2015

International Journal of Computational Engineering Research

Volume 5 Issue 2, February 2015

International Journal of Computational Engineering Research (IJCER) is dedicated to protecting personal information and will make every reasonable effort to handle collected information appropriately. All information collected, as well as related requests, will be handled as carefully and efficiently as possible in accordance with IJCER standards for integrity and objectivity..]

IJCER Open access Journal

Editorial Board

Editor-In-Chief

Editorial Committees

Contents:

ISSN (e): 2250 – 3005 || Vol, 05 || Issue,02 || February – 2015 ||
International Journal of Computational Engineering Research (IJCER)

Continuous Wavelet Transform (CWT) based Analysis of Very Fast Transient over Voltages of 132 KV Power Transformer

K.Prakasam[1], D.Prabhavathi[2], ,Dr.M.Suryakalavathi[3], Dr.B.Ravindranath Reddy[4]

[1]*Department of Electrical and Electronics Engineering, Sri Sivani College of Engineering,srikakulam,A.P,INDIA.*
[2]*Department of Electrical and Electronics Engineering, Sri Sivani College of Engineering,Srikakulam,A.P,INDIA.*
[3]*Department of Electrical and Electronics Engineering, JNTUH, Hyderabad,INDIA.*
[4]*Department of Electrical and Electronics Engineering, JNTUH, Hyderabad,INDIA.*

ABSTRACT

This paper results the most accurate results of Very Fast Transient over Voltages of 132 KV transformer caused by the switching operation. A 132KV transformer is designed using MATLAB simulin, the VFTOs generated by the switching operations have been analyzed and are presented. The VFTOs generated due to Disconnector switching operation can cause insulation failure at very high voltage levels. The reasons of these problems are travelling waves which is generated during switching operations in a gas-insulated substation (GIS). Calculation of Very Fast Transient Overvoltage has been carried out using MATLAB7.8 for various switching.

Keywords—*disconnect or, High voltage level, MAT LAB, Switching, Switching operations, Travelling Very Fast Transient over voltages, Wavelet transform,*

I. INTRODUCTION

Very Fast Transient Over voltages (VFTOs) generated by switching operations. This type of overvoltages is dangerous for the transformer insulation due to a short rise time, which can cause non-linear voltage distribution along transformer windings. In some special cases, the turn-to-turn voltage can rise near the transformer basic insulation level [1]. These problems can either lead to direct break down or initiation of partial discharge which deteriorate the insulation. After a short time this can result in an insulation breakdown. These over voltages occur inside the winding and are difficult to measure and detect. Electromagnetic transients may appear with a wide range of frequencies that vary from several Hz to several hundreds of MHz transients and faster electromagnetic transients. The latter type of transients can occur for a shorter duration ranging from microseconds to several cycles. Frequency ranges are classified into groups for the ease of developing models accurate enough due to frequency behavior of power components. An accurate mathematical representation of each power component can generally be developed for a specific frequency range (CIGRE, 1990). One of the reasons of generated VFTOs is re-strikes and pre-strikes during opening or closing of switching devices. Very Fast Transients (VFT), also known as Very Fast Front Transients, belong to the highest frequency range of transients in power systems. According to the classification proposed by the CIGRE Working Group 33–02, VFT may vary from 100 kHz up to 50 MHz (1990). According to IEC 71–1, the shape of a very fast transient over voltage is ‘‘usually unidirectional with time to peak<0.1 ms, total duration<3 ms, and with superimposed oscillations at frequency 30 kHz<f<100 MHz’’ (1993). The VFTOs in transformer windings have always been troublesome therefore it is important to analyze the wave both in time domain and frequency domain, therefore the wavelet transform is implemented. There are several works on VFTOs but this method is efficient and can be used to compute the effect of VFTOs on transformer.

In this paper a 132KV transformer is designed using Mat lab software of version 7.8, the VFTOs generated by switching conditions are calculated and are analyzed by wavelet transform and the result is tabulated and discussed.

Dis-connector Switch (DS) operation typically involves slow moving contacts which results in numerous discharges during operation .For example, a floating section of switchgear between a disconnect switch and an open breaker (load side may be disconnected from an energized Gas insulated system (supply side). For capacitive currents below—1 amp, are-strike occurs every time the voltage between the connects exceeds the dielectric strength of the gaseous medium between them. Each re-strike generates a spark, which equalizes the potentials between the switch **contacts. Following spark extinction, the supply and load side potentials will deviate according to the AC supply** voltage variation and the discharge characteristics of the load side respectively. Another spark will result when the voltage across the electrode gap dependent breakdown voltage UB and the potential difference of the load and supply side U. Each Dis-connector Switch (DS) operation generates a large number of ignitions between the moving contacts. The number of ignitions depends on the speed of the contacts. The largest and steepest surge voltages are generated only by those breakdowns at the largest contact gap

Dis-connector Switch (DS) operation typically involves slow moving contacts which results in numerous discharges during operation .For example, a floating section of switchgear between a disconnect switch and an open breaker (load side may be disconnected from an energized Gas insulated system (supply side). For capacitive currents below—1 amp, are-strike occurs every time the voltage between the connects exceeds the dielectric strength of the gaseous medium between them. Each re-strike generates a spark, which equalizes the potentials between the switch contacts. Following spark extinction, the supply and load side potentials will deviate according to the AC supply voltage variation and the discharge characteristics of the load side respectively. Another spark will result when the voltage across the electrode gap dependent breakdown voltage and the potential difference of the load and supply side. Each Disconnect or Switch (DS) operation generates a large number of ignitions between the moving contacts. The number of ignitions depends on the speed of the contacts. The largest and steepest surge voltages are generated only by those breakdowns at the largest contact gap.

II. WAVELET TRANSFORM

A wavelet is a waveform of effectively limited duration that has an average value of zero. The driving force behind wavelet transforms (WTs) is to overcome the disadvantages embedded in short time Fourier transform (STFT), which provides constant resolution for all frequencies since it uses the same window for the analysis of the inspected signal x (t). On the contrary, WTs use multi-resolution, that is, they use different window functions to analyze different frequency bands of the signal x (t). Different window functions ψ(s,b,t);which are also called son wavelets, can be generated by dilation or compression of a mother wavelet ψ(t) , at different time frame. A scale is the inverse of its corresponding frequency. WTs can be categorized as discrete WTs or continuous WTs. For vibration-based fault diagnosis, usually continuous WTs are employed. A continuous type of wavelet transform (CWT) that is applied to the signal x (t) can be defined as,

$$w(a,b) = \frac{1}{\sqrt{a}} \int_{-\infty}^{\infty} f(t)\psi\left(\frac{t-b}{a}\right)dt \qquad (2.1)$$

Where

- a is the dilation factor,
- b is the translation factor and
- $\psi(t)$ is the mother wavelet.
- $1/\sqrt{a}$ is an energy normalization term that makes wavelets of different scale has the same amount of energy.

A continuous wavelet transform (CWT) is used to divide a continuous-time function into wavelets. Unlike Fourier transform, the continuous wavelet transform possesses the ability to construct a time-frequency representation of a signal that offers very good time and frequency localization. In mathematics, the continuous wavelet transform of a continuous, square-integrable function $x(t)$ at a scale $a > 0$ and translational value $b \in \mathbb{R}$ is expressed by the following integral

$$X_w(a,b) = \frac{1}{\sqrt{|a|}} \int_{-\infty}^{\infty} x(t)\psi^*\left(\frac{t-b}{a}\right) dt \qquad (2.2)$$

where $\psi(t)$ is a continuous function in both the time domain and the frequency domain called the mother wavelet and $*$ represents operation of complex conjugate. The main purpose of the mother wavelet is to provide a source function to generate the daughter wavelets which are simply the translated and scaled versions of the mother wavelet. To recover the original signal $x(t)$, inverse continuous wavelet transform can be exploited.

$$x(t) = \int_0^\infty \int_{-\infty}^\infty \frac{1}{a^2} X_w(a,b) \frac{1}{\sqrt{|a|}} \tilde{\psi}\left(\frac{t-b}{a}\right) db\ da \tag{2.3}$$

$\tilde{\psi}(t)$ is the dual function of $\psi(t)$. And the dual function should satisfy

$$\int_0^\infty \int_{-\infty}^\infty \frac{1}{|a^3|} \psi\left(\frac{t_1-b}{a}\right) \tilde{\psi}\left(\frac{t-b}{a}\right) db\ da = \delta(t-t_1). \tag{2.4}$$

Sometimes, $\tilde{\psi}(t) = C_\psi^{-1} \psi(t)$, where

$$C_\psi = \frac{1}{2} \int_{-\infty}^{+\infty} \frac{|\hat{\psi}(\zeta)|^2}{|\zeta|} d\zeta \tag{2.5}$$

is called the admissibility constant and $\hat{\psi}$ is the Fourier transform of ψ. For a successful inverse transform, the admissibility constant has to satisfy the admissibility condition:

$$0 < C_\psi < +\infty.$$

It is possible to show that the admissibility condition implies that $\hat{\psi}(0) = 0$, so that a wavelet must integrate to zero.

III. MODEL DEVELOPMENT OF 132KV TRANSFORMER

Despite the advancement in electrical measurement techniques and equipment, quantifying the VFTO at such high frequencies remains challenging. Actual measurement in the GIS during planning stage is not practically possible. Designers must use numerical tools to calculate the VFTO associated with switching operations in a GIS. This informs the design decision process to achieve a more robust and reliable system with adequate insulation levels for all equipments used. The existing technical literature shows that with good modeling techniques and appropriate assumptions, numerical tools can provide reasonably accurate predictions of the VFTO magnitude and their rate of rise [1], [2], [3], [4], [5], [6], [7]. The simulation studies reported here was performed using MAT LAB software, version of 7.8. Switching events in a GIS generates transients with frequencies in the range of hundreds of kHz up to tens of MHz. These transients cannot be calculated if conventional techniques of modelling and simulation are used.

Coaxial conductors in gas insulated substations have higher specific capacitance to earth. GIS is also characterized by lower surge impedance and inductance as well as larger gradient of the electric field between pre-strike and re-strike arcs in SF6 under pressure. This causes very fast transients with surge fronts of very short durations. Due to the geometrical structure of GIS and its low surge impedance, travelling waves reflection at the GIS entrance could rapidly result in sizeable over voltages at any open end within the GIS (i.e. due to multiple reflections). A disconnect or is represented by a PI section comprises of two travelling wave models, two capacitors to ground and a capacitor across the breaking contacts as shown in fig 1. A circuit breaker is represented by a PI circuit with five travelling wave models and four capacitors. Decaying resistance (R0e-t/T) in series with a small resistance, r of 0.5 Ω to take care of the residual spark resistance [11].

$$R = R\,e^{-}(t / T) + r \tag{3.1}$$

The value of R0 is taken as $1x10^6$ MΩ and T as 1 ns. This gives a resistance whose value varies from very high value (MΩ) to a low value of 0.5 Ω within 30 ns.

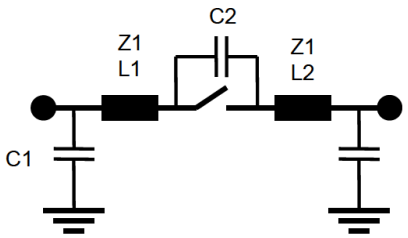

Fig.1 Dissconnector

Where, Z1 = 35 Ω, L1 = 640 mm, L2 = 450 mm, C1 = 25 pF and C2 = 2.5 pF

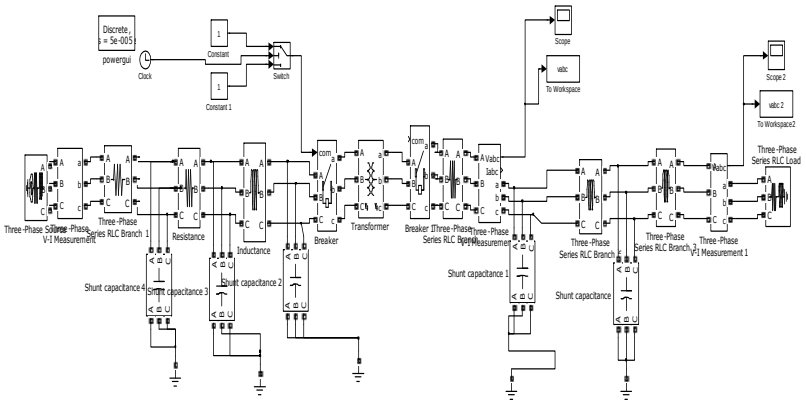

Mat lab simulink Schematic Diagram of 132KV Power Transformer

IV. RESULTS AND DISCUSSIONS

A 132KV power transformer is modelled using mat lab software and the model of dissconnector is used for switching conditions.The diss connector is provided at the transformer primary side with the operating times of 4/60 to 10/60 micro seconds.The conventional result of three phase voltage when transformer is subjected to switching condition is shown in fig 4.1 and the result extrated by wavelet transform is shown in fig 4.2.Also individual phases of transformer are subjected to switching conditions and their resultant voltages are captured and shown in figs 4.3,4.5 and 4.7 .The continious wavelet transform is applied to extract the results of phase A, phase B and phase c and are shown in fig 4.4, 4.6 and 4.8.from the results it can be observed that there is error in the conventional methods of evaluation of VFTOs and wavelet transform gives an accurate result of VFTOs.the values are calculated and are tabulated in the table 1 taking peak value of VFTOs and Rise time of the waves forms.to analys the VFTOs db wavelet transform is used with the level of Db7.The 50 Hz frequency signal is generated at the sampling period of 0.0002 and scale of 69.19.Tab;e 1 gives the result of conventional method.table II gives the result extracted by the wavelet transform.the error between conventinal and wavelet transform is evaluated as 2.66% in magnitude of VFTOs and 5.3% error in rise time.Hence it is concluded that the wavelet transform gives very accurate result and is more efficient.

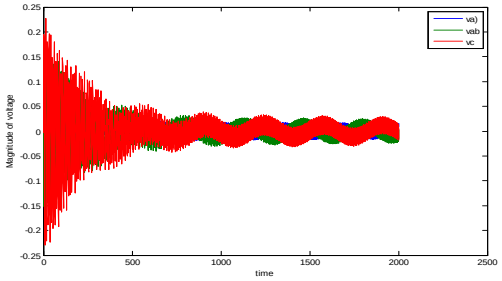

Fig.4.1 Three phase voltage waveform due to switching of three phase at transformer

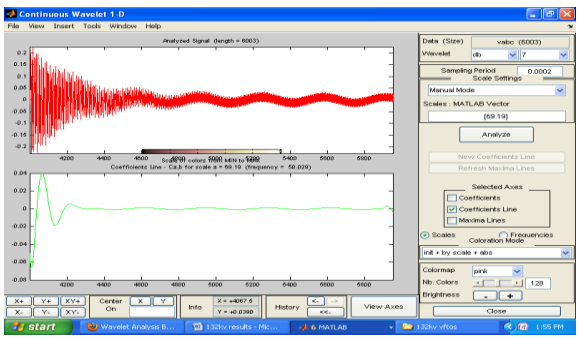

Fig.4.2 Wavelet result of Three phase voltage waveform due to switching of three phase at transformer

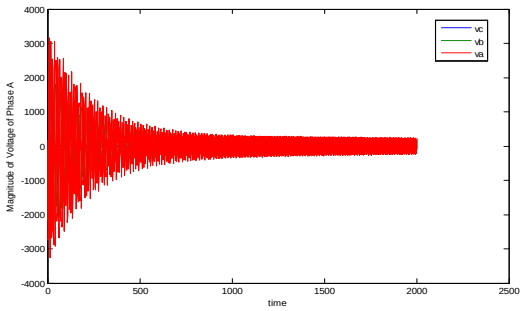

Fig.4.3 Voltage waveform due to switching in Phase A at transformer

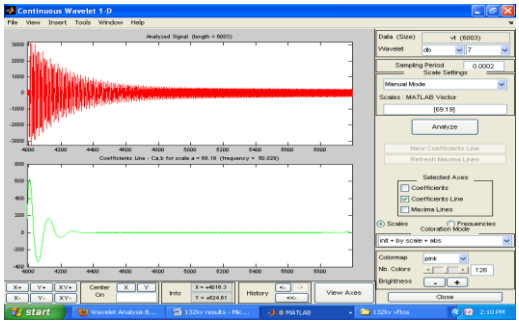

Fig.4.4 Wavelet result of Voltage due to switching in Phase A at transformer

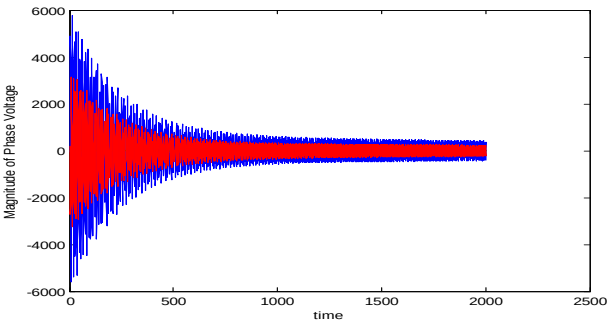

Fig.4.5 Voltage waveform due to switching in Phase B at Transformer

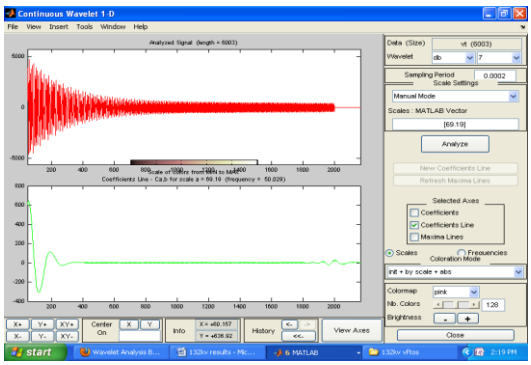

Fig.4.6 Wavelet result of Voltage waveform due to switching in Phase B at Transformer

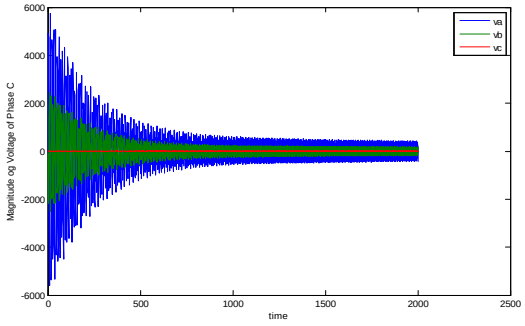

Fig.4.7 Voltage waveform due to switching in Phase C at Transformer

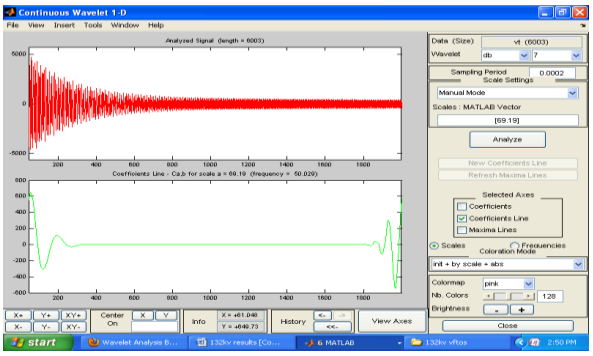

Fig.4.8 Wavelet result of Voltage waveform due to switching in Phase C at Transformer

Table I

Mode of Operation	Voltage Magnitude	Rise Time in (Nanoseconds)
Closing condition	2.45	75
Opening condition	1.35	64

Table II

Mode of Operation	Voltage Magnitude	Rise Time in (Nanoseconds)
Closing condition	2.19	79
Opening condition	1.56	54

V. CONCLUSIONS

A model is developed for the prediction of the VFTO phenomena in the 132KV power transformer. The peak magnitude of Very fast transient over voltages generated during switching event have calculated for a 132kv GIS transformer for a particular switching operation. The VFTOs generated by switching operation are evaluated by both conventional and wavelet transform and by comparing both the methods it is observed that the error evaluated as 2.66% in magnitude of VFTOs and 5.3% in rise time .Hence it is concluded that wavelet transform is so accurate and can be used for practical applications for better performance.

VI. ACKNOWLEDGEMENTS

The authors wish to gratefully acknowledge Smt.Dr.M.Suryakalavathi, Prof Dept of E.E.E, J.N.T.U.H, Hyderabad and her support for the completion of this work. The authors also wish to gratefully acknowledge Dr.B.Ravindranath Reddy for the support given in the completion of this research work.

REFERENCES

[1] U. Riechert et. Al, "Very Fast Transient Overvoltages during Switching of Bus-Charging Currents by 1100 kV Disconnector", *CIGRE* 2010, A3_107_2010.

[2] S. Ynabu et. al, "Estimation of Fast Transient Overvoltage in Gas- Insulated Substation.," *IEEE Trans. Power Delivery*, vol. 5, No. 4, Nov 1990.

[3] Susumu Matsumura, Tohei Nitta, " Surge Propagation in Gas Insulated Substation", *IEEE Trans. Power Apparatus and Systems*, Vol. PAS-100, No.6 June 1981.

[4] S.A. Boggs et. al, "The Modelling of Statistical Operating Parameters and the Computation of Operation-Induced Surge Waveforms for GIS Disconnectors", *Cigre*, 1984, Paper 13-15.

[5] Z. Haznadar et. al, "More Accurate Modelling of Gas Insulated Substation Components in Digital Simulations of Very Fast Electromagnetic Transients.", *Transaction on Power Delivery*, Vol 7 No. 1 January 1992.

[6] J. F. de Lima Filho et. al, "Tucurui's 500 kV SF6 Gas-Insulated Substation Fast Transients – Analysis, Modeling and Field Test Comparisons", *International Conference on Power System Transients*, 1995.

[7] P. Rohrbach, "550 kV GIS VFT Simulations as a Support for Transformer Design", *International Conference on Power System Transients*, 2001.

[8] IEEE Fast Front Transients Working Group, "Modeling Guidelines for Fast Transients", *IEEE Trans on Power Delivery*, Vol 11, No 1, January 1996, p 493-506.

[9] IEEE Very Fast Front Transients Working Group, "Modeling Guidelines for Very Fast Front Transients in Gas Insulated Substation".

[10] V. Vinod Kumar, "Influence of Switching Conditions on the VFTO Magnitudes in a GIS", *IEEE Trans on Power Delivery*, Vol. 16, No. 4, October 2001.

[11] H. W Dommel, "Transformer models in the simulation of electromagnetic transients", *Proc 5th Power Systems Computing Conference*, Cambridge, England, September 1-5, 1975.

[12] A. Morched, B. Gustavsen, M. Tartibi, "A Universal Model for Accurate Calculation of Electromagnetic Transients on Overhead Lines and Underground Cables", *IEEE Transactions on Power Delivery*, Vol. 14, No. 3, pp. 1032-1038, July 1999.

[13] *High-voltage switchgear and controlgear – Part 102 : Alternating current disconnectors and earthing switch*, BS EN 62271-102 :2002.

Biographies and Photographs

2) K.Prakasam, Born in 1973 April 20, his B.Tech degree from KSRM College of Engineering SV university in 1997 and M.Tech degree from SV university in the year 2004. He has specialized in Power Systems operation and Control Systems. his research interests include Simulation studies on Transients of different power system equipment. He has 16 years of experience. He is presently working as Prof .Prof and HOD of Dept of EEE, *Sri Sivani College of Engineering*, Srikakaulam, Andhrapradesh, INDIA

1)D.Prabhavathi Born in 1976 august 27, her B.Tech degree from KSRM college of Engineering, kadapa , SV university, and M.Tech degree from SV University in the year 2004.She has specialized in Power Systems operation and control. Her research interests include Simulation studies on faults identification in UG cable of LT and HT. She has 12 years of experience. She is currently working as .Prof, dept of E.E.E *Sri Sivani College of Engineering*, Srikakaulam, Andhrapradesh ,INDIA..

3) Dr. M. Surya Kalavathi, Born on 8th July 1966, Obtained her B.Tech degree from S.V. U. in 1988 and M.Tech from S.V.U. in the year 1992.Obtained her doctoral degree from JNTU, Hyderabad and Post Doctoral from CMU, USA. She is presently working as Professor (EEE) in JNTUH College of Engineering, Kukatpally, Hyderabad. Published 16 Research Papers and presently guiding many Ph.D. Scholars. She has specialized in Power Systems, High Voltage Engineering and Control Systems. Her research interests include Simulation studies on Transients of different power system equipment. She has 18 years of experience. She has invited for various lectures.

4) Bhumanapally.Ravindhranh Reddy, Born on 3rd September, 1969. Got his B.Tech in Electrical & Electronics Engineering from the J.N.T.U. College of Engg., Anantapur in the
year 1991. Completed his M.Tech in Energy Systems in IPGSR of J.N.T.University Hyderabad in the year 1997. Obtained his doctoral degree from JNTU, INDIA

ISSN (e): 2250 – 3005 || Vol, 05 || Issue,02 || February – 2015 ||
International Journal of Computational Engineering Research (IJCER)

Wavelet based detection and location of faults in 400kv, 50km Underground Power Cables

D.Prabhavathi[1], K.Prakasam[2], Dr.M.Suryakalavathi[3], Dr.B.Ravindranath Reddy[4]

[1]*Department of Electrical and Electronics Engineering, Sri Sivani College of Engineering,Srikakulam,A.P.INDIA*
[2]*Department of Electrical and Electronics Engineering, Sri Sivani College of Engineering,Srikakulam,A.P,INDIA*
[3]*Department of Electrical and Electronics Engineering, JNTUH, Hyderabad, INDIA.*
[4]*Department of Electrical and Electronics Engineering, JNTUH, Hyderabad, INDIA.*

ABSTRACT

In this paper, a method for detection and location of fault in a power line is presented. This method can be applied for both transmission and distribution power lines of underground cables. The proposed method is capable to determine type of fault the fault location upon its occurrence, based on the data available from the measuring equipment. The algorithm presented uses the fault steady-state data (voltages and currents) and the system parameters, to calculate the fault location. The influence of the fault resistance that depends on the design characteristics of the power line is disregarded. The proposed method has been modeled in mat lab simulink of version 7.8.

KEYWORDS: *Cables, distribution, Fault location, Fault diagnosis, steady state, transmission, underground, wavelet,*

I. INTRODUCTION

Detection and Location of faults in power transmission lines is one of the main concerns for all the electric utilities as the accurate detection and fault location can help to restore the power supply in the shortest possible time. Fault location methods for transmission lines are broadly classified as impedance based method which uses the steady state fundamental components of voltage and current values [1–3], travelling wave (TW) based method which uses incident and reflected TWs observed at the measuring end(s) of the line [4, 5], and knowledge based method which uses artificial neural network and/or pattern recognition techniques [6,7]. All the above methods use the measured data either from one end of the transmission line or from all ends. Fault analysis methods are an important tool used by protection engineers to estimate power system currents and voltages during disturbances. It provides information for protection system setting, coordination and efficiency analysis studies. Today, three approaches are used in the industry for such analysis: classical symmetrical components, phase variable approach and complete time-domain simulations [19]. Classical fault analysis of unbalanced power systems is based on symmetrical components approach [20, 21]. However, in un transposed feeders with single-phase or double- phase laterals, the symmetrical component methods do not consider accurately these specific characteristics [22]. Hence, symmetrical components based techniques may not provide accurate results for power distribution systems, which are normally characterized by those asymmetries. With industrial computer facilities improvement, the fault analysis phase variable approach has been proposed to substitute the symmetrical components methods on distribution systems [23]. In the phase variable approach, system voltages and currents are related through impedance and admittance matrices based on phase frame representation, considering the typical distribution systems asymmetries. However, fault analysis is still fault resistance dependant [24]. Due to fault resistance stochastic nature, typical fault analysis studies consider the fault paths as an ideal short-circuit. To overcome this limitation, recent studies suggest the usage of fault resistance estimation algorithms [25–27]. These works provide a fault resistance estimate using symmetrical components or modal analysis techniques, restricting the application on balanced systems with equally transposed lines. The usage of artificial intelligence has also been recently proposed in order to overcome the fault resistance effects in classical power system protection [28] and fault location [29] applications.

II. WAVELET TRANSFORMS

A wavelet is a waveform of effectively limited duration that has an average value of zero. The driving force behind wavelet transforms (WTs) is to overcome the disadvantages embedded in short time Fourier transform (STFT), which provides constant resolution for all frequencies since it uses the same window for the analysis of the inspected signal x (t). On the contrary, WTs use multi-resolution, that is, they use different window functions to analyze different frequency bands of the signal x (t). Different window functions ψ(s,b,t);which are also called son wavelets, can be generated by dilation or compression of a mother wavelet ψ(t) , at different time frame. A scale is the inverse of its corresponding frequency. WTs can be categorized as discrete WTs or continuous WTs. For vibration-based fault diagnosis, usually continuous WTs are employed. A continuous type of wavelet transform (CWT) that is applied to the signal x (t) can be defined as,

$$w(a,b) = \frac{1}{\sqrt{a}} \int_{-\infty}^{\infty} f(t)\psi\left(\frac{t-b}{a}\right)dt \qquad (2.1)$$

Where

- a is the dilation factor,
- b is the translation factor and
- $\psi(t)$ is the mother wavelet.
- $1/\sqrt{a}$ is an energy normalization term that makes wavelets of different scale has the same amount of energy.

A continuous wavelet transform (CWT) is used to divide a continuous-time function into wavelets. Unlike Fourier transform, the continuous wavelet transform possesses the ability to construct a time-frequency representation of a signal that offers very good time and frequency localization. In mathematics, the continuous wavelet transform of a continuous, square-integrable function $x(t)$at a scale $a > 0$and translational value $b \in \mathbb{R}$is expressed by the following integral

$$X_w(a,b) = \frac{1}{\sqrt{|a|}} \int_{-\infty}^{\infty} x(t)\psi^*\left(\frac{t-b}{a}\right) dt \qquad (2.2)$$

where $\psi(t)$is a continuous function in both the time domain and the frequency domain called the mother wavelet and $*$ represents operation of complex conjugate. The main purpose of the mother wavelet is to provide a source function to generate the daughter wavelets which are simply the translated and scaled versions of the mother wavelet. To recover the original signal $x(t)$, inverse continuous wavelet transform can be exploited.

$$x(t) = \int_0^{\infty} \int_{-\infty}^{\infty} \frac{1}{a^2} X_w(a,b) \frac{1}{\sqrt{|a|}} \tilde{\psi}\left(\frac{t-b}{a}\right) db\, da \qquad (2.3)$$

$\tilde{\psi}(t)$is the dual function of $\psi(t)$. And the dual function should satisfy

$$\int_0^{\infty} \int_{-\infty}^{\infty} \frac{1}{|a^3|} \psi\left(\frac{t_1-b}{a}\right) \tilde{\psi}\left(\frac{t-b}{a}\right) db\, da = \delta(t-t_1). \qquad (2.4)$$

Sometimes, $\tilde{\psi}(t) = C_{\psi}^{-1}\psi(t)$, where

$$C_{\psi} = \frac{1}{2} \int_{-\infty}^{+\infty} \frac{|\hat{\psi}(\zeta)|^2}{|\zeta|} d\zeta \qquad (2.5)$$

is called the admissibility constant and $\hat{\psi}$is the Fourier transform of ψ. For a successful inverse transform, the admissibility constant has to satisfy the admissibility condition:

$$0 < C_{\psi} < +\infty.$$

It is possible to show that the admissibility condition implies that $\hat{\psi}(0) = 0$, so that a wavelet must integrate to zero.

III. PROPOSED SYSTEM

A 400KV, 100MVA, 50km, 50Hz power cable is considered and is designed using Mat lab simulink with Simpower systems block sets. Since the length of the line is small**,** the leakage current can be neglected and the shunt part of the line can be neglected and with the series impedance an accurate detection can be obtained.

To induce a fault in the power line, a point in the line has to be connected to ground through a small resistance (fault resistance), fig1 and Fig.2 represents a single-ended power line with a fault at distance x from point A.

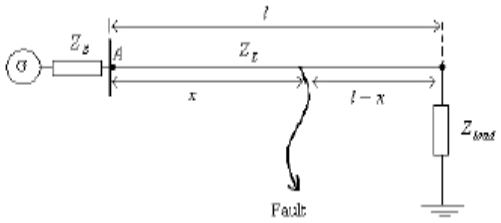

Fig, 1 One - end power cable of 50Km long

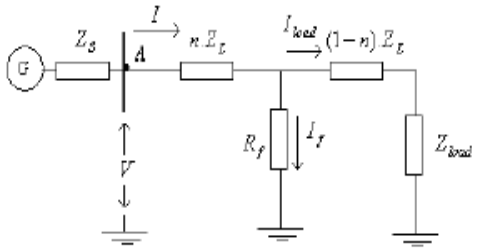

Fig.2 Representation of a single-ended power line with a fault at distance x from point A.

Z = The source impedance. ,Z_L = The line impedance

load Z =The load impedance. : load Z ,l = The line length.

X=The length from the fault location equipment (point A) to the fault.

V= The measured voltage. I = Measured current R_f = The fault resistance

I_f = Fault current, I = Load current

n = the per unit length from the measuring equipment (point A) to the fault: n = x/l

The mat lab simulink modeling is obtained from the mathematical modeling of the power cable and is shown in fig.4.1.The various fault are carried and the detection and location of faults were analysed.

IV. SIMULATION STUDIES OF PROPOSED SYSTEM

This section presents the simulation results to evaluate the developed fault location algorithm. The developed fault location algorithm is implemented in Mat lab. The model has been created with a toolbox of Matlab/Simulink® called SimPowerSystems®. It is a collection of blocks that allow the modeling of different elements that usually are present on power systems. It uses the Simulink as simulation engine. The studied power system is a 400KV, 50 Hz, 50 km underground cable transmission line system. The simulation of the algorithm is focused on a single phase-to- ground fault, a type of fault that occupies about 90% of all of the transmission line faults. The results of the simulations are the voltage and current waveforms of the three phases at the header of the line, the same information that can be obtained from real faults. The voltage and current phasors are found taking the fundamental frequency by using the fast Fourier transform. With the phasors and the model of the network, now the algorithms can be computed. The Simulink model used to simulate the algorithm used is shown in the Figure. 4.1. Continuous wavelet transform is applied to extract the accurate detection and location of the faults.

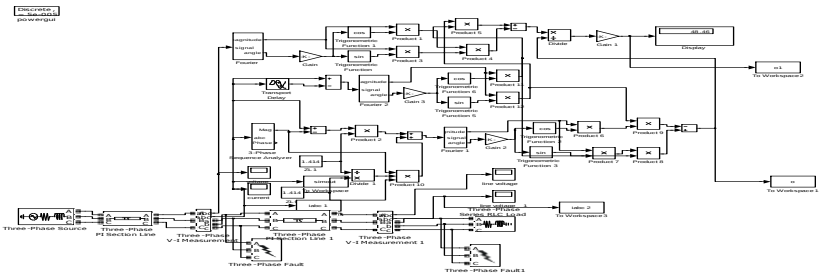

4.1. MATLAB Simulink model of 400KV, 50Km Three phase UG cable

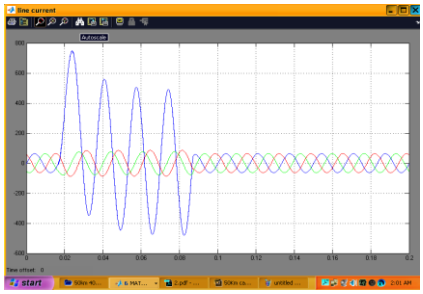

Fig.4.2.Single line to ground fault current (AG fault)

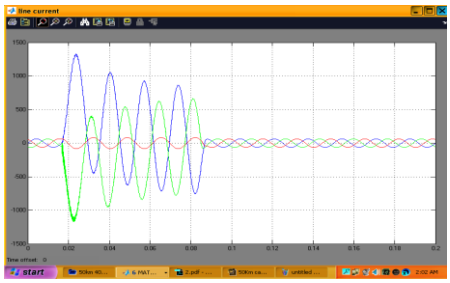

Fig.4.3.Double line to ground fault current (ABG fault)

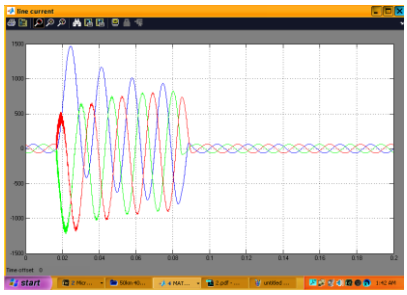

Fig.4.4.Three Phase to ground fault current (ABCG fault)

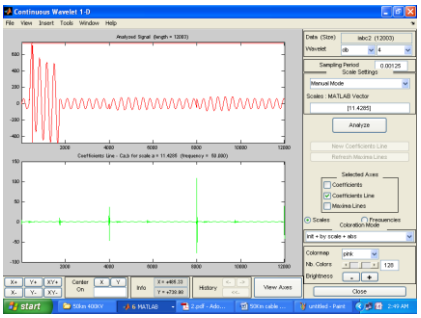

Fig 4.5.Single line to earth fault (AG) at 50km by wavelet transforms

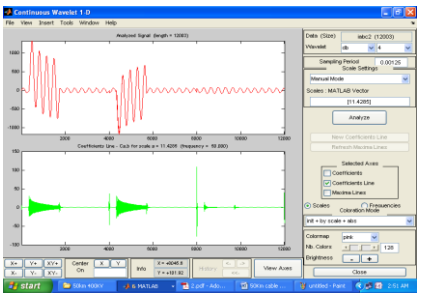

Fig 4.6.Double line to earth fault (ABG) at 50km by wavelet transforms

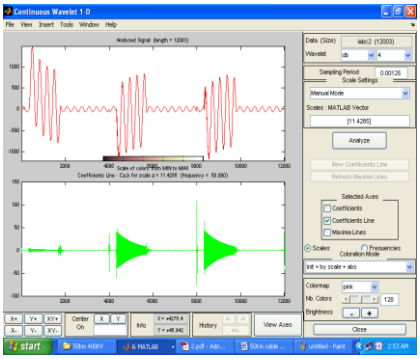

Fig 4.7.Tripple line to earth fault (ABCG) at 50km by wavelet transforms

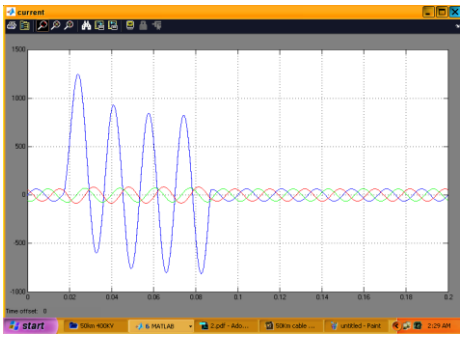

Fig.4.8.Single line to ground fault current (AG fault) at 25km

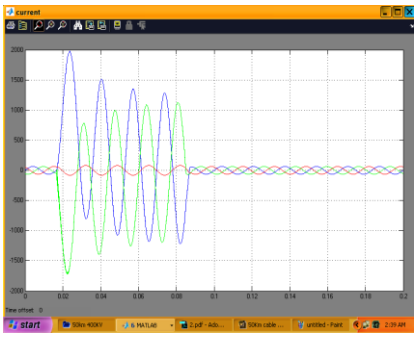

Fig.4.9.Double line to ground fault current (ABG fault) at 25km

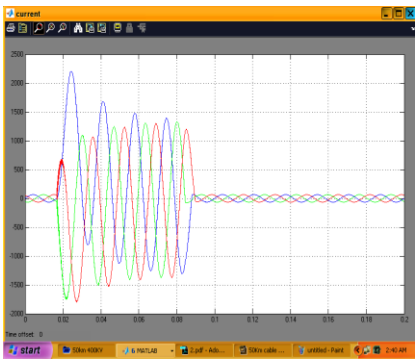

Fig.4.10.Tripple line to ground fault current (ABCG fault) at 25km

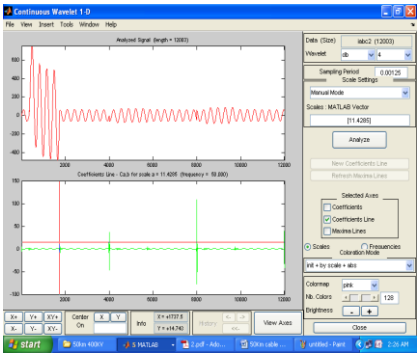

Fig 4.11.Single line to earth fault (AG) at 25km by wavelet transforms

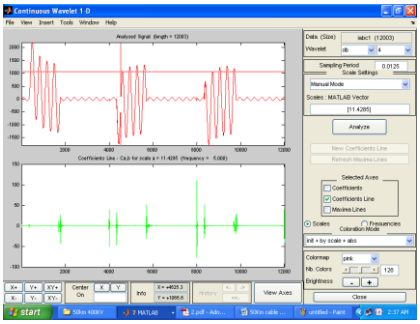

Fig 4.11.Double line to earth fault (ABG) at 25km by wavelet transforms

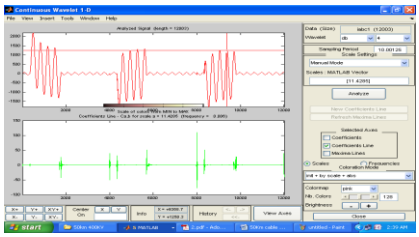

Fig 4.11.STripple line to earth fault (ABCG) at 25km by wavelet transforms

Table-1

LG Fault		
Actual Distance(km)	Measured Distance(km)	% Error
25	24.58	1.68
50	51.45	-2.9

Table-2

LLG Fault		
Actual Distance(km)	Measured Distance(km)	% Error
25	25.1	-0.4
50	49.58	0.8

Table-3

LLLG Fault		
Actual Distance(km)	Measured Distance(km)	% Error
25	25.87	-3.4
50	53.18	-6.36

The estimation accuracy is evaluated by the percentage error calculated as per the following equation

$$\frac{Actual\ fault\ location - estimated\ fault\ location}{Total\ lenghth\ of\ the\ line} X100$$

Where the location of the fault is defined as the distance between the bus at which the measuring equipment are installed, and the fault point. As can be seen, the fault location estimates are satisfactory. The location fault is estimated in wavelet transform between the two peaks of the waveform.

V. CONCLUSIONS

This paper presents detection and location of fault in 400KV underground .The proposed algorithm uses the steady-state data (voltages and currents), available by the measuring equipment, to calculate the fault location. The influence of the fault resistance is disregarded. The proposed method can be used to built a stand-alone fault locating equipment and as a part of a protective device as an impedance relay. Simulation studies have shown that the proposed algorithm can yield quite accurate estimates of the fault detection and location. The resultant of all types of faults are shown in figures 4.2 to 4.7 for fault at 50km and from figures 4.8 to 4.11 for faults at 25km.The resultant values of all faults are tabulated in table I, table II and table III. From this it can be observed that the wavelet transform gives better results in detection and location of faults. The maximum error in this analysis is -6.36%

REFERENCES

[1] Filomena AD, Resener M, Salim RH, Bretas AS. Extended impedance-based fault location formulation for unbalanced underground distribution systems. In: IEEE PESGM-conversion & delivery of electrical energy in the 21st century; 2008 July. p. 1– 8.

[2] Amir AA, Ramar K. Accurate one-end fault location for overhead transmission lines in interconnected power systems. Int J Electr Power Energy Syst 2010;32(5):383–9.

[3] Abdel-Fattah M, Lehtonen M. A new transient impedance-based algorithm for earth fault detection in medium voltage network

[4] Bo ZQ, Johns AT, Aggarwal, AK. A novel fault locator based on the detection of fault generated high frequency transients. In: Proceedings of 6th IEE developments in power systems protection conference; March 1997. p. 197– 200. [5] Evrenosoglu CY, Abur A. Travelling wave based fault location for teed circuits. IEEE Trans Power Deliv 2005;20(2):1115–21.

[6] Anamika Jain, Kale VS, Thoke AS. Application of artificial neural networks to transmission line faulty phase selection and fault distance location. In: IASTED, Chiang Mai, Thailand; 29–31 March 2006. p. 262–7.

[7] Fernandez RMC, Rojas HND. An overview of wavelet transforms applications in power systems. In: 14th PSCC, Sevilla, Spain; 2002. p. 1–8.

[8] Lee H. Development of accurate traveling wave fault locator using global positioning satellites. In: 20th Annual western protective relay conference, Spokane Washington, USA; October 1993. p. 197–204.

[9] Jiang F, Bo ZQ, Weller G, Chin SM, Redfern MA. A GPS based fault location scheme for distribution line using wavelet transform technique. In: international conference on power system transients, Budapest, Hungary, June 1999. p. 224–8.

[10] Elhaffar A, Lehtonen M. An improved GPS current traveling-wave fault locator in EHV transmission networks using few recordings. In: Proceedings of international conference on future power systems, Schiphol–Amsterdam, Netherlands; 1–5 November 2005.

[11] Silva MD, Oleskovicz M, Coury DV. Hybrid fault locator for three-terminal lines based on wavelet transforms. Electr Power Syst Res 2008;78(11):1980–8.

[12] Lin YH, Liu CW, Yu CS. A new fault locator for three-terminal transmission lines—using two-terminal synchronized voltage, current phasors. IEEE Trans Power Deliv 2002;17(2):452–9.

[13] Chen CS, Liu CW, Fast and accurate fault detection/location algorithms for double-circuit/three-terminal lines using phasor measurement units. J Chin Inst Eng 2003;26(3):289–99.

[14] Ngu EE, Ramar K. Single-ended traveling wave based fault location on two terminal transmission lines. In: IEEE TENCON, Singapore; 23rd–26th November, 2009. p. 1–4. ISBN: 978-1-4244-4547-9.

[15] Zheng XY, Li XM, Ding JY, Duan ZY. Study on impedance-traveling wave assembled algorithm in one-terminal fault location system for transmission lines. In: 3rd International conference on electric utility deregulation & restructuring and power technologies; April 2008. p. 1123–6.

[16] Yerekar SR. Fault location system for transmission lines in one-terminal by using impedance-traveling wave assemble. <http://eeeic.eu/proc/ technical_program_cd.html> [accessed August 2009].

[17] Dong XZ, Chen Z, He XZ, Wang KH, Luo CM. Optimizing solution of fault location. IEEE Power Eng Soc Summer Meet 2002;3:1113–7.

[18] Rajendra S, McLaren PG. Traveling wave techniques applied to the protection of teed circuits: multi-phase/multi-circuit system. IEEE Trans Power Apparat Syst 1985 Dec;104:3351–7.

[19] Halpin SM, Grigsby LL. A comparison of fault calculation procedures for industrial power distribution systems: the past, the present and the future. In: Proceedings of the IEEE international conference on industrial technology; 1994.

[20] Halpin SM, Grigsby LL, Gross CA, Nelms RM. An improved fault analysis algorithm for unbalanced multi-phase power distribution systems. IEEE Trans Power Deliv 1994;9(3):1332–8.

[21] Anderson PM. Analysis of faulted power systems. New York (USA): IEEE; 1995.

Acknowledgements

The authors wish to gratefully acknowledge Smt.Dr.M.Suryakalavathi, Prof Dept of E.E.E, J.N.T.U.H, Hyderabad and her support for the completion of this work. The authors also wish to gratefully acknowledge Dr.B.Ravindranath Reddy, Deputy Executive Engineer, J.N.T.U.H, and Hyderabad for the support given in the completion of this research work.

Biographies and Photographs

1)D.Prabhavathi Born in 1976 august 27, her B.Tech degree from KSRM college of Engineering, kadapa , SV university, and M.Tech degree from SV University in the year 2004.She has specialized in Power Systems operation and control. She is currently working as Assoc.Prof, dept of E.E.E *Sri Sivani College of Engineering*, Srikakaulam, Andhrapradesh,INDIA. Her research interests include Simulation studies on faults identification in UG cable of LT and HT. She has 13 years of experience.

2) K.Prakasam, Born in 1973 April 20, his B.Tech degree from KSRM College of Engineering SV university in 1997 and M.Tech degree from SV university in the year 2004. He has specialized in Power Systems operation and Control Systems. His research interests include Simulation studies on Transients of different power system equipment. He has 16 years of experience. He is presently working as Prof .Prof and HOD of Dept of EEE, *Sri Sivani College of Engineering*, Srikakaulam,Andhrapradesh,INDIA

3) Dr. M. Surya Kalavathi, Born on 8th July 1966, Obtained her B.Tech degree from S.V. U. in 1988 and M.Tech from S.V.U. in the year 1992.Obtained her doctoral degree from JNTU, Hyderabad and Post Doctoral from CMU, USA. She is presently working as Professor (EEE) in JNTUH College of Engineering, Kukatpally, Hyderabad. Published 16 Research Papers and presently guiding many Ph.D. Scholars. She has specialized in Power Systems, High Voltage Engineering and Control Systems. Her research interests include Simulation studies on Transients of different power system equipment. She has 18 years of experience. She has invited for various lectures.

4) Bhumanapally.Ravindhranh Reddy, Born on 3rd September, 1969. Got his B.Tech in Electrical & Electronics Engineering from the J.N.T.U. College of Engg., Anantapur in the year 1991. Completed his M.Tech in Energy Systems in IPGSR of J.N.T.University Hyderabad in the year 1997.Obtained his doctoral degree from JNTU, INDIA

ISSN (e): 2250 – 3005 || *Vol, 05* || *Issue,02* || *February – 2015* ||
International Journal of Computational Engineering Research (IJCER)

Effect of mainstream air velocity on velocity profile over a rough flat surface

Arunima Singh[1], A. Kumar[2], M. Mallick[3]
[1] *(Department of Civil Engineering, National Institute of Technology, Rourkela)*
[2] *(Department of Civil Engineering, National Institute of Technology, Rourkela)*
[3] *(Department of Civil Engineering, National Institute of Technology, Rourkela)*

ABSTRACT

In turbulent flow, the boundary layer is defined as the thin region on the surface of a body in which viscous effects are important. The boundary layer allows the fluid to stick at the surface and thus having the velocity of the surface and to increase towards the mainstream. Roughness is a component of surface texture. It is quantified by the vertical deviations of a real surface from its ideal form. To study the variations of velocity profiles at boundary layer and their influences especially in turbulence zone, the approaches were done.

KEYWORDS: *Boundary layer, Velocity profile, Turbulence, wind tunnel, laminar zone, turbulent zone, boundary layer parameters, surface roughness.*

I. INTRODUCTION

We experience wind turbulence in everyday life. It affects all the structures and objects within the atmospheric boundary. Turbulence is the chaotic and seemingly random motion of fluid parcels. Turbulence has mechanical and convective origins. Shear forces cause mechanical turbulence while buoyant instabilities (due to the intermingling of fluid parcels with different densities) cause convective turbulence. Atmospheric turbulence differs from turbulence generated in a laboratory or in pipe flow. In the atmosphere, convective turbulence coexists with mechanical turbulence. Roughness is a component of surface texture. It is quantified by the vertical deviations of a real surface from its ideal form. Each of the roughness parameters is calculated using a formula for describing the surface. Although these parameters are generally considered to be "well known" a standard reference describing each in detail is Surfaces and their Measurement. Roughness is often closely related to the friction and wear properties of a surface. In turbulent flow, the boundary layer is defined as the thin region above the surface of a body in which viscous effects are important. The boundary layer allows the fluid to stick at the surface and thus having the velocity of the surface and to increase towards the mainstream.

The study, by K. V. S. Namboodiri, Dileep Puthillam Krishnan et.al (2014), discussed the features of wind turbulence, and surface roughness parameter over the coastal boundary layer of the Peninsular Indian Station, Thumba Equatorial Rocket Launching Station. James Cardillo & Yi Chen, Guillermo Araya (2013) had shown that the dynamic multi-scale approach can be successfully extended to simulations which incorporate surface roughness. They observed that inner peak values of Reynolds stresses increase when considering outer units.

The research of G.R. Spedding, A. Hedenstro¨m, L. C. Johansson (2009) showed that DPIV can measure the background turbulence, and therefore its instantaneous structure. The measurements also reveal certain challenges in investigating the aerodynamic performance of small-scale flying devices. A variety of atmospheric boundary layer parameters are examined as a function of wind direction in both urban and suburban settings in Oklahoma City, Oklahoma, derived from measurements during the Joint Urban 2003 field campaign, by Cheryl Klipp (2007). Shuyang Cao, Tetsuro Tamura (2006) had done Wind tunnel experiments to study the effects of surface roughness on the turbulent boundary layer flow over a two-dimensional steep hill, accompanied by a relatively steady and large separation, sometimes called a separation bubble. Carolyn D. Aubertine, John K. Eaton, Simon Song (2004) studied the effects of wall roughness were examined experimentally for two different rough-wall cases involving flow over a ramp with separation and reattachment. For these cases, the roughness Reynolds number was matched at two different momentum thicknesses Reynolds numbers. Both flow conditions were fully rough. R. A. Antonia, P-A. Krogstad (2000) explained the classical treatment of rough wall turbulent boundary layers consists in determining the effect, the roughness has on the mean velocity profile.

This effect is usually described in terms of the roughness function DU+. The general implication is that different roughness geometries with the same DU+ will have similar turbulence characteristics, at least at a sufficient distance from the roughness elements. The study by Stefan Emeis (1990) had shown the Pressure drag of obstacles in the atmospheric boundary layer is computed with a mesoscale numerical model of the troposphere. Different parts of the drag can be separated from the numerical results: total pressure drag is determined from the surface pressure distribution, hydrostatic drag from the temperature distribution in the atmosphere, and form drag as a residual. The paper of J. Blom, L. Wartena (1969) described the development of a turbulent boundary layer in a neutral atmosphere downwind of an abrupt change of surface roughness. Both a single change and two subsequent changes are treated.

II. EXPERIMENTALSET-UP

The set-up mainly consists of a wind tunnel which is a large tube with air moving inside. The wind tunnels are used to study the aerodynamic behaviour of an object. Researchers use wind tunnels to learn more about any air moving or wind influenced objects. The wind tunnel used in this project is a low speed wind tunnel in the Hydraulic Machines Laboratory located at National Institute of Technology, Rourkela, Odisha. The wind tunnel is able to produce a wind velocity of up to 45 m/s. The specifications of wind tunnel are tabulated below:

Table 1. Wind tunnel specifications

Components	Length (m)	Inlet (m)	Outlet (m)
Effuser	1.3	2.1×2.1	2.1×2.1
Test section	8	0.6×0.6	0.6×0.6
Diffuser	5	0.6	1.3

The experimental variables include three constant free stream velocities of 12, 12.5 and13.5m/son flat plates of 40 grade roughness. Emery papers of 40 grade to produce a roughness projection of 375μm was used in the experiment. All the experiments were carried out at room temperature (250 to 270C). A total of 17 numbers of sections at the intervals of 5 cm were taken along the centre-line of the flat plate. At a particular section, velocity measurement along vertical height at an interval of 2 mm and up to a height of maximum velocity were recorded in the turbulentregion.The same procedure was repeated for varying sections and varying incoming main stream velocities. The observation data were used for plotting of graphs and further studies. Some of the principal equipments used to carry out the experiment are Rough flat Plates of 40 grade, Digital Veloci Manometer, Telescopic pitot-tube, Special trolley arrangement and Tachometer.

III. RESULTS ANDDISCUSSION

From the experimental data, the graphs of velocity profiles are plotted first. That is obtained by plotting graph of Velocity (v) vs height (y) at different sections for every constant free stream velocities.
Then graphs for velocity vs height at different freestream velocities (V) for each particular turbulent section were shown. At last but not the least, the graphs of velocity (v) vs boundary layer thickness (δ) for different free stream velocities were developed.

3.1VelocityProfiles : Here we observed the regularity and variations in the patterns for increasing velocities with the rise in vertical height at different sections in the zone of turbulence.

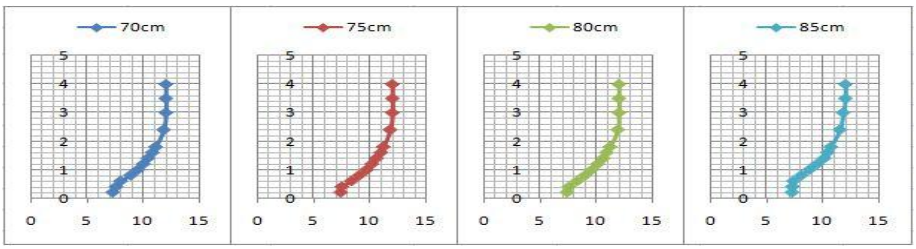

Figure 1.Velocity profiles at various sections for V_1

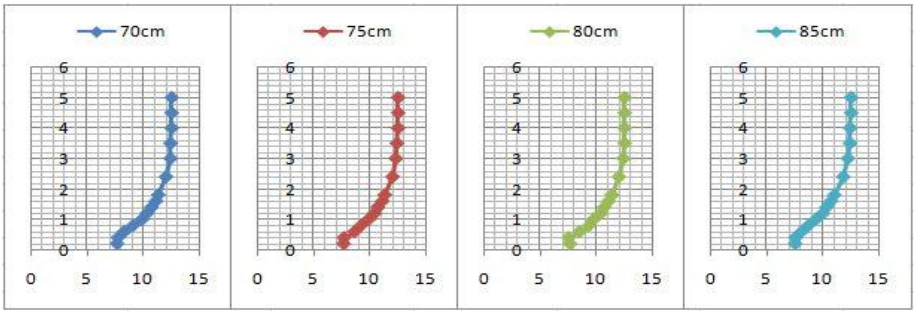

Figure 2.Velocity profiles at various sections for V_2

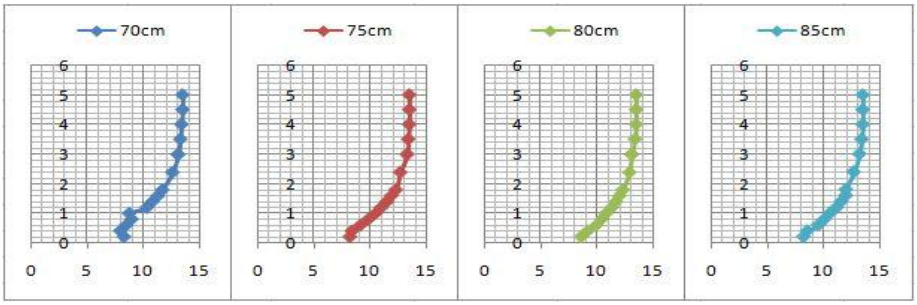

Figure 3.Velocity profiles at various sections for V_3

3.2Velocity Variations at Each Section for Different Main Stream Velocities

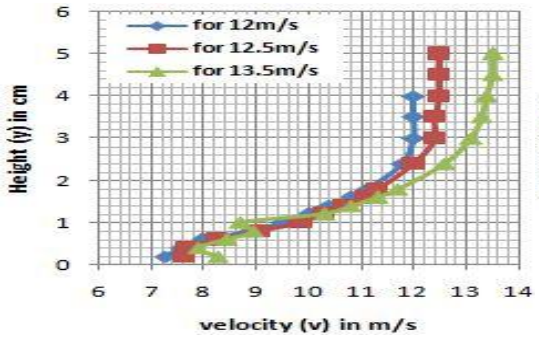

Figure 4.Velocity varriations at 70cmsection for different free streamvelocities.

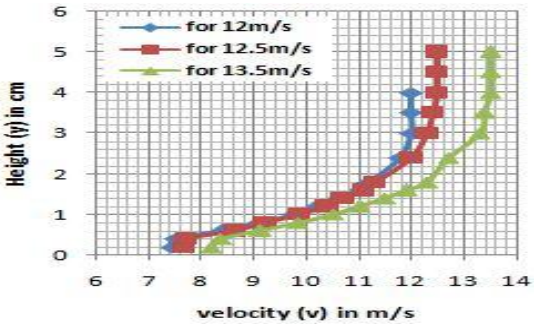

Figure 5.Velocity varriations at 75cmsection for different free streamvelocities.

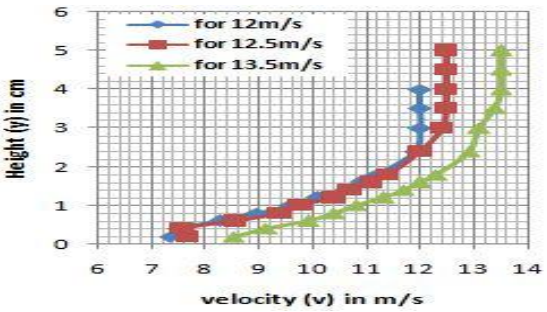

Figure 6.Velocity varriations at 80cmsection for different free streamvelocities.

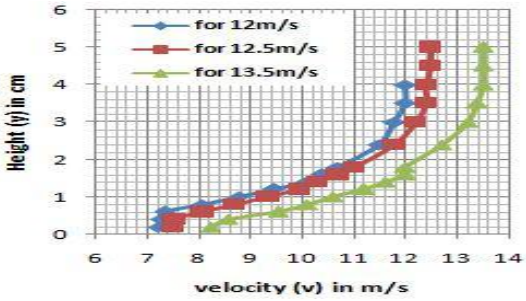

Figure 7.Velocity varriations at 85cmsection for different free streamvelocities.

3.3Plot of Boundary Layer Thicknesses at Different Sections for All the Free Stream Velocities & Vice-Versa

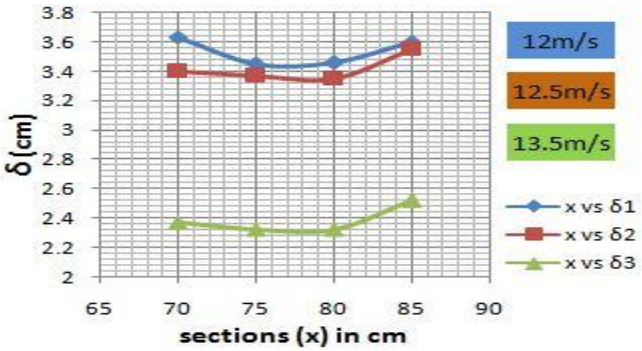

Figure 8.Plot of boundary layer thicknesses at turbulent sections for different free stream velocities.

IV. CONCLUSION

From the analysis of the experimental data and plots, it has been concluded that at a particular location, the velocity is significantly influenced by the incoming free stream velocity. It has been obtained that velocity at a given location above the surface increases with increase in mainstream velocity. Again, it has been found that for a given mainstream velocity, boundary layer thickness increases as the distance from the leading edge increases. Also, it is has been concluded that at a particular section, the boundary layer thickness decreases with increase in mainstream velocity.

REFERENCES

[1]. K. V. S. Namboodiri, Dileep Puthillam Krishnan, et al. (2014) "Coastal Boundary Layer Characteristics of Wind, Turbulence, and Surface Roughness Parameter over the Thumba Equatorial Rocket Launching Station", Journal of Climatology.Volume 2014, Article ID 504178, 21 pages.

[2]. James Cardillo & Yi Chen (2013) "DNS of a turbulent boundary layer with surface roughness". Journal of Fluid Mechanics/ Volume 729 /, pp 603-637 Cambridge University Press.

[3]. Hedenström, Anders, et al. (2009) "High-speed stereo DPIV measurement of wakes of two bat species flying freely in a wind tunnel." Experiments in Fluids 46.5: 923-932.

[4]. Klipp, Cheryl (2007), "Wind direction dependence of atmospheric boundary layer turbulence parameters in the urban roughness sublayer." Journal of Applied Meteorology and Climatology 46.12: 2086-2097.

[5]. B. Massey and J. Ward-Smith,(2006) "Mechanics of Fluids", Taylor and Francis, 8th Edition.

[6]. Cao, Shuyang, and Tetsuro Tamura. (2006), "Experimental study on roughness effects on turbulent boundary layer flow over a two-dimensional steep hill." Journal of wind engineering and industrial aerodynamics 94.1 (2006): 1-19.

[7]. Aubertine, Carolyn D., John K. Eaton, et al. (2004) "Parameters controlling roughness effects in a separating boundary layer." International journal of heat and fluid flow 25.3 (2004): 444-450.

[8]. F.M. White, (2003) "Fluid Mechanics", McGraw-Hill, 5th Edition.

[9]. B.R. Munson, D.F. Young, et al. (2002), "Fundamentals of Fluid Mechanics", John Wiley, 4th Edition.

[10]. Blom, J., and L. Wartena. (1969) "The influence of changes in surface roughness on the development of the turbulent boundary layer in the lower layers of the atmosphere." Journal of the Atmospheric Sciences 26.2 (1969): 255-265.

ISSN (e): 2250 – 3005 || *Vol, 05* || *Issue,02* || *February – 2015* ||
International Journal of Computational Engineering Research (IJCER)

Effectiveness of Shear Wall-Frame Structure Subjected to Wind Loading in Multi-Storey Building

Tarun Shrivastava[1], Prof. Anubhav Rai[2], Prof. Yogesh Kumar Bajpai[3]
[1] *Student of M-Tech Structural Engineering, Gyan Ganga Institute of Technology & Sciences Jabalpur ,*
[2] *Asst. Prof. Department of Civil Engineering, Gyan Ganga Institute of Technology & Sciences Jabalpur*
[3.] *HOD, Department of Civil Engineering, Gyan Ganga Institute of Technology & Sciences Jabalpur*

ABSTRACT:
This paper represent the shear-wall frame behavior in a multi-storey building subjected to wind loading. The different cases are prepared with different configuration of shear wall. Comparative graphical representation of different models (cases) on the basis of different parameters such as lateral deformation, storey drift index, maximum bending moment and shear forces are also discussed.

KEYWORDS: *Multi-storey building, lateral load. lateral deformation, storey drift index, maximum bendina moment. maximum shear forces. wind behavior.*

I. INTRODUCTION

A multi-storey building is subjected to lateral loads due to wind loads and earthquake loading. In this paper we analyzed the eight storey multi-storey building with different configuration of shear wall subjected to wind loading. Shear wall-frame is known as the combination of shear wall and rigid frame, which tend to deflect in shear mode as well as flexural mode. We analyzed the wall-frame structure for determining the different parameters- maximum lateral deformation, storey drift index, maximum bending moment , maximum shear forces.

II. PROBLEM FORMULATION

The bare frame of 8-storey R.C.C. structure in medium soil has a ground plan of 20m x 18m the maximum height of the structure is 25.6m.

Analyze the wind load on the frame.
The size of the beam is = 300mm x 400mm
Exterior column size = 400mm x 550mm
Interior column size = 400mm x 600mm

The height of the floor is 3.2m . Assuming wind pressure 1.5KN/m^2. Assuming special moment resisting frame is used. A structure is without in-fill walls.
Analysis is done with bending axis in XX- direction.
There are 3 different models are prepared with different different position of shear wall the cases are as follows:
MODEL-1 Exterior wall-frame case
MODEL-2 Middle Interior wall-frame case
MODEL-3 Core shear wall case

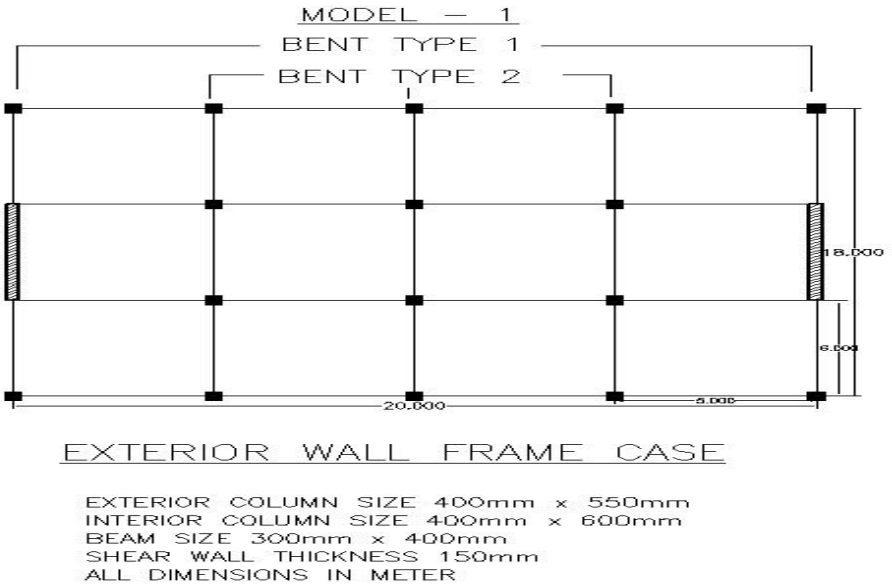

Figure -1 Exterior wall frame case

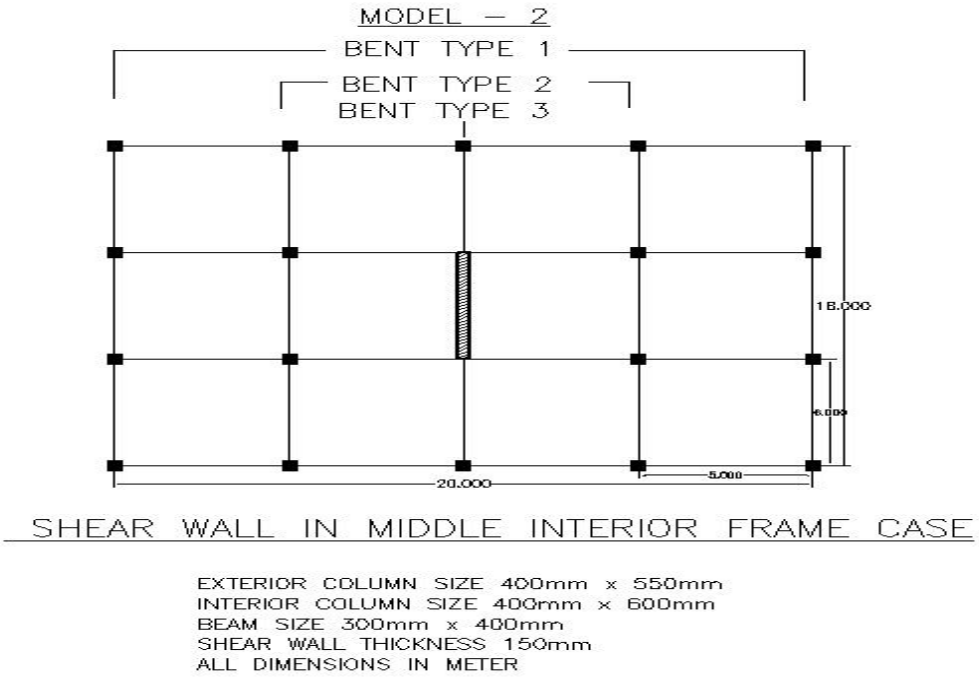

Figure-2 Shear wall in middle interior frame case

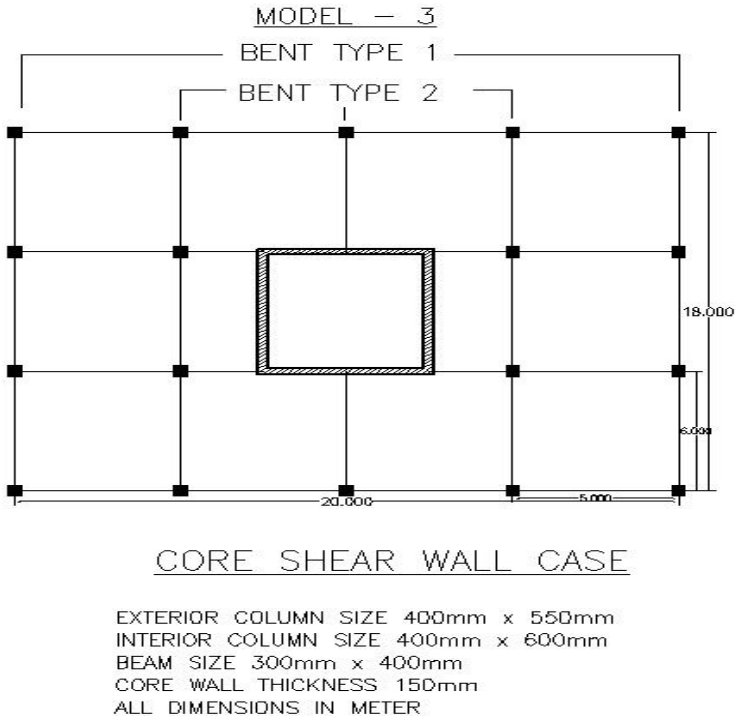

Figure 3 Core shear wall case

III. RESULT & DISCUSSIONS

(i)Method adopted for the analysis as per reference[2]. After the analysis of the problem we calculate the different values structural parameters as tabulated below:

Table 1

COMPARATIVE RESULTS OF DIFFERENT PARAMETERS OF DIFFERENT CASES WHICH IS SUBJECTED TO WIND LOADING								
S.NO.	MODEL NO.	MODEL NAME	TOTAL $(EI)_t$ in KN-m^2	TOTAL SHEAR RIGIDITIES $(GA)_t$ in KN	MAXIMUM LATERAL DEFORMATION at TOP in mm	MAXIMUM STOREY DRIFT INDEX at TOP	MAXIMUM MOMENT AT BASE in KN-m	MAXIMUM SHEAR AT BASE in KN
1	MODEL-1	EXTERIOR WALL-FRAME CASE	11,01,68,000	3,63,346.12	7.894	0.000369	5505.024	721.92
2	MODEL-2	SHEAR WALL IN ONLY MIDDLE INTERIOR FRAME CASE	5,63,19,200	3,20,200	12.011	0.000536	4915.2	652.8
3	MODEL-3	CORE SHEAR WALL CASE	38 x 10^7	21.778 x 10^4	3.687	0.000187	8060.928	706.56

(ii) Comparative graphical representation of different parameters as shown in figure-

Figure 4 Comparative representation of maximum displacement wind loading

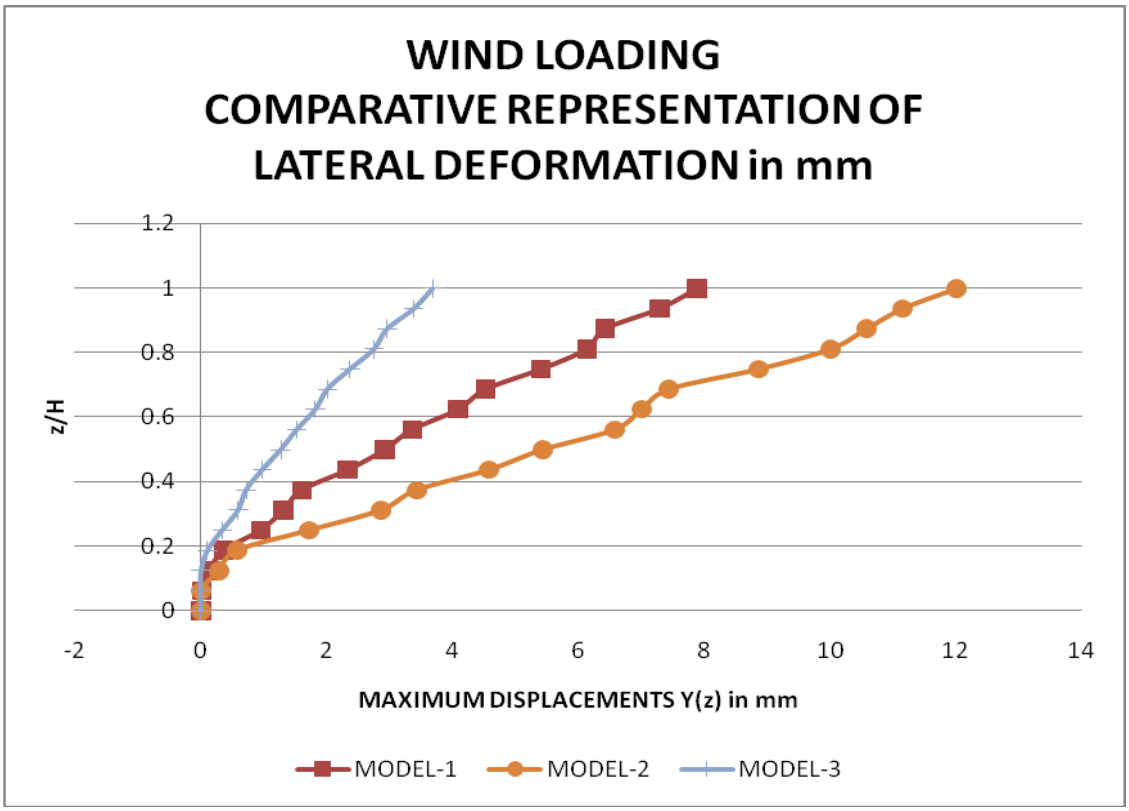

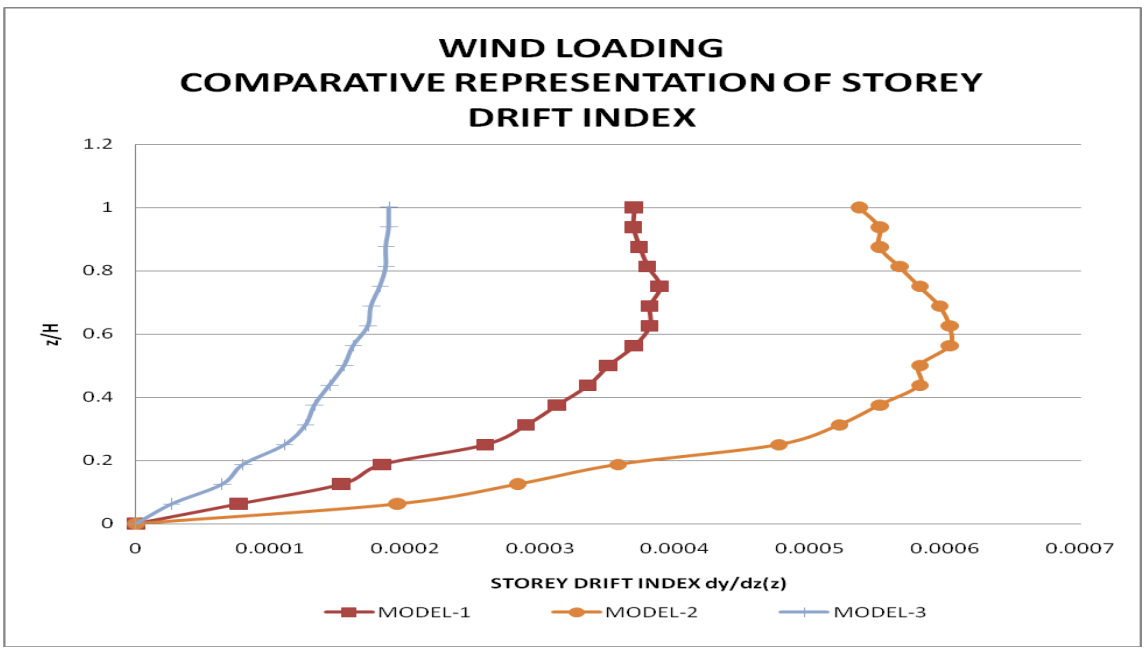

Figure-5 comparative representation of storey drift index due to wind loading
Figure-6 Comparative representation of bending moment in KN-m

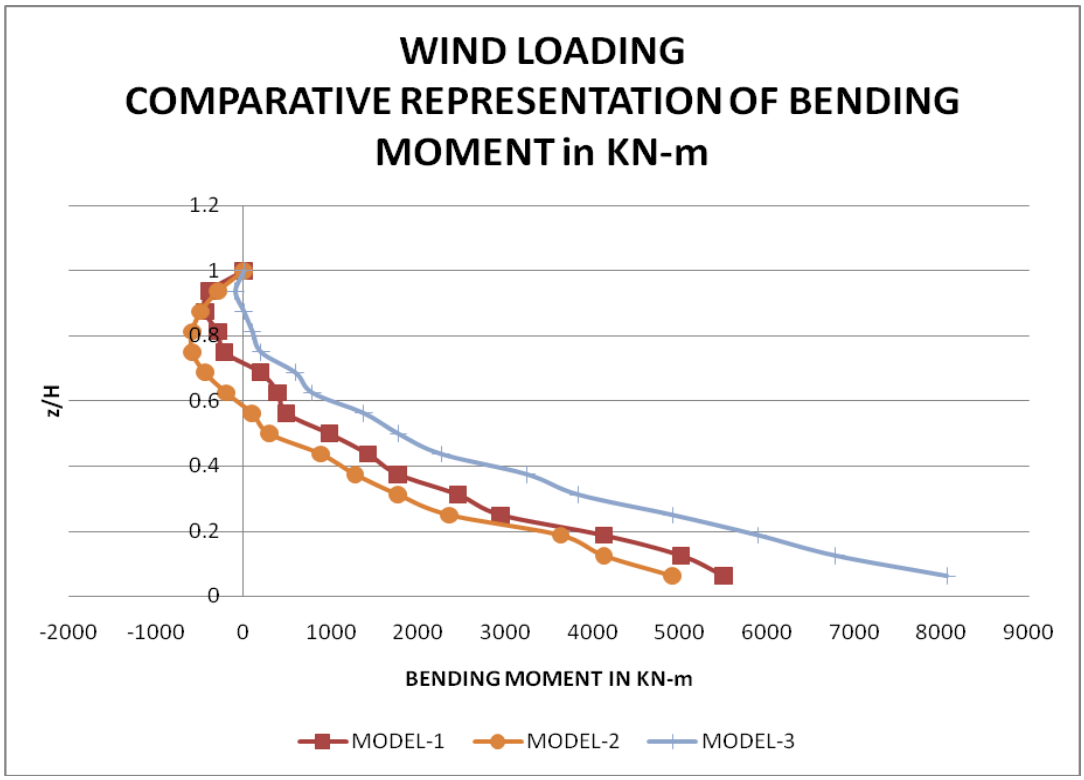

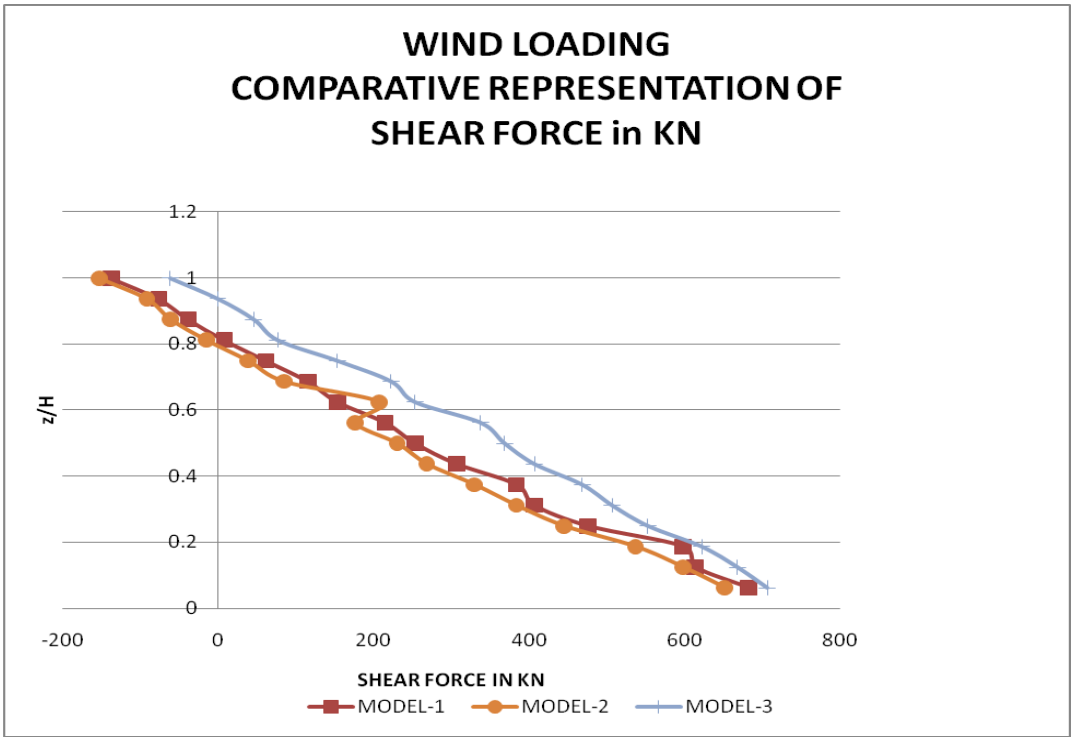

Figure-7 Comparative representation of shear forces inKN

(iii) Moment carrying capacity by shear wall and frame as shown in figure-

Figure-8 (MODEL-1) Moment carrying capacity by wall and frame in KN-m

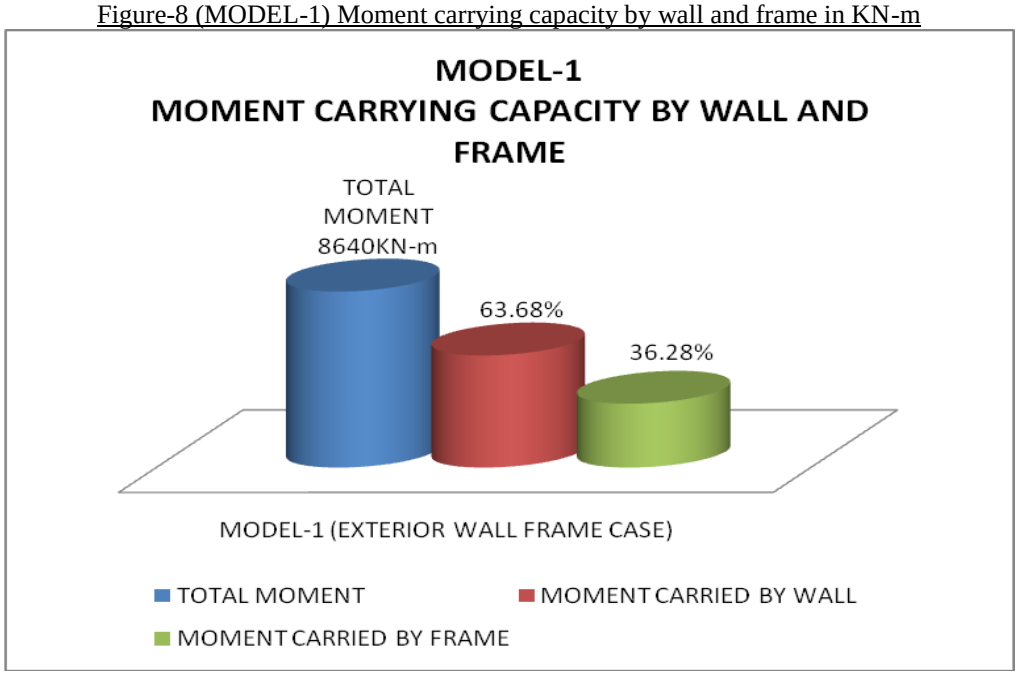

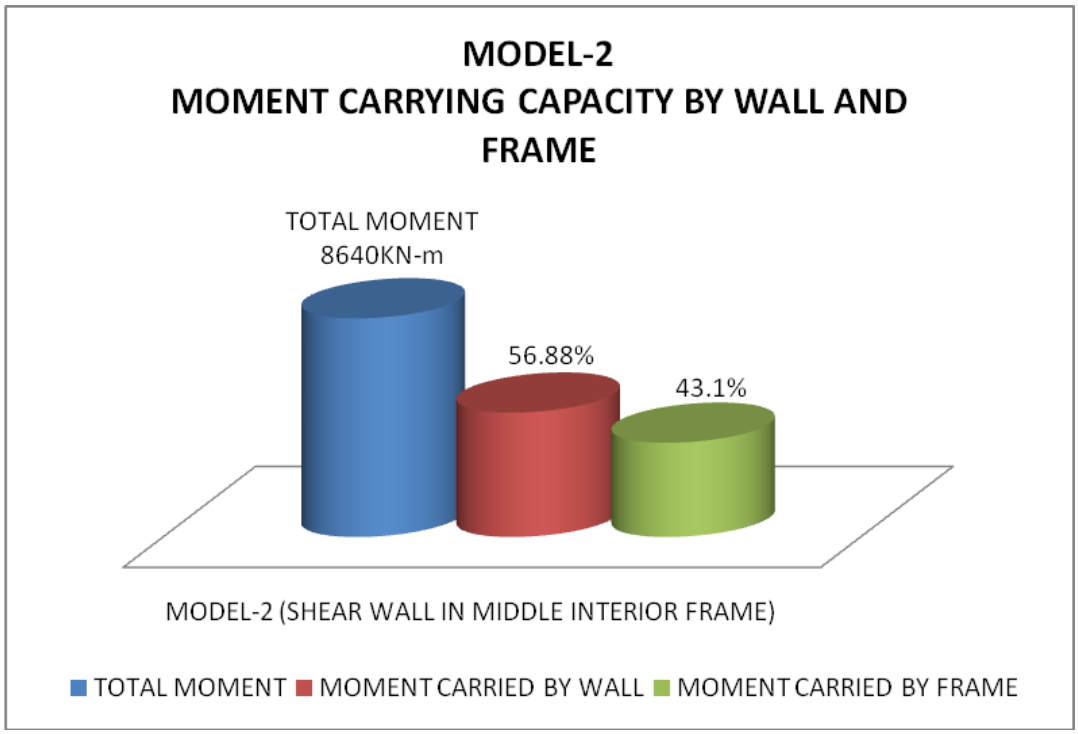

Figure-9 (MODEL-2) Moment carrying capacity by wall and frame in KN-m

Figure-10 (MODEL-3) Moment carrying capacity by wall and frame in KN-m

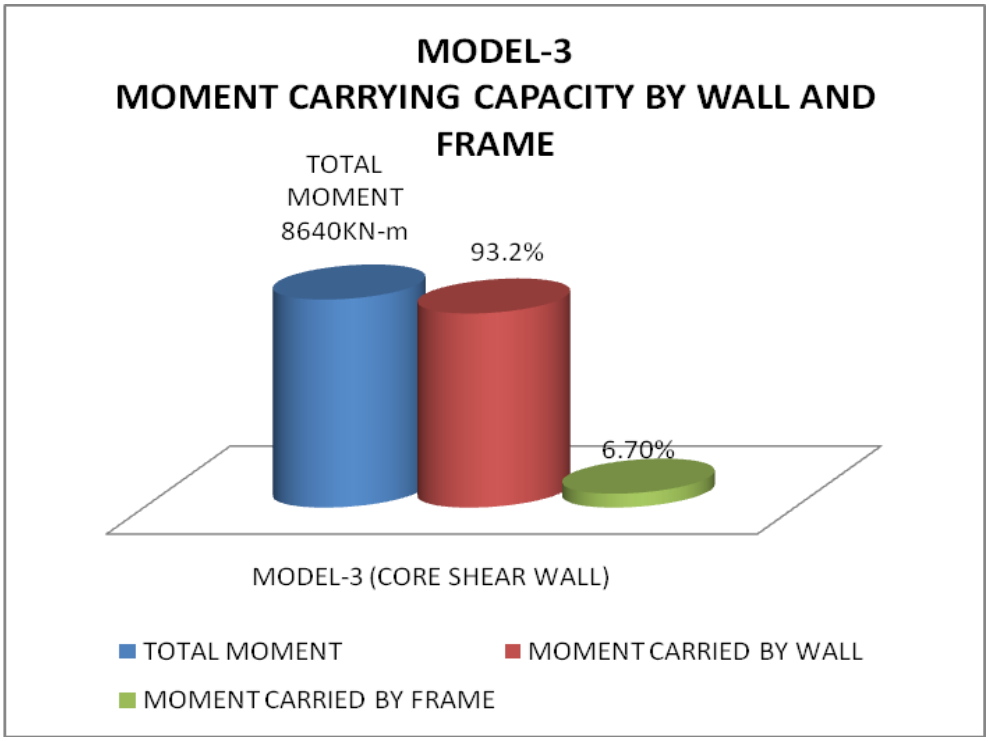

(iv) Shear force carrying capacity by Shear wall and frame as shown in figure

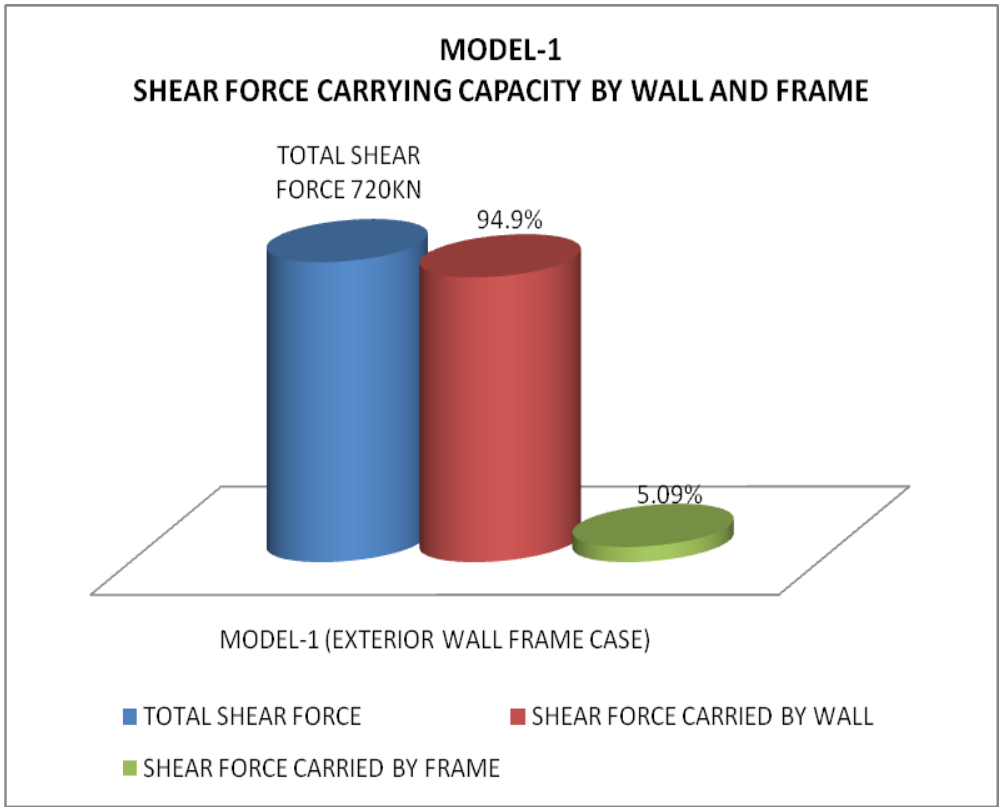

Figure-11 (MODEL-1) Shear force carrying capacity by wall and frame in KN-m

Figure-12 (MODEL-2) Shear force carrying capacity by wall and frame in KN-m

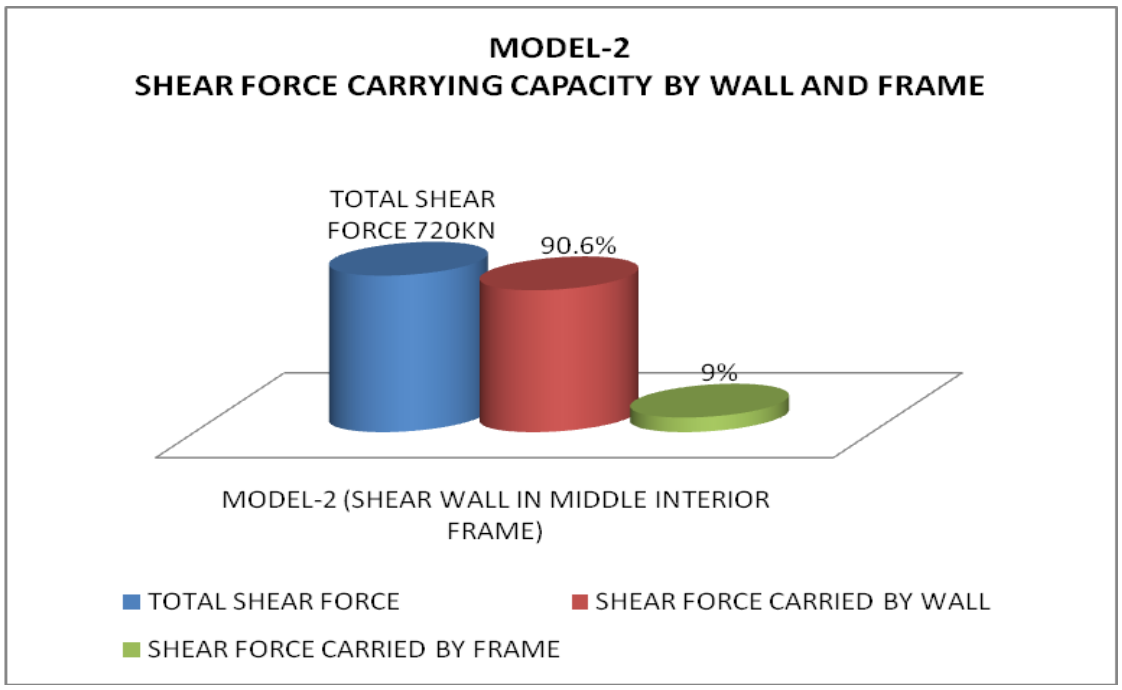

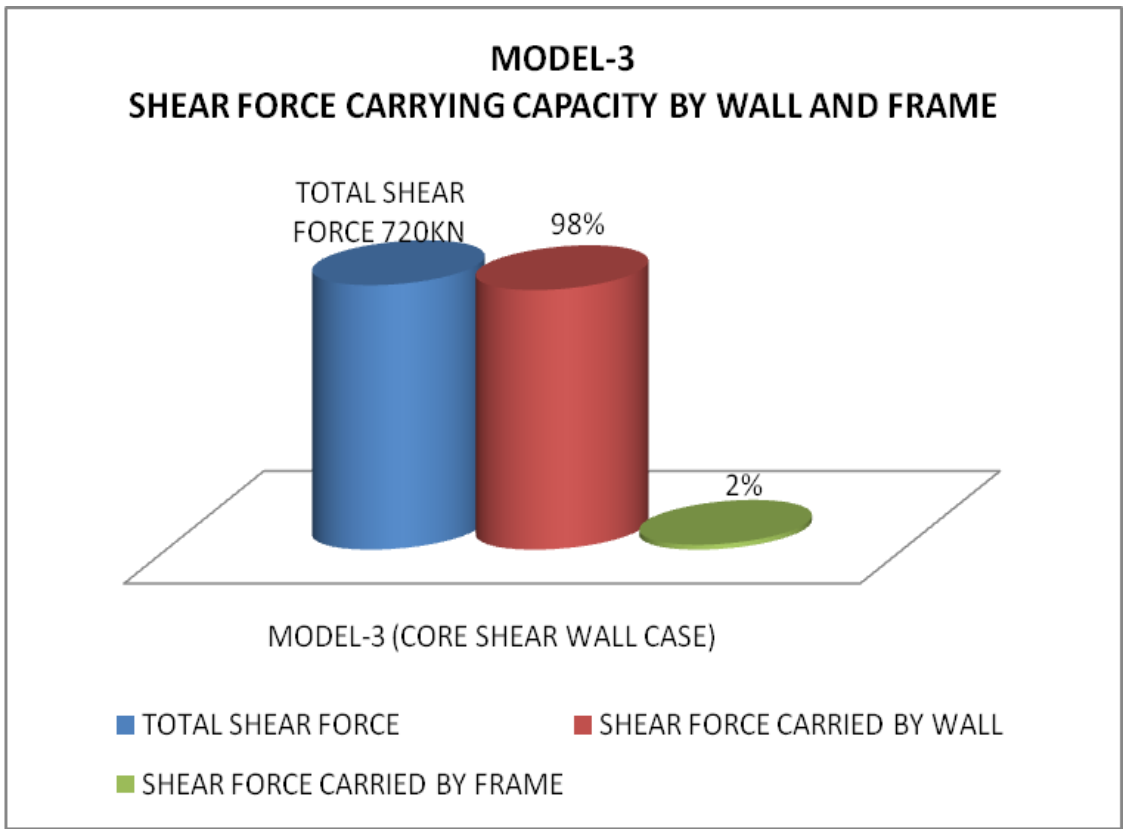

Figure-13 (MODEL-3) Shear force carrying capacity by wall and frame in KN-m

IV.CONCLUSION

1. As from result the maximum lateral deformation in MODEL-2 is 12.011mm, in MODEL-1 it is 7.894mm and in MODEL-3 it is 3.687mm. This indicated that the MODEL-3 is stiffer structure against the lateral loads.
2. The drift index is minimum in MODEL-3 the drift index is minimum (table-1) which will be more useful for taller buildings preventing the damage of internal partition and outer cladding and architectural fitting.
3. As from figure-10 (MODEL-3) the wall shares 93.2% of the total moment and the frame shares only 6.7%, while in MODEL-1 (figure-8) the wall shares 63.68% of the moment and frame takes 36.28% and in MODEL-2, 56.88% in wall and 43.1% in the frame. It is concluded that the MODEL-3 (with core wall) is providing more rigidity consequently bearing large moments and distributing a small share to frame which is relatively flexible.
4. As from figure -13 MODEL-3 the wall shares 98% of the total shear but in model-2 it is about 90.6% in MODEL-1 and is about 94.9% inspite the total base shear of the each model is roughly same.
5. It is concluded that effectiveness of the core wall is not helping too much in reducing the base shear. Effectiveness of the shear wall frame is providing more lateral stiffness; Rigidness to the structure against lateral loads minimizing the maximum lateral deformation , drift index, taking maximum share of the moment full filling it's purpose for which it is provided for.

REFERENCES

[1] Alfa Rasikan, M.G Rajendran " Wind Behavior of Building with and without Shear wall" (IJERA) Vol.3, Issue 2, March-April 2013 page480-485.

[2] Bryan Stafford Smith and Alex Coull " Tall Building Structures: Analysis and Design" 2011 Reprint Edition , Wiley India Pvt. Ltd.

[3] P.P. Chandurkar[1], Dr, P.S. Pajgade[2],"Seismic Analysis of RCC Building with and without Shear Wall" Vol.3, Issue 3 2013 page1805-1810 [1]post graduate student in structural engineering, Department of civil Engineering, Prof.[2], megha institte of technology and research bandera.

[4] Anuj Chandiwala "Earthquake Aanalysis of Building Configuration With Different Position of Shear Wall" Vol.2 Issue 12 2012 page 343-353 Adhoc Lecturer in Sarvajanic College of Engineering & Technology , Athvalines, Surat, Gujrat, India.

[5] [1],Prof. S.S. Patil, [2],Miss. S.A. Ghadge, [3],Prof. C.G. Konapure, [4], Prof. Mrs. C.A. Ghadge " Seismic Analysis of High-Rise Building by Response Spectrum Method" IJCER vol-3 Issue 3 2013 [1,3],Department of Civil Engineering, W.I.T. College of Engineering Solapur Maharashtra [2],Student, W.I.T. College of Engineering, Solapur Maharashtra [4],Department of Civil Engineering. S.T.B. College of Engineering, Tuljapur, Maharashtra.

ISSN (e): 2250 – 3005 || Vol, 05 || Issue,02 || February – 2015 ||
International Journal of Computational Engineering Research (IJCER)

Skinput: Advance Input Technology

Shaikh Abdur Rehman Mohammed Sadique[1], Pragnesh N Shah[2]
[1]Dept of Electronics, Pillai Institute of Information Technology, Engineering, Media Studies & Research, University Of Mumbai
[2]Professor,Dept of Electronics Pillai Institute Of Information Technology, Engineering, Media Studies & Research, University Of Mumbai

ABSTRACT

In this paper we are describing about the new input sensing technology that is skinput. Skin put technology enabled device acts as an input interface. It provides a new input technique based on bio-acoustic sensing that allows the skin to be used as a finger input surface. This also allows the body to be annexed as an input surface without the need for the skin to be invasively instrumented with sensors, tracking markers, or other items.

KEYWORD: *Skin put, Bio-acoustic, Finger, Pico-Projector, Palm, Proprioception.*

I. INTRODUCTION

Skin put is a technology which uses the surface of the skin as an input device. Our skin produces natural and distinct mechanical vibrations when tapped at different places. However, skin is fundamentally different from conventional, off-body touch surfaces. As skin is stretchable, it allows for additional input modalities, such as pulling, pressing and squeezing. This increases the input space for on-skin interactions and enables more varied forms of interaction, for instance more varied gestures. This opens up a new interaction space, which is largely unexplored. We aim to contribute to the systematic understanding of skin as an input modality and of its specific capabilities. To start with, we focus on input on the upper limb (i.e. upper arm, forearm, hand and fingers), for this is the most frequently used location. Devices with significant computational power and capabilities can now be easily carried on our bodies. Appropriating the human body as an input device is appealing not only because we have roughly two square meters of external surface area, but also because much of it is easily accessible by our hands (e.g., arms, upper legs, torso). In this paper, we present our work on Skinput – a method that allows the body to be appropriated for finger input using a novel, non-invasive, wearable bio-acoustic sensor.

II. THEORATICAL REVIEW

Skin put using touch on palm or hand surface. : As computing becomes more mobile, there is an increasing need to develop more advanced input tools and methods. Screens are smaller, cameras are more ubiquitous, and touch technology is everywhere. Yet entering text, choosing graphics entities, performing drag-and-drop, and so on are still difficult. One real struggle in dealing with small screens is surface area. Current mobile-devices screens have enough clarity that you can detect tiny objects, even as presbyopia set in. Skinput combines simple bio-acoustic sensor and some sophisticated machine learning to enable people to use their finger or forearms as touch pads. It has been, found that different types of finger taps on different parts of the hand and forearm produce unique acoustic signatures as per the study conducted by Carnegie mellon university Machine learning parses the features into a unique interpretation of the different taps. Skinput gives new meaning to the term "touch typing."

Figure 1: Skinput uses bio-acoustic sensor and sophisticated machine learning to turn the human palm into a touch pad.

More than touch : Skin is fundamentally different from off body touch surfaces, opening up a new and largely unexplored interaction space. We investigate characteristics of the various skin-specific input modalities, analyze what kinds of gestures are performed on skin, and study what are preferred input locations.. As skin is stretchable, it allows for additional input modalities, such as pulling, pressing and squeezing. This increases the input space for on-skin interactions and enables more varied forms of interaction, for instance more varied gestures.

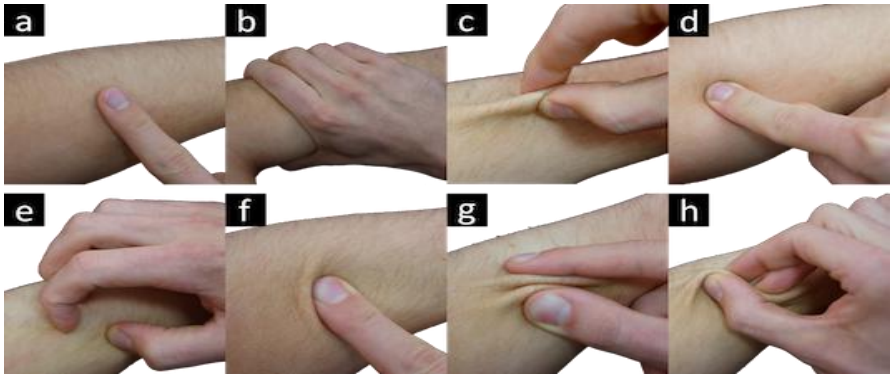

Figure 2: Input modalities: (a) touch, (b) grab, (c) pull, (d) press, (e) scratch, (f) shear, (g) squeeze and (h) twist.

The flexible nature of skin affords not only touching, but also pulling, shearing, squeezing, and twisting. Skin is capable of sensing various levels of contact force, which enables pressing. Lastly, the physiological properties of the touching finger or hand further add to the expressiveness, touch can be performed with the fingernails, resulting in scratching, or the full hand can enclose another body part resulting in grabbing. The resulting set of eight modalities as shown in Figure 2. It was derived from established modalities of conventional touch interfaces and from results of studies on the biomechanics of skin. These modalities are ranging from on-surface interaction to intense skin deformations. More complex gestures, e.g. rubbing or shaking, can be performed by using these basic input modalities. Note that these modalities are defined from a user perspective and not from a technology-centered one.

III. PRINCIPLE

The principle on which this technology works is bio-acoustic. Whenever there is a finger taps on the skin, the impact creates acoustic signals, which can be captured by a bio-acoustic sensing device. Some amount of energy is lost to the external environment in the form of sound waves. Apart of the rest energy travels along the surface of the skin and the rest is transmitted inward till it's get reflected from the bone. Depending on the type of surface on which the disturbance is created, the amplitude of the wave varies. For example, on a soft surface (forearm) the amplitude is larger as compared to a hard surface (elbow) where the amplitude is smaller. In addition to the underneath surface, the amplitude of the wave also varies with the force of disturbance. Variations in bone density, size and the different filtering effects created by soft tissues and joints create distinct acoustic locations of signals, which are sensed, processed and classified by software. Interactive capabilities can be linked to different locations on the body. The average body surface area of an adult is 1.73 m^2, is 400 times greater than a touch-screen phone 0.004 m^2. Sailors and tattoo parlors have long seen opportunities for the body as a display. Skinput adds interactivity via a Pico-projector and vibration sensing tap an image projected on your arm, and the resulting arm vibrations control an application. [4]

IV. WORKING

Skin put uses acoustic information, to capture this information a wearable armband that is non-invasive and easily removable is employed. The Skin put sensor and the processing techniques used to segment, analyze, and classify bio-acoustic signals are studied in this section. The working is based on acoustic signals through density of tissues. Your tap on the arm translates through sensors into an instruction on a menu. The graphic display appears on your arm or hand, wherever the display is set up to be located, and from then on it's like using a cell phone. Arm is better, because the graphic display on your arm is about 200 times bigger. You can use Skinput to control devices you carry, like a dashboard setup. So in theory you can control your phone, your iPOD, etc, with one tap on your arm. It really does look impressive. [6]

Bio-Acoustics : When a finger taps the skin, several distinct forms of acoustic energy are produced. Some energy is radiated into the air as sound waves; this energy is not captured by the Skinput system. Among the acoustic energy transmitted through the arm, the most readily visible are transverse waves, created by the displacement of the skin from a finger impact as shown in Figure 4. When shot with a high-speed camera, these appear as ripples, which propagate outward from the point of contact. The amplitude of these ripples is correlated to both the tapping force and to the volume and compliance of soft tissues under the impact area. In general tapping on soft regions of the arm creates higher amplitude transverse waves than tapping on boney areas (e.g., wrist, palm, fingers), which have negligible compliance. [5] In addition to the energy that propagates on the surface of the arm, some energy is transmitted inward, toward the skeleton as shown Figure 5. These longitudinal (compressive) waves travel through the soft tissues of the arm, exciting the bone, which is much less deformable then the soft tissue but can respond to mechanical excitation by rotating and translating as a rigid body.

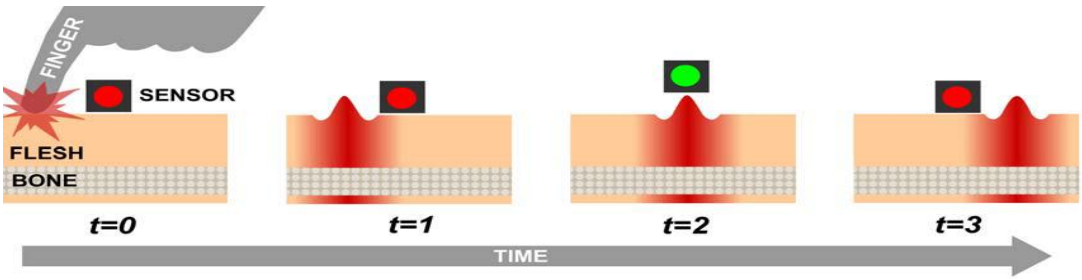

Figure 4: Transverse wave propagation: Finger impacts displace the skin, creating transverse waves (ripples). The sensor is activated as the wave passes underneath it.

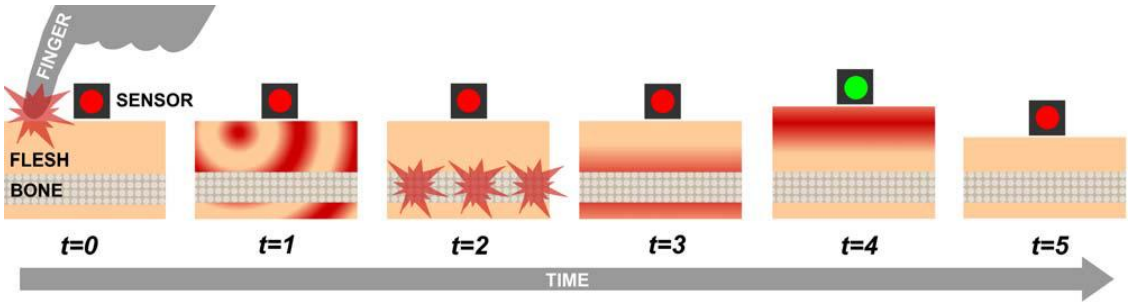

Figure 5: Longitudinal wave propagation: Finger impacts create longitudinal (compressive) waves that cause internal skeletal structures to vibrate. This, in turn, creates longitudinal waves that emanate outwards from the bone (along its entire length) toward the skin.

The two separate highlight forms of conduction transverse waves moving directly along the arm surface, and longitudinal waves moving into and out of the bone through soft tissues because these mechanisms carry energy at different frequencies and over different distances. Similarly, it is also believed that joints play an important role in making tapped locations acoustically distinct. Bones are held together by ligaments, and joints often include additional biological structures such as fluid cavities. This makes joints behave as acoustic filters. The design of a novel, wearable sensor for bio-acoustic signal acquisition as shown in following figure describes an analysis approach that enables our system to resolve the location of finger taps on the body. The robustness and limitations of the system has been assessed through user study. The broader space of bio-acoustic input been explored through prototype applications and additional experimentation

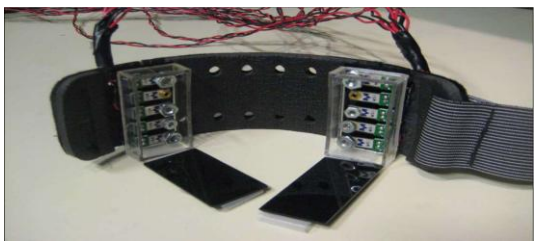

Figure 6: A wearable, bio-acoustic sensing array built into an armband. Sensing elements detect vibrations transmitted through the body. The two sensor packages shown above each contain five, specially weighted, cantilevered piezo films, responsive to a particular frequency range.

Armband : Final prototype, as shown in Figures 6 and 7, features two arrays of five sensing elements, incorporated into an armband form factor. Based on pilot data collection, we selected a different set of resonant frequencies for each sensor package as mentioned in Table 1. The upper sensor package was turned to be more sensitive to lower frequency signals, as these were more prevalent in fleshier areas. Conversely, lower sensor array was tuned to be sensitive to higher frequency signals, in order to capture signals transmitted through then denser bones. [5] In this prototype system, a Mackie Onyx 1200F audio interface was employed to digitally capture data from the ten sensors. This was connected via Fire wire to a conventional desktop computer, where a thin client written in C interfaced with the device using the Audio Stream Input/ Output (ASIO) protocol.

Figure 7. Prototype armband

.Upper array	25 Hz	27Hz	30Hz	38Hz	78Hz
Lower array	25Hz	27Hz	40Hz	44Hz	64Hz

Table 1: Resonant frequencies of elements in the two sensor packages

Each channel was sampled at 5.5 kHz, a sampling rate that would be considered too low for speech or environmental audio, but was able to represent the relevant spectrum of frequencies transmitted through the arm. This reduced sample rate makes this technique readily portable to embedded processors. For eg, the ATmega168 processor employed by the Arduino platform can sample analog readings at 77kHz with no loss of precision, and could therefore provide the full sampling power required for Skinput 55kHz total . Data was then sent from thin client over a local socket to primary application, written in Java. This program performs three key functions. First, it provided a live visualization of the data from ten sensors, which was useful in identifying acoustic features as shown in the following figure. Second, it segmented inputs from the data stream into independent instances i.e. taps. Third, it classified these input instances. The audio stream was segmented into individual taps using an absolute exponential average of all ten channels as shown in figure 8, red waveform. When an intensity threshold was exceeded as figure 8, upper blue line, the program recorded the timestamp as a potential start of a tap. If the intensity did not fall below a second, independent "closing" threshold as in figure 8, lower purple line between 100ms and 700ms after the onset crossing a duration found to be the common for finger impacts, the event was discarded. If start and end crossings were detected that satisfied these criteria, the acoustic data in that period i.e. plus a 60ms buffer on either end was considered an input event as in figure 8, vertical green regions. Although simple, this heuristic proved to be highly robust, mainly due to the extreme noise suppression provided by our sensing approach.

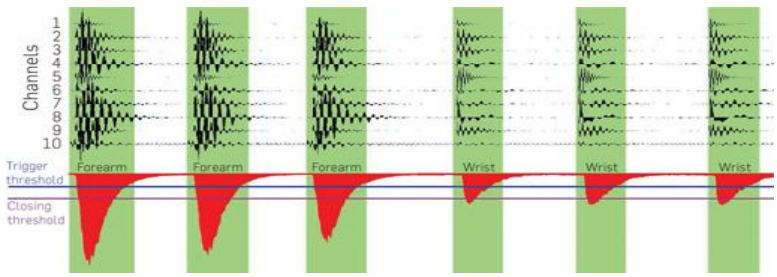

Figure 8: ten channels of acoustic data generated by three finger taps on the forearm, followed by three taps on the wrist. The exponential average of the channels is shown in red. Segmented input windows are highlighted in green. Note how different sensing elements are actuated by the two locations.

Experiments and Discussing: In this section the results and experiments conducted by Carnegie Mellon University on arm as well as the fore-arms is discussed.

Fingers (Five Locations): One set of gestures tested had participants tapping on the tips of each of their five fingers. The fingers offer interesting affordances that make them compelling to appropriate for input. Foremost, they provide clearly discrete interaction points, which are even already well-named. In addition to five finger tips, there are 14 knuckles five major, nine minor, which, taken together, could offer 19 readily identifiable input locations on the fingers alone Second, exceptional finger to finger dexterity, as demonstrated when counted by tapping on our fingers. Finally, the fingers are linearly ordered, which is potentially useful for interfaces like number entry, magnitude control (e.g., volume), and menu selection. At the same time, fingers are among the most uniform appendages on the body, with all but the thumb sharing a similar skeletal and muscular structure. This drastically reduces acoustic variation and makes differentiating among them difficult.

Whole Arm (Five Locations): Another gesture set investigated the use of five input locations on the forearm and hand: arm, wrist, palm, thumb and middle finger as shown in figure 7. These locations was selected for two main reasons First, they are distinct and named parts of the body e.g. wrist these locations in three different conditions. One condition placed the sensor above the elbow, while another placed it below. This was incorporated into the experiment to measure the accuracy loss across this significant articulation point (the elbow). Additionally, participants repeated the lower placement condition in an eyes-free context: participants were told to close their eyes and face forward, both for training and testing. This condition was included to gauge how well users could target on-body input locations in an eyes-free context (e.g., driving).

Forearm (Ten Locations): Fifth and final experimental condition used ten locations on just the forearm as in figure 6 Not only was this a very high density of input locations unlike the whole-arm condition, but it also relied on an input surface the forearm with a high degree of physical uniformity unlike, e.g., the hand.

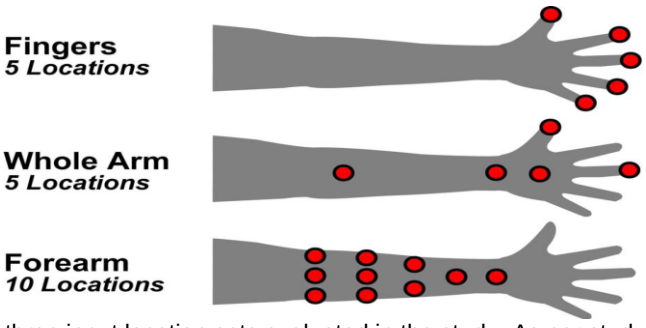

Figure 9. Figure 7: The three input location sets evaluated in the study. As per study conducted at Carnegie mellon university by Chris Harrison, Desney tan, Dan morris.

Now lets discuss the results of the above mention experiments .Five finger Despite multiple joint crossings and ~40cm of separation between the input targets and sensors, classification accuracy remained high for the five-finger condition, averaging 87.7% (SD=10.0%, chance=20%) across participants. with errors tending to be evenly distributed over the other digits. When classification was incorrect, the system believed the input to be an adjacent finger 60.5% of the time; only marginally above prior probability (40%). This suggests there are only limited acoustic continuities between the fingers. The only potential exception to this was in the case of the pinky, where the ring finger constituted 63.3% percent of the misclassifications.

Whole Arm

The below-elbow placement performed the best, posting a 95.5% (SD=5.1%, chance=20%) average accuracy. Moving the sensor above the elbow reduced accuracy to 88.3% (SD=7.8%, chance=20%), a drop of 7.2%. This is almost certainly related to the acoustic loss at the elbow joint and the additional 10cm of distance between the sensor and input targets. Figure 8 shows these results.

Forearm

Classification accuracy for the ten-location forearm condition stood at 81.5% (SD=10.5%, chance=10%), a surprisingly strong result for an input set The goal of this exercise was to explore the tradeoff between classification accuracy and number of input locations on the forearm, which represents a particularly valuable input surface for application designers.

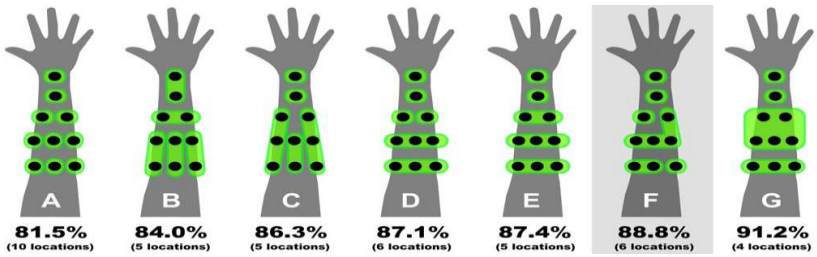

Figure 9: Higher accuracies can be achieved by collapsing the ten input locations into groups. A-E and G were created using a design-centric strategy. F was created following analysis of per-location accuracy data. As per study conducted at Carnegie mellon university by Chris Harrison, Desney tan, Dan morris.

Feasibility of the given technology : Skin put is yet in its nurturing stage but when fully developed it can be used as an input for almost any electronic device. Through skin put we can play games with just the movement of our hands. This will introduce a totally new era of gaming.. At the same time, bodies have clear physical limitations; you get tired holding your arm still. Unless the goal is to get into better shape, such mundane factors impose real constraints on what interfaces you're likely to actually adopt. Piezoelectric sensors used to measure the deformation. Today, such sensors are commonly used as guitar pick-ups. Increasingly diverse and cheap sensing technologies make this a really exciting time for inventing new interactive systems further step is to flesh out the design space of alternatives, understand their trade-offs, and build theories. This exploration will require tools (and curricula) for rapidly and flexibly creating interfaces with rich sensing and machine learning.[4]

V. CONCLUSION

In this paper, we have presented the approach to appropriating the human body as an multi input surface where multiple acoustic sensors can be togetherly interfaced sensing multiple touches and impressions. It described a novel, wearable bio-acoustic sensing array built into an armband in order to detect and localize finger taps on the forearm and hand. Results from experiments have shown that our system performs very well for a series of gestures, even when the body is in motion. Additionally, it have presented initial results demonstrating other potential uses of our approach, which we hope to further explore in future work. These include single-hand, multi-hand gestures, taps with different parts of the finger, and differentiating between materials and objects. We conclude with descriptions of several prototype applications that demonstrate the rich design space we believe Skinput enables.

REFERENCES

[1] Martin Weigel, Vikram Mehta, Jurgen steimle More Than Touch: Understanding How People Use Skin as an Input Surface for Mobile Computing CHI '14 Proceedings of the SIGCHI Conference on Human Factors in computing System Pages 179-188 ACM 2014
[2] David J. Kasik Advanced Graphics Technology May/June 2011 96
[3] Lauren Goode "The Skinny on Touch Technology"
[4] Scott Klemmer Skintroducing the Future Communication of the ACM 2011 VOL.54 NO.8
[5] Chris Harrison, Desney Tan, Dan Morris Skinput: Appropriating the Body as an Input Surface Communications of the ACM, Vol. 54 No. 8, Pages 111-118
[6] Paul Wallis How to wear a working computer display on your skin. 2010

AUTHOR INFORMATION

Shaikh
M.E
PANVEL

AbdurRehman
Electronics P.I.I.T

Prof. Pragnesh N Shah
Dept. Of Electronics P.I.I.T PANVEL

ISSN (e): 2250 – 3005 || Vol, 05 || Issue,02 || February – 2015 ||
International Journal of Computational Engineering Research (IJCER)

A Study Of Activation Parameters For Viscous Flow Process Of Tetrabutyl Ammonium Iodide In Binary Mixture Of N,N-Dimethylformamide And Ethylmethylketone At Different Temperatures.

Baljeet Singh Patial
Department of Chemistry, BTC DAV College, Banikhet (Dalhousie), Distt. Chamba, H.P.(India)

ABSTRACT:

Viscosities and densities of tetrabutylammonium iodide (Bu_4NI) in N,N-Dimethylformamide (DMF), ethylmethyl ketone (EMK) and DMF + EMK solvent mixtures containing 0, 20, 40, 60, 80 and 100 mol % of DMF at 298, 308 and 318K have been reported. The viscosity data have been analysed in terms A- and B- viscosity coefficients of the Jones Dole equation. Both A- and B coefficients have found to be positive over the entire solvent composition range at all temperatures. Partial molal volumes ($\overline{V}_2^\circ$) have also been calculated which have been used along with B- values to calculate the activation parameters for viscous flow process electrolytic solution. The activation parameters have been examined as a function of solvent composition to interpret the solution behaviour of tetraethyl ammonium bromide (Bu_4NI) in binary mixture of DMF-EMK. The behaviuor of these suggests strong ion-solvent interactions in these systems and that Bu_4NI act as structure-maker in EMK+DMF mixed solvents.

I. INTRODUCTION

Studies on the behavior of ions in mixed water + non-aqueous solvents have received a lot of attention in the recent past[1-2]. However, similar studies of electrolytes in non-aqueous solvents are scare in the literature. Precise data on electrolytes in mixed solvents find applications in many industrial processes, as they provide a wide choice of solutions with appropriate properties[3-5]. Viscosity studies of electrolytic solutions in mixed solvent system is one of the most fundamental transport properties that play a vital role in understanding the solution behavior of the electrolytes[6]. An attempt has been made to investigate the ion-solvent interactions of tetrabutyl ammonium iodide (Bu_4NI)in N,N-dimethylformamide (DMF) and ethylmethylketone (EMK) mixtures. It is found that the character of molecular interaction considerably influences the solvation of ions. Thus, DMF+EMK mixed solvents would be interesting media for the study of ion-solvent and solvent – solvent interactions of Bu_4NI. The present investigation reports the viscosity studies of tetraethyl ammonium bromides (Bu_4NI) in N, N-Dimethylformamide (DMF), ethylmethyl ketone (EMK) and DMF + EMK mixtures at 298, 308 and 318 K. Studies of viscosity of ionic solutions are of great help in characterizing the structure and properties of solutions. The viscosity B-coefficients of this salt in the given mixture are analysed in terms of ion-solvent interactions. The viscosity B-coefficients of given electrolyte at different temperature have also been used to estimate the transition parameters for viscous flow process of the electrolyte in DMF- EMK mixtures. These parameters are the true representatives of the behaviour of ions in a given solution.

II. MATERIALS AND METHODS

Tetraethyl ammonium bromide (Bu_4NI) of analytical grade, Fluka, was dried and used as described earlier[3-5]. Solvent DMF (extrapure AR grade; S D Fine Chemicals Ltd.) was purify methods reported in our previous works[3-5,7]. Viscosity measurements were carried out as described elsewhere[8-9]. Viscosity values were found to be good agreement with those reported in literature[8-9,10]. The densities of pure solvent, solvent system and various electrolytic solutions were measurement with the help of a sealable type of pycnometer (supplied by M/s. Harsh & Co., Ambala Cantt.) of 20 cm^3 capacity). The viscosities and densities of the above electrolyte in DMF, EMK and DMF+EMK solvent systems were measured at 298,308 and 318K. The overall accuracy of the viscosity and density measurements in this study was estimated to be ± 0.2% and ± 0.1% respectively.

III. RESULTS AND DISCUSSION

Densities and viscosities of tetraethyl ammonium bromides (Bu_4NI) in N, N-Dimethylformamide (DMF), ethylmethyl ketone (EMK) and DMF – EMK mixtures containing 0, 20, 40, 50, 60, 80 and 100 mol% of DMF in the concentration range (0.02-0.1) mol dm^{-3} at 298, 308 and 318 K. The viscosity data of present solutions were analysed by using the Jones-Dole equation[11]:

$$\eta/\eta_o = \eta_r = 1 + AC^{1/2} + BC \qquad \text{------(1)}$$

arranged in the form of straight line equation as:

$$\Psi = \frac{(\eta_r - 1)}{C^{1/2}} A + BC^{1/2} \qquad \text{------(2)}$$

where η and η_o respectively, are viscosities of solution and solvent, η_r is relative viscosity of solution, A is Falkenagen Coefficient[12] and is a measure of ion – ion interactions theoretically. On the other hand, B is empirical and is a function of ion-solvent interactions and C is the molar concentration.

Furthermore, the viscosity data is also examined in the light of the transition state theory of the relative viscosity of various electrolytic solutions proposed by Feaken et al[6].

According to theory, viscosity B-coefficient is given as:

$$B = \frac{\overline{V}_1^o - \overline{V}_2^o}{1000} + \frac{\overline{V}_1^o \left[\frac{\Delta G_2^* - \Delta G_1^*}{RT}\right]}{1000} \qquad \text{-------(3)}$$

where $\overline{V}_1^o$ and $\overline{V}_2^o$ are the partial molar volumes of the solvent and solute respectively, ΔG^*_1 and ΔG^*_2 are the free energy activation for viscous flow per mole of pure solvent and solute solution respectively.

The free energy activation, ΔG^*_1 for viscous flow process per mole of pure solvent system is estimated using Erying's equation[13]:

$$\Delta G^*_1 = RT \ln(\eta_o \overline{V}_1^o)/hN \qquad \text{------(4)}$$

where R, h and N are gas constant, Planck's constant respectively, $\overline{V}_1^o$ is the molar volume mass of the solvent and T is the absolute temperature.

ΔG^*_2, the free energy activation for viscous flow per mole of pure solvent is derived from equation (3) as:

$$\Delta G_2^* = \Delta G_1^* + \left(\frac{RT}{\overline{V}_1^o}\right)\left[1000B - \left(\overline{V}_1^o - \overline{V}_2^o\right)\right] \qquad \text{----- (5)}$$

The molar volume $\overline{V}_1^o$, of the pure solvent system has been determined from the relation:

$$\overline{V}_1^{\,0} = \frac{x_1 M_1 + x_2 M_2}{\rho_{mixt.}} \qquad \text{------(6)}$$

where x_i refers to the mole fraction of the solvent component i, M_i is the molar mass of the solvent mixture and $\rho_{mixt.}$ is the density of the mixture.

The values of the partial molar volume, $\overline{V}_2^{\,0}$ of solute solution are obtained by the use of least square treatment to the plots of the use of ϕ_v, apparent molar volumes of solution versus $C^{1/2}$ in accordance with Masson's emperical[14]:

$$\phi_V = \phi_V^o + S_V^* + C^{1/2} \qquad \text{--------(7)}$$

where $\phi_V^o \left(= \overline{V}_2^o\right)$ is the partial molar volume of the solution and S_V^* is the experimental slope.

The apparent molar volume, ϕ_v is calculated from the density data by using flowing expression:

$$\phi_V = 1000\frac{(\rho_o - \rho)}{C\rho_o} + \frac{M_2}{\rho_o} \qquad \text{--------(8)}$$

Where ρ_o and ρ are densities of solvent and solution, respectively; C is molar concentration of electrolyte and M_2 is its molecular weight.

The plots of ψ (= $(\eta/\eta_o - 1)/C^{1/2}$) versus $C^{1/2}$ to be linear over the whole concentration range of studied electrolytes at different solvent composition and temperatures. Jones-Dole viscosity A-and B-coefficient have obtained from these plots by the least square fitting method. Table-1 gives these values for various solvent compositions at 298, 308 and 318 K.

Table -1: Experimentally determined viscosity A ($dm^{2/3}$ $mol^{-1/2}$) and B (dm^3 mol^{-1}) -coefficients of Bu_4NI in DMF -EMK mixtures at different temperatures.

Temperatures	Mole Fraction of DMF											
	1.00		0.80		0.60		0.40		0.20		0.00	
	$Ax10^2$	B	$Ax10_2$	B	$Ax10_2$	B	$Ax10^2$	B	$Ax10^2$	B	$Ax10^2$	B
298 K	1.16	1.22	1.33	1.19	1.57	1.17	2.40	1.16	3.25	1.15	3.63	1.14
308 K	1.47	1.14	2.15	1.10	3.24	1.07	6.86	1.05	1.00	1.03	8.14	1.02
318 K	3.29	1.04	9.53	1.01	9.97	0.98	1.38	0.96	1.42	0.95	1.45	0.94

Viscosity A-coefficients in all the cases are found to be positive. Most of the studies in pure and mixed solvents have been reported positive A-coefficient[3-5,15]. Some authers[2,16] have also reported negative A-coefficients. But it has been suggested that negative A-coefficient have no physical significance[17] and may have arisen due to some systematic error in viscosity measurements. Comparing B- values reported in Table 1 for Bu_4NI in DMF and EMK with those reported in literature can check the accuracy of the present viscosity data. The B-coefficients for studied electrolyte are positive which is common feature for most of the solvents[3-5,17-18]. The positive B-coefficients value attributed to strong ion-solvent interaction in the system. The positive B-coefficients in the present work, however show only slight increase with the addition of DMF in DMF+EMK mixtures. This observation fairly consistent with the viscosity studies of Prasad et al[18] and Baljeet et al[3] in DMF+H_2O mixtures, Gill et al[19] in DMF + Ac mixtures and Baljeet et al[5] in DMF+EMK mixtures.
The present results, therefore, indicate the ideal behavior of DMF + EMK mixtures as suggested in literature[3-5,18,19].
It is clear from Table 1 that viscosity B- coefficients for the given electrolyte decrease with decrease in Temperature. This is found to be consistent with the works reported in litrature[18].
The activation parameters for viscous flow process, like ΔH^*, $T\Delta S^*$ and ΔG_2^* obtained for Bu_4NI in DMF + EMK mixtures at 298,308 and 318 K are summarized in Table 2 and Table 3.

Table-2 Free energy of activation, ΔG_1^*(kJ mol^{-1}) and apparent molar volume, $\overline{V}_1^\circ$(dm^3 mol^{-1}) for DMF, EMK and DMF+EMK mixtures at different temperatures.

X_{DMF}	Temperatures					
	298K		308K		318K	
	$\overline{V}_1^\circ$	ΔG_1^*	$\overline{V}_1^\circ$	ΔG_1^*	$\overline{V}_1^\circ$	ΔG_1^*
1.00	77.4	23.9	79.0	24.4	78.2	25.0
0.80	79.8	23.6	81.5	24.1	80.6	24.6
0.60	82.2	23.4	84.1	23.9	83.1	24.3
0.40	84.7	23.1	86.8	23.5	85.7	24.0
0.20	87.4	22.8	89.7	23.2	88.5	23.6
0.00	90.2	22.5	92.9	23.0	91.4	23.4

Table 3- Activation parameters, $\overline{V}_2^\circ$(dm^3 mol^{-1}), ΔG_2^*(k J mol^{-1}), $T\Delta S^*$(k J mol^{-1}) and ΔH^*(k J mol^{-1}) for Bu_4NI in DMF, EMK and DMF+ EMK mixtures at different temperatures.

X_{DMF}	Temperatures											
	298K				303K				308K			
	$\overline{V}_2^\circ$	ΔG_2^*	$T\Delta S^*$	ΔH^*	$\overline{V}_2^\circ$	ΔG_2^*	$T\Delta S^*$	ΔH^*	$\overline{V}_2^\circ$	ΔG_2^*	$T\Delta S^*$	ΔH^*
1.00	364.4	72.3	41.7	114.0	368.2	71.1	43.1	114.2	371.3	69.6	44.5	114.1
0.80	362.2	69.3	44.7	114.0	364.5	68.1	46.2	114.3	369.5	66.7	47.7	114.4
0.60	360.1	67.1	47.7	114.8	362.4	65.5	49.3	114.8	367.2	64.0	50.9	114.9
				1								
0.40	356.8	65.0	50.7	115.7	358.1	63.0	52.4	115.4	362.9	61.7	54.1	115.8
0.20	354.2	63.1	53.6	116.7	354.6	61.2	55.4	116.4	361.1	59.6	57.2	116.2
0.00	351.7	61.3	56.6	117.9	353.3	59.3	58.5	117.8	358.0	57.6	60.4	118.0

The present solvent system possesses ideal structure[20] as explained above. However, $\Delta G^*_2 > \Delta G^*_1$ for present electrolyte over the entire composition ranges suggest some structure making effect of this electrolyte. In fact, Feakens et al[6] have shown that $\Delta G^*_2 > \Delta G^*_1$ for electrolytes that are structure makers. This is found to be consistent not only with the fact that the B coefficients for Bu_4NI in dipolar-aprotic solvents [3-5,21,22], but also the fact that ΔG^*_2 decreases with rise in temperature. Similarly, the decrease in ΔG^*_2 with addition of DMF manifests the reduction in dipolar association of DMF[5, 23] on account of inter molecules interactions between DMF and EMK. Similar argument must hold well in respect of $T\Delta S^*$ values. The $T\Delta S^*$ values increase almost linearity with the increase in DMF concentration in DMF+EMK mixtures at 298, 308 and 318K. Moreover, the relative magnitude of positive ΔH^* and $T\Delta S^*$ for Bu_4NI in DMF+EMK mixtures suggest that the transition state is associated with bond breaking and decrease in order, however small it may be. The data further reveal that ΔH^* and $T\Delta S^*$ values for given salt decrease1 almost regularly with the addition of DMF in the mixture over the entire solvent composition range. Scrutiny of activation parameters for Bu_4NI in DMF+ EMK system further reveals that a comparable amount of structure is disrupted in the viscous flow process by Bu_4N^+ ions, as the relative magnitude of ΔH^* and $T\Delta S^*$ values for this salt is observed to be independent of solvent composition. This is found to be consistent with the experimental fact that (i) Bu_4N^+ ions, due to their larger size and small surface charge density is weakly solvated in this system and (ii) that there is no significant structural consequence of intermolecular interactions between the solvent components due to their dipolar aprotic natures. The experimental evidences as reported by Baljeet[3-4] Parker[20] and Gill[24] substantiate both these facts.

REFRENCES:

[1]. Osinska S T; Cem. Soc. Rev., 29A(1993).
[2]. Ali A & Nain A K; J Chem. Res.,(S)(1994)80.
[3]. Patial B S, IOSR-JAC, 8(2)(Feb.2015)01-04
[4]. Patial B S, IOSR-JAC, 7(Dec.2014)01-05.
[5]. Patial B S , Chauhan S, Chauhan M S & Syal V K, Ind. J. of Chem., 41A(2002)2039.
[6]. Feakens D, Freementle J & Lawrence K G, J. Chem. Soc. Faraday Trans 1,70(1974)795.
[7]. Reddick J A, Burger W B & Sankano T K,Tecknique in Chemistry Vol.II 4th edition(John Wiley, N.Y.,1986).
[8]. Syal V K, Patial B S & Chauhan S, Acoust. Lett., 23(2000)137.
[9]. Syal V K, Patial B & Chauhan S, Ind. J. Pure and Appl. Phys. 37(1999)366.
[10]. Kaminsky M, Disc. Faraday Soc. 24(1957)1716.
[11]. Jone G & Dole M, J. Am. Chem. Soc.,51(1929)2950.
[12]. Falkenhagen H & Dole M, Phys. Z.,30(1929)611; Falkenhagen H and Vernon E L, Phys. Z.33(1932)140.
[13]. Glasston S, Laider K J & Erying H, The Theory Process (Mcgraw-Hill,NewYork)(1941)477.
[14]. Masson D O; Philos. Mag. 8(1929)218.
[15]. Gill D S & Singh B, J. Chem.Soc. Faraday Trans.1,84(1988)4417.
[16]. Jauhar S P, Banait J S, Guruya P S & Narula S P, Ind. J. Chem.,19A(1980)797.
[17]. Harmed H S & Owen B B, physical chemistry of electrolyte, 3rd Edn(Reinhold, New York)1975.
[18]. Prasad M N & Agarwal M M, Ind. J. Chem. 14A(1976)322
[19]. Gill D S & Cheema J S, Z. Phys. Chem.(N.F.),134(1983)205.
[20]. Parker A J, Chem. Rev., 69(1969)1; Quart. Rev.,16(1962)163.
[21]. Syal V K, Chauhan S & Chauhan M S, Ind. J. Chem., 29A(1990)693.
[22]. Gill D S & Sharma A N; J Chem Soc Faraday Trans1;78(1982)475.
[23]. Choi Y S, Huh Y D & Bonner O D, Spectrochem. Acta Part A, 41(1985)1127.
[24]. Gill D S, Kumari N & Chauhan M S, J. Chem. Soc. Faraday Trans1,81(1985)687.

ISSN (e): 2250 – 3005 || *Vol, 05* || *Issue,02* || *February – 2015* ||
International Journal of Computational Engineering Research (IJCER)

Optimized Compressive Strength Modeling of Mixed Aggregate in Solid Sandcrete Production

P.N. Onuamah
Civil Engineering Department, Enugu State University of Science and Technology, Enugu, Nigeria.

ABSTRACT

The paper presents the report of an investigation into the model development and optimization of the compressive strength of 60/40 sand/quarry dust solid sandcrete block. Quarry dust is a massive waste in quarry sites and can be combined with sand at studied ratios. The study applies the Scheffe's optimization approach to obtain a mathematical model of the form $f(x_{i1},x_{i2},x_{i3,,}x_{i4})$*, where* x_i *are proportions of the concrete components, viz: cement, sand, quarry dust and water. Scheffe's experimental design techniques are followed to mould various solid block samples measuring 450mm x 225mm x 150mm and tested for 28 days strength. The task involved experimentation and design, applying the second order polynomial characterization process of the simplex lattice method. The model adequacy is checked using the control factors. Finally a software is prepared to handle the design computation process to take the desired property of the mix, and generate the optimal mix ratios.*

KEYWORDS*: Sandcrete, Pseudo-component, Simplex-lattice, Optimization, binary Mixtures*

I. INTRODUCTION

The construction of structures is a regular operation which heavily involves sandcrete blocks for load bearing or non-load bearing walls. The cost/stability of this material has been a major issue in the world of construction where cost is a major index. Concrete is an indispensable material of construction of civil engineering structures, and the ease or cost of its production accounts for the level of success in environmental upgrading involving the construction of new roads, buildings, dams, water structures and the renovation of such structures. To produce the sandcrete several primary components such as cement, sand, aggregates and some admixtures are to be present in varying quantities and qualities. Unfortunately, the occurrence and availability of these components vary very randomly with location and hence the attendant problems of excessive or limited quantities of the materials occurring in different areas. Where the scarcity of one component prevails exceedingly, the cost of the sandcrete production increases geometrically as such problems obviate the need to seek alternative materials for partial or full replacement of the scarce component when it is possible to do so without losing the quality of the concrete.

1.1 **Optimization Concept**

Every activity that must be successful in human endeavour requires planning. The target of planning is the maximization of the desired outcome of the venture. In order to maximize gains or outputs it is often necessary to keep inputs or investments at a minimum at the production level. The process involved in this planning activity of minimization and maximization is referred to as optimization, (Orie O.U. and Osadebe N.N., 2009). In the science of optimization, the desired property or quantity to be optimized is referred to as the objective function. The raw materials or quantities whose amount of combinations will produce this objective function are referred to as variables. The variations of these variables produce different combinations and have different outputs. Often the space of variability of the variables is not universal as some conditions limit them. These conditions are called constraints. For example, money is a factor of production and is known to be limited in supply. The constraint at any time is the amount of money available to the entrepreneur at the time of investment. Hence or otherwise, an optimization process is one that seeks for the maximum or minimum value and at the same time satisfying a number of other imposed requirements (Majid, K.I., 1974). The function is called the objective function and the specified requirements are known as the constraints of the problem.

Everybody can make concrete but not everybody can make structural concrete. Structural concrete are made with specified materials for specified strength. Concrete is heterogeneous as it comprises sub-materials. Concrete is made up of fine aggregates, coarse aggregates, cement, water, and sometimes admixtures. David and Galliford (2000), report that modern research in concrete seeks to provide greater understanding of its constituent materials and the possibilities of improving its qualities. For instance, Portland cement has been partially replaced with ground granulated blast furnace slag (GGBS), a by–product of the steel industry that has valuable cementitious properties (Ecocem Ireland Ltd, 1993).

1.2 Concrete Mix optimization

The task of concrete mix optimization implies selecting the most suitable concrete aggregates from the data base (Genadij and Juris, 1998). Several methods have been applied. Examples are by Mohan (2002), Simon (2003), Lech (1999), Czarneki (1994). Nordstrom and Munoz (1994) proposed an approach which adopts the equilibrium mineral assemblage concept of geochemical thermodynamics as a basis for establishing mix proportions. Bloom and Bentur (1995) reports that optimization of mix designs require detailed knowledge of concrete properties. Low water-cement ratios lead to increased strength but will negatively lead to an accelerated and higher shrinkage. Apart from the larger deformations, the acceleration of dehydration and strength gain will cause cracking at early ages.

1.3 **Modeling**

Modeling means setting up mathematical equation or construction of physical or other systems. Many factors of different effects occur in nature in the world simultaneously dependently or independently. When they interplay they could inter-affect one another differently at equal, direct, combined or partially combined rates, to generate varied natural constants in the form of coefficients and/or exponents. The challenging problem is to understand and asses these distinctive constants by which the interplaying factors underscore some unique natural phenomenon towards which their natures tend, in a single, double or multi phase systems. For such assessment a model could be constructed for a proper observation of response from the interaction of the factors through controlled experimentation followed by schematic design where such simplex lattice approach of the type of Henry Scheffe (1958) optimization theory could be employed. Also entirely different physical systems may correspond to the same mathematical model so that they can be solved by the same methods. This is an impressive demonstration of the unifying power of mathematics (Erwin Kreyszig, 2004).

II. LITERATURE REVIEW

In the past ardent researchers have done works in the behavior of concrete under the influence of its components. With given proportions of aggregates the compressive strength of concrete depends primarily upon age, cement content, and the cement-water ratio (Reynolds, C. and Steedman, J.C, 1981). Of all the desirable properties of hardened concrete such as the tensile, compressive, flexural, bond, shear strengths, etc., the compressive strength is the most convenient to measure and is used as the criterion for the overall quality of the hardened concrete (Majid, K.I., 1974). Every activity that must be successful in human endeavour requires planning whose target is the maximization of the desired outcome of the venture. (Orie O.U. and Osadebe N.N., 2009). Optimization process is one that seeks for the maximum or minimum value and at the same time satisfying a number of other imposed requirements (Majid, K.I., 1974). Modern research in concrete seeks to provide greater understanding of its constituent materials and possibilities of improving its qualities (David and Galliford, 2000). The task of concrete mix optimization implies selecting the most suitable concrete constituents from the data base (Genadij and Juris, 1998). Optimization of mix designs require detailed knowledge of concrete properties (Bloom and Bentur, 1995). The task of concrete mix optimization implies selecting the most suitable concrete aggregates from a data base (Genadji and Juris, 1998). Mathematical models have been used to optimize some mechanical properties of concrete made from Rice Husk Ash (RHA), - a pozolanic waste (Scheffe 1958, Obam and Osadebe's, 2007) .

The inclusion of mound soil in mortar matrix resulted in a compressive strength value of up to 40.08N/mm2, and the addition of 5% of mound soil to a concrete mix of 1:2:4:0.56 (cement: sand: coarse aggregate: water) resulted in an increase of up to 20.35% in compressive strength, (Felix et al, Alu and Sulaiman, 2000).Simplex is a structural representation (shape) of lines or planes joining assumed positions or points of the constituent materials (atoms) of a mixture, and they are equidistant from each other (Jackson N., 1983). When studying the properties of a q-component mixture, which are dependent on the component ratio only the factor space is a regular (q-1)–simplex (S. Akhnazarov and V. Kafarov , 1982). Simplex lattice designs are saturated, that is, the proportions used for each factor have m + 1 equally spaced levels from 0 to 1 (x_i = 0, 1/m, 2/m, … 1), and all possible combinations are derived from such values of the component concentrations, that is, all possible mixtures, with these proportions are used (S. Akhnazarov and V. Kafarov, 1982).

Sandcrete blocks are masonry units used in all types of masonry constructions such as interior and exterior load bearing walls, fire walls party walls, curtain walls, panel walls, partition, backings for other masonry, facing materials, fire proofing over structured steel members, piers, pilasters columns, retaining walls, chimneys, fireplaces, concrete floors, patio paving units, curbs and fences (R.C.Smith, 1973). The block is defined by ASIM as hollow block when the cavity area exceeds 25% of the gross cross-sectional area, otherwise it belongs to the solid category (R.C.Smith, 1973). Obodo (1999) stated that methods of compaction during moulding has a marked effect on the strength of sandcrete blocks. Hence, it was found that blocks from factories achieving compaction by using wooden rammers had higher strength than those compacted by mechanical vibration, except when the vibration is carried out with additional surcharge.

III. BACKGROUND THEORY

This is a theory where a polynomial expression of any degrees, is used to characterize a simplex lattice mixture components. In the theory only a single phase mixture is covered. The theory lends path to a unifying equation model capable of taking varying mix component variables to fix equal mixture properties. The optimization that follows selects the optimal ratio from the component ratios list that is automatedly generated. This theory is the adaptation to this work of formulation of response function for compressive strength of sandcrete block.

3.1 Simplex Lattice

Simplex is a structural representation (shape) of lines or planes joining assumed positions or points of the constituent materials (atoms) of a mixture (Jackson N., 1983), and they are equidistant from each other. Mathematically, a simplex lattice is a space of constituent variables of X_1, X_2, X_3,……, and X_i which obey these laws:

$$\left.\begin{array}{l} X_i < 0 \\ X \neq \text{negative} \\ 0 \leq x_i \leq 1 \\ \sum_{i=1} x_i = 1 \end{array}\right\} \quad \ldots\ldots\ldots\ldots\ldots\ldots\ldots\ldots\ldots\ldots\ldots\ldots\ldots\ldots\ldots\ldots\ldots\ldots\ldots\ldots\ldots\ldots 3.1$$

That is, a lattice is an abstract space.
To achieve the desired strength of concrete, one of the essential factors lies on the adequate proportioning of ingredients needed to make the concrete. Henry Scheffe, (1958), developed a model whereby if the compressive strength desired is specified, possible combinations of needed ingredients to achieve the compressive strength can easily be predicted by the aid of computer, and if proportions are specified the compressive strength can easily be predicted.

3.2 **Simplex Lattice Method**

In designing experiment to attack mixture problems involving component property diagrams the property studied is assumed to be a continuous function of certain arguments and with a sufficient accuracy it can be approximated with a polynomial (Akhnazarova and Kafarov, 1982, pp 242). When investigating multi-components systems the use of experimental design methodologies substantially reduces the volume of an experimental effort. Further, this obviates the need for a special representation of complex surface, as the wanted properties can be derived from equations while the possibility to graphically interpret the result is retained.

As a rule the response surfaces in multi-component systems are very intricate. To describe such surfaces adequately, high degree polynomials are required, and hence a great many experimental trials. A polynomial of degree n in q variable has C^n_{q+n} coefficients. If a mixture has a total of q components and x_1 be the proportion of the i^{th} component in the mixture such that,

$$x_i >= 0 \ (i=1,2, \ldots q), \quad . \quad . \quad . \quad . \quad . \quad . \quad . \quad . \quad (3.2)$$

then the sum of the component proportion is a whole unity i.e.

$$X_1 + x_2 + x_3 + x_4 = 1 \text{ or } \sum x_i - 1 = 0 \ \ldots . \quad .. \quad .. \quad .. \quad (3.3)$$

where i = 1, 2, …., q… Thus the factor space is a regular (q-1) dimensional simplex. In (q-1) dimensional simplex if q = 2, we have 2 points of connectivity. This gives a straight line simplex lattice. If q=3, we have a

triangular simplex lattice and for q = 4, it is a tetrahedron simplex lattice, etc. Taking a whole factor space in the design we have a (q,m) simplex lattice whose properties are defined as follows:

i. The factor space has uniformly distributed points,
ii. Simplex lattice designs are saturated (Akhnarova and Kafarov, 1982). That is, the proportions used for each factor have m + 1 equally spaced levels from 0 to 1 (x_i = 0, 1/m, 2/m, … 1), and all possible combinations are derived from such values of the component concentrations, that is, all possible mixtures, with these proportions are used.

Hence, for the quadratic lattice (q,2), approximating the response surface with the second degree polynomials (m=2), the following levels of every factor must be used 0, ½ and 1; for the fourth order (m=4) polynomials, the levels are 0, 1/4, 2/4, 3/4 and 1, etc; Scheffe, (1958), showed that the number of points in a (q,m) lattice is given by

$$C_{q+m-1} = q(q+1) \ldots (q+m-1)/m! \quad \ldots\ldots\ldots\ldots \quad .. \quad .. \quad .. \quad .. \quad (3.4)$$

3.2.1**The (4,2) Lattice Model**

The properties studied in the assumed polynomial are real-valued functions on the simplex and are termed responses. The mixture properties were described using polynomials assuming a polynomial function of degree m in the q-variable x_1, x_2 ……, x_q, subject to equation 3.1, and will be called a (q,m) polynomial having a general form:

$$\hat{Y}= b_0 + \sum_{i\le 1\le q} b_i X_i + \sum_{i\le 1<j\le q} b_{ij} X_i X_{ij} + \ldots + \sum_{i\le 1<j<k\le q} b_{ijk} + \sum b_{i1i2\ldots in} X_{i1} X_{i2} \ldots X_{in} \quad \ldots\ldots \quad .. \quad .. \quad (3.5)$$

$$\hat{Y} = b_0 + b_1X_1 + b_2X_2 + b_3X_3 + b_4X_4 + b_{12}X_1X_2 + b_{13}X_1X_3 + b_{14}X_1X_4 + b_{24}X_2X_4 + b_{23}X_2X_3 + b_{34}X_3X_4$$
$$b_{11}X^2_1 + b_{22}X^2_2 + b_{33}X^2_3 + b_{44}X^2_4 \quad \ldots \quad \ldots \quad (3.6)$$

where b is a constant coefficient.

The relationship obtainable from Eqn (3.6) is subjected to the normalization condition of Eqn. (3.3) for a sum of independent variables. For a ternary mixture, the reduced second degree polynomial can be obtained as follows:
From Eqn. (3.3)

$$X_1 + X_2 + X_3 + X_4 = 1 \quad \ldots\ldots\ldots\ldots\ldots\ldots\ldots\ldots\ldots\ldots\ldots\ldots (3.7)$$

i.e

$$b_0 X_2 + b_0X_2 + b_0 X_3 + b_0X_4 = b_0 \quad \ldots\ldots\ldots\ldots\ldots\ldots\ldots\ldots\ldots\ldots\ldots\ldots (3.8)$$

Multiplying Eqn. (3.7) by X_1, X_2, x_3, x_4, in succession gives

$$X_1^2 = X_1 - X_1X_2 - X_1X_3 - X_1X_4$$
$$X_2^2 = X_2 - X_1X_2 - X_2X_3 - X_2X_4 \quad \ldots\ldots\ldots\ldots\ldots\ldots\ldots\ldots\ldots\ldots (3.9)$$
$$X_3^2 = X_3 - X_1X_3 - X_2X_3 - X_3X_4$$
$$X_4^2 = X_4 - X_1X_4 - X_2X_4 - X_3X_4$$

Substituting Eqn. (3.8) into Eqn. (3.9), we obtain after necessary transformation that

$$\hat{Y} = (b_0 + b_1 + b_{11})X_1 + (b_0 + b_2 + b_{22})X_2 + (b_0 + b_3 + b_{33})X_3 + (b_0 + b_4 + b_{44})X_4 +$$
$$(b_{12} - b_{11} - b_{22})X_1X_2 + (b_{13} - b_{11} - b_{33})X_1X_3 + (b_{14} - b_{11} - b_{44})X_1X_4 + (b_{23} - b_{22} - b_{33})X_2X_3 + (b_{24} - b_{22} - b_{44})X_2X_4 + (b_{34} - b_{33} - b_{44})X_3X_4 \quad \ldots \ldots \ldots (3.10)$$

If we denote

$$\beta_i = b_0 + b_i + b_{ii}$$
and $$\beta_{ij} = b_{ij} - b_{ii} - b_{jj},$$

then we arrive at the reduced second degree polynomial in 6 variables:

$$\hat{Y} = \beta_1X_1 + \beta_2X_2 + \beta_3X_3 + \beta_4X_4 + \beta_{12}X_1X_2 + \beta_{13}X_1X_3 + \beta_{14}X_1X_4 + \beta_{23}X_2X_{23} + \beta_{24}X_2X_4 + \beta_{34}X_3X_4$$
$$\ldots \quad \ldots \quad (3.11)$$

Thus, the number of coefficients has reduced from 15 in Eqn 3.6 to 10 in Eqn 3.11. That is, the reduced second degree polynomial in q variables is

$$\hat{Y} = \sum \beta_i X_i + \sum \beta_{ij} X_i \quad .. \quad .. \quad .. \quad .. \quad .. \quad .. \quad (3.12)$$

3.2.2 Construction of Experimental/Design Matrix

From the coordinates of points in the simplex lattice, we can obtain the design matrix. We recall that the principal coordinates of the lattice, only a component is 1 (Table 3.1) zero.

Table 3.1 Design matrix for (4,2) Lattice

N	X_1	X_2	X_3	X_4	Y_{exp}
1	1	0	0	0	Y_1
2	0	1	0	0	Y_2
3	0	0	1	0	Y_3
4	0	0	0	1	Y_4
5	½	1/2	0	0	Y_{12}
6	½	0	1/2	0	Y_{13}
7	1//2	0	0	1/2	Y_{14}
8	0	1/2	1/2	0	Y_{23}
9	0	1/2	0	1/2	Y_{24}
10	0	0	1/2	1/2	Y_{34}

Hence if we substitute in Eqn. (3.11), the coordinates of the first point (X_1=1, X_2=0, X_3=0,and X_4=0, Fig (3.1), we get that $Y_1 = \beta_1$.

And doing so in succession for the other three points in the tetrahedron, we obtain

$$Y_2 = \beta_2,\ Y_3 = \beta_3,\ Y_4 = \beta_4 \quad . \quad . \quad . \quad . \quad . \quad . \quad . \qquad (3.13)$$

The substitution of the coordinates of the fifth point yields

$$Y_{12} = ½\ X_1 + ½X_2 + ½X_1.{}^1/_2X_2$$
$$= ½\ \beta_1 + ½\ \beta_2 + {}^1/_4\ \beta_{12}$$

But as $\beta_i = Y_i$ then

$$Y_{12} = ½\ \beta_1 - ½\ \beta_2 - {}^1/_4\ \beta_{12}$$

Thus

$$\beta_{12} = 4\ Y_{12} - 2Y_1 - 2Y_2 \quad . \quad . \quad . \quad . \quad . \qquad (3.14)$$

And similarly,

$$\beta_{13} = 4\ Y_{13} - 2Y_1 - 2Y_2$$
$$\beta_{23} = 4\ Y_{23} - 2Y_2 - 2Y_3$$

etc.

Or generalizing,

$$\beta_i = Y_i \text{ and } \beta_{ij} = 4\ Y_{ij} - 2Y_i - 2Y_j \quad . \quad . \quad . \quad . \quad . \quad . \qquad .(3.15)$$

which are the coefficients of the reduced second degree polynomial for a q-component mixture, since the four points defining the coefficients β_{ij} lie on the edge. The subscripts of the mixture property symbols indicate the relative content of each component X_i alone and the property of the mixture is denoted by Y_i.

3.2.3 Actual and Pseudo Components

The requirements of the simplex that

$$\sum_{X=1} Xi = 1$$

makes it impossible to use the normal mix ratios such as 1:3, 1:5, etc, at a given water/cement ratio. Hence a transformation of the actual components (ingredient proportions) to meet the above criterion is unavoidable. Such transformed ratios say $X_1^{(i)}$, $X_2^{(i)}$, and $X_3^{(i)}$ and $X_4^{(i)}$for the i^{th} experimental points are called pseudo components. Since X_1, X_2 and X_3 are subject to $\sum Xi = 1$, the transformation of cement:sand:quarry dust :water at say 0.30 water/cement ratio cannot easily be computed because X_1, X_2, X_3 and X_4 are in pseudo expressions $X_1^{(i)}$, $X_2^{(i)}$, $X_3^{(i)}$ and $X_4^{(i)}$.For the i^{th} experimental point, the transformation computations are to be done.

The arbitrary vertices chosen on the triangle are A_1(1:6.25:3.75:0.32), A_2(1:5.64:3.36:30) A_3(1:4.88:2.92:0.29), and A_4(1:6.26:3.74:0.37), based on experience and earlier research reports.

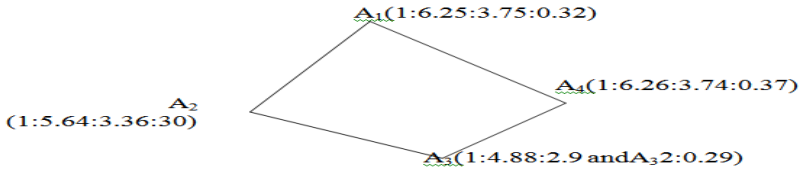

Fig 3.1 Tetrahedral Simplex

3.2.4 Transformation Matrix

If Z denotes the actual matrix of the i^{th} experimental points, observing from Table 3.2 (points 1 to 3),

$BZ = X = 1$ . . . . . .(3.16)

where B is the transformed matrix.

Therefore, $B = I.Z^{-1}$

Or $B=Z^{-1}$ . . . . . (3.17)

For instance, for the chosen ratios A_1, A_2, A_3 and A_4 (fig. 3.6),

$$Z = \begin{pmatrix} 1 & 6.25 & 3.75 & 0.32 \\ 1 & 5.64 & 3.36 & 0.30 \\ 1 & 4.88 & 2.92 & 0.29 \\ 1 & 6.26 & 3.74 & 0.37 \end{pmatrix} \quad . \quad . \quad . \quad . \quad . \quad . \quad (3.18)$$

From Eqn 3.17,

$B = Z^{-1}$

$$Z^{-1} = \begin{pmatrix} -0.55 & 1.00 & 4.09 & -3.55 \\ -17.53 & 27.14 & -12.79 & 3.18 \\ 30.52 & -44.29 & 19.68 & -5.91 \\ -10.39 & -14.29 & 6.49 & 18.18 \end{pmatrix}$$

Hence,

$B Z^{-1} = Z. Z^{-1}$

$$= \begin{pmatrix} 1 & 6.25 & 3.75 & 0.32 \\ 1 & 5.64 & 3.36 & 0.30 \\ 1 & 4.88 & 2.92 & 0.29 \\ 1 & 6.26 & 3.74 & 0.37 \end{pmatrix} \begin{matrix} -0.55 \\ -17.53 \\ 30.52 \\ -10.39 \end{matrix} \begin{pmatrix} 1.00 & 4.09 & -3.55 \\ 27.14 & -12.79 & 3.18 \\ -44.29 & 19.68 & -5.91 \\ -14.29 & 6.49 & 18.18 \end{pmatrix}$$

$$= \begin{matrix} 0 \\ 0 \\ 0 \end{matrix} \begin{pmatrix} 1 & 0 & 0 & 0 \\ 0 & 1 & 0 & 0 \\ 0 & 0 & 1 & 0 \\ 0 & 0 & 0 & 1 \end{pmatrix}$$

Thus, for actual component Z, the pseudo component X is given by

$$X \begin{pmatrix} X_1^{(i)} \\ X_2^{(i)} \\ X_3^{(i)} \\ X_4^{(i)} \end{pmatrix} = B \begin{pmatrix} -0.55 & 1.00 & 4.09 & -3.55 & Z_1^{(i)} \\ -17.53 & 27.14 & -12.79 & 3.18 & Z\ Z_2^{(i)} \\ 30.52 & -44.29 & 19.68 & -5.91 & Z_3^{(i)} \\ -10.39 & -14.29 & 6.49 & 18.18 & Z_4^{(i)} \end{pmatrix} \begin{pmatrix} \\ \\ \\ \end{pmatrix}$$

which gives the X_i(i=1,2,3,4) values in Table 3.2.

The inverse transformation from pseudo component to actual component is expressed as

$AX = Z$ . . . . . (3.19)

where A = inverse matrix

$A = Z X^{-1}$.

From Eqn 3.16, X = BZ, therefore,

$$A = Z.(BZ)^{-1}$$
$$A = Z.Z^{-1}B^{-1}$$
$$A = IB^{-1}$$
$$= B^{-1} \quad . \quad . \quad . \quad . \quad . \quad . \quad . \quad . \quad . \quad (3.20)$$

This implies that for any pseudo component X, the actual component is given by

$$\begin{pmatrix} Z_1^{(i)} \\ Z_2^{(i)} \\ Z_3^{(i)} \\ Z_4^{(i)} \end{pmatrix} = \begin{matrix} 1 \\ B\ 1 \\ 1 \\ 1 \end{matrix} \begin{pmatrix} 6.25 & 3.75 & 0.32 \\ 5.64 & 3.36 & 0.30 \\ 4.88 & 2.92 & 0.29 \\ 6.26 & 3.74 & 0.37 \end{pmatrix} \times \begin{pmatrix} X_1^{(i)} \\ X_2^{(i)} \\ X_3^{(i)} \\ X_4^{(i)} \end{pmatrix} \quad . \quad . \quad . \quad . \quad . \quad (3.21)$$

Eqn 3.21 is used to determine the actual components from points 5 to 10 , and the control values from points 11 to 13 (Table 3.2).

Table 3.2 Values for Experiment

N	X_1	X_2	X_3	X_4	RESPONSE	Z_1	Z_2	Z_3	Z_4
1	1	0	0	0	Y_1	1.00	6.25	3.75	0.32
2	0	1	0	0	Y_2	1.00	5.64	3.36	0.3
3	0	0	1	0	Y_3	1.00	4.88	2.92	0.29
4	0	0	0	1	Y_4	1.00	6.26	3.74	0.37
5	½	1/2	0	0	Y_{12}	1.00	5.945	3.555	0.31
6	½	0	1/2	0	Y_{13}	1.00	5.565	3.335	0.305
7	1/2	0	0	1/2	Y_{14}	1.00	6.255	3.745	0.345
8	0	1/2	1/2	0	Y_{23}	1.00	5.26	3.14	0.295
9	0	1/2	0	1/2	Y_{24}	1.00	5.95	3.55	0.335
10	0	0	1/2	1/2	Y_{34}	1.00	5.57	3.33	0.33
Control points									
11	0.25	0.25	0.25	0.25	Y_{1234}	1.00	5.76	3.44	0.32
12	0.5	0.25	0.25	0	Y_{1123}	1.00	5.76	3.45	0.31
13	0.25	0.5	0	0.25	Y_{1224}	1.00	5.95	3.55	0.32

3.2.5 Use of Values in Experiment

During the laboratory experiment, the actual components were used to measure out the appropriate proportions of the ingredients: cement, sand, aggregate dust and water were for casting the samples. The values obtained are presented in Tables in section 5.

3.3 Adequacy of Tests

This is carried out by testing the fit of a second degree polynomial (Akhnarova and Kafarov 1982). After the coefficients of the regression equation has been derived, the statistical analysis is considered necessary, that is, the equation should be tested for goodness of fit, and the equation and surface values bound into the confidence intervals. In experimentation following simplex-lattice designs there are no degrees of freedom to test the equation for adequacy, so, the experiments are run at additional so-called control points.

The number of control points and their coordinates are conditioned by the problem formulation and experiment nature. Besides, the control points are sought so as to improve the model in case of inadequacy. The accuracy of response prediction is dissimilar at different points of the simplex. The variance of the predicted response, S_Y^2, is obtained from the error accumulation law. To illustrate this by the second degree polynomial for a ternary mixture, the following points are assumed:

X_i can be observed without errors (Akhanarova and Kafarov, 1982).

The replication variance, S_Y^2, is similar at all design points, and

Response values are the average of n_i and n_{ij} replicate observations at appropriate points of the simplex

Then the variance $S_{\hat{Y}i}$ and $S_{\hat{Y}ij}$ will be

$$(S_{\hat{Y}}^2)_i = S_Y^2/n_i \quad . \quad . \quad . \quad . \quad . \quad . \quad . \quad . \quad (3.22)$$
$$(S_{\hat{Y}}^2)_{ij} = S_Y^2/n_{ij}. \quad . \quad . \quad . \quad . \quad . \quad . \quad . \quad . \quad (3.23)$$

In the reduced polynomial,

$$\hat{Y} = \beta_1X_1 + \beta_2X_2 + \beta_3X_3 + \beta_4X_4 + \beta_{12}X_1X_2 + \beta_{13}X_1X_3 + \beta_{14}X_1X_4 + \beta_{23}X_2X_{23} + \beta_{24}X_2X_4 + \beta_{34}X_3X_4 \quad . \quad . \quad . \quad .(3.24)$$

If we replace coefficients by their expressions in terms of responses,

$\beta_i = Y_i$ and $\beta_{ij} = 4Y_{ij} - 2Y_i - 2Y_j$

$\hat{Y} = Y_1X_1 + Y_2X_2 + Y_3X_3 + Y_4X_4 + (4Y_{12} - 2Y_1 - 2Y_2)X_1X_2 + (4Y_{13} - 2Y_1 - 2Y_3)X_1X_3 + (4Y_{14} - 2Y_1 - 2Y_4)X_1X_4 + (4Y_{23} - 2Y_2 - 2Y_3)X_2X_3 + (4Y_{24} - 2Y_2 - 2Y_4)X_2X_4 + (4Y_{34} - 2Y_3 - 2Y_4)X_3X_4$

$= Y_1(X_1 - 2X_1X_2 - 2X_1X_3 - 2X_1X_4) + Y_2(X_2 - 2X_1X_2 - 2X_2X_3 - 2X_2X_4) + Y_3(X_3 - 2X_1X_3 + 2X_2X_3 + 2X_3X_4) + Y_4(X_4 - 2X_1X_4 + 2X_2X_4 + 2X_3X_4) + 4Y_{12}X_1X_2 + 4Y_{13}X_1X_3 + 4Y_{14}X_1X_4 + 4Y_{23}X_2X_3 + 4Y_{24}X_2X_4 + 4Y_{34}X_3X_4$ . . . . . .(3.25)

Using the condition $X_1+X_2+X_3 = 1$, we transform the coefficients at Y_i

$X_1 - 2X_1X_2 - 2X_1X_3 = X_1 - 2X_1(X_2 + X_3)$

$= X_1 - 2X_1(1 - X_1) = X_1(2X_1 - 1)$ and so on. . (3.26)

Thus

$\hat{Y} = X_1(2X_1 - 1)Y_1 + X_2(2X_2 - 1)Y_2 + X_3(2X_3 - 1)Y_3 + X_4(2X_4 - 1)Y_4 + 4Y_{12}X_1X_2 + 4Y_{13}X_1X_3 + 4Y_{14}X_1X_4 + 4Y_{23}X_2X_3 + 4Y_{24}X_2X_4 + 4Y_{34}X_3X_4$ . . . . . (3.27)

Introducing the designation

$a_i = X_i(2X_1 - 1)$ and $a_{ij} = 4X_iX_j$ . . . . . (3.27a)

and using Eqns (3.22) and (3.230) give the expression for the variance $S_{\hat{Y}}^2$.

$$S_{\hat{Y}}^2 = S_Y^2 \left(\sum_{1\le i\le q} a_{ii}/n_i + \sum_{1\le i<j\le q} a_{jj}/n_{ij}\right) \quad . \quad . \quad . \quad . \quad .. \quad (3.28)$$

If the number of replicate observations at all the points of the design are equal, i.e. $n_i = n_{ij} = n$, then all the relations for $S_{\hat{Y}}^2$ will take the form

$S_{\hat{Y}}^2 = S_Y^2\xi/n$ . . . . . .(3.29)

where, for the second degree polynomial,

$$\xi = \sum_{1\le i\le q} a_i^2 + \sum_{1\le i<j\le q} a_{ij}^2 \quad . \quad . \quad (3.30)$$

As in Eqn (3.30), ξ is only dependent on the mixture composition. Given the replication Variance and the number of parallel observations n, the error for the predicted values of the response is readily calculated at any point of the composition-property diagram using an appropriate value of ξ taken from the curve.

Adequacy is tested at each control point, for which purpose the statistic is built:

$t = \Delta_Y/(S_{\hat{Y}}^2 + S_Y^2) = \Delta_Y n^{1/2}/(S_Y(1 + \xi)^{1/2}$ . . . . . .(3.31)

where $\Delta_Y = Y_{exp} - Y_{theory}$ . . . . . .(3.32)

and n = number of parallel observations at every point.

The t-statistic has the student distribution, and it is compared with the tabulated value of $t_{\alpha/L}(V)$ at a level of significance α, where L = the number of control points, and V = the number for the degrees of freedom for the replication variance.

The null hypothesis is that the equation is adequate is accepted if $t_{cal} < t_{Table}$ for all the control points.

The confidence interval for the response value is

$\hat{Y} - \Delta \le Y \le \hat{Y} + \Delta$ . . . . . (3.33)

$\Delta = t_{\alpha/L,k} S_{\hat{Y}}$ . . . . . (3.34)

where k is the number of polynomial coefficients determined.

Using Eqn (3.29) in Eqn (3.34)

$\Delta = t_{\alpha/L,k} S_Y(\xi/n)^{1/2}$ . . . . . (3.35)

IV. METHODOLOGY

4. Introduction

To be a good structural material, the material should be homogeneous and isotropic. The Portland cement, sandcrete or concrete are none of these, nevertheless they are popular construction materials (Wilby, 1963).The necessary materials required in the manufacture of the sandcrete in the study are cement, sand, aggregate dust and water.

4.1 Materials

The sand material were collected at the Iyioku River sand basin in Enugu State and conformed to BS 882and belongs to zone 2 of of the ASHTO classification.

The water for use is pure drinking water which is free from any contamination i.e. nil Chloride content, pH =6.9, and Dissolved Solids < 2000ppm. Ordinary Portland cement is the hydraulic binder used in this project and sourced from the Dangote Cement Factory, and assumed to comply with the Standard Institute of Nigeria (NIS) 1974, and kept in an air-tight bag. The aggregate dust was got from the Ishiagu quarry site and conformed to a maximum size of 2mm.

4.2 Preparation of Samples

The sourced materials for the experiment were transferred to the laboratory. The pseudo components of the mixes were designed following the background theory from where the actual variables were developed. The component materials were mixed at ambient temperature according to the specified proportions of the actual components generated in Table 3.2. In all, two solid blocks of 450mm x225 x150mm for each of ten experimental points and three control points were cast for the compressive strength test, cured for 28 days after setting and hardening.

4.3 Strength Test

After 28 day of curing, the blocks were crushed to determine the sandcrete block strength, using the compressive testing machine to the requirements of BS 1881:Part 115 of 1986.

V. RESULT AND ANALYSIS

5.1 Determination of Replication Error And Variance of Response

To raise the experimental design equation models by the lattice theory approach, two replicate experimental observations were conducted for each of the ten design points. Below is the table which contain the results of two repetitions each of the 10 design points plus three Control Points of the (4,2) simplex lattice, and show the mean and variance values per test of the observed response, using the following mean and variance equations below:

$$\ddot{Y} = \sum_{i}(Y_r)/r \quad . \quad . \quad . \quad . \quad . \quad . \quad . \quad 5.1$$

where $\hat{Y}$ is the mean of the response values and

r =1,2.

$$S_Y^2 = \sum^{n}[(Y_i - \ddot{Y}_i)^2]/(n-1) \quad . \quad . \quad . \quad . \quad . \quad . \quad 5.2$$

where n =13.

Table 5.1 Result of the Replication Variance of the Compressive Strength Response for 450mm x225 x150mm Block

Experiment No (n)	Repetition	Response f_c (N/mm$^{2)}$	Response Symbol	$\sum Y_r$	$\ddot{Y}_r$	$\sum(Y_r - \ddot{Y}_r)^2$	S_i^2
1	1A	3.03	Y_1	4.96	2.48	0.61	0.05
	1B	1.93					
2	2A	2.52	Y_2	5.41	2.71	0.07	0.01
	2B	2.89					
3	3A	2.46	Y_3	4.95	2.48	0.00	0.00
	3B	2.49					
4	4A	3.01	Y_4	5.36	2.68	0.22	0.02
	4B	2.95					
5	5A	2.91	Y_{12}	5.24	2.62	0.17	0.01
	5B	2.33					
6	6A	3.25	Y_{13}	5.71	2.86	0.31	0.03
	6B	2.46					
7	7A	3.30	Y_{14}	7.10	3.55	0.13	0.01
	7B	3.80					
8	8A	2.68	Y_{23}	4.92	2.46	0.10	0.01
	8B	2.24					
9	9A	3.63	Y_{24}	5.98	2.99	0.82	0.07

	9B	2.35					
10	10A 10B	3.14 2.78	Y_{34}	5.92	2.96	0.06	0.01
Control Points							
11	11A 11B	2.73 3.51	C_{1234}	6.24	3.12	0.30	0.03
12	12A 12B	2.59 3.88	C_{1123}	6.47	3.24	0.83	0.07
13	13A 130B	3.68 4.10	C_{1224}	7.78	3.89	0.09	0.01
						3.37	0.31

Replication Variance

$S_Y^2 = \sum S_i^2 = 0.31$

That's

Replication error $S_Y = (0.31)^{1/2} = 0.56$

5.2 Determination of Regression Equation for the Compressive Strength. From Eqns 3.15 and Table 5.1 the coefficients of the reduced second degree polynomial is determined as follows:

$B_1 = 2.48$
$\beta_2 = 2.71$
$\beta_3 = 2.48$
$\beta_4 = 2.68$
$\beta_{12} = 0.11$
$\beta_{13} = 1.51$
$\beta_{14} = 3.88$
$\beta_{23} = -0.52$
$\beta_{24} = 1.19$
$\beta_{34} = 1.53$

Thus, from Eqn (3.11),

$$\hat{Y}_c = 2.48X_1 + 2.71X_2 + 2.48X_3 + 2.68X_4 + 0.11X_1X_2 + 1.51X_1X_3 + 3.88X_1X_4 - 0.52X_2X_3 + 1.19X_2X_4 + 1.53X_3X_4 \quad . \quad . \quad . \quad . \quad . \quad . \quad . \quad (5.3)$$

Eqn 5.3 is the mathematical model of the compressive strength of hollow sandcrete block based on 28-day strength.

5.3 Test of Adequacy of the Compressive strength Model

Eqn 5.4, the equation model, will be tested for adequacy against the controlled experimental results.

We recall our statistical hypothesis as follows:

1. Null Hypothesis (H_0): There is no significant difference between the experimental values and the theoretical expected results of the compressive strength.
2. Alternative Hypothesis (H_1): There is a significant difference between the experimental values and the theoretical expected results of the compressive strength.

5.3.1 t-Test for the Compressive strength Model

If we substitute for X_i in Eqn 5.4 from Table 3.3, the theoretical predictions of the response ($\hat{Y}$) can be obtained. These values can be compared with the experimental results (Table 5.1). For the t-test (Table 5.2), a, ξ, t and Δ_y are evaluated using Eqns 3.31, 3.32, 3.35, 3.27a and 3.30 respectively.

Table 5.2 t-Test for the Test Control Points

N	CN	I	J	a_i	a_{ij}	a_i^2	a_{ij}^2	ξ	Ÿ	Ŷ	Δ_y	t
1	C_1	1	2	-0.125	0.250	0.016	0.063		3.12	3.07	0.05	0.12
		1	3	-0.125	0.250	0.016	0.063					
		1	4	-0.125	0.250	0.016	0.063					
		2	3	-0.125	0.250	0.016	0.063					
		2	4	-0.125	0.250	0.016	0.063					
		3	4	-0.125	0.250	0.016	0.063					
						0.094	0.375	0.15				
2	C_2	1	2	0.000	0.500	0.000	0.250		3.24	2.71	0.53	1.16
		1	3	0.000	0.500	0.000	0.250					
		1	4	0.000	0.000	0.000	0.000					
		2	3	0.000	0.250	0.000	0.063					
		2	4	0.000	0.000	0.000	0.000					
		3	4	0.000	0.000	0.000	0.000					
						0.000	0.563	0.32				
3	C_3	1	2	-0.125	0.500	0.016	0.250		3.89	3.05	0.84	1.84
		1	3	-0.125	0.000	0.016	0.000					
		1	4	-0.125	0.250	0.016	0.063					
		2	3	-0.125	0.000	0.016	0.000					
		2	4	-0.125	0.500	0.016	0.250					
		3	4	-0.125	0.000	0.016	0.000					
						0.094	0.563	0.33				

Significance level $\alpha = 0.05$,
i.e. $t_{\alpha/L}(V) = t_{0.05/3}(13)$, where L=number of control points.

From the Student's t-table, the tabulated value of $t_{\alpha/L}(V) = t_{0.05/3}(13)$ is found to be 2.450 which is greater than the calculated t-values in Table 5.2. Hence we can accept the Null Hypothesis.

From Eqn 3.35, with k=10 and $t_{\alpha/k,v} = t_{0.05/k}(13) = 3.01$,
Δ = 0.46 for C_{1234}, 0.67 for $C_{1124 =0.26}$, and 0.68 for C_{1224},
which satisfies the confidence interval equation of
Eqn 3.33 when viewed against most response values in Table 5.2.

5.2 Computer Program

The computer program is developed for the model. In the program any Compressive Strength can be specified as an input and the computer processes and prints out possible combinations of mixes that match the property, to the following tolerance:

Compressive Strength - 0.001 N/mm^2,

Interestingly, should there be no matching combination, the computer informs the user of this. It also checks the maximum value obtainable with the model.

5.2.1 Choosing a Combination

It can be observed that the strength of 3.55 N/sq mm yielded 4 combinations. To accept any particular proportions depends on the factors such as workability, cost and honeycombing of the resultant lateritic concrete.

VI CONCLUSION

Henry Scheffe's simplex design was applied successfully to prove that the Compressive Strength of sandcrete is a function of the proportion of the ingredients (cement, quarry dust,sand and water), but not the quantities of the materials. The maximum compressive strength obtainable with the compressive strength model is 3.55N/sq mm. See the computer run outs which show all the possible lateritic concrete mix options for the desired Compressive Strength property, and the choice of any of the mixes is the user's. One can also draw the conclusion that the maximum values achievable, within the limits of experimental errors, is quite below that obtainable using sand as aggregate. This is due to the predominantly high silt content of quarry dust. It can be observed that the task of selecting a particular mix proportion out of many options is not easy, if workability and other demands of the resulting sandcrete have to be satisfied. This is an important area for further research work. The project work is a great advancement in the search for the applicability of sandcrete in sandcrete mortar production in regions where sand is extremely scarce with the ubiquity of quarry dust.

Recommendations : From the foregoing study, the following could be recommended:

i) The model can be used for the optimization of the strength of concrete made from cement, quarry dust,sand and water.

ii) Quarry dust aggregates cannot adequately substitute sharp sand aggregates for heavy construction.

iii) More research work need to be done in order to match the computer recommended mixes with the workability of the resulting concrete.

iii) The accuracy of the model can be improved by taking higher order polynomials of the simplex.

```
'QBASIC BASIC PROGRAM THAT OPTIMIZES THE PROPORTIONS OF SANDCRETE MIXES
'USING THE SCHEFFE'S MODEL FOR CONCRETE COMPRESSIVE STRENGTH
CLS
C1$ = "(ONUAMAH.HP) RESULT OUTPUT ": C2$ = "A COMPUTER PROGRAM "
C3$ = "ON THE OPTIMIZATION OF A 4-COMPONENT SANDCRETE MIX"
PRINT C2$ + C1$ + C3$
PRINT
'VARIABLES USED ARE
'X1, X2, X3,X4, Z1, Z2, Z3,Z4, Z$,YT, YTMAX, DS

'INITIALISE I AND YTMAX
I = 0: YTMAX = 0
   FOR MX1 = 0 TO 1 STEP .01
  FOR MX2 = 0 TO 1 - MX1 STEP .01
   FOR MX3 = 0 TO 1 - MX1 - MX2 STEP .01
     MX4 = 1 - MX1 - MX2 - MX3
     YTM = 2.48 * MX1 + 2.71 * MX2 + 2.48 * MX3 + 2.68 * MX4 + .11 * MX1 * MX2 + 1.51 * MX1 *
MX3 + 3.88 * MX1 * MX4 - .52 * MX2 * MX3 + 1.19 * MX2 * MX4 + 1.53 * MX3 * MX4
     IF YTM >= YTMAX THEN YTMAX = YTM
   NEXT MX3
  NEXT MX2
 NEXT MX1
INPUT "ENTER DESIRED STRENGTH, DS = "; DS

'PRINT OUTPUT HEADING
PRINT
PRINT TAB(1); "No"; TAB(10); "X1"; TAB(18); "X2"; TAB(26); "X3"; TAB(34); "X4"; TAB(40);
"YTHEORY"; TAB(50); "Z1"; TAB(58); "Z2"; TAB(64); "Z3"; TAB(72); "Z4"
PRINT
'COMPUTE THEORETICAL STRENGTH, YT
 FOR X1 = 0 TO 1 STEP .01
  FOR X2 = 0 TO 1 - X1 STEP .01
   FOR X3 = 0 TO 1 - X1 - X2 STEP .01
    X4 = 1 - X1 - X2 - X3
    YT = 2.48 * X1 + 2.71 * X2 + 2.48 * X3 + 2.68 * X4 + .11 * X1 * X2 + 1.51 * X1 * X3 + 3.68 * X1 *
X4 - .52 * X2 * X3 + 1.19 * X2 * X4 + 1.53 * X3 * X4
     IF ABS(YT - DS) <= .001 THEN
     'PRINT MIX PROPORTION RESULTS
     Z1 = X1 + X2 + X3 + X4: Z2 = 6.25 * X1 + 5.64 * X2 + 4.88 * X3 + 6.26 * Z4: Z3 = 3.75 * X1 + 3.36
* X2 + 2.92 * X3 + 3.74 * X4: Z4 = .32 * X1 + .3 * X2 + .29 * X3 + .37 * X4
     I = I + 1
     PRINT TAB(1); I; USING "##.###"; TAB(7); X1; TAB(15); X2; TAB(23); X3; TAB(32); X4;
TAB(40); YT; TAB(48); Z1; TAB(56); Z2; TAB(62); Z3; TAB(70); Z4
     PRINT
     PRINT
     IF (X1 = 1) THEN 550
    ELSE
     IF (X1 < 1) THEN GOTO 150
    END IF
```

```
150       NEXT X3
        NEXT X2
      NEXT X1
    IF I > 0 THEN 550
    PRINT
    PRINT "SORRY, THE DESIRED STRENGTH IS OUT OF RANGE OF MODEL"
    GOTO 600

550 PRINT TAB(5); "THE MAXIMUM VALUE PREDICTABLE BY THE MODEL IS "; YTMAX; "N / Sq
mm "
600 END
```

A COMPUTER PROGRAM (ONUAMAH.HP) RESULT OUTPUT ON THE OPTIMIZATION OF A 4-COMPONE
NT SANDCRETE MIX

ENTER DESIRED STRENGTH, DS = ? 2.4511

No	X1	X2	X3	X4	YTHEORY	Z1	Z2	Z3	Z4
1	0.000	0.130	0.870	0.000	2.451	1.000	4.979	2.977	0.291
2	0.000	0.430	0.570	0.000	2.451	1.000	7.030	3.109	0.294
3	0.010	0.280	0.710	0.000	2.452	1.000	6.949	3.052	0.293
4	0.010	0.290	0.700	0.000	2.452	1.000	6.949	3.056	0.293

THE MAXIMUM VALUE PREDICTABLE BY THE MODEL IS 3.552508 N / Sq mm

Press any key to continue

A COMPUTER PROGRAM (ONUAMAH.HP) RESULT OUTPUT ON THE OPTIMIZATION OF A 4-COMPONE
NT SANDCRETE MIX

ENTER DESIRED STRENGTH, DS = ? 3.6

No	X1	X2	X3	X4	YTHEORY	Z1	Z2	Z3	Z4

SORRY, THE DESIRED STRENGTH IS OUT OF RANGE OF MODEL

Press any key to continue

REFERENCE

[1]. Akhanarova, S. and Kafarov, V., Experiment and Optimization in Chemistry and Chemical Engineering, MIR Publishers, Mosco, 1982, pp. 213 - 219 and 240 – 280.

[2]. Adepegba D, (1975), "A Compressive Study on the Normal Concrete with Concretes which contain Laterite Fines Instead of Sand". Bldg Sccp. 135-141.

[3]. Aribisale, O. A. (1990),"Input of Local Materials in Building as a Means of Reducing Cost of Building Construction", The Quantity Surveyor, pp. 4-7.

[4]. Balogun, I.A. and Adepegba, D., (1982), "Effects of Varying Sand Content in Laterized Concrete", Inst. J. Cement Campus. Light Wt. Concrete, 4235-4241).

[5]. Berkovich, I., (1983), "Block Making From Soil", African Technical Review, pp. 116-118.

[6]. Bloom, R. and Benture, A. "Free and restrained Shrinkage of Normal and High Strength Concrete", int. ACI Material Journal, Vol. 92, No. 2, pp. 211-217.

[7]. BS 817, Methods of Mix Design, 1975.

[8]. Chemleva, T., and Mikeshina, N., In Collected papers: new Ideas in Experimental Design, Edited by Nalimov, Nauka.

[9]. Dalvi, Ashok, D., Bacon, W. Gordon, Osborne, Robert, C. (March 7-10, 2004), PDAC 2004 International Convention, Trade Show & Investors Exchange.

[10]. David, J., Galliford, N., Bridge Construction at Hudersfield Canal, Concrete, Number 6, 2000.

[11]. Department of Environment, Design of Normal Concrete Mixes, Huso Ltd, 1968 ACI-Standard 181, 1986.

[12]. Ecocem Island Ltd, Ecocem GBBS Cement. "The Technically Superior and Environmentally Friendly Cement", 56 Tritoville Road Sand Dublin 4 Island, 19.

[13]. Erwin, K., Advanced Engineering Mathematics, 8th Edition, John Wiley and Sons, (Asia) Pte. Ltd, Singapore, pp. 118-121 and 240 – 262.

[14]. Felix, F.U., Al, O.C., and Sulaiman, J., "Mound Soil as a Construction Material in Civil Engineering, Vol. 12, No. 13, pp. 205-211, 2000.

[15]. Garmecki, L., Garbac, A., Piela, P., Lukowski, P., Material Optimization System: Users Guide, Warsaw University of Technology Internal Report, 1994.

[16]. Genedij, S. and Juris, B., "Concrete Design and Optimization", 2nd Int. Symposium in Civil Engineering, Budapest, 1988.

[17]. Hughes, B.P., Proceedings of the Symposium on Advances in Concrete, Concrete Society, London, 1971, pp. 315-332.

[18]. Jackson, N., Civil Engineering Materials, RDC Arter Ltd, Hong Kong, 1983.

[19]. Kateregga, J.K., (1985), "Improvement and Use of Earth Construction Products for low Cost Housing", Proceedings of a Symposium on Appropriate Building** This reference is incomplete.

[20]. Majid, K.I., Optimum Design of Structure, Butterworths and Co., Ltd, London, pp. 16, 1874.

[21]. Mohan, Muthukumar, M. and Rajendran, M., "Optimization of Mix Proportions of Mineral Aggregates Using Box Jenken Design of Experiments", Ecsevier Applied Science, Vol. 25, Issue 7, pp. 751-758, 2002.

[22]. Nzeh, R.E. and Osadebe, N.N., Osadebe Notebook in Standardization of Concrete Blocks strength through Mathematical Modeling and Precision", M. Eng. Thesis, Department of Civil Engineering, University of Nigeria, Nsukka, 2000.

[23]. Nordstrom, D.K. and Munoz, J.I., Geotechnical Thermodynamics, Blackwell Scientific Publications, Boston, 1994.

[24]. Obam, S.O. and Osadebe, N.N., "Mathematical Models for Optimization of some Mechanical properties of Concrete made from Rice Husk Ash, Ph.D Thesis, of Nigeria, Nsukka, 2007.

[25]. Obodo D.A., Optimization of Component Mix in Sandcrete Blocks Using Fine Aggregates from Different Sources, UNN, 1999.

[26]. Orie, O.U., Osadebe, N.N., "Optimization of the Compressive Strength of Five Component Concrete Mix Using Scheffe's Theory – A case of Mound Soil Concrete", Journal of the Nigerian Association of Mathematical Physics, Vol. 14, pp. 81-92, May, 2009.

[27]. Osuji, S.O.U., "Concrete Mix Design Approach Based on the Optimum Characteristics of Some Binary Mixtures", M.Eng. Thesis, University of Benin, Benin City, 1998.

[28]. Reynolds, C. and Steedman, J.C., Reinforced Concrete Designers Handbook, View point Publications, 9th Edition, 1981, Great Britain.

[29]. Schefe, H., (1958), Experiments with Mixtures, Royal Statistical Society journal. Ser B., Vol. 20, 1958. pp 344-360, Rusia.

[30]. Simon, M., (1959), "Concrete Mixture Optimization Using Statistical Models, Final Report, Federal Highway Administration, National Institutes and Technology, NISTIR 6361, 1999.

[31]. R.C.Smith, (1973), "Materials of Construction", Mc Graw-Hill Book Company, USA.

[32]. Takafumi, N., Fminori, T., Kamran, M.N. Bernardino, M.C. and Alessandro P.F., (2009), "Practical Equations for the Elatic Modulus of Concrete", ACI Structural Journal, September-October, 2009, Vol. 106, No. 5.

[33]. Tardy Yves, (1997), Petrology of Laterites and Tropical Soils. ISBN 90-5410-678-6, http://www.books.google.com/books. Retrieved April 17, 2010.

[34]. Ukamaka, N.T., (2007), "Static Analysis and Design of Laterized Concrete Cylinderical Shells for Farm Storage", Ph.D Thesis, University of Nigeria, Nsukka, 2007.

[35]. Wilby, C.B., Structural Concrete, Butterworth, London, UK, 1983.

[36]. Yamaguchi, Kosei., (2003), Iron Isotope Composition of Fe-Oxide as a measure of Water-rock Interaction: An Example from Precambrian Tropical Laterite in Botswana, 2003-2004.

ISSN (e): 2250 – 3005 || Vol, 05 || Issue,02 || February – 2015 ||
International Journal of Computational Engineering Research (IJCER)

Character recognition of Devanagari characters using Artificial Neural Network

Richa Patil[1], Varunakshi Bhojane[2]
[1](Information Technology ,PIIT/ Mumbai University, India)
[2](Information Technology PIIT / Mumbai University, India)

ABSTRACT:
In this paper we have presented a novel approach for recognizing the handwritten characters in Devanagari script .This paper describes the method and different techniques used for handwritten character recognition system for Devanagari script .In second stage we extract features of the characters into consideration like types of spine ,intersection points ,directional changes and shirolekha .we have used neural network as a classifier which takes the extracted features as input . The proposed algorithm uses the scripting properties the recognition rate achieved with this technique is 80%.

Keywords *- data collection, extracting feature, image normalization, neural network, Segmentation.*

I. INTRODUCTION

This paper analyses different challenges and approaches that are related to Devanagari handwritten character the script in this paper that is taken into consideration is Devanagari which is also script for Hindi, Marathi, Nepali and Sanskrit languages. About More than 450 people use this script.

II. DEVANAGARI SCRIPT

Since 19th century Devanagari has been commonly used scripting language.it is a standardized script .it is the most adopted writing system in the world which consist of 33 consonant and 11 vowels. The modifiers are another constituent symbols which make recognition of Devanagari script more challenging. since character recognition was based on handwritten characters there are number of factor which come into consideration like

- writing of a person
- width of the pen
- speed of writing

In case of Devanagari language the concept of uppercase and lowercase is absent ,Character in Devanagari are formed by holes,strokes and curves

2 block diagram of recognition system

The schematic block diagram of handwritten Devanagari recognition system consist of various stages is shown below.

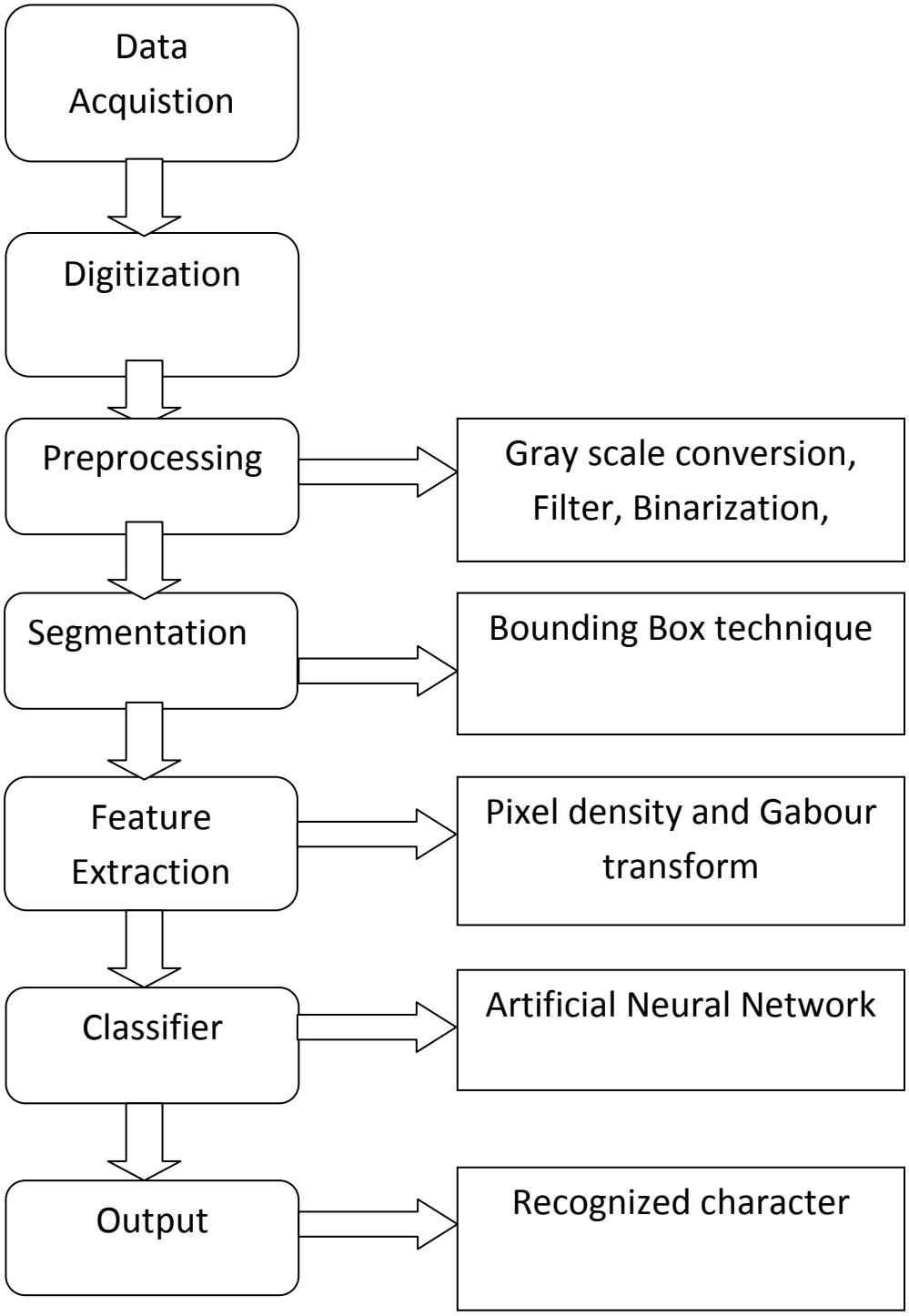

Figure 1

2.1 **Data Acquistion** -Handwritten data samples of character are acquired on paper from different people.

2.2 **Digitization**- The data samples are now scanned using any device which can be a scanner. A flat-bed scanner is used at 300dpi which converts the data on the paper being scanned into a bitmap image [1]

2.3 **Preprocessing** –The digitized image so obtained was in gray tone and stored in TIF format [2]

Preprocessing removes discontinuity and distortion in the input character and convert the character in form of recognizable form .The process which comes under preprocessing are.

- Binarization
- Inversion
- Noise Reduction
- Normalization

2.3.1 Binarization

For testing purpose the character are first written on plain paper with pen or marker pen .These images that are stored via paint are nothing but RGB images. These images are then converted to white and black images with a threshold values of 0.5 to get a true binary image that is 0s for all background pixel and 1s for all foreground pixel.

2.3.2 inversion

The binary images consist of a black foreground as font and white as background. The number pixel in background exceed the one as compared to foreground so we can say number of 1s will atleast be 10 times as compared to number of 0s . We conventionally work with 1s leaving 0s here since we are working only on 1s so we have less number of calculation hence we invert the image so that background is black and foreground is white which gives appearance just like DOS screen.

2.3.3 Noise Reduction

Digital images become prone to different type of noise. Noise is result of error which during image acquisition process gives pixel values that do not reflect true intensities. Noise causes disconnected line segments ,bumps and gaps in lines ,filled loops etc [3].Noise can be introduce by scanner CCD detector, electronic transmission of data .Median filter ,wiener filter and various other filters are used to deal and remove this noise .Gaussian filter is used to smoothing the images and median filter are used to replace the intensity of character image.

2.3.4 normalization

Normalization is the process of converting a random sized images into a standard size image. It is a technique used to reduce shape variation.

2.4 Segmentation – segmentation is a process which analyze the digitalized images provided by a scanning device.This image localize the limit of each character and isolate them from each other .the various steps in segmentation are

(1) The binarized image is checked for Interline space among words.

(2) If interline spaces are detected then the image is segmented into set of paragraphs across the interline gap.

(3) The character in image are now detected and considered as individual objects.

(4) Features are now extracted for these bounding object in feature extraction step.

Figure 2. Character Segmentation

2.5 Feature extraction-

The aim of this step is to recognizing structure and to extract discriminant information from an image of a character and to reduce its dimensions of its representation .In character recognition as in pattern recognition task ,plays a major role in improving the recognition accuracy[4]The feature extraction method we used is Gabor transform which for different sides and we got various output as

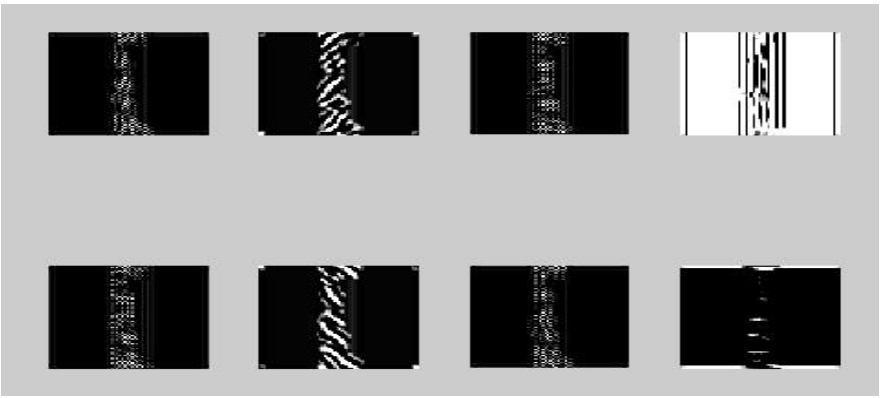

Figure 3 Feature extraction of a character

These technique gives feature like Area, Centroid, Eccentricity , EquiDiameter , Majoraxislength, Extent, Minoraxislength, orientation, perimeter.

2.6 Classification

The extracted features act as an input in the classification process.A bag-of-key feature are used as an input and given to classifier such as ANN.Here we have used Probablistic ANN to recognize character the feature extracted from the character are given as input to ANN.

2.6.1 Probabilistic Neural Network (PNN)

In a PNN, the operations are organized into a multilayered feedforward network with four layers:

- Input layer
- Hidden layer
- Pattern layer/Summation layer
- Output layer

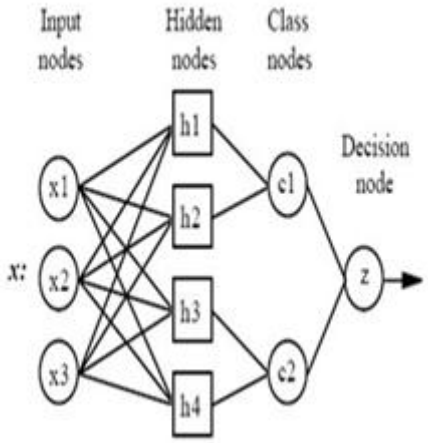

Figure 4 PNN architecture

III. CONCLUSION

A lot of research work exists in the survey for Devanagari Handwritten recognition.. In this paper, we have projected various aspects of each phase of offline Devanagari character recognition process that have been used. Researchers have used many character set for research. The following key challenges are more to be carried out by researchers by increasing number of holes and strokes and mixed words.

REFERENCES

Journal Papers:

[1] Gunjan Singh et al, Recognition of Handwritten Hindi Characters using Backpropagation Neural Network / *(IJCSIT) International Journal of Computer Science and Information Technologies, Vol. 3 (4) , 2012,4892-4895*

[2] Sneha U.Bohra et al ./ Handwritten Character Recognition for major Indian Scripts:*A Survey International Journal of Computer Science & Engineering Technology*

[3] Vikas J Dongre,Vijay H Mankar, A Review of Research on Devnagari Character Recognition, *International Journal of Computer Applications (0975 – 8887) Volume 12– No.2, November 2010*

[4] Sushma shelke, Shaila Apte, Multistage Handwritten Marathi Compound Character Recognition Using Neural Networks, *Journal of Pattern Recognition Research 2 (2011)* 253-268.

ISSN (e): 2250 – 3005 || *Vol, 05* || *Issue,02* || *February – 2015* ||
International Journal of Computational Engineering Research (IJCER)

Impact of Using RHA and CD in Replacement of Cement for Mix

Dr.A.S.Kanagalakshmi[1,] J.Caroline Saro[2,] V.Jayashree[3]

1. *Professor, Panimalar Engineering College, Chennai*
2. *Student, Dept of Civil Engineering Panimalar Engineering College, Chennai*
3. *Student, Dept of Civil Engineering Panimalar Engineering College, Chennai*

ABSTRACT

The introduction of sustainable development to overcome issues of natural resource depletion has been gaining increased attention. The major objective of this study is to address the potential use of both agricultural and industrial wastes namely RHA (Rice Husk Ash) and CD (Copper Dust) as raw material in production of concrete. This study is an experimental investigation performed on replacement of copper dust and rice husk in cement concrete. It enhances the mechanical properties of concrete cube subjected to split tensile test and compressive strength test .This study provides comparison between the performance of using copper dust and rice husk cement concrete, as a strengthening material of concrete cube. The samples were tested and proved its promising results which were found to be increased compressive strength upto 25% and increased split tensile strength upto 40%.

KEYWORDS:*CD, RHA, mix design, compressive strength, split tensile strength, electrical resistivity*

I. INTRODUCTION

Globally, approximately 600 million tons of rice paddy is produced each year. On average 20% of the rice paddy is husk, giving an annual total production of 120 million tons. In the majority of rice producing countries much of the husk produced from the processing of rice is either burnt or dumped as a waste.The treatment of rice husk as a 'resource' for energy production is a departure from the perception that husks present disposal problems. The concept of generating energy from rice husk has great potential, particularly in those countries that are primarily dependant on imported oil for their energy needs. Rice husks are one of the largest readily available but most under-utilized biomass resources, being an ideal fuel for electricity generation.If a long term sustainable market and price for rice husk ash (RHA) can be established, then the viability of rice husk power or co-generation plants are substantially improved. Many more plants in the 2 - 5 MW range can become commercially viable around the world and this biomass resource can be utilized to a much greater extent than at present.Copper dust consists primarily of silica sand, coated with a thin film of burnt carbon, residual binder (bentonite, sea coal, resins) and dust. Copper dust can be used in concrete to improve its strength and other durability factors. Copper dust can be used as a partial replacement of cement or as a partial replacement of fine aggregates or total replacement of fine aggregate and as supplementary addition to achieve different properties of concrete. The physical and chemical characteristics of foundry sand will depend in great part on the type of casting process and the industry sector from which it originates. In modern foundry practice, sand is typically recycled and reused through many production cycles. Industry estimates that approximately 100 million tons of sand is used in production annually of that 6 - 10 million tons are discarded annually and are available to be recycled into other products and in industry. The automotive industries and its parts are the major generators of foundry sand. Foundries purchase high quality size-specific silica sands for use in their molding and casting operations.

II. MATERIALS AND METHODS

The following materials are used for replacing cement and sand

- Rice husk ash
- Copper dust

2.1. RICE HUSH ASH (RHA)

Rice husk is unusually high in ash compared to other biomass fuels – close to 20%. The ash is 92% - 95% silica, highly porous and lightweight, with a very high external surface area. Its absorbent and insulating properties are useful to many industrial applications.

RHA is a general term describing all types of ash produced from burning rice husks. In practice, the type of ash varies considerably according to the burning technique. The silica in the ash undergoes structural transformations depending on the conditions (time, temperature etc) of combustion.

At 550°C – 800°C amorphous ash is formed and at temperatures greater than this, crystalline ash is formed. These types of silica have different properties and it is important to produce ash of the correct specification for the particular end use.

2.1.1. CONSEQUENCES

- The addition of RHA to cement has been found to enhance cement properties:
- The addition of RHA speeds up setting time, although the water requirement is greater than for OPC (Ordinary Portland Cement).
- At 35% replacement, RHA cement has improved compressive strength due to its higher percentage of silica.
- RHA cement has improved resistance to acid attack compared to OPC
- More recent studies have shown RHA has uses in the manufacture of concrete for the marine environment. Replacing 10% Portland cement with RHA can improve resistance to chloride penetration.
- Several studies have combined fly ash and RHA in various proportions. In general, concrete made with Portland cement containing both RHA and fly ash has a higher compressive strength than concrete made with Portland cement containing either RHA or fly ash on their own.

2.2. COPPER DUST

Copper dust is high quality silica sand with uniform physical characteristics. It is a by- product of ferrous and nonferrous metal casting industries, where sand has been used for centuries as a molding material because of its thermal conductivity. It is a byproduct from the production of both ferrous and nonferrous metal castings. The raw sand is normally of a higher quality than the typical bank run or natural sands used in fill construction sites. The sands form the outer shape of the mould cavity. These sands normally rely upon a small amount of betonies clay to act as the binder material. Depending upon the geometry of the casting, sands cores are inserted into the mould cavity to form internal passages for the molten metal. Once the metal has solidified, the casting is separated from the moulding and core sands in the shakeout process. In the casting process, moulding sands are recycled and reused multiple times. Eventually, however, the recycled sand degrades to the point that it can no longer be reused in the casting process. At that point, the old sand is displaced from the cycle as by-product, new sand is introduced, and the cycle begins again. Although there are other casting methods used, including die casting and permanent mould casting, sand casting is by far most prevalent mould casting technique.Sand is used in two different ways in metal castings as a moulding material, which focuses the external shape of the cast part and as cores that form internal void spaces in products such as engine blocks. Since sand grains do not naturally adhere to each other so binders must be introduced to cause the sand to stick together and holds its shape during the introduction of molten metal into mould and cooling of casting.

2.3. METHODOLOGY

2.3.1. COLLECTION OF RAW MATERIALS

The raw materials used in our project are rice husk ash (RHA), copper dust. Copper dust has been collected from the sterlite, Tuticorin and RHA from rice mill Rajapalayam.

2.3.2. TESTING OF RAW MATERIALS

The following tests have been conducted for the collected raw materials to know about their characteristics.

RICE HUSK ASH

- Specific gravity
- Fineness

COPPER DUST

- Specific gravity
- Fineness
- Crushing value

2.3.2.1. DETERMINATION OF SPECIFIC GRAVITY

Specific gravity is determined by pycnometer using the following formula,

FORMULA:

Specific gravity of the soil = $\frac{(w2 - w1)}{[(w2 - w_1) - (w3 - w_4)]}$

Where,

W1 - empty weight of the pycnometer/density bottle.

W2 - weight of pycnometer/density bottle with copper alone.

W3 - weight of pycnometer/density bottle with copper and water.

W4 - weight of pycnometer/density bottle with water alone.

MATERIALS	SPECIFIC GRAVITY
CEMENT	3.15
SAND	2.65
COARSE AGGREGATE	2.76
RICE HUSK ASH	2.52
COPPER DUST	4.16

2.3.2.2. DETERMINATION OF FINENESS OF RHA

Fineness of RHA is determined using Sieve Analysis method.

As a result percentage of fineness of the RHA=75%

III. CUBE CASTING AND TESTING

The mix design of concrete has been done according to DOE (department of environment) guidelines for M20 grade. Based upon the quantities of ingredient of the mixes, the quantities of RHA, COPPER DUST for 20%, 30% and 40% replacement by weight have been estimated and mixes have been made.

3.1. PROPORTIONING OF CONCRETE MIX

MIX1- Control concrete

MIX2- Concrete with 30% Rice husk Ash

MIX3 - Concrete with 20% RHA + 30% Copper Dust

MIX4 - Concrete with 20% RHA + 40% Copper Dust

MIX5 - Concrete with 30% RHA +30% Copper Dust

MIX6 - Concrete with 30% RHA +40% Copper Dust

3.1.2. MIX DESIGN FOR NORMAL CONCRETE

Characteristic compressive strength required in the field at 28days = 20 N/mm^2

Maximum size of aggregate = 20mm

Degree of quality control = good

Type of exposure = mild

3.1.3 TARGET MEAN STRENGTH OF CONCRETE

The target mean strength for specified characteristic cube Strength is

$$\mathbf{fck = fck + (t*s)}$$

Where,

fck = characteristic compressive strength at 28 days

s = standard deviation for each grade of concrete, which shall be determined separately according to

IS: 456-1978.

t = a statistical value depending on expected of low results (risk factor) according to IS: 456-1978.

$$fck = fck + (t*s)$$

$$= 20+ (1x4.6)$$

$$= 24.6\ N/mm^2.$$

3.1.4. DESIGN STIPULATIONS

Characteristic compressive strength

required in the field at 28days = 20 N/mm2

Maximum size of aggregate = 20mm

Degree of quality control = good

Type of exposure = Mild

3.1.5. TEST DATA FOR MATERIALS

Specific gravity of cement =3.15

Specific gravity of fine aggregates =2.65

Specific gravity of coarse aggregates =2.78

3.1.6. SELECTION OF WATER – CEMENT RATIO

$$\mathbf{C = ((100-PW)/(100-0.7P)\{W/C+0.3F\}}$$

Where, $\mathbf{p =100F/(C+F)}$

Fly ash content, $\mathbf{F =pC/ (100-p)}$

(i.e.). p is the percentage of fly ash in the. total cementitious material.

W -is the free water content

W/(C+0.3F) is the free water / cementitious ratio for design strength.

The free water/ cementitious material ratio w/c + F should then be compared with the specified value.

Hence the total cementitious material content is =300kg/m3

The free water/cementitious material ratio is =0.65

3.1.7. CALCULATION OF WATER CONTENT

Cement content satisfies the durability requirement. But water/cementitious material ratio does not satisfy the durability requirement. Therefore adopt water/ cementitious material ratio of 0.65, instead of 0.51

Then water content = 300*0.65

= 195.2 kg/m3

3.1.8. CALCULATION OF COARSE AND FINE AGGREGATE CONTENT

For water content of 195kg/m3, average specific gravity of 2.65 of aggregates, the wet density of concrete comes to 2420 kg/m3.

Hence the total weight of aggregates

=2420-(300+195+0)

=1925.4 kg/m^3.

For free water/cementitious material ratio of 0.50, and for F.A 40% passing through 600µ sieve, and for slump of 30-60 mm the proportion of F.A is =40%.

Weight of F.A = (40/100)*1925.4

= 770.2 kg/m^3

Weight of C.A = 1925.4-770.2

= 1152.6 kg/m^3

The above weights of F.A, C.A are to be adjusted depending upon the free moisture content and absorption characteristics of aggregates. The corresponding correction is also to be made in the quantity of actual water added. And also consequent changes in the quantities of aggregates.

Then trial mixes are made to see that the concrete satisfies all the requirements in plastic conditions and strength at 28days. If not, minor adjustment is made in the quantities of material worked out.

TABLE 1 MIX PROPORTION

Water kg/m^3	**Cement kg/m^3**	**RHA kg/m^3**	**Sand kg/m^3**	**Coarse aggregate kg/m^3**
195	300	0	770.2	1152.5
0.65	1	0	2.5	3.5

3.2. MIX DESIGN FOR 20% RHA+40% COPPER DUST CONCRETE

Design stipulations

Characteristic compressive strength required in the field at 28days = 20 N/mm^2

Maximum size of aggregate = 20mm

Degree of quality control = good

Type of exposure = Mild

3.2.1. TEST DATA FOR MATERIALS

Specific gravity of cement =3.15

Specific gravity of fine aggregates =2.65

Specific gravity of coarse aggregates =2.78

3.2.2. SELECTION OF WATER – CEMENT RATIO

C= ((100-PW)/(100-0.7P){W/C+0.3F}

Where, **p =100F/(C+F)**

Fly ash content, **F=pC/(100-p)**

(i.e.).,p is the percentage of fly ash in the total cementitious material.

W is the free water content

W/(C+0.3F)is the free water / cementitious ratio for design strength.

The free water/ cementitious material ratio w/c + F should then be compared with the specified value.

For slump of 60mm, for maxim size aggregate of 20mm, in case of crushed aggregate, the approximate water content is 210kg/m^3.Since 20percent of flu ash is used,

Therefore the water content =195kg/m^3

Then cement content =279.1kg/m^3

Fly ash content, F = pC/(100-p) = 69.7kg/m3

Hence the total cementitious material content is 348.8kg/m^3. The free water/cementitious material ratio is (195/348.8)=0.56.

3.2.3. CALCULATION OF WATER CONTENT

Cement content satisfies the durability requirement. But water/cementitious material ratio does not satisfy the durability requirement. Therefore adopt water/ cementitious material ratio of 0.56, instead of 0.51

Then water content = 348.8*0.56

= 195.33 kg/m^3.

3.2.4 CALCULATION OF COARSE AND FINE AGGREGATE CONTENT

For water content of 195kg/m^3, average specific gravity of 2.65 of aggregates, the wet density of concrete comes to 2420 kg/m^3.

Hence the total weight of aggregates

=2420-(295+279.1+69.7)

=1875.8 kg/m^3

For free water/cementitious material ratio of 0.50, and for F.A, 40% passing through 600µ sieve, and for slump of 30-60 mm the proportion of F.A is =40%.

Weight of F.A = (40/100)*1875.8

=750.32 kg/m^3

Weight of C.A =1875.8-750.32

=1125.5 kg/m^3.

The above weights of F.A, C.A are to be adjusted depending upon the free moisture content and absorption characteristics of aggregates. The corresponding correction is also to be made in the quantity of actual water added. And also consequent changes in the quantities of aggregates.

Then trial mixes are made to see that the concrete satisfies all the requirements in plastic conditions and strength at 28days. If not, minor adjustment is made in the quantities of material worked out.

Table 2 Mix proportion

Water kg/m^3	Cement kg/m^3	RHA kg/m^3	Sand kg/m^3	Coarse aggregate kg/m^3
195	279.1	69.7	750.32	1125.5
0.56	1	0.25	2.68	3.9

Thus, for all replacements the mix design has done similarly.

IV. CASTING OF SPECIMENS

For each mix, cited in above table, good number of 150mm side cube were casted. Immediately after casting, these specimens were covered with wet burlap at the casting site for 24 hours. Following this the test specimens were transferred to the curing tank. The cubes were tested for 7-days and 28-days strengths. The test results are shown in table. It is seen that the nature curves for normal concrete with RHA and Copper Dust concrete were similar.

4.1. Test for compressive strength

Age at test: Usually testing is done after 7 days and 28 days, the days being measured from the time the water is added to the dry ingredients.

COMPRESSIVE TEST RESULTS OF SPECIMEN

S.No	REPLACEMENT OF CEMENT BY RHA	7th DAY COMPRESSIVE STRENGTH	28th DAY COMPRESSIVE STRENGTH
1	Control Concrete	21.47	**27.35**
2	30% Rice husk Ash	16.19	**24.45**
3	**20% RHA & 30% Copper Dust**	**21.27**	**29.92**
4	20% RHA & 40% Copper Dust	21.56	**30.34**
5	30% RHA & 30% Copper Dust	17.61	**26.98**
6	**30% RHA & 40% Copper Dust**	**13.03**	**22.78**

(20% RHA and 40% CD is advisable)

7 DAYS COMPRESSIVE STRENGTH

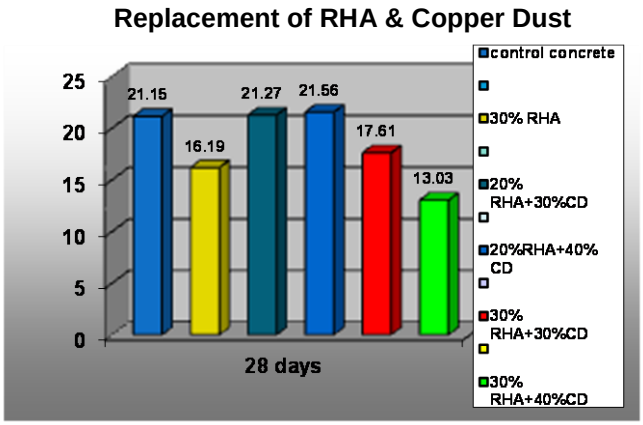

Fig 1 compressive strength result after replacement for 7days

28 DAYS COMPRESSIVE STRENGTH

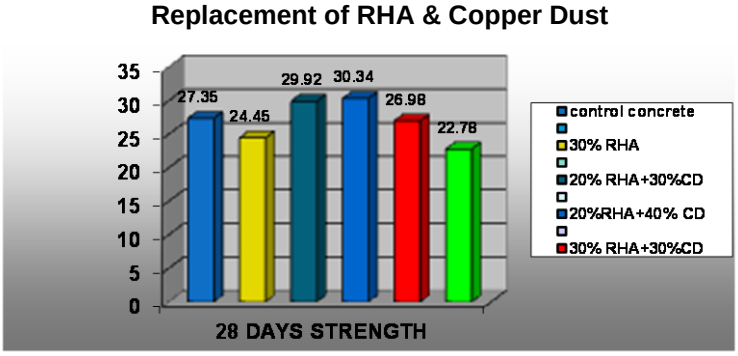

Fig 2 increased compressive strength result after replacement for 28days

4.2. Test for split tensile strength

Age at test: Usually testing is done after 7 days and 28 days, the days being measured from the time the water is added to the dry ingredients.

Table 3 Tensile test results of specimen

S.No	REPLACEMENT OF CEMENT BY RHA	7th DAY TENSILE STRENGTH	28th DAY TENSILE STRENGTH
1	Control Concrete	3.77	**4.9**
2	30% Rice husk Ash	2.66	**5.0**
3	20% RHA & 30% Copper Dust	4.68	**5.39**
4	**20% RHA & 40% Copper Dust**	**3.75**	**6.17**

5	30% RHA & 30% Copper Dust	3.07	**4.78**
6	**30% RHA & 40% Copper Dust**	**2.85**	**3.49**

(20% RHA and 40% CD is advisable)

7 DAYS SPLIT-TENSILE STRENGTH

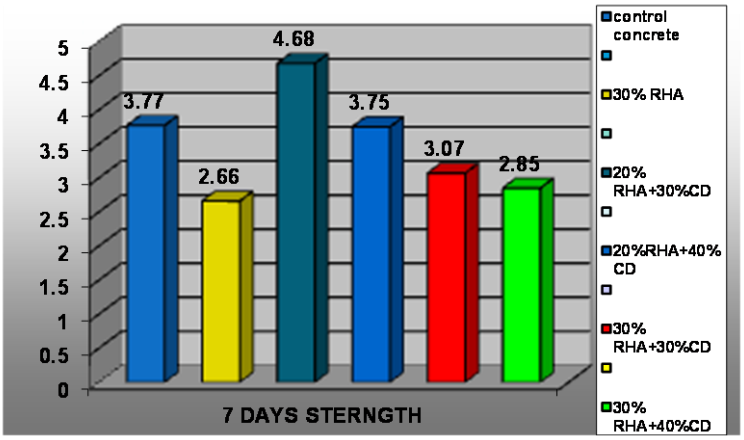

Fig 3 increased split tensile strength result after replacement for 7days

28 DAYS SPLIT-TENSILE STRENGTH

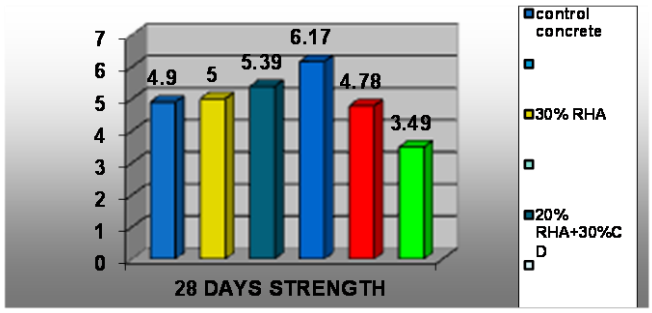

Fig 4 increased split tensile strength result after replacement for 28days

V. ELECTRICAL RESISTIVITY TEST

Resistivity is fundamental property of a particular material. The electrical resistivity of any material is defined as the resistance, in ohms, between opposite faces of unit cube of the material.

Thus, if þ is the resistivity of concrete then,

Þ=RA/L ohm m

R -Resistance

Þ – Resisstivity

A –Area of the specimen in m^2

L - Length between electrodes in 'm'.

Generally the conventional concrete does not conduct electricity. The resistivity of conventional concrete varies from 6.54×103 ohm m to 11.40×103 ohm m, Hence it acts as a pure resister.

R=V/I

R-Resistivity

V- Voltage applied to the conductive specimen 230v

I – Alternate current taken by the conductive specimen.

R=230/0.1

= 2300

=2.3×103 ohm m

VI. CONCLUSION

- ✓ The RHA used in this study was efficient as a pozzolanic material because it contains high amorphous silica of 88.32%
- ✓ From the test results it was found that concrete with 20% **RHA** and 40% **COPPER DUST** have shown high compressive strength. Hence up to 20% RHA replacement would not adversely affect the strength and mechanical properties.
- ✓ The addition of RHA and **copper dust** to a concrete mix improved the mechanical properties of concrete with respect to compressive strength and it is nearly about upto 25%.
- ✓ Split Tensile Strength has shown an increase with increase in replacement levels of **copper dust upto 40%** with fine aggregate.
- ✓ Split Tensile Strength also increased with increase in age.

REFERENCE

[1]. IS 10262 -2009 Indian Standard recommended guide lines for concrete mix design (2009)
[2]. IS 383-1970 code for properties of aggregates (1970)
[3]. ACI report 234R-96
[4]. Akihiko, Y. and Takashi, Y. "Study of utilisation of copper slag as fine aggregate for concrete", Ashikaya Kogyo Daigaku Kenkyu Shuroku, Vol. 23, pp. 79-85, 1996.
[5]. Al-Jabri, K. and Makoto Hisada. "Copper slag as sand replacement for high performance concrete", Cement & Concrete Composites, Vol. 31, pp.483- 488, 2009.
[6]. Al-Jabri, K., Taha, R. and Al-Ghassani, M. "Use of copper slag and cement by-pass dust as cementitious materials" Cement, Concrete Aggregates, Vol. 24, No.1, pp. 7-12, 2005.
[7]. Al-Jabri, K.S., Abdullah, H., Al-Saidy and Ramzi Taha. "Effect of copper slag as a fine aggregate on the properties of cement mortars nd concrete", Construction and Building Materials, Vol. 25, pp. 933-938, 2011.
[8]. Al-Jabri, K.S., Taha, R.A., Al-Hashmi, A. and Al-Harthy, A.S. "Effect of copper slag and cement by-pass dust addition on mechanical properties of concrete", Construction and building materials, Vol. 20, pp.322-331, 2006.
[9]. Al-Jabri, K.S., Makoto Hisada, Abdulla, H.A. and Al-oraini, S.K. "Performance of high strength concrete made with copper slag as a fine aggregate", Construction and building materials, Vol.23, pp. 2132-2140, 2009.
[10]. AUSTRALIAN JOURNAL OF BASIC AND APPLIED SCIENCES ,3(3) : 1616-1622,2009 ISSN 1991-8178 (2009, INSInet publication)
[11]. Sakr. K., 2006 Effects of Silica fume and Rice husk ash on the properties of concrete Journal materials in civil engineering 18(3) 367-376
[12]. METHA, P. K., Rice husk ash – a unique supplementary cementing material, in: V.M. Malhotra (Ed), Proceedings of the International Symposium on Advances in Concrete Technology. CANMET/ACI, Athens, Greece, May, 1992, pp. 407-430.
[13]. Abichou T. Benson, C. Edil T., 1998a.Database on beneficial reuse of foundry by- products. Recycled materials in geotechnical applications, Geotech. Spec. Publ.No.79, C. Vipulanandan and D.Elton, eds., ASCE, Reston, Va., 210-223
[14]. Bentur A. (2002), Cementitious Materials – Nine Millennia and A New Century: Past, Present and future. Journal of Materials in Civil Engineering 2002: 14(1): 1-22.
[15]. Coutinho SJ. (2003), The combine benefit of CPF and RHA in improving the durability of concrete structures. Cement and Concrete Composites 2003: 25(1):5159. Gastaldine ALG, Isaia GC, Gomes NS.
[16]. Shetty M.S., Concrete Technology, S.Chand and Company Pvt.Ltd. New Delhi, India (1991).
[17]. Eddine BT, Salah MM: Solid waste as renewable source of energy: current and future possibility in Algeria. Int. J. Energy Environ. Eng. 2012.
[18]. Batayneh M, Marie I, Asi I: Use of selected waste materials in concrete mixes. Waste Manag 2007, 27:1870–1876.
[19]. Shi-cong K, Bao-jian Z, Chi-sun P: Feasibility study of using recycled fresh concrete waste as coarse aggregates in concrete. Construct Build Mater 2012.

ISSN (e): 2250 – 3005 || *Vol, 05* || *Issue,02* || *February – 2015* ||
International Journal of Computational Engineering Research (IJCER)

Performance Analysis of Ad-hoc on Demand Distance Vector Routing (AODV) and Dynamic Source Routing (DSR) routing Protocols for Mobile Ad-hoc Networks

Bhushan Ramesh Ratnaparakhi[1], Prof. Ranjana R. Gite[2], Prof. Dattatray S. Babe[3]

[1] *Student of Dept. of Electronics and Telecommunications , Vidyalankar Institute of Technology Mumbai*
[2] *Assistant Professor Dept. of Electronics and Telecommunications , Vidyalankar Institute of Technology Mumbai*
[3] *Assistant Professor Dept. of Electronics and Telecommunications, Vidyalankar Institute of Technology Mumbai*

ABSTRACT

Now a day Mobile Ad hoc Networks (MANETs) are a new generation of networks offering unrestricted mobility without any underlying infrastructure. This MANETs research program has mainly focused on developing an efficient routing mechanism in such a highly dynamic and resource constrained network [1]. Most of these routing protocols assume a trusted, safe and cooperative environment. This performance analysis project work is related to various Mobile Ad hoc Networks (MANETs) routing protocols such as Ad-hoc on Demand Distance Vector Routing (AODV), Dynamic Source Routing (DSR), and Optimized Link State Routing (OLSR) [1-4]. On the bases of different routing protocols as mention earlier we can stimulate using network simulator software which generates different graphs as result. And then see Comparative analysis effects on routing protocol parameters as based on graph of Mobile Ad-hoc Networks (MANETs) on the bases of various simulation environments such as area, number of node, testing field, traffic load etc. Following parameters are considered for performance analysis Routing Overhead, End-to-End Delay and Throughput. The proposed work analyses various performance parameter of the routing protocols and suggesting which method is superior among them and study graphs obtain in Network stimulating software (NS-2) for Mobile Ad-hoc Networks (MANETs). In this paper we took Ad-hoc on Demand Distance Vector Routing (AODV) and Dynamic Source Routing (DSR) protocol, this two routing protocols simulate for same network area parameter in NS-2 environment to observe various results and conclude the study on bases of graph which we obtained as a result.

Keywords: Area, AODV, DSR, MANETs, Number of Node, Network Simulator 2 (NS-2), OLSR, Routing Protocols.

I. INTRODUCTION

A Mobile Ad hoc Networks (MANETs) is a collection of mobile devices that can communicate with each other without the use of a predefined infrastructure or centralized administration [1]. Mobile Ad hoc Networks are new generation of networks offering unrestricted mobility without any underlying infrastructure [1-2]. A mobile Ad hoc network is a dynamically self-organizing network without any central administrator or infrastructure support. It is composed of mobile terminals and that communicates with one to other and broadcast through radio transmission. In ad hoc wireless networks, communicating data is vulnerable to lots of potential attacks due to their characteristics of having dynamic topology, limited bandwidth and energy constraints [1-4].

Mobile Ad hoc Networks are the new generation of networks which offers unrestricted mobility without fail of any underlying infrastructure. In ad hoc wireless networks, communicating data is vulnerable to lots of potential attacks due to their unique characteristics of having dynamic topology, limited bandwidth and energy constraints in the protocols [1-4]. In addition to that freedom of mobility, a MANET can be constructed quickly at a low cost, as it does not rely on existing network infrastructure. Due to this flexibility, a MANET is attractive for applications such as emergency operations, vehicle networks, disaster relief, military service, casual meetings, campus networks, maritime communications, robot networks, and so on. Dynamic topology, limited bandwidth and energy constraints this are the negative points of this network [1-3]. Routing protocols are mainly classified in reactive and proactive routing protocols. In reactive routing protocols, such as the Ad hoc On Demand Distance Vector (AODV) protocol nodes find routes only when required and Dynamic Source Routing (DSR) is also an on-demand protocol and features similar route discovery as AODV [6]. A source route is appended to all packets and intermediate nodes only when use this source route to forward data. Scope of this project is based on mentioned routing protocols.

1.2 Approach of network

This infrastructure network made up of networks with wired and fixed gateways. A mobile host communication with a bridge in network primarily called base station available within communication radius. This area of infrastructure network defined in program. The mobile unit that is node can move random geographically while it is communicating. In this ad hoc network all nodes are mobile and can be connected dynamically in random manner. When mobile unit goes out of range of one base station then it connects automatically with new base station and start communicating and information exchange happened in between two nodes this information in the form of data packets. The nodes in network function like routers which found and maintain routes to other node. The node in mobile ad hoc network can be cell phone, laptop, PDA and any device to capable of do communication. This is the overview of our Mobile Ad hoc Networks (MANETs).

1.3 Classification of MANETs Routing Protocols

The routing protocols of MANETs can be classified in three main types. Figure 1 shows diagrammatical classification of MANETs along with some relative examples routing protocols.

Routing protocols mainly classified in two types such as reactive and proactive routing protocols. In reactive routing protocol, the Ad hoc On Demand Distance Vector (AODV) protocol nodes find routes only when required and Dynamic Source Routing (DSR) is also an on-demand protocol and features similar route discovery as AODV. A source route is appended to all packets and intermediate nodes, and it uses this source route to forward data. In proactive routing protocols Optimized Link State Routing (OLSR) protocol has come.

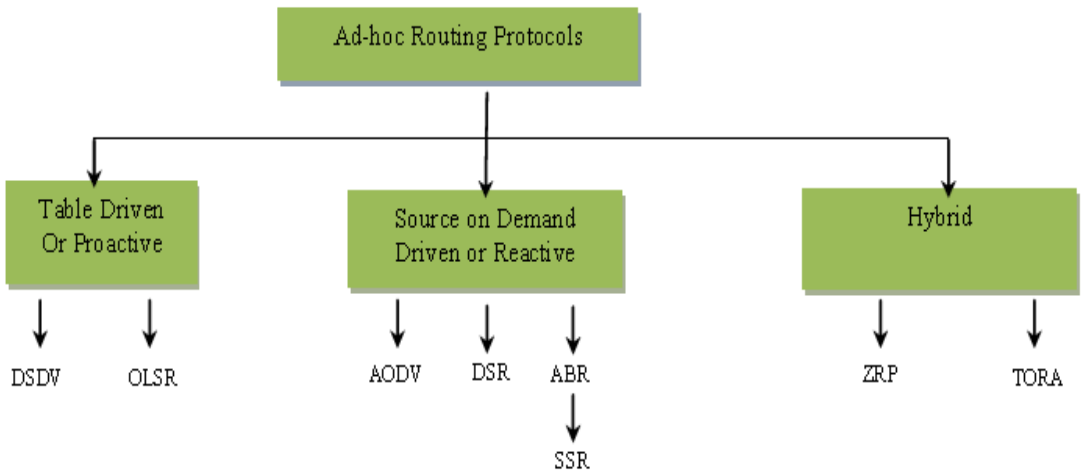

Figure 1. Classification of MANETs Routing protocols [5].

This classifation chats gives the direct differencial view about the routing protocols in mobile network.

II. MAIN INTRODUCTION ABOUT AODV AND DSR ROUTING PROTOCOLS IN MANETS

2.1 Ad Hoc on Demand Distance Vector Routing (AODV)

Mobile Ad hoc network is one of branch in wireless networks for mobile node. This mobile wireless network is very popular now a day due to its unique characteristics. Basically routing protocols mainly classified in two types such as reactive and proactive routing protocols. In reactive routing protocol, the Ad hoc On Demand Distance Vector (AODV) protocol nodes find routes only when required and features similar route discovery. A source route is appended to all packets and intermediate nodes, and it uses this source route to forward data. It is the most important routing protocol in mobile wireless networks. The Ad Hoc On-Demand Distance Vector routing protocol (AODV) is an improvement of the Destination-Sequenced Distance Vector routing protocol (DSDV) [5]. DSDV has its efficiency in creating smaller ad-hoc networks. This is the main important functioning of Ad Hoc On-Demand Distance Vector routing protocol (AODV) in MANETs.

Reactive protocols discover routes only when needed. When node wants to communicate with another node then it checks its existing information with destination route node. If this checking is positive then communication established between source and destination node and further data exchange is going to be happened. The RREQ request in (Figure 2) is from source to destination gives discovers the path towards destination. After sending RREQ packet request to destination then destination node send back the RREP packet request send back to source. These RREP packets decide the shortest routing path between sources to destination.

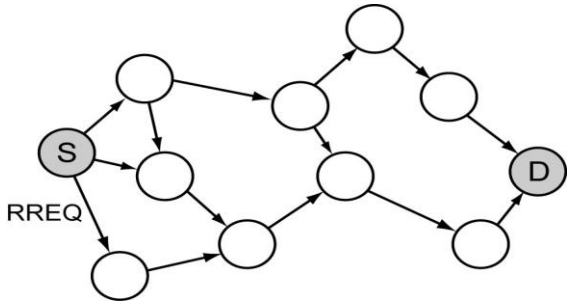

Figure 2. A RREQ Source to Destination path generation [5]

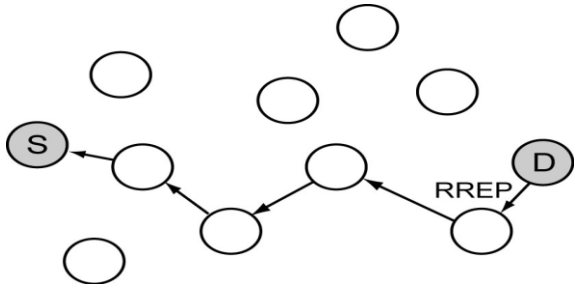

Figure 3. A RREP Packet send back to Source [5]

Advantages:

- AODV tries to minimize the number of required broadcasts.
- It creates the routes on-demand basis.
- Need lower delay for connection setup.
- Destination sequence numbers are used to find the latest route to the destination.

Disadvantages:

- Does not follow the unidirectional links.
- Periodic route formation creates unnecessary bandwidth consumption.

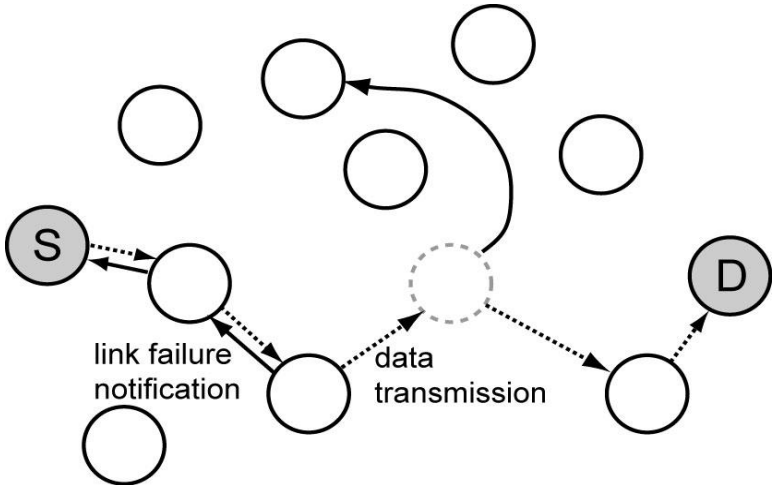

Figure 4. AODV link notification [5].

2.2 Dynamic Source Routing (DSR)

These Dynamic Source Routing protocol come under reactive routing protocol in classification of routing techniques of mobile Ad hoc network. The Dynamic Source Routing (DSR) protocol is an on-demand routing protocol based on source routing. In the source routing technique, a sender determines the exact sequence of nodes through which to propagate a packet [5]. The list of intermediate nodes for routing is explicitly contained in the packet's header. DRS are a simple form and effective routing protocol design for use of multi-hop wireless ad hoc networks of mobile nodes. It is type of self-organizing and self-configuring network.

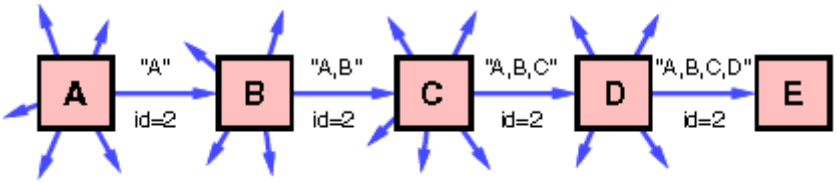

Figure 5: DSR discovery route A source to E destination.

Advantages:

- Self-organize
- Self-configuring
- Less End-to-End delay.

Disadvantages:

- Only find path one node to other.
- Path directory added to next upcoming path.

III. NETWORK SIMULATION ENVIRONMENTS

The Network simulator is a name for series of discrete event network simulators, specifically **ns-1**, **ns-2** and **ns-3**. All of them are discrete-event network simulator. It is tool in which wireless networks simulation can be done due genuine limitations to high cost of implementation, area limitations, etc. In 1996-97, ns version 2 (ns-2) was initiated based on a refactoring by Steve McCanne. Use of Tcl was replaced by MIT's Object Tcl (OTcl), an object-oriented dialect Tcl [1]. The core of ns-2 is also written in C++, but the C++ simulation objects are linked to shadow objects in OTcl and variables can be linked between both language realms. Simulation scripts are written in the OTcl language, an extension of the Tcl scripting language [3-4].

At this time ns-2 consists of over 300,000 lines of source code, and there is probably a comparable amount of contributed code that is not integrated directly into the main distribution is many forks of ns-2 exist, both maintained and unmaintained. It runs on GNU/Linux, FreeBSD, Solaris, Mac OS X and Windows versions that support Cygwin. It is licensed for use under version 2 of the GNU General Public License [5-6].

3.1 Workflow for simulation

There is some general process of creating a simulation given in as per several steps. These steps are as follows:

- Topology definition: to ease the creation of basic facilities and define their interrelationships, ns-2 has a system of containers and helpers that facilitates this process.
- Model development: models are added to simulation (for example, UDP, IPv4, point to-point devices and links, applications); most of the time this is done using helpers.
- Node and link configuration: models set their default values (for example, the size of packets sent by an application or MTU of a point-to-point link); most of the time this is done using the attribute system.
- Execution: simulation facilities generate events, data requested by the user is logged.
- Performance analysis: after the simulation is finished and data is available as a time stamped event trace. This data can then be statistically analysed with tools like R to draw conclusions.
- Graphical Visualization: raw or processed data collected in a simulation can be graphed using tools like Gnuplot, matplotlib or XGRAPH [5].

3.2 Strategy for simulation work

For the simulation purpose latest version 2.35 of NS-2 has been used in this project work. This setup is done on the windows operating system, for do this work we have to install Oracle VM virtual box on windows 7 computer. Then Oracle VM virtual box gives the platform of LINUX operating system to run Ubuntu 12.04 (32 bit) in this virtual system to do actual simulation of project operation NS-2 network simulating software.

3.2.1 Scenario

- Topology of 1000*1000 is taken for simulation.
- Nodes are moving at constant random speed.
- Nodes are being generated randomly at random position.
- Nodes are generated at random time as if few nodes are entering into the topology.
- Radio propagation model used is Two-Ray Ground.
- Movement is linear and node speed is constant for a simulation.
- Antenna model used is Omni Antenna.

3.2.2 Node characteristics

- Link Layer Type: Logical Link (LL) type
- MAC type: 802_11
- Network Interface type: wireless
- Queue type: Drop-Tail
- Channel type: wireless
- The simulation parameters are listed in Table.

3.2.3 Performance matrix

The following different performance matrices are evaluated the behavior of AODV, DSR routing protocols wireless network of mobile ad hoc networks MANETs. For this work some parameters are taken into consideration.

- Routing Overhead.
- Throughput.
- End-to-End Delay.

Table 1. Simulation Parameters for NS-2.

PARAMETERS	VALUES
Simulator	NS-2 (version- 2.35)
Channel type	Channel/ wireless channel
Network interface type	Phy/ wireless phy
Mac type	Mac/ 802_11
Link layer type	LL
Antenna	Antenna/ Omni antenna
Maximum pack in ifq	50
Area (M*M)	1000*1000
Number of mobile node	60
Mac 802_11 RTS Threshold	3000
Source type	UDP/ TCP
Simulation time	80 sec.
Routing protocols	AODV and DSR

3.3 Information to Simulation model

The objective of this project is the performance evaluation of two routing protocol for mobile ad hoc networks by using an open-source network simulation tool called NS-2. Two routing protocols: AODV, DSR have been considered for performance evaluation in this work. The simulation environment has been conducted with the LINUX operating system, because NS-2 works with Linux platform only. This gives the overview related to project.

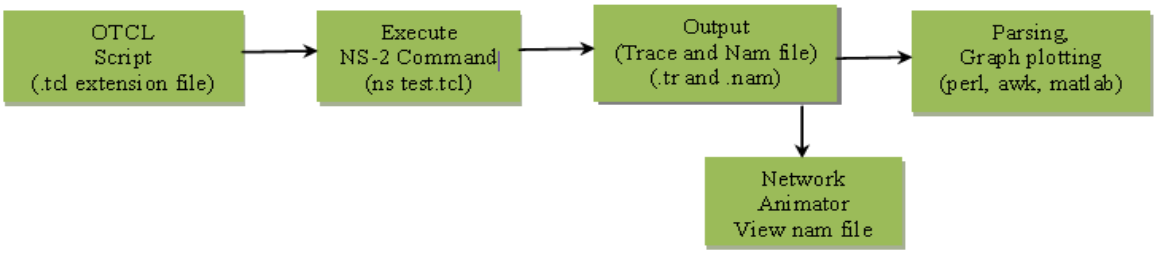

Figure 6. Simulation overview [5]

Whole simulation study is divided into two parts; one is create the node that may be cell phone, internet or any other devices. NS-2 output window is called NAM (Network Animator) file, which shows the node movement and communication occurs between various nodes in various conditions or to allow the users to visually appreciate the movement as well as the interactions of the mobile nodes. And another one is graphical analysis of trace file (.tr). Trace files contain the traces of event that can be further processed to understand the performance of the network.

Figure 6 of simulation overview depicts the overall process give the overview about how a network simulation is conducted under NS-2. Output files such as trace files have to be parsed to extract useful information. The parsing can be done using the *awk* command (in UNIX and LINUX, it is necessary to use gwak for the windows environment) or Perl script. The results have been analyzed using Excel or Matlab.

A software program which can shorten the process of parsing trace files (Xgraph and TraceGraph) has also been used in this project. However, it doesn't work well when the trace file is too large. To generate trace file and nam file, we call tcl script in CYGWIN command shell. By varying the simulation parameter shown in table 1, we can see the graphical variation between various performance metrics like Routing Overhead, End-to-End Delay with node speed and Throughput etc.

3.4 Nam file

NAM is a Tcl/TK based animation tool for viewing network simulation traces and real world packet traces. A network animator that provides packet-level animation and protocol-specific graphs to aid the design and debugging of new network protocols have been described. Taking data from network simulators such as ns or live networks, NAM was one of the first tools to provide general purpose, packet-level, and network animation, before starting to use NAM, a trace file needs to create [7]. This trace file is usually generated by NS. Once the trace file is generated, NAM can be used to animate it. A snapshot of the simulation topology in NAM for 60 mobile nodes is shown in figure 7 which is visualized the traces of communication or packets movements between mobile nodes.

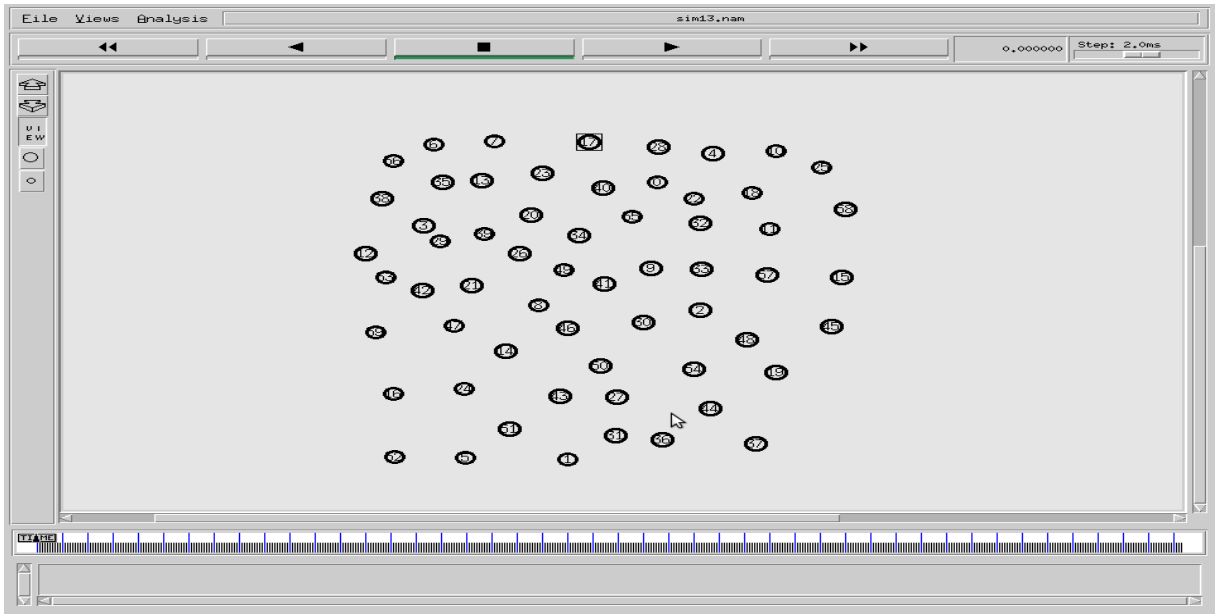

Figure 7. Nam window snapshot for mobile nodes.

4. Actual project NAM windows in project

Following various Nam windows are taken from run time of project with some time interval to show the working of node on that time period. These images are gives the actual field simulation happened at that time. Nam window shows original view of run time project on screen with node activity. This Nam window is user define, space is created accordingly in object program file. In this project proj.tcl is program file.

Below table give some indications related to colours and diagrams available in simulation window.

Table 2. Indicative parameter for simulating nam window in NS-2

Sr. no	Parameters	Indication to images
1	Number in circle	Node
2	Node in green circle	Source node
3	Node in red circle	Destination node
4	Black dotted lines	Packet transmission between nodes
5	Black square	Packet data loss

This figure 8 shows the initial image of NAM window at time 0 sec.

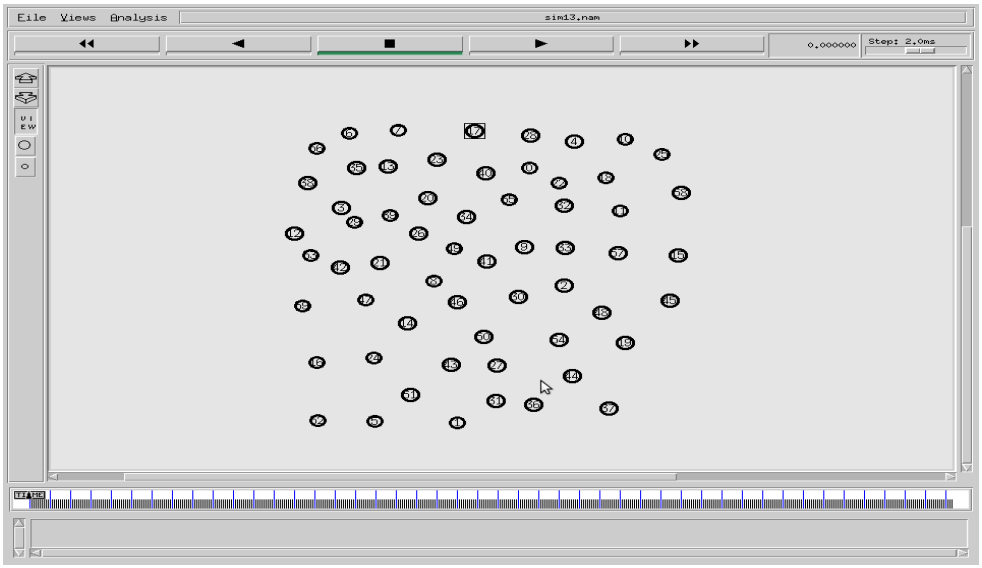

Figure 8. Initial time nam window at (o sec.) time

This figure 9 shows the image of NAM window at time 10 sec.

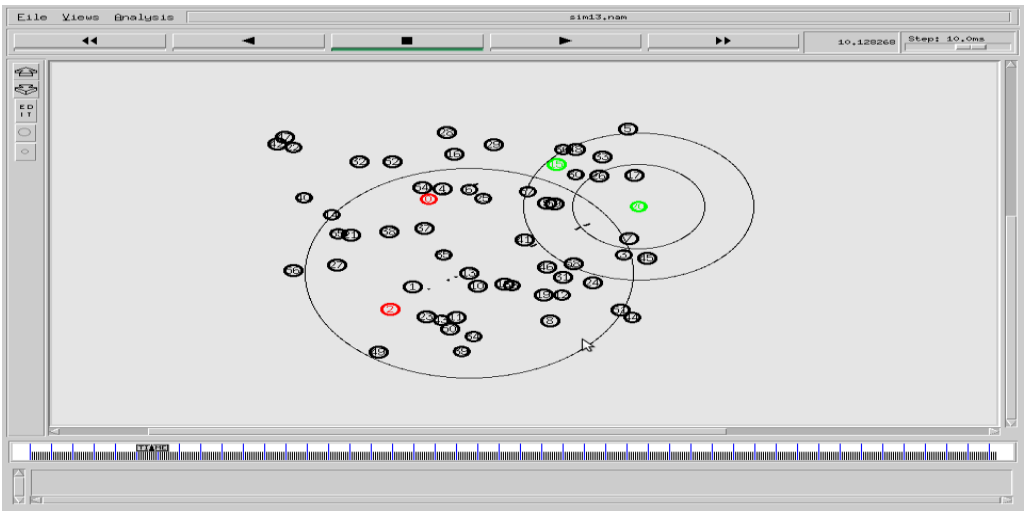

Figure 9. Nam window with (10 sec.) time

This figure 10 image shows at time of 21 sec interval.

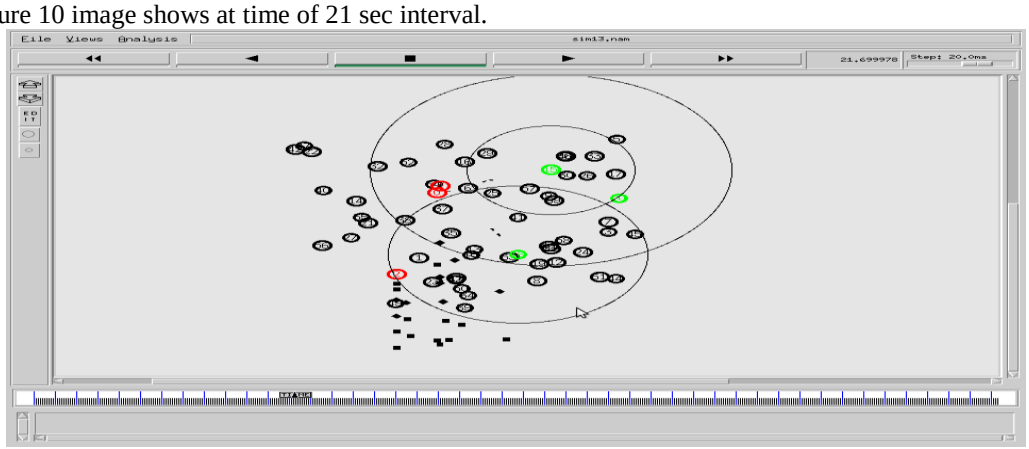

Figure 10. Nam window at (21 sec.) time

Figure 11 at interval of 32 sec. shows the last NAM window which shows all packet data transmission and packet losses in the actual scenario.

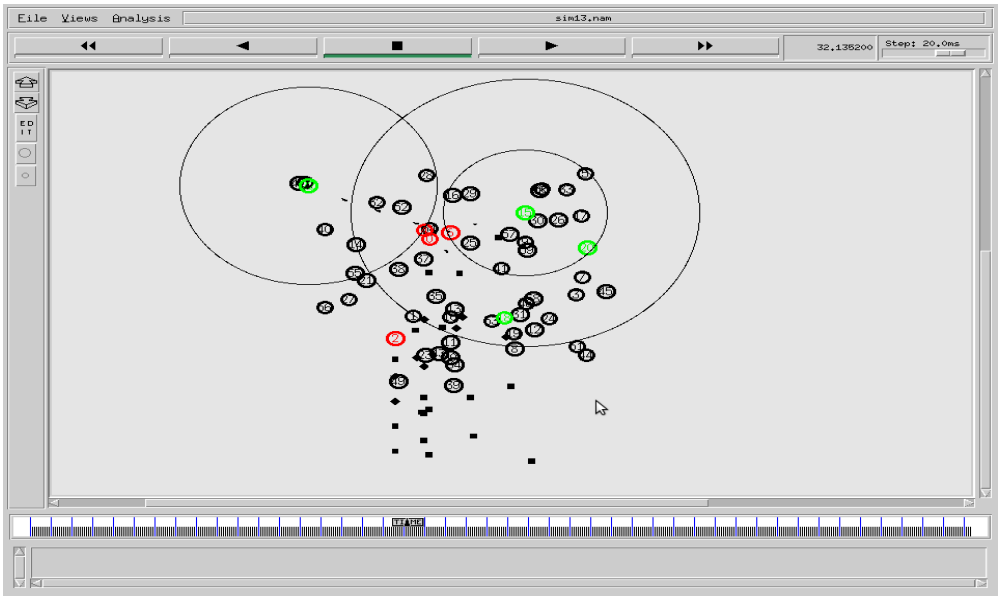

Figure 11. Nam window at (32 sec.) time

V. RESULTING GRAPH OF PROJECT

Below graphs are created from actual output data obtained in run time simulation. This output data can be converted in various graphs for observation made by using Microsoft excel Tool in windows.

- **Routing Overhead**- Routing Overhead is one of the performance parameter which gives the analytical study of routing protocols by using such parameters we can able to tell which on is good. Basically Routing Protocol is the performance parameter to find the best shortest routing path in between two consecutive nodes. High value graph shows the better performance and gives the best routing overhead.

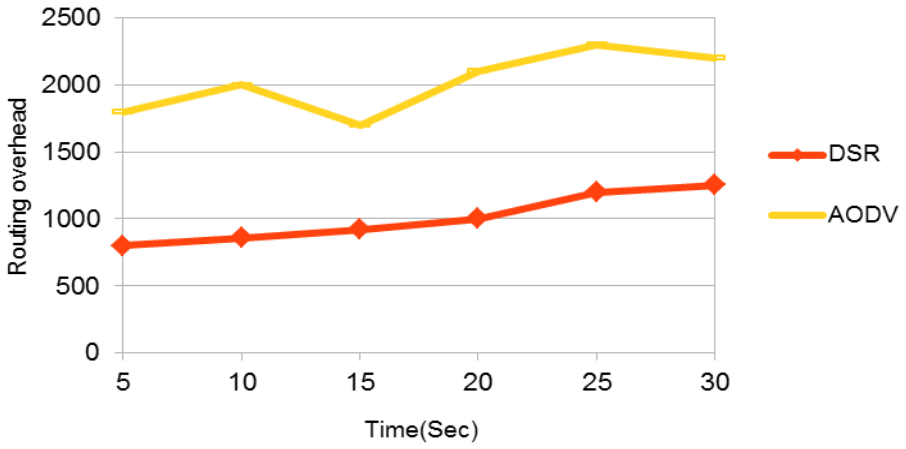

Figure 12. Routing Overhead Vs Time (Sec.)

- **Throughput**- Throughput is the no of packets that is passing through the channel in a particular time period. Unit of this throughput is Kbps. As per the observation when graph shows the high reading at the particular time period. That shows the higher is the throughput better is the particular Routing Protocol.

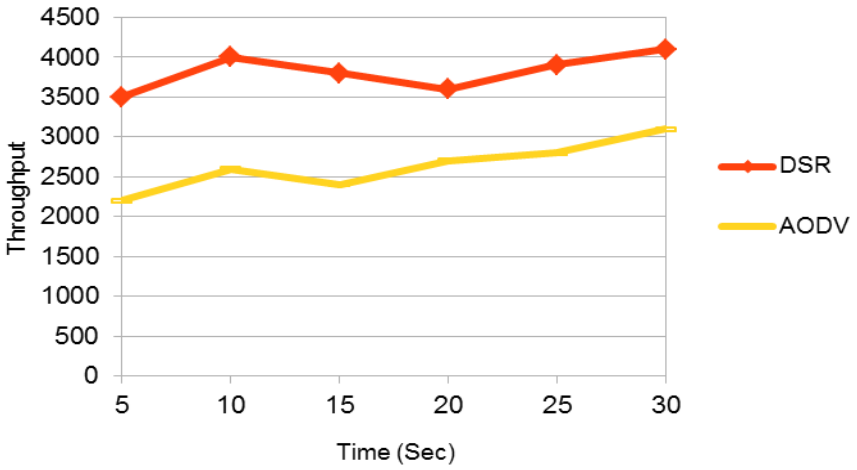

Figure 13: Throughput vs. Time (Sec.)

- **End-to-End Delay**- In which specific packet is transmitting from source node to destination node and calculating the difference between send time and received time is called End-to-End Delay. Many factors like route discovery, queening propagation and transfer time gives the performance of delay. In this case if value with lower reading graph shows better End-to-End delay and this routing protocol is good.

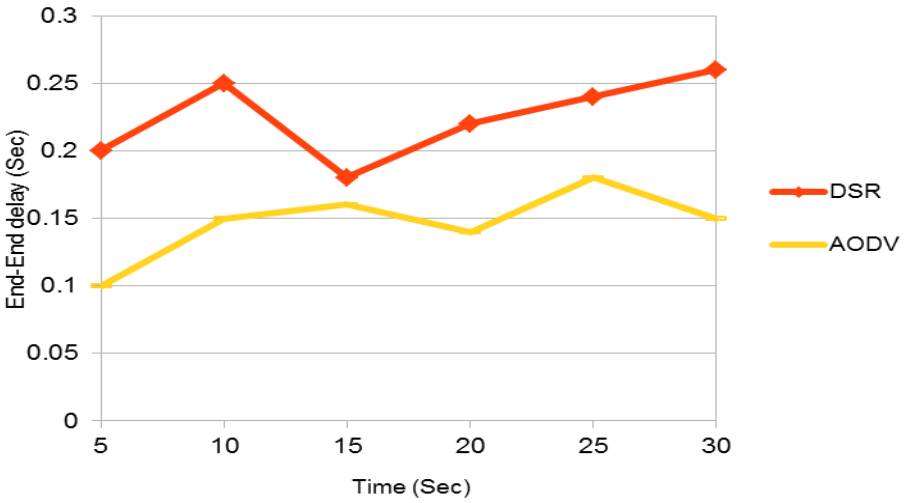

Figure 14. End-to-End delay Vs Time

VI. CONCLUSION

Conclusion of this project is based on the graphs which are obtained in actual run time simulation. Simulation did in Network Simulator (NS-2) specifically in network simulator 2.35 versions. Figure 12 shows the output graph of Routing Overhead as graph of higher value give the better routing protocol among the two, in this case AODV is superior according to definition of routing protocol which mentioned above. As per the definition of Throughput mentioned above higher value reading in Figure 13 which is DSR is the superior at the time of throughput part. As per the End-to-End delay concept Figure 14 give the clear indication that AODV has lesser value reading that's why AODV is having good End-to-End delay. From the observation of all graphical result obtained in Network Simulator we can conclude that AODV routing protocol is best among the two i.e., DSR and AODV.

VII. ACKNOWLWDGEMENTS

Authors like to do special thanks to Electronics and Telecommunication Engineering Department, Vidyalankar Institute of Technology, Mumbai University, India for providing appropriate information and related stuff. This work is accomplished and is successfully brought into existence due to the guidance and thorough attention of my guides Prof. Dattatray S. Bade sir and Prof. Ranjana R. Gite madam. I also wanted to do special thanks to my co-guide Prof. Ranjana R. Gite (Assistant Professor in Department of Electronics and Telecommunication, Vidyalankar Institute of Technology) for giving me her valuable time and co-operation. I would like to give a special thanks to my both guides to giving me a best opportunity to do a project work in area like Mobile Ad-hoc Networking. Kindly thanks to all staff members of Electronics and Telecommunication Department, my classmates for giving me there time and support for various problems and college authorities of Vidyalankar Institute of Technology.

REFERENCES

[1] Zeyad M Alfawaer, Saleem Al zoubi, "A proposed security subsystem for Ad hoc Wireless Networks", International forum on Computer Science Technology and Application, June 2009.

[2] Yih-Chun Hu, David B. Johnson and Adrian Perrig, "SEAD: Secure Efficient Distance Vector Routing for Mobile Wireless Ad hoc Networks", In Fourth IEEE Workshop on Mobile Computing Systems and Applications (WMCSA '02), June 2002, pp. 3-13, June 2002.

[3] Yih-Chun Hu, Adrian Perrig and David B. Johnson, "Ariadne: A Secure on Demand Routing Protocol for Ad-hoc Networks", in Proceedings of the 8th annual international conference on Mobile computing and networking (MobiCom) '02, September 23-26, 2002, Atlanta, Georgia, USA.

[4] Panagiotis, Papadimitratos and Zygmunt J. Haas, "Secure Routing for Mobile Ad hoc Networks", In Proc. SCS Communication Networks and Distributed Systems Modeling and Simulation Conference(CNDS2002), San Antonio, TX, January 27-3 1, 2002.

[5] S.k. Gupta and R.k. saket, "Performance matric comparison of AODV AND DSDR routing protocols in MANETs using NS2", proceeding in volume 7, issue 3, IJRRAS, June 2011.

[6] S. Ci et al., "Self-Regulating Network Utilization in Mobile Ad-Hoc Wireless Networks," IEEE Trans. Vehic. Tech., vol. 55, no. 4, July 2006, pp. 1302–10.

[7] B. Wu et al, "A Survey of Attacks and Countermeasures in Mobile Ad Hoc Networks," Wireless/Mobile Network Security, Springer, vol. 17, 2006.

[8] M. Zapata and N. Asokan, "Securing Ad Hoc Routing Protocols", ACM Wise, 2002.

[9] P. Yi et al., "A New Routing Attack in Mobile Ad Hoc Networks," Int'l. J. Info. Tech., vol. 11, no. 2, 2005.

[10] L. Buttyan and J.P Hubaux, "Stimulating cooperation in self-organizing mobile ad hoc networks", ACM/Kluwer Mobile Networks and Applications, vol. 8, no. 5, pp. 579 – 592, Oct 2003.

ISSN (e): 2250 – 3005 || Vol, 05 || Issue,02 || February – 2015 ||
International Journal of Computational Engineering Research (IJCER)

Wimax Emulator to Enhance Media and Video Quality

[1] Supriya. L. Shitole, [2] Prof.Ranjana.R. Gite
[1]M.E (EXTC), VIT/ Mumbai University, Mumbai, Maharashtra, India
[2]EXTC Dept, VIT/Mumbai University Mumbai, Maharashtra, India

ABSTRACT

Worldwide interoperability for Microwave Access (WiMAX) is one amongst the forthcoming generations (4G) promising networks to cover a number of the consumers' desires. It's a promising technology that's supposed to deliver mounted and additional recently, mobile broadband connectivity. It's a forthcoming technology it's primarily supposed to overcome the drawbacks of previous version. It's developed primarily because of the coverage area is larger compare all different networks, high information rates, it's simply deployable and secure Quality of service. WiMax may be a new technology handling provision of information over long distance using wireless communication methodology in many alternative ways that supported. IEEE 802.16 WiMax is claimed as another broadband instead of cable and telephone circuits. Worldwide interoperability for Microwave Access (WiMAX) technology will concentrate on Quality of Service (QoS). Quality of Service is an important parameter to evaluate performance of any Network. During this article, Quality of video is improved using WiMAX emulator. Applications like video and audio streaming, on-line play, video conferencing, voice over IP (VoIP) and File Transfer Protocol (FTP) demand a large range of QOS necessities like bandwidth and delay. IEEE 802.16 normal referred to as WIMAX provides broadband wireless access with QOS requirements. These paper have designed a system using WiMAX and RTP to enhance quality of media and video transmitted over network. These paper are progressing to use NS2 emulator so it will use external packets for simulation. These papers are using Ns2 for showing the complete network completely.

I. INTRODUCTION

In today's rising computational era everyone needs a device that's computationally robust enough to satisfy individuals want. WiMAX is that the one. WiMAX has already been adopted worldwide by operators attracted by promises of enormous throughput and coverage for broadband wireless access. Broadband may be a generic term used to describe high-speed networking services, that's a collection of data communication technologies with the capability to transmit vital amounts of information at a high rate, Supporting the delivery of a variety of digital services some or all of which may occur at the same time. It's typically a symmetrical service permitting quick in and outbound knowledge capability. There are several devices use to provide broadband connection like Wi-Fi.

Wi-Fi is generally used to give a Wi-Fi enabled device like computer, cell phone or personal digital assistant an Internet/LAN connection when in proximity of access purpose. Wi-Fi can even be used to produce a mesh network. Wi-Fi additionally permits connectivity in peer-to-peer mode. That allows devices directly connected to every different. WiMAX on the opposite hand, with its higher bandwidth and longer reach is planned to be connecting Wi-Fi hotspot for every different and to alternative a part of the internet providing a wireless different to cable and provide high speed mobile information and telecommunication service. This paper is shown on improving media and video quality by using WiMAX emulator. Since this paper is functioning in wireless networking area, on Ns2 primarily based WiMAX emulator. Emulator is same like simulator it uses external packets for simulation so it's known as emulator. During this case, emulator uses real time video frames for simulation. This paper will generate emulator in Ns2. These papers have used Ns2 as a result of its fully developed and analysis on Ns3 continues to be going. Ns2 has 2 main components Otcl and C++. Otcl is at front end and C++ resides at back end. Otcl is scripting language. Object creation is completed in Otcl and object

invocation is completed in C++. These papers have preferred WiMAX technology for transmission of media and video because of its following advantages:

• WiMAX will handle up to speed of 70 Mbps.

• WiMAX typically blankets a radius of 30 miles (50 km).

• WiMAX has most frequency of 10-66 gigahertz frequency.

• In WiMAX, large numbers of individuals get access to tower at same time whereas Wi-Fi user need to kind of fight to remain connected with specified access purpose.

• WiMAX proposes the complete range of security

These papers have designed a system using WiMAX and RTP to enhance quality of video and media transmitted over network. This paper has used RTP because of its features like recovering lost segments and re-sequencing of packets at application layer. This method design implements features like multicasting facility in network and to cut back packet drop ratio using WiMAX technology and RTP protocol.

Objective of the paper

• The applications logical ensue one module to a different among the system.

• The application is functioning consistent with the necessity specifications.

• The application is reliable and strong and it will recover graciously from failures.

• The application is simple to use and maintain as this paper as secure.

1.1 Technology Preview

NS2

NS-2 is an event driven packet level network simulator developed as a part of the VINT project (Virtual net Tested). This was a collaboration of the many institutes as well as UC Berkeley, AT and T, XEROX PARC and ETH. Version one of NS was developed in 1995 and with version two released in 1996. Version two enclosed a scripting language referred to as Object orientating Tcl (OTcl). It's an open source software system package accessible for each Windows 32 and Linux platforms. NS-2 has several and increasing uses including:

• To assess the performance of existing network protocols.

• To assess new network protocols before use.

• To run massive scale experiments impossible in real experiments.

• To simulate kind of IP networks.

1.1.1 NS2 Features

NS-2: Network simulator version two

• Discrete event simulator.

• Open source, supported two languages.

• C++, for the object oriented simulator, quick to run, slower to alter.

• OTcl, Object Tool command language, interpreter accustomed execute user's command, scripts, slower to run however modified quickly.

1.1.2 Support

• Wired networks: P2P links, LAN.

• Wireless networks: (Ad-hoc, Mobile, WLAN, Bluetooth, Satellite).

• Support emulation.

II. LITERATURE SURVEY

[1] Mojtaba Seyedzadegan and Mohamed Othman proposed IEEE 802.16: WiMAX summary, WiMAX architecture that WiMAX may be a new technology handling provision of information over long distance using wireless communication methodology in many various ways in which. Supported IEEE 802.16 WiMAX is claimed as another broadband instead of cable and telephone circuit. It's a fast technical summary and covers: WiMAX overview (Fundamental Concept; Technology; standard update) and WiMAX architecture. WiMAX Technology is facing several hurdles in market whereas it's some great benefits that create it a technology of nowadays.

[2] Gyan Prakash, Sadhana Pal proposed WiMAX Technology and Its Applications presents the features of the worldwide interoperability for Microwave Access (WiMAX) technology and future applications of WiMAX. A discussion is given by comparison WIMAX with DSL (Digital subscriber line) & Cable and wireless local area network (Wi-Fi). WiMAX may be a global broadband wireless standard. Several developing countries merely don't have the infrastructure to support either cable or telephone circuit broadband technologies. In fact, several such countries are already wide using proprietary broadband wireless technologies. Even in such regions to this paper, it's impossible that either Cable or telephone circuit technologies would disappear. The basic infrastructure usually dictates that the most affordable solutions can predominate. In several areas in developing nations, it should be cheaper to deploy Cable and telephone circuit within the cities a minimum of for fixed applications, whereas WiMAX can dominate outside of major cities.

[3] Min Xing, Siyuan Xiang, Lin Cai, proposed a time period adaptive algorithmic rule for Media and video streaming over Multiple Wireless Access Networks that the way to with efficiency and cost-effectively utilizes multiple links to boost media and video streaming quality desires investigation. So as to take care of high media and video streaming quality whereas reducing the wireless service price. In this, first, they formulate the media and video streaming method over multiple links as an MDP drawback. To realize smooth and top quality media and video streaming, this paper outlines many actions and reward functions for every state. Second, this paper proposes a depth-first period of time search algorithmic rule. The proposed adaptation algorithmic rule can take many future steps into consideration to avoid playback interruption and accomplish higher smoothness and quality.

III. PROBLEM DEFINATION

The major limitation are Specialized instrumentation required for utilizing full practicality of wimax you wish specialized hardware with dedicated antennas. Interference might have an effect on connectivity because the wimax uses radio waves; it's susceptible to interference caused by different instrumentation. The major limitation with any wireless technology is that it's very exhausting to satisfy its security desires. Same is that the case with Wimax the hackers can even attack this connection and may steal some helpful info. The intruders are capable enough of repetition the Mac frames therefore they will break the safety codes. The hackers will even hijack the full network by creating use of denial of service attack. This security threat will devastate the complete connections. Another limitation that comes with the Wimax is that hackers have devised manner to masquerade because the base station during this way, the confidential information is accessed. The concerned departments like Wimax forum try exhausting to overcome this major limitation as this may cause the individuals to refrain from using this technology. Numerous software's present within the market alter the hackers and crackers to decipher the codes and exploit info. Therefore given that the range is low the Wimax technology operates considerably.The infrastructure demand for 802.16 technologies needs distributed network that is complicated and costly to make. The technology is therefore costly that solely massive names like Intel are able to manufacture silicone chips that are integrated with the PCs to extend the efficiency of the system. The marketplace for Wimax continues to be not terribly attractive as there are not enough hardware devices that support this technology. Immense investment is needed to produce equipments that may correspond with this technology. But during this time of recession who would invest such amount quantity in new technology like Wimax. Moreover people are a lot of familiar with use Wi-Fi and that they notice it a lot of users friendly. Thus it's not possible for them to change to the current new technology.

The IT experience required to take care of its security is additionally rare. In different words we will say that individuals don't seem to be attentive to handling the pros and cons related to this technology. This technology has didn't prove it as an independent technology. Individuals take into account it as a 3G technology and also the one exchange broadband wired DSL. The Wimax claims to figure well with the mobile technologies, however still they're not adopted. This is often due to the restricted devices that add accordance with WiMax. The antennas that enhance the efficiency of network are extremely tiny and their electricity power demand is more.

Generally for transmitting videos and something Wi-Fi technology is employed. It's not reliable due to its speed. This paper are coming up with our system to get rid of issues with videos like slow streaming, and slow transmission rate of packets. This paper is transmitting our packets through Network emulator. These papers are getting to use WiMAX technology and RTP for it. WiMAX technology is employed over Wi-Fi. There are several drawbacks of Wi-Fi over WiMAX.

- Wi-Fi is slower than WiMAX. Wi-Fi will transmit up to 54 mbps only. WiMAX will transmit up to 70 Mbps.
- Wi-Fi range is minimum i.e. 30m only as compared to WiMAX (50 km).
- Wi-Fi frequency is extremely low i.e. 5 gigahertz as compared to WiMAX.

These papers are progressing to use NS2 emulator so it will use external packets for simulation. These papers are using Ns2 for showing the complete network nearly. To implement WiMAX physically isn't cheap to us; therefore this paper is using NS2.

IV. PROPOSED METHODOLOGY

4.1 System Architecture

The proposed network architecture is shown in Fig.3. 1. During this design, one computer is employed as a media server and several other Clients are used as video clients. One pc running ns-2 is employed as a WiMAX network emulator that mimics the impairments introduced by the wireless channel in time period. The media and video streaming packets generated by the media server are fed within the WiMAX emulator then multicast to clients. Every client will then show the received video stream severally. The network simulator ns-2 could be a distinct event simulator targeted at networking analysis.

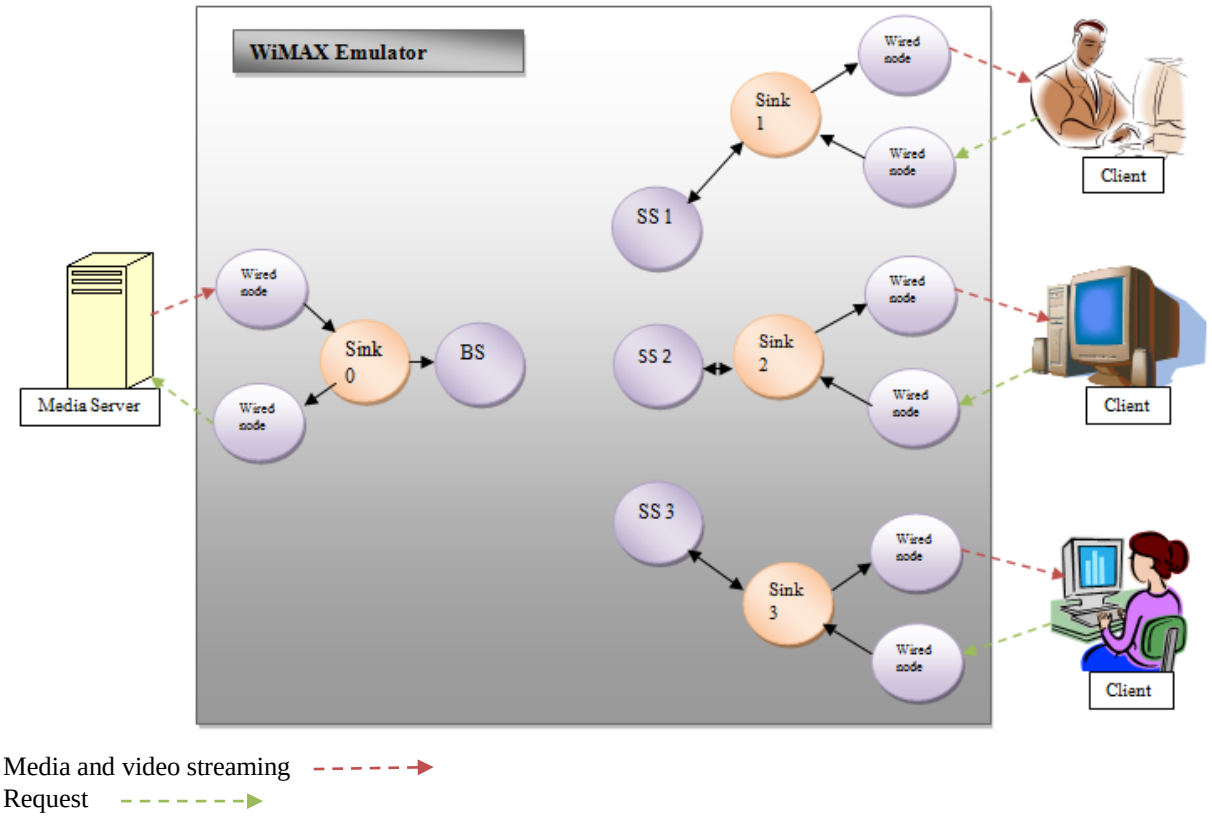

Figure 4.1: System architecture

Ns-2 provides modules for simulation of communication protocol, routing, and multicast protocols over wired and wireless (local and satellite) networks. A similar ns-2 WiMAX module utilized in the system level simulator of WiMAX Forum is additionally utilized in this emulator.

4.1.1. System Feature

1. WiMAX Transmission

• Description and Priority

The media and video streaming aren't quick. They continuously take more time to load. Particularly for multimedia system information, dependability isn't as necessary as timely transmission. Therefore this paper is using WiMAX technology for quick transmission. Ultimately quality of media and video gets improved because of WiMAX.

• Response Sequences

User means that client request for media and Video packets then Packets are transmitted through Ns2 emulator using this feature i.e. WiMAX. Ultimately transmission rate raised.

2. Functional necessities

• Clients should be within the range of WiMAX i.e. 50 km. It needs massive power for transmission.
• It is needed to put in a further WiMAX card to extend the efficiency and strength of the signals.
• The antennas that enhance the efficiency of network are extremely tiny and their electricity power demand is additional.

4.2 Data Flow Diagram

The Data flow diagram (DFD) is that the graphical illustration of the processes and also the flow of information among them. An information flow diagram illustrates the processes, information stores, external entities and therefore the connecting information flows in an exceedingly system. it's a typical observe to draw a context- level information flow diagram initial which shows the interaction between the system and outdoors entities. This context- level DFD is then "exploded" into a close DFD.

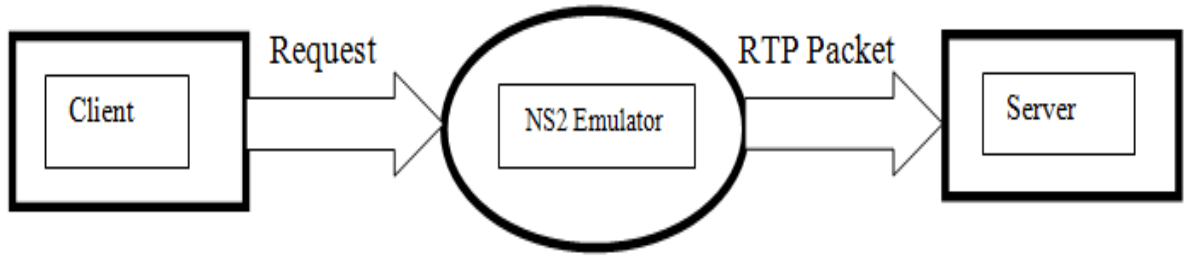

Figure 4.2.1 Data flow diagram1

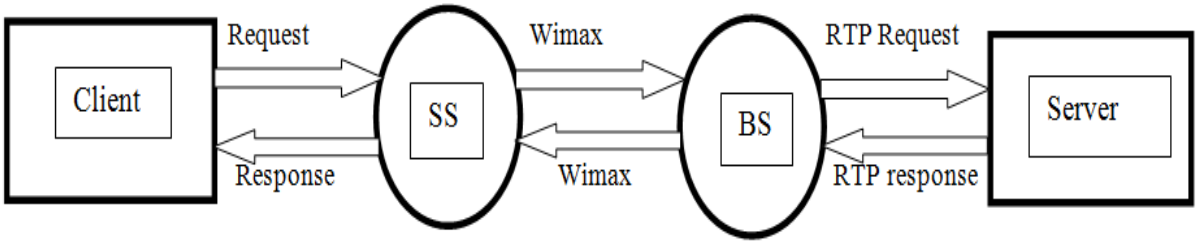

Figure 4.2.2 Data flow diagram2

V.CONCLUSION

Thus this paper presented an NS-2 based mostly IEEE 802.16 network emulator for supporting media and video streaming services. The proposed emulator will emulate completely different channels and real propagation conditions. The video is displayed on client aspect and permits for analysis of application-level media and video streaming metrics. The performance of the proposed emulator was evaluated once time period services are taken under consideration. Wi-Fi and WiMAX transmission are compared through this overall transmission of media and video from server. Finally this paper have Shown that if WiMAX technology is employed instead of Wi-Fi. This paper got additional responsibility and sensible network performance overall.

REFERENCES

[1] Mojtaba Seyedzadegan and Mohamed Othman "IEEE 802.16: WiMAX Overview, WiMAX Architecture "International Journal of Computer Theory and Engineering, Vol. 5, No. 5, October 2013.

[2] Gyan Prakash, Sadhana Pal, International Journal of Engineering Research and Applications (IJERA) "WIMAX Technology and Its Applications"

[3] Min Xing, Student Member, IEEE, Siyuan Xiang, Member, IEEE, and Lin Cai, Senior Member, IEEE"A Real-Time Adaptive Algorithm for Media and video streaming over Multiple Wireless Access Networks" VOL. 32, NO. 4, APRIL 2014

[4] Mehdi Alasti and Behnam Neekzad, ClearwireJie Hui and Rath Vannithamby, Intel Labs" Quality of Service in WiMAX and LTE Networks"

[5] Johan ElgeredA, A.SafaeiMoghaddamA, and Benjamin Vedder B, "How Quality of Service (QoS) is achieved in WiMAX (IEEE 802.16)"

[6] Sanjay Kumar Dhurandher, Isaac Woungang, Mohammad S. Obaidat, Fellow, IEEE, Kirti Kumar, Mamta Joshi, and Monika Verma. "A Distributed Adaptive Admission Control Scheme for Multimedia Wireless Mesh Networks".

ISSN (e): 2250 – 3005 || Vol, 05 || Issue,02 || February – 2015 ||
International Journal of Computational Engineering Research (IJCER)

Anonymous Communication for Providing More Privacy and Security

[1]Satish .K. Hatwar , [2] Prof.Vijay.M. Purohit
[1]M.E (EXTC), VIT/ Mumbai University Mumbai, Maharashtra, India
[2]EXTC Dept, VIT/Mumbai University, Mumbai, Maharashtra, India

ABSTRACT

A peer-to-peer network within which interconnected nodes ("peers") shares resources amongst one another without the utilization of centralized administrative systems. In communication network, the foremost common problems are privacy and security. During this network, anonymity is additionally crucial issue. The foremost anonymity for peer-to-peer users involved with the users' identities and actions which may be discovered by the other members. An intruder will get info regarding the content of the information, the sender's and receiver's identities. There are several approaches proposed to produce anonymous peer-to-peer communications. This paper provides anonymous communication with additional privacy and security. Anonymous approaches are designed with the subsequent 3 goals: to safeguard the identity of provider, to safeguard the identity of requester and to safeguard the contents of transferred information between them. This paper presents a new peer-to-peer approach to realize anonymity between a requester and a provider in peer-to-peer networks with trustworthy servers known as supper node in order that the provider won't be able to determine the requester and no alternative peers will determine the two act parties with certainty. This paper shows that the proposed algorithmic rule improved reliableness and has a lot of security. This algorithmic rule, based on onion routing and organization, protects transferring information against traffic analysis attack. The ultimate goal of this anonymous communications algorithmic rule is to permit a requester to speak with a provider in such a way that no-one will confirm the requester's identity and therefore the content of transferred information.

I. INTRODUCTION

In today's rising computational area everyone needs a communication network with full privacy and security. The user need security their personal data and their privacy. Protecting their data and respecting their privacy is prime to maintaining their trust. The privacy and security programs govern in such the simplest way that user data from ensuring the confidentiality of their personal communications and protecting and securing their data. The user is also involved regarding privacy and security of their personal data as they use communication networks. This paper facilitate them user manage a good range of privacy and security which will have an effect on them once using communication network.

Risk includes:

1) Confidentiality of their personal and personal communication
2) Collection of their personal problems
3) Security of their personal data
4) Use of their personal data

There were several approaches to provide privacy and security in wireless communication area. One amongst the means will offer the privacy and security to user data by anonymous communication. In fact, anonymity will be considered a special encryption on the messages to hide correlations between the messages and also the senders. The anonymizing method is performed throughout publishing, communication, searching, and retrieving. Therefore, protecting the messages in communication is important for anonymity. There are several approaches proposed to produce anonymous communications. Existing System are:

Crowds

These are an anonymous web dealing protocol and one amongst the oldest anonymizer networks and only offer requester anonymity. A crowd contains a closed group of collaborating nodes known as jondos and uses a trustworthy third party as centralized crowd membership server referred to as mixer. The new jondo requests crowd membership from the blender, then the blender replies with a listing of all current crowd members. After that, the blender in- forms all previous members of the new member. The requester node selects at random a jondo from the member list and forwards the request to that. The subsequent nodes decide at random whether to forward the request to a different node or to send it to the server.

Hordes

Hordes provide requester anonymity by adopting the Crowds probabilistic forwarding mechanism, and reach provider anonymity by acting a multicast transmission. Since the replying path is that the shortest multicast path from the provider to the requester, Hordes significantly reduces the latency. However, peers in Hordes should participate within the multicast relaying, that incurs an enormous traffic and wastes the bandwidth.

The limitations of existing system contain some attacks against the anonymous communication. The attacker is also system members or intruders from outside.

Therefore to beat the limitation of existing systems there's another conception of using third party as a trusty node is named as supper node in peer to peer network. A peer-to-peer network may be a dynamic and scalable set of computers (also referred as peers). The peers will join or leave the network at any time. The fundamental idea of a peer-to-peer network is to create a virtual layer over the application or network layer. In such AN overlay network all peers interconnect with one another. All peers are both the resource consumers and providers. Currently, file-sharing is that the most well-liked application in peer-to-peer systems.

Peer-to-peer networks are often divided into structured and unstructured categories. Structured peer-to-peer networks map every peer similarly as the index data of every resource into a globally position like Distributed Hash Table (DHT) in an exceedingly highly organized structure. This paradigm has 2 main drawbacks that limit the implementation in real world. First, it cannot support the fuzzy question and second, the DHT structure has massive overhead to individual peers and too tough to maintenance. In Unstructured peer-to-peer networks, peers will join and leave networks merely and there don't seem to be any structured patterns there. This paper focuses on the unstructured peer to-peer networks as a result of this sort of network are best to implement and provide security and anonymity.

There are 3 totally different roles that every peer will play in peer-to-peer networks: a provider (also known as a responder, host or publisher) to supply services upon requests, a requester (also known as AN initiator) to request services, and a proxy (also known as an intermediate peer) during which routs information from a peer to a different peer. Consistent with these roles there are 3 aspects of anonymity in peer-to-peer networks.

Provider anonymity that hides the identity of a provider against different peers, requested anonymity that hides a requester's identity and Mutual anonymity that hides each provider's and requester's identities. Within the most demanding version, achieving mutual anonymity needs that neither the requester, nor the provider will determine one another, nor no alternative peers will determine the two act parties with certainty.

1.1. DUAL-PATH TECHNIQUES FOR REQUESTER ANONYMITY

This paper present the algorithmic rule for achieving requester anonymity with the help of trustworthy third party referred to as supper node that solely keeps networks map. Every peer should send a trigger signal to supper node either sporadically or once it desires to join/leave the network. The ultimate goal of anonymous peer-to-peer networks is to cover the user identities, like the user's ID and IP address. The proposed algorithmic rule is that the means that the requester will connect with arbitrary provider and transfer information with it, in order that any peers like

Provider cannot find the requester's identity. The fundamental principle is relay messages from requester to provider through multiple intermediate peers so truth origin and destination of the messages is hidden from alternative peers. The requester creates a dual-path that contains a path to send request and another to induce respond from provider so the provider cannot compromise the requester's identity. The transferred information between requester and provider is encrypted to safeguard it against eavesdropping. So, during this algorithmic rule there are 2 methods to attach requester to provider: request path and response path. Each of them is initiated by requester at random. The requesters will modification these methods at random whereas connecting to provider at any time. Fig.1.1. illustrates a request and response paths within the network.

Each peer should join the network for obtaining services. The new peer requests a listing of peers within the networks from the supper node. The supper node replies with a listing of all current peers. Afterward supper node informs all peers of the new member. For departure the networks, the peer should send a removing signal for informing the supper node that it desires to go away there. Then, the supper node updates the list of peers what is more it announces alternative peers automatically. Every peer should send a trigger signal to the

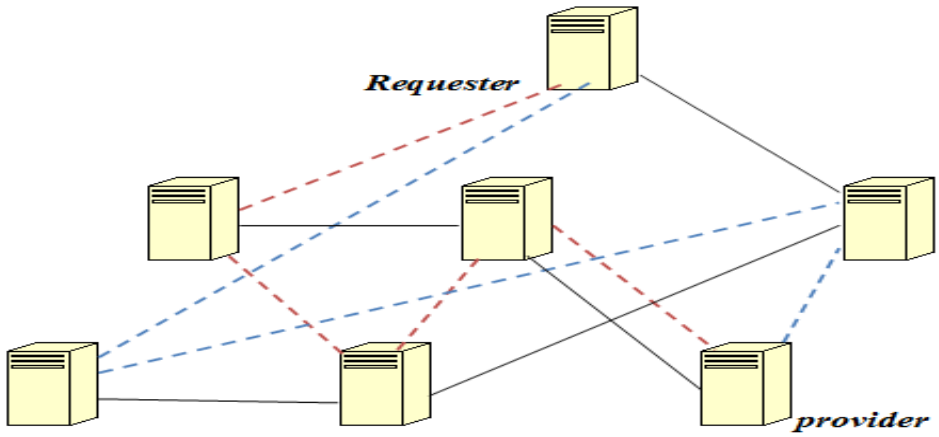

Fig.1.1.Dual path paradigm

Supper node sporadically, to inform the supper node that it's alive. When an amount of time, if the supper node doesn't sense any trigger signal from a peer, it'll take away the peer from the list.

II. LITERATURE SURVEY

[1] A. K. Datta, M. Gradinariu, M. Raynal, and G. Simon proposed Anonymous Publish/Subscribe in P2P Networks, the fundamental plan of a peer-to-peer network is to create a virtual layer over the application or network layer. In such an overlay network all peers interconnect with one another. All peers are both the resource consumers and providers. Currently, file-sharing is that the most well liked application in peer-to-peer systems.

[2] R.-Y. Xiao proposed Survey on anonymity in unstructured peer-to-peer systems that Peer-to-peer networks will be divided into structured and unstructured categories. Structured peer-to-peer networks map every peer still because the index info of every resource into a globally position like Distributed Hash Table (DHT) during an extremely organized structure. This paradigm has two main drawbacks that limit the implementation in real world. First, it cannot support the fuzzy question and Second, the DHT structure has massive overhead to individual peers and too tough to maintenance. In Unstructured peer-to-peer networks, peers will join and leave networks merely and there don't seem to be any structured patterns there. This paper focuses on the unstructured peer-to- peer networks as a result of this sort of network are best to implement and provide security and anonymity.

[3] L. Xiao, Z. Xu and X. Zhang Mutual anonymity Protocols for Hybrid Peer-to-Peer Systems proposed there are 3 completely different roles that every peer will play in peer-to-peer networks: a provider (also known as a responder, host or publisher) to provide services upon requests, a requester (also known as an initiator) to request services, and a proxy (also known as an intermediate peer) during which routs information from a peer to a different peer. consistent with these roles there are 3 aspects of anonymity in peer-to-peer networks: provider anonymity that hides the identity of a provider against alternative peers, Requester anonymity that hides a requester's identity and Mutual anonymity that hides each provider's and requester's identities. Within the most demanding version, achieving mutual anonymity needs that neither the requester, nor the provider will determine one another, nor no alternative peers will determine the two communication parties with certainty.

[4] Satoshi Togawa, Kazuhide Kanenishi and Yoneo Yano Peer-to-Peer File Sharing Communication Detection System using the Traffic Feature Extraction proposed a traffic visual image system for P2P communication detection, and that we explained a configuration of the paradigm system. And, we have a tendency to explained the results of experimental use and examine. This technique extracts records of P2P communication activities from the collected IP packets and therefore the collected DNS question results, and presents the administrator with a feature map. We have a tendency to develop a paradigm system and experimented to verify its effectiveness. It had been shown that an administrator may examine the results of the feature map.

III. PROBLEM DEFINATION

The limitations of existing system contain some attacks against the anonymous communication. The attackers could also be system members or intruders from outside. The ultimate target is to locate the requester, provider, and what they're transferring.

Time-to-Live Attacks: Time-to-live counters verify the utmost number of hops for a message and are utilized in most peer-to-peer networks to avoid flooding. If an attacker will send a request to a node with such a low time-to-live counter that the packet can most likely not be forwarded, any response relieves that note as the provider.

Denial of Service Attacks: Denial of service attacks may be significantly awkward once nodes will act anonymously, as this might mean that the node acting a Denial of service attack couldn't be known and removed from the system. Whereas anonymous systems cannot stop all Denial of service attacks.

Statistical Attacks: Any attackers are able to get statistical data over a period of long term. Net- works could probably safe for a single run however could reveal data regarding the identities of their peers once all the noticeable messages of a longer run are analyzed for patterns.

Traffic analysis: Making use of the traffic information of a communication to extract data. Interception and cryptanalytic are 2 techniques to analyze the transferred information. The reliable anonymous approach must safe against these types of attacks.

To overcome the on top of limitations exists by the previous systems like Crowds, Hordes, Tor, etc., this paper implementing a system with anonymous communication. During this system, maintaining the anonymity of the sender and also the privacy of the information being transferred between requester and provider.

IV. PROPOSED METHODOLOGY

The proposed approach provides requester anonymity to safeguard the identity of the requester and therefore the transferred information against different peers specially the intruders. The proposed algorithmic rule relies on Onion Routine mechanize. Onion Routing is that the technique during which the requester and also the provider communicate with one another anonymously by means of some intermediate peers referred to as onion routers. During this technique, messages route between onion routers. The messages encrypted with onion router's public key. Every onion router learns solely the identity of consequent onion router.

4.1. Process

1) A requester sends a signal to the supper node and requests a list of all current peers.
2) The supper node replies to the peer and sends a list of the live peers within the networks.
3) The requester chooses 2 sets of peers arbitrarily. One in all them is employed for request and therefore the different and also for the response.
4) The requester, requests via the request path and also the response path is embedded in request path by the requester
5) When the provider needs to response the request, it sends the respond message to the peer that determines within the tail of the received message from the requester

4.2. System architecture

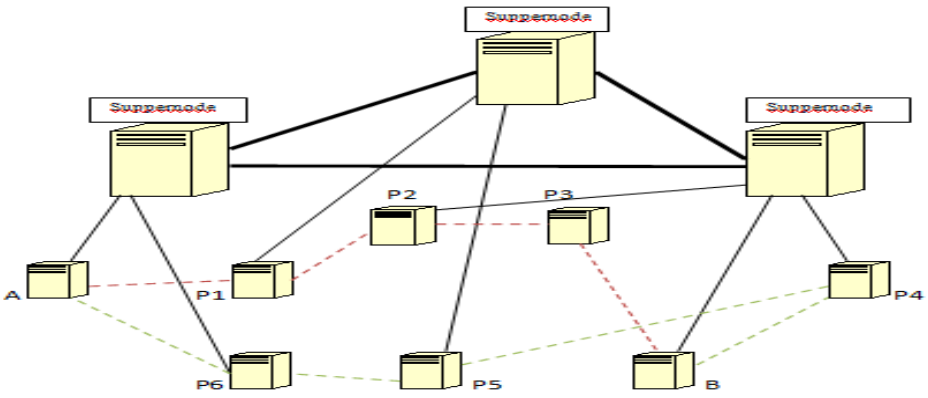

Request Path
Response Path
Communication between Peers and Suppernodes

Fig.4.2.1. System design

Let's take into account peers P1, P2 and P3 that are chosen arbitrarily by requester for request path and P4, P5 and P6 that are chosen for response path. Additionally think about M, the message that the requester needs to send. During this figure, "A" acts as a requester and "B" acts as a provider. "A" creates 2 methods to communicate with "B" and sends messages via them. "A" should rely messages through P1, P2 and P3 (request path) to send them to provider. Additionally "A" receives the response of its request through P4, P5 and P6 (response path).

After the requester (A) creates the Dual-Path, currently it should create the packet of the messages. To create the packets, the requester (A) should encode the messages by intermediate peers public keys during a layer by layer structure, like onion routing mechanism.

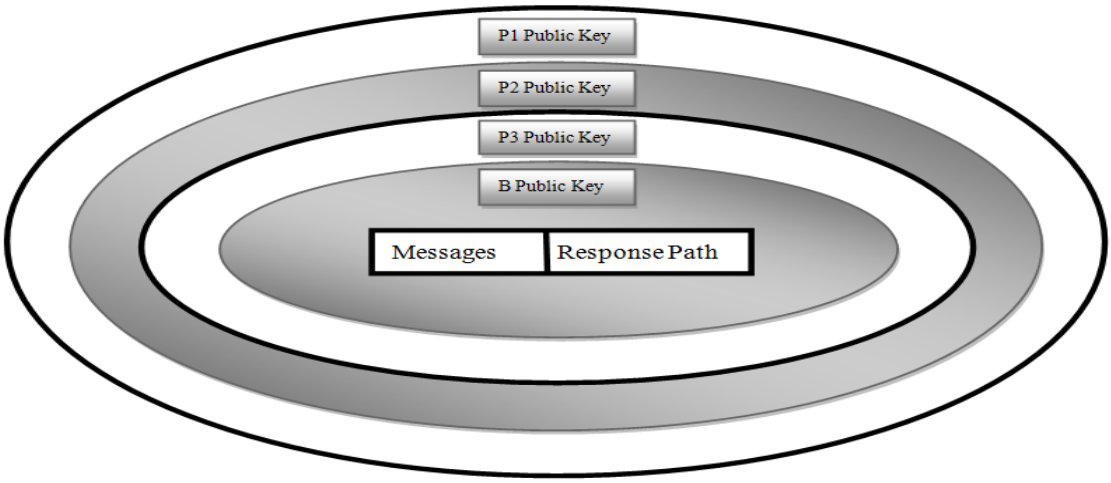

Fig.4.2.2. The structure of request path in wrapped message

When the provider (B) receives the packets, it extracts the message and also the response path packet. Every response packet has 2 elements, the "Next Peer" and also the "Tail". The "Next Peer" part contains subsequent peer during which the message should be sent to that. When extracting the response path packet by provider (B), it encrypts the response message by P4 public key and attaches the Tail" a part of response path packet at end of it. Currently the provider (B) sends the wrapped message to P4. P4 does same method and sends the received messages to P5. P5 sends the messages to P6 and finally P6 sends the messages to the requester (A).

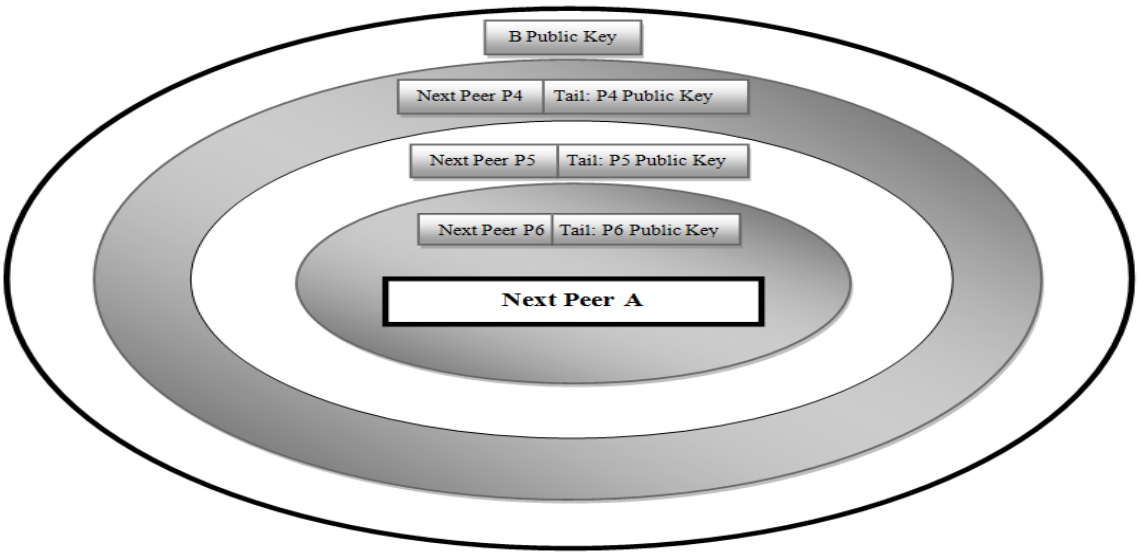

Fig.4.2.3. The structure of response path in wrapped message

4.3. Data Flow

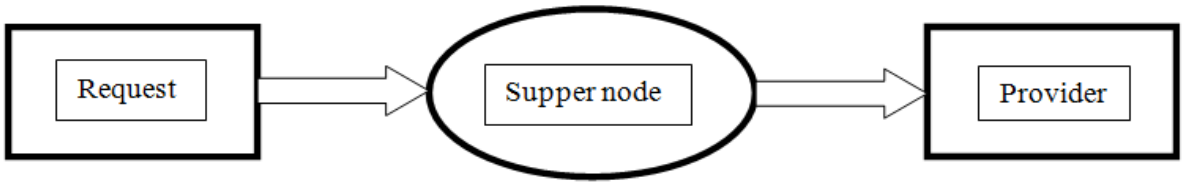

Fig.4.3.1.Data Flow 1

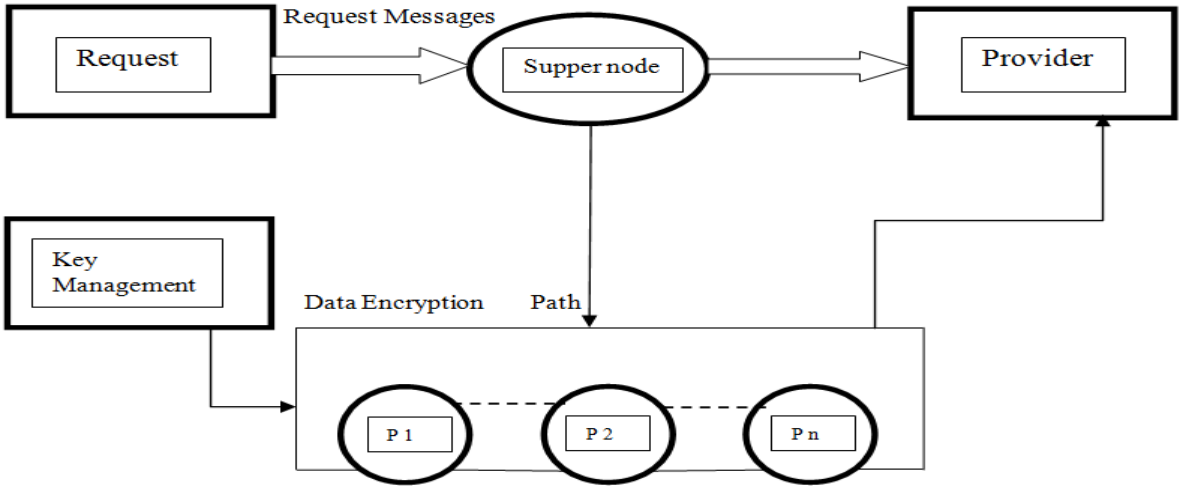

Peer: P1, P2…Pn

Fig.4.3.2.Data Flow 2

V.CONCLUSION

The proposed peer-to-peer anonymous algorithmic rule provides versatile layer for the requester to decide on dual-path to attach to the provider. This algorithmic rule provides additional responsibility and additional Security. additionally it will increase its fault tolerance because the connection between the requester and also the provider isn't depend upon intermediate peers, and if every intermediate peer downs, the requester will modification the dual- path to continue its connectivity. We tend to algorithmic rule our rule for achieving requester anonymity with the help of trusty third party referred to as supper node that only keeps networks map. Super-nodes are used to recover the group formation of network nodes. Super-nodes are generated based on this data to represent the closeness between nodes.

REFERENCES

[1] *A. K. Datta, M. Gradinariu, M. Raynal, and G. Simon*, Anonymous Pub- lish/Subscribe in P2P Networks, in Proc. International Parallel and Distributed Pro- cessing Symposium (IPDPS'03), pp. 47a, 2003.

[2] *R.-Y. Xiao*, Survey on anonymity in unstructured peer-to-peer systems, Journal of Computer Science and Technology, pp. 660-671, 2008.

[3] *L. Xiao, Z. Xu, and X. Zhang*, Mutual Anonymity Protocols for Hybrid Peer-to-Peer Systems, in Proc. of the 23rd International Conference on Distributed Comput- ing Systems, pp. 68.

[4] *Satoshi Togawa, Kazuhide Kanenishi and Yoneo Yano*, Peer-to-Peer File Sharing Communication Detection System using the Traffic Feature Extraction.2006 IEEE International Conference on Systems, Man, and Cybernetics October 8-11, 2006, Taipei, Taiwan.

[5] *Guowei Huang, Zhi Chen, Qi Zhao Gongyi Wu*, Activity Monitoring to Guarantee File Availability in Structured P2P File-sharing Systems. 26th IEEE International Symposium on Reliable Distributed Systems

[6] *Bing Li and Dijiang Huang*, Modeling Anonymous MANET Communications Using Super-nodes. 2013 IEEE Military Communications Conference.

ISSN (e): 2250 – 3005 || Vol, 05 || Issue,02 || February – 2015 ||
International Journal of Computational Engineering Research (IJCER)

Independent Functions of Euler Totient Cayley Graph

[1,] K.J. Sangeetha, [2,] B. Maheswari
[1,] PGT Mathematics, A.P. Model School, Kammanapalli, Chittoor dist.
[2,] Department of Applied Mathematics, Sri Padmavati Women's University,
Tirupati - 517502, Andhra Pradesh, India.

ABSTRACT

Graph Theory is the fast growing area of research in Mathematics. The concepts of Number Theory, particularly, the "Theory of Congruence" in Graph Theory, introduced by Nathanson[7], paved the way for the emergence of a new class of graphs, namely, ***"Arithmetic Graphs". Cayley graphs*** *are another class of graphs associated with the elements of a group. If this group is associated with some arithmetic function then the Cayley graph becomes an Arithmetic graph. The Cayley graph associated with Euler Totient function is called an* ***Euler Totient Cayley graph*** *and in this paper we study the independent Functions of Euler Totient Cayley graphs. This paper is devoted to the study of independent functions of Euler Totient Cayley Graph in two cases when n is prime and when n is non-prime.*

KEYWORDS: *Euler Totient Cayley Graph, independent set, independent function.*

I. INTRODUCTION

The concept of the domination number of a graph was first introduced by Berge [3] in his book on graph theory. Ore [8] published a book on graph theory, in which the words 'dominating set' and 'domination number' were introduced. Allan and Laskar [1], Cockayne and Hedetniemi [4], Arumugam [2], Sampath kumar [9] and others have contributed significantly to the theory of dominating sets and domination numbers. An introduction and an extensive overview on domination in graphs and related topics are given by Haynes et al. [5].

II. EULER TOTIENT CAYLEY GRAPH AND ITS PROPERTIES

Definition 2.1: The **Euler totient Cayley** graph is defined as the graph whose vertex set V is given by $Z_n = \{0, 1, 2, ..., n-1\}$ and the edge set is E = {(x, y) / x – y ∈ S or y – x ∈ S} and is denoted by $G(Z_n, \varphi)$. where S denote the set of all positive integers less than n and relatively prime to n. That is $S = \{r / 1 \le r < n \text{ and } GCD(r, n) = 1\}$, $|S| = \varphi(n)$.

Now we present some of the properties of Euler totient Cayley graphs studied by Madhavi [6].

1. The graph $G(Z_n, \varphi)$ is $\varphi(n)$ – regular and has $\frac{n\varphi(n)}{2}$ edges.
2. The graph $G(Z_n, \varphi)$ is Hamiltonian and hence it is connected.
3. The graph $G(Z_n, \varphi)$ is Eulerian for n ≥ 3.
4. The graph $G(Z_n, \varphi)$ is bipartite if n is even.
5. The graph $G(Z_n, \varphi)$ is complete if n is a prime.

III. INDEPENDENT SETS AND INDEPENDENT FUNCTIONS

Definition 3.1: Let G(V, E) be a graph. A subset I of V is called an **independent set (IS)** of G if no two vertices of I are adjacent in G.

Definition 3.2: Let G(V, E) be a graph. A function $f : V \to [0,1]$ is called an **independent function (IF),** if for every vertex $v \in$V with $f(v) > 0$, we have $\sum_{u \in N[v]} f(u) = 1$.

RESULTS

Theorem 3.3: Let I be an IS of $G(Z_n, \varphi)$. Let a function $f : V \to [0,1]$ be defined by

$$f(v) = \begin{cases} 1, & \text{if } v \in I, \\ 0, & \text{otherwise} \end{cases}.$$

Then f becomes an IF of $G(Z_n, \varphi)$.

Proof: Consider $G(Z_n, \varphi)$. Let I be an IS of $G(Z_n, \varphi)$.

Let f be a function defined as in the hypothesis.

Case 1: Suppose n is a prime. Then $G(Z_n, \varphi)$ is a complete graph. So every single vertex forms an IS of $G(Z_n, \varphi)$ and every neighbourhood N[v] of $v \in V$ consists of n vertices.

Then $\sum_{u \in N[v]} f(u) = 1 + \underbrace{0 + 0 + \ldots\ldots + 0}_{(n-1)-times} = 1, \quad \forall v \in V$.

Hence f is an IF of $G(Z_n, \varphi)$.

Case 2: Suppose n is not a prime. Then $G(Z_n, \varphi)$ is $|S|$- regular graph. Let $|S| = r$.

Let I be an independent set of $G(Z_n, \varphi)$. Then $|I| > 1$.

If $v \in I$ then $f(v) > 0$ and since v contains no other vertex of I in its neighbourhood we have

$$\sum_{u \in N[v]} f(u) = 1 + \underbrace{0 + 0 + \ldots\ldots\ldots + 0}_{(r-1)-times} = 1.$$

Thus f is an IF of $G(Z_n, \varphi)$.

Therefore f is an IF of $G(Z_n, \varphi)$ for any n.

Remark 3.4: Let $f : V \to [0,1]$ be defined by

$$f(v) = \begin{cases} k, & \text{if } v \in I, \\ 0, & \text{otherwise} \end{cases}.$$

where 0 < k < 1.

Then f cannot be an IF of $G(Z_n, \varphi)$.

This is because for $v \in I$, $\sum_{u \in N[v]} f(u) = k < 1$.

So for $f(v) > 0$, $\sum_{u \in N[v]} f(u) = k < 1$, which implies that f cannot be an IF.

Illustration 3.5: Consider $G(Z_{11}, \varphi)$. The graph is given below.

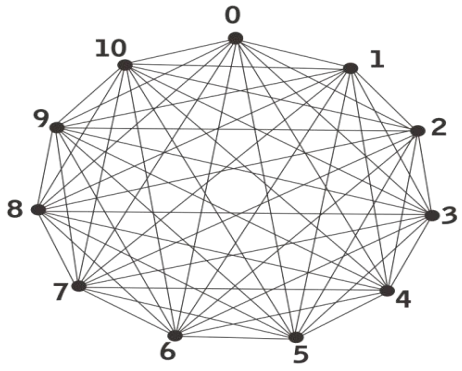

Figure 1: G(Z_{11},φ)

Let $I = \{0\}$ be the IS of $G(Z_{11}, \varphi)$.

Then $f(v) = \begin{cases} 1, & \text{if } v = 0 \\ 0, & \text{if } v = 1, 2, 3, ..., 10. \end{cases}$

$\Rightarrow \sum_{u \in N[v]} f(u) = 1, \ \forall v \in V$ with $f(v) > 0$.

Thus f is an IF of $G(Z_{11}, \varphi)$.

Illustration 3.6: Consider $G(Z_8, \varphi)$. The graph is given below.

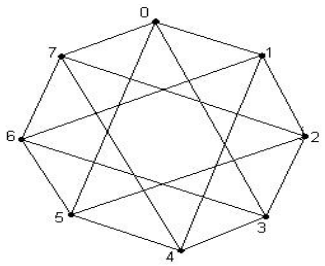

Figure 2: G(Z_8,φ)

The graph is $|S| = 4 -$ regular.

Let $I = \{0, 4\}$ be an IS of $G(Z_8, \varphi)$.

Then the summation values taken over every neighbourhood N[v] of $v \in V$ is given below.

v:	0	1	2	3	4	5	6	7
$f(v)$:	1	0	0	0	1	0	0	0
$\sum_{u \in N[v]} f(u)$:	1	2	0	2	1	2	0	2

$\Rightarrow \sum_{u \in N[v]} f(u) = 1, \ \forall \ v \in V$ with $f(v) > 0$.

Hence f is an IF of $G(Z_8, \varphi)$.

Theorem 3.7: Let $f : V \to [0, 1]$ be a function defined by

$$f(v) = \frac{1}{r+1}, \ \forall v \in V.$$

where $r > 0$ denotes the degree of $v \in V$. Then f becomes an IF of $G(Z_n, \varphi)$.

Proof: Consider $G(Z_n, \varphi)$.

Let $f(v) = \frac{1}{r+1}, \forall v \in V$, where $r > 0$ denotes the degree of the vertex $v \in V$.

Case 1: Suppose n is a prime. Then every neighbourhood N[v] of $v \in V$ consists of n vertices. Then $r = n - 1$.

Now

$$\sum_{u \in N[v]} f(u) = \underbrace{\frac{1}{r+1} + \frac{1}{r+1} + ... + \frac{1}{r+1}}_{(n-times)} = \frac{r+1}{r+1} = 1.$$

$\Rightarrow \sum_{u \in N[v]} f(u) = 1, \quad \forall v \in V$ *with* $f(v) > 0$.

Thus f is an IF of $G(Z_n, \varphi)$.

Case 2: Suppose n is not a prime. Then $G(Z_n, \varphi)$ is $|S| -$ regular graph and $|S| = r$.

Now

$$\sum_{u \in N[v]} f(u) = \underbrace{\frac{1}{r+1} + \frac{1}{r+1} + \ldots\ldots\ldots + \frac{1}{r+1}}_{(|S|+1-times)} = \frac{r+1}{r+1} = 1.$$

$$\Rightarrow \sum_{u \in N[v]} f(u) = 1, \quad \forall v \in V \text{ with } f(v) > 0.$$

Therefore f is an IF of $G(Z_n, \varphi)$ for every n.

Illustration 3.8: Consider $G(Z_7, \varphi)$. The graph is shown below.

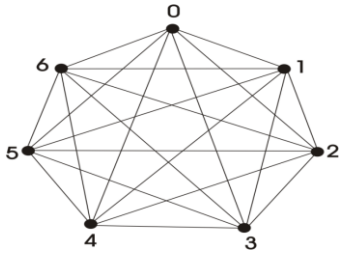

Figure 3: G(Z_7,φ)

Every neighbourhood N[v] of $v \in V$ consists of 6 vertices.

Then $r + 1 = 6 + 1 = 7$.
Now define a function $f : V \to [0,1]$ by

$$f(v) = \frac{1}{7}, \ \forall v \in V.$$

$$\text{Then} \quad \sum_{u \in N[v]} f(u) = \underbrace{\frac{1}{7} + \frac{1}{7} + \ldots\ldots\ldots + \frac{1}{7}}_{7-times} = \frac{7}{7} = 1.$$

$$\Rightarrow \sum_{u \in N[v]} f(u) = 1, \ \forall v \in V \text{ with } f(v) > 0.$$

Thus f is an IF of $G(Z_7, \varphi)$.

Illustration 3.9: Consider $G(Z_{15}, \varphi)$. The graph is shown below.

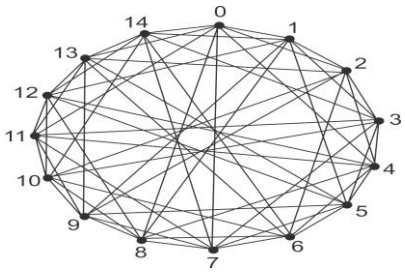

Figure 4: G(Z_{15},φ)

It is a $|S| = 8$ - regular graph.

$$\text{Then} \quad \sum_{u \in N[v]} f(u) = \underbrace{\frac{1}{8} + \frac{1}{8} + \ldots\ldots\ldots + \frac{1}{8}}_{|S|+1-times} = \frac{8}{8} = 1.$$

$$\Rightarrow \sum_{u \in N[v]} f(u) = 1, \ \forall v \in V \text{ with } f(v) > 0.$$

Thus f is an IF of $G(Z_{15}, \varphi)$.

Theorem 3.10: Let $f : V \to [0,1]$ be a function defined by

$$f(v) = \begin{cases} r, & \text{if } v = v_i \in V, \\ 1 - r, & \text{if } v = v_j \in V,\ v_i \neq v_j, \\ 0, & \text{otherwise} \quad . \end{cases}$$

where $0 < r < 1$.

Then f becomes an IF of $G(Z_n, \varphi)$, when n is a prime.

Proof: Consider $G(Z_n, \varphi)$, when n is a prime. Since it is a complete graph, every neighbourhood N[v] of $v \in V$ consists of n vertices.

Then

$$\sum_{u \in N[v]} f(u) = r + (1 - r) + \underbrace{0 + 0 + \ldots\ldots + 0}_{(n-2)-times} = r + (1 - r) = 1.$$

$$\Rightarrow \sum_{u \in N[v]} f(u) = 1, \ \forall\ v \in V \quad with \quad f(v) > 0.$$

Thus f is an IF of $G(Z_n, \varphi)$.

Theorem 3.11: A function $f : V \to [0,1]$ is an IF of $G(Z_n, \varphi)$ if and only if $P_f \subseteq B_f$.

Proof: Consider $G(Z_n, \varphi)$.

Suppose $f : V \to [0,1]$ is an IF of $G(Z_n, \varphi)$.

The boundary set $B_f = \left\{ u \in V \Big/ \sum_{u \in N[v]} f(u) = 1 \right\}$.

Positive set $P_f = \{ u \in V \,/\, f(u) > 0 \}$.

Let $v \in P_f$. Then $f(v) > 0$.

Since f is an IF, for all $f(v) > 0$, $\sum_{u \in N[v]} f(u) = 1$.

$\Longrightarrow v \in B_f$.

Therefore $P_f \subseteq B_f$.

Conversely, suppose $v \in P_f$. Then $v \in B_f$, since $P_f \subseteq B_f$.

Then $\sum_{u \in N[v]} f(u) = 1, \quad for \quad f(v) > 0.$

$\Longrightarrow f$ is an IF of $G(Z_n, \varphi)$.

REFERENCES

[1]. Allan, R. B., Laskar, R. C. − On domination and independent domination numbers of a graph, Discrete Math, 23 (1978), 73-76.
[2]. Arumugam, S. − Uniform Domination in graphs, National Seminar on graph theory and its Applications, January (1983).
[3]. Berge, C. − The Theory of Graphs and its Applications, Methuen, London (1962).
[4]. Cockayne, E. J., Hedetniemi, S. T. − Towards a theory of domination in graphs, Networks, 7 (1977), 247 – 261.
[5]. Haynes, T. W., Hedetniemi, S. T., Slater, P. J − Fundamentals of domination in graphs, Marcel Dekker, Inc., New York (1998).
[6]. Madhavi, L. − Studies on domination parameters and enumeration of cycles in some Arithmetic Graphs, Ph.D.Thesis,submitted to S.V.University, Tirupati, India, (2002).
[7]. Nathanson, Melvyn, B. − Connected components of arithmetic graphs, Monat. fur. Math, 29 (1980), 219 – 220.
[8]. Ore, O. − Theory of Graphs, Amer. Math. Soc. Colloq. Publ. vol. 38. Amer. Math. Soc., Providence, RI, (1962).
[9]. Sampath Kumar, E. − On some new domination parameters of a graph. A survey. Proceedings of a Symposium on Graph Theory and Combinatorics, Kochi, Kerala, India, 17 – 19 May (1991), 7 – 13.

ISSN (e): 2250 – 3005 || *Vol, 05* || *Issue,02* || *February – 2015* ||
International Journal of Computational Engineering Research (IJCER)

An Experimenatl Study on Heat Transfer Behaviors of A Welded - Aluminum Minichannel Heat Exchanger

Thanhtrung Dang[1], Thanhnghia Nguyen[2] and Tronghieu Nguyen[1]
[1]*Ho Chi Minh University of Technology and Education, Vietnam*
[2]*Quy Nhon Vocational College, Vietnam*

ABSTRACT:
This paper presented an investigation for heat transfer behaviors of a welded-Aluminum minichannel heat exchanger (MNHE) using experimental method. In this study, the results show that the welding Aluminum method for MNHE is less efficiency than the bonding PMMA method at high mass flow rate of water. For water having the inlet temperature of 62℃ and mass flow rate of 4.1g/s, the heat transfer rate of the welded- Aluminum MNHE is 118W and the heat transfer rate of the bonded-PMMA MNHE is 132W. It is an important key to select a method for design a minichannel heat exchanger.
KEYWORDS: *Temperature, heat transfer, heat exchanger, minichannel, experimental.*

I. INTRODUCTION

Enhancing heat transfer efficiency and decreasing size are attractive investigations. Regarding to these fields, Dixit and Ghosh [1] studied the effect of heat in-leak for two stream cross flow minichannel heat exchangers with unmixed fluids. The analytical results have been used for predicting the outlet fluid temperatures. With experimental data, one of the end plates in a crossflow-type multistream, minichannel heat exchanger has been subjected to deliberate external heat input given electrically. Experimental result obtained is employed to validate the fluid exit temperatures predicted by the developed model under the same conditions of external heat ingress. The variation in the exit fluid temperatures has been recorded as a function of this external heat in-leak entering the exchanger through one of its outer surfaces. Ray et al. [2] investigated nanofluids performance in a compact minichannel plate heat exchanger. Three nanofluids (comprising of aluminum oxide, copper oxide and silicon dioxide nanoparticles in ethylene glycol and water mixture) have been studied theoretically to compare their performance in a compact minichannel plate heat exchanger. Comparisons have been made on the basis of three important parameters; equal mass flow rate, equal heat transfer rate and equal pumping power. The results show that for a dilute particle volumetric concentration of 1%, all the nanofluids show improvements in their performance over the base fluid. From experiments on a 0.5% aluminum oxide nanofluid, preliminary correlations for the Nusselt number and the friction factor for nanofluid flow in a plate heat exchanger has been derived. This apparatus will be useful to test different kinds of nanofluids. Effect of inlet configuration on the refrigerant distribution in a parallel flow minichannel heat exchanger was studied by Kim et al. [3]. The refrigerant R-134a flow distribution was experimentally investigated for a round header/ten flat tube test section simulating a brazed aluminum heat exchanger. Three different inlet configurations (parallel, normal, vertical) were studied. It is shown that normal and vertical inlet yielded similar flow distribution. The flow distribution was the worst for the parallel inlet configuration. Dixit and Ghosh [4] reviewed micro- and mini-channel heat sinks and heat exchangers for single phase fluids. Miniature heat exchangers have the potential to provide energy efficient systems. In addition, their characteristics of compactness, small size and lesser weight have attracted widespread applications. Literatures related co-current, counter-current and cross-current micro- and mini-channel heat exchangers have been discussed. Sohel et al. [5] studied heat transfer enhancement of a minichannel heat sink using Al_2O_3–H_2O nanofluid. The thermal performances of a minichannel heat sink are experimentally investigated for cooling of electronics using nanofluid coolant instead of pure water. The Al_2O_3–H_2O nanofluid including the volume fraction ranging from 0.10 to 0.25 vol.% was used as a coolant. The experimental results showed the higher (up to 18%) improvement of the thermal performances using nanofluid instead of pure distilled water. Peyghambarzadeh et al. [6] experimentally studied overall heat transfer coefficient in the application of dilute nanofluids in the car radiator. Nanofluids showed greater heat transfer performance comparing with water. Increasing liquid and air Re increases the overall heat transfer coefficient. Increasing the inlet liquid temperature decreases the overall heat transfer coefficient. Nieh et al. [7] employed oxide nano-coolant in air-cooled radiator for heat dissipation.

They produced the Al_2O_3 and TiO_2 nano-coolant by the two-step synthesis method. The heat dissipation capacity and the efficiency factor of the nano-coolant are higher than ethylene glycol. The results showed that the enhanced ratio of the pressure drop and pumping power is not obvious. Dang et al. [8, 9] studied the minichannel heat exchangers to replace for a scooter radiator using experimental method. The results of this study show that minichannel heat exchangers have higher heat transfer rate than that obtained from scooter radiator, but the size of minichannel heat exchangers is about 64% (with three passes) and about 55.7% (with five passes) the size of scooter radiator. However, in [1-7], authors did not study effect of pass number of the heat exchangers on heat transfer behaviors; in [8,9], authors did not use heat exchangers with welding Aluminum instead of bonding PMMA (Polymethymethacrylate) on minichannels. From the relevant literatures above, it is important to study a minichannel heat exchanger with welding Aluminum on minichannels. In the following section, the heat transfer characteristics of the welded Aluminum minichannel heat exchanger (MNHE) will be compared with those of the bonded PMMA MNHE in [9]. All dimensions of two heat exchangers are the same.

II. METHODOLOGY

To design and fabricate the welded-Aluminum MNHE, the governing equations are mentioned [8-10]. The energy balance equation for this minichannel heat exchanger is expressed by:

$$m_w c_w (T_{w,i} - T_{w,o}) = m_a c_a (T_{a,o} - T_{a,i}) \quad (1)$$

Where m is mass flow rate (subscripts w and a stand for water and air sides, respectively), c is specific heat, $T_{w,i}$, $T_{w,o}$, $T_{a,i}$, and $T_{a,o}$ are inlet and outlet temperatures of water and air sides, respectively.
The maximum heat transfer rate, Q_{max} is evaluated by

$$Q_{max} = (mc)_{min} (T_{w,i} - T_{a,i}) \quad (2)$$

The effectiveness (NTU method) is determined by

$$\varepsilon = \frac{Q}{Q_{max}} \quad (3)$$

Heat flux is calculated by

$$q = \frac{Q}{A} \quad (4)$$

Or $q = k \Delta T_{lm}$ (5)

Where Q is heat transfer rate, q is heat flux, A is heat transfer area, k is overall heat transfer coefficient, and ΔT_{lm} is log mean temperature difference.
The log mean temperature difference is calculated by:

$$\Delta T_{lm} = \frac{\Delta T_{max} - \Delta T_{min}}{\ln \frac{\Delta T_{max}}{\Delta T_{min}}} \quad (6)$$

A welded-Aluminum MNHE was designed, based on the above equations. All dimensions of this heat exchanger are the same with the minichannel heat exchanger in [9]. Model (including 48 channels for the water side with the length of 110 mm) is divided into five passes. The channels have a rectangular cross-section, with the width of 1 mm and the depth of 1 mm, the distance between two channels is 1mm. The separating walls have the width of 2 mm. The manifolds of MNHE are rectangular in shape, with the width of 10 mm and the depth of 1 mm. Air side has 54 fins; the cross-section is rectangular, with the depth of 10 mm and the length of 140 mm. The distance between two fins is 1 mm and the thickness of fin is 1 mm. All dimensions are shown in Fig.1.

To seal this MNHE, five Aluminum plates were welded on the five fluid passes of substrate by welding precise technology. After welding, the heat exchanger was filed to get as a smooth plate.

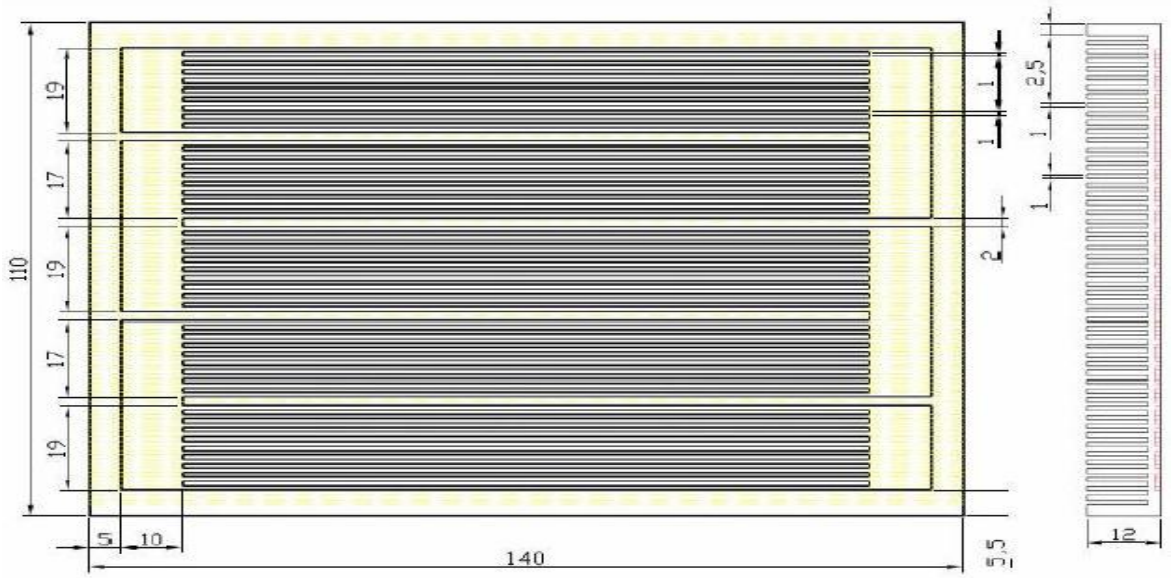

Fig.1. Dimensions of the model

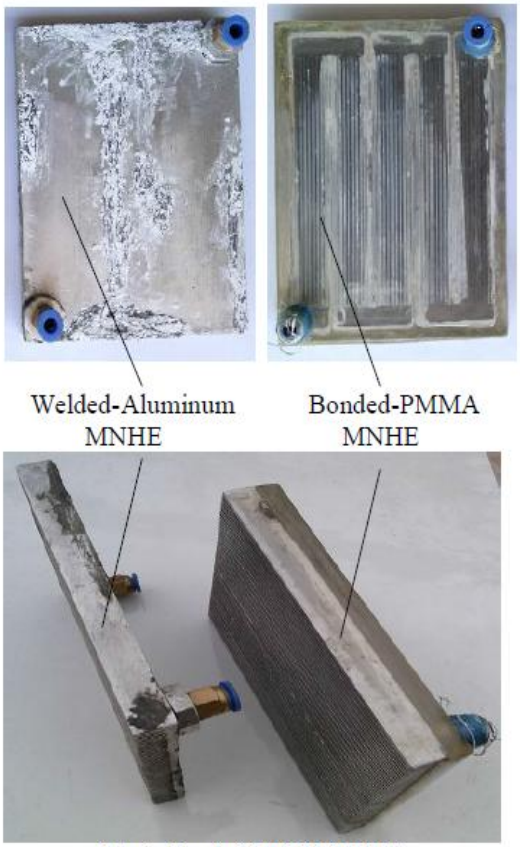

Fig.2. Bonded-PMMA MNHE and welded–Aluminum MNHE

A comparison between the bonded-PMMA MNHE and the welded-Aluminum MNHE is shown in Fig. 2. The onded-PMMA MNHE is the heat exchanger which mentioned in [9]. With the bonded-PMMA MNHE, a layer of PMMA was bonded on the fluid side of substrate by UV light process

Experimental setup

The experimental system consists of the test sample (the Bonded-PMMA MNHE or the Welded-Aluminum NHE), syringe system, and overall testing loop, as shown in Fig.3. Experiment data obtained from the two heat exchangers are under the constant room temperature condition of 30°C.

Table 1. Accuracies and ranges of testing apparatuses

Testing apparatus	Accuracy	Range
Thermocouples	± 0.1 °C	0 ~100 °C
Precision balance	± 0.0015 g	0.0000 ~ 210g
Anemometer	± 3 %	0 ~ 45 m/s

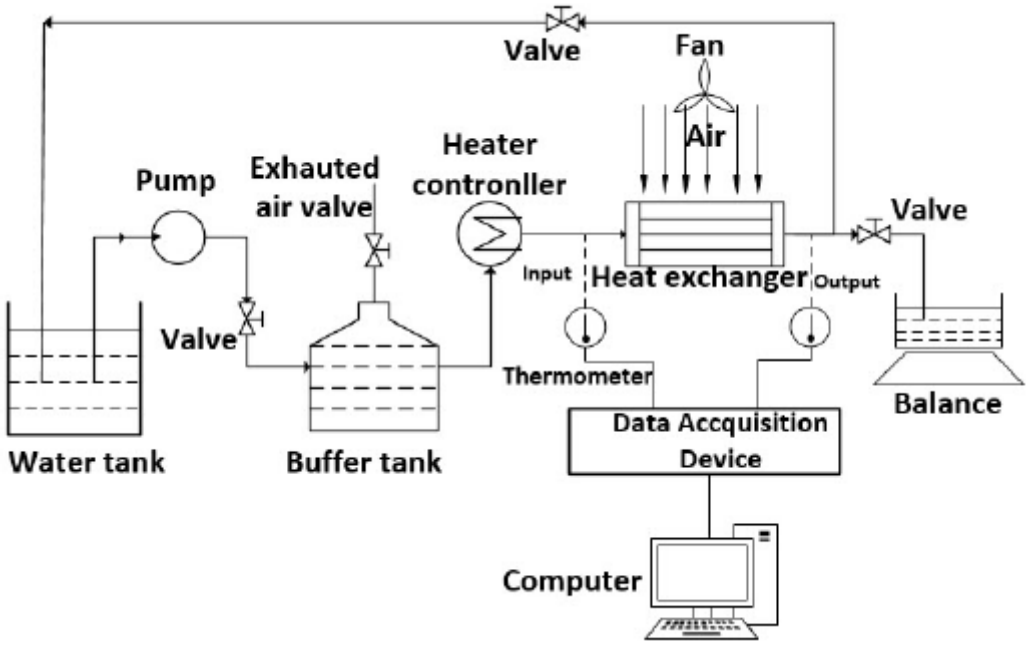

Fig.3. Schematic diagram of the test loop

Accuracies and ranges of testing apparatuses are listed in Table 1. A picture of test loop is shown in Fig. 4. Equipments used for the experiments are listed as follows [8, 9]: - Thermocouples, Model PT-100, made by Omega - Pump, VSP-1200, made by Tokyo Rikakikai - Heater, Model AXW-8, made by Medilab- nemometer, AVM-03, made by Prova - Micro electronic balance, Model TP - 214, made by Denver.

Fig.4. Photo of the test loop

III. RESULTS AND DISCUSSION

The study was done in the case of varying the mass flow rate of water.

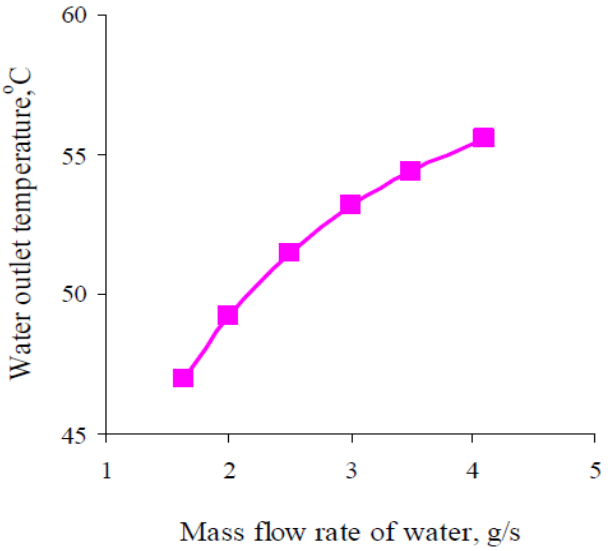

Fig.5. Water outlet temperature versus mass flow rate of water

The experimental data obtained under the ambient temperature of 30°C; the air velocity was fixed at 2 m/s; the mass flow rate of water was varying from 1.64 to 4.1g/s, and the water inlet temperature was fixed at 62°C. The experimental conditions in this study are the same conditions in [9].

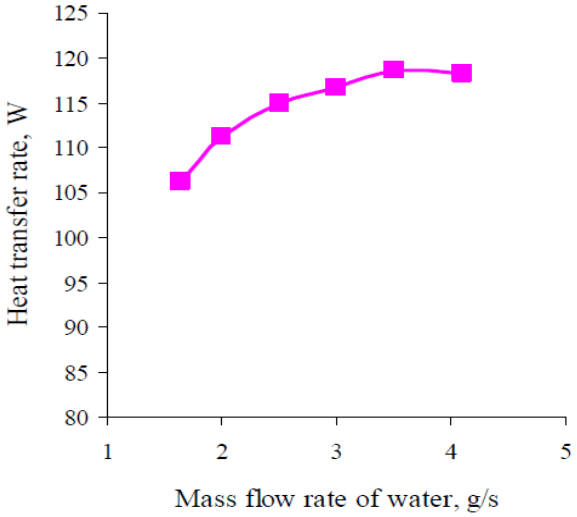

Fig.6. Heat transfer versus mass flow rate of water

When the mass flow rate of water increases, the water outlet temperature increases, it leads to the water temperature difference decreases. Figure 5 shows a relationship between the water outlet temperature and the mass flow rate of water. Because that the mass flow rate term increases more strongly than the temperature difference term, so the heat transfer rate of the heat exchanger increases as rising mass flow rate of water, as shown in Fig. 6. However, when the mass flow rate of water is over 3g/s, the heat transfer rate of the heat exchanger slowly increases. It is explained that at low mass flow rate of water, the force of water is weak, the welded-Aluminum plates and the separating walls of channels do not have gaps. But at high mass flow rate of water, the force of water is strong, the welded- Aluminum plates and the separating walls of channels have gaps, water runs for both the minichannels and gaps between the welded- Aluminum plates and the separating walls of channels. So the fluid flow is not minichanel heat transfer state. Comparisons between the welded-Aluminum MNHE and the bonded-PMMA MNHE are shown in Fig. 7 and Fig. 8. All conditions for these comparisons are the same. It is observed that as the mass flow rate is lower than 3g/s, the heat transfer rate obtained from the welded-Aluminum MNHE is higher than that obtained from the bonded-PMMA MNHE. It means that the welded-Aluminum MNHE was reinforced heat transfer by the welded- Aluminum plate which the thermal

conductivity of Aluminum is higher than PMMA. For the welded-Aluminum MNHE, the heat transfer rate of 111W was achieved for water having the inlet temperature of 62°C and mass flow rate of 2g/s. For the bonded-PMMA MNHE, the heat transfer rate of 103W was achieved for water having the inlet temperature of 62°C and mass flow rate of 2g/s. However, when the mass flow rate is over 3g/s, the heat transfer rate obtained from the welded-Aluminum MNHE is lower than that obtained from the bonded-PMMA MNHE. It is due to Aluminum is flexible, so water flows for both the minichannels and the gaps between the welded- Aluminum plates and the separating walls of channels. With the bonded-PMMA MNHE, the thickness of PMMA is 10mm, it is strong enough, so it has not have the gaps between the PMMA plate and the separating walls of channels. For the welded-Aluminum MNHE, the heat transfer rate of 118W was achieved for water having the inlet temperature of 62°C and mass flow rate of 4.1g/s. For the bonded PMMA MNHE, the heat transfer rate of 132W was achieved for water having the inlet temperature of 62°C and mass flow rate of 4.1g/s.

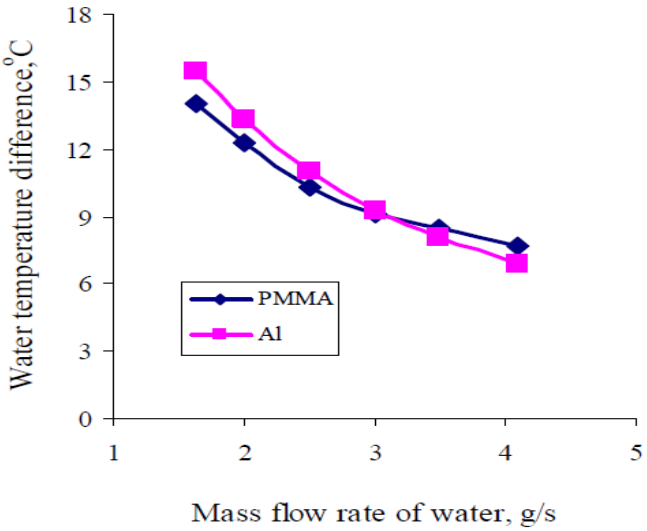

Fig.7. Comparison between the welded-Aluminum MNHE and the bonded-PMMA MNHE for the water temperature difference

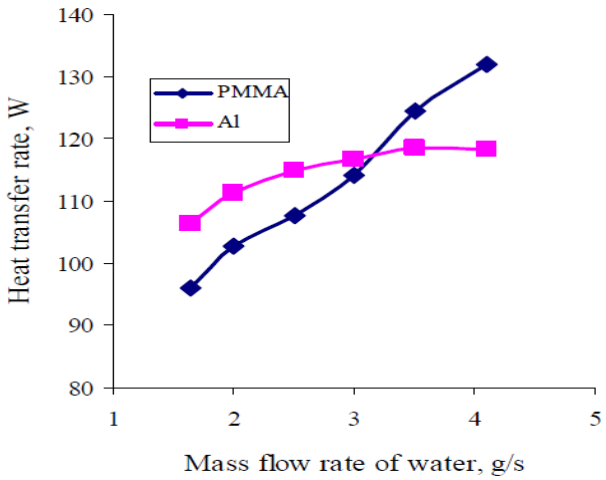

Fig.8. Comparison between the welded-Aluminum MNHE and the bonded-PMMA MNHE for heat transfer rate

From Figs. 5-8, it is indicated that at low mass flow rate of water, the heat transfer rate of the welded-Aluminum NHE is higher than the heat transfer rate of the bonded-PMMA MNHE. However, at high mass flow rate of water, the heat transfer rate of the welded- Aluminum MNHE is lower than the heat transfer rate of the bonded-PMMA MNHE. In this study, these results show that the welding Aluminum method for MNHE is less efficiency than the bonding PMMA method; it is an important key to select a method for design a minichannel heat exchanger.

IV. CONCLUSION

An investigation for a welded-Aluminum MNHE has done by experimental method. This heat exchanger has also compared with the bonded-PMMA MNHE. For water having the inlet temperature of 62°C and mass flow rate of 2g/s, the heat transfer rate of the welded-Aluminum MNHE is 111W and the heat transfer rate of the bonded-PMMA MNHE is 103W. For water having the inlet temperature of 62°C and mass flow rate of 4.1g/s, the heat transfer rate of the welded-Aluminum MNHE is 118W and the heat transfer rate of the bonded-PMMA MNHE is 132W. In this study, the welding Aluminum method for MNHE is less efficiency than the bonding PMMA method. It is an important key to select a method for design a minichannel heat exchanger.

V. ACKNOWLEDGMENTS

The supports of this work by the projects (Project No. T2014-22TĐ/KHCN-GV and Project No. T2015-TĐ/KHCN-GV sponsored by the specific research fields at Ho Chi Minh City University of Technology and Education, Vietnam) are deeply appreciated

REFERENCES

[1] Tisha Dixit and Indranil Ghosh, Theoretical and experimental studies of crossflow minichannel heat exchanger subjected to external heat ingress, Applied Thermal Engineering, Vol. 73, Issue 1, 2014, pp. 162–171

[2] Dustin R. Ray, Debendra K. Das, and Ravikanth S. Vajjha, Experimental and numerical investigations of nanofluids performance in a compact minichannel plate heat exchanger, International Journal of Heat and Mass Transfer, Vol. 71, 2014, pp. 732–746

[3] Nae-Hyun Kim, Do-Young Kim, and Ho-Won Byun, Effect of inlet configuration on the refrigerant distribution in a parallel flow minichannel heat exchanger, International Journal of Refrigeration, Vol. 34, Issue 5, 2011, pp. 1209– 1221

[4] Tisha Dixit and Indranil Ghosh, Review of micro- and mini-channel heat sinks and heat exchangers for single phase fluids, Renewable and Sustainable Energy Reviews Vol. 41, 2015, pp. 1298–1311

[5] M.R. Sohel, S.S. Khaleduzzaman, R. Saidur, A. Hepbasli, M.F.M. Sabri, and I.M. Mahbubul, An experimental investigation of heat transfer enhancement of a minichannel heat sink using Al2O3–H2O nanofluid, International Journal of Heat and Mass Transfer, Vol. 74, 2014, pp. 164– 172

[6] S.M. Peyghambarzadeh, S.H. Hashemabadi, M. Naraki, and Y. Vermahmoudi, Experimental study of overall heat transfer coefficient in the application of dilute nanofluids in the car radiator, Applied Thermal Engineering, Vol. 52, Issue 1, 2013, pp. 8–16

[7] Hwa-Ming Nieh, Tun-Ping Teng, and Chao- Chieh Yu, Enhanced heat dissipation of a radiator using oxide nano-coolant, International Journal of Thermal Sciences, Vol. 77, 2014, pp. 252–261

[8] Thanhtrung Dang, Daly Minh Nao, Ngoctan Tran, and Jyh-Tong Teng, A Novel Design for a Scooter Radiator Using Minichannel, International Journal of Computational Engineering Research (IJCER), June 2013, Vol 03, Issue 6, pp. 41-49.

[9] Thanhtrung Dang, Minhhung Doan, Batan Le, and Jyh-tong Teng, Enhancing heat transfer efficiency of minichannel heat exchangers by increasing the pass number, The 2nd International Conference on Green Technology and SustainableDevelopment 2014 (GTSD14), Ho Chi Minh city, Oct 29-30, 2014, pp. 261-265

[10] Satish Kandlikar, Srinivas Garimella, Dongqing Li, Stephane Colin, Michael King, Heat Transfer and Fluid Flow in Minichannels and Microchannels, Elsevier, November 2005.

ISSN (e): 2250 – 3005 || Vol, 05 || Issue,02 || February – 2015 ||
International Journal of Computational Engineering Research (IJCER)

Application of DRP scheme solving for rotating disk-driven cavity

Reui-Kuo Lin [1,*], Shun-Feng Tsai [2] , Kwan Ouyang [3]

1, Department of Marine Engineering, Taipei College of Maritime Technology, No. 212, Sec. 9, Yen Ping N. Rd.,Shihlin Dist., Taipei 11174, Taiwan, Republic of China (R.O.C)

2, Department of Marine Engineering, National Taiwan Ocean University, No.2, Beining Rd., Jhongjheng District, Keelung City 202, Taiwan, Republic of China (R.O.C)

3, Department of Marine Engineering, Taipei College of Maritime Technology, No. 212, Sec. 9, Yen Ping N. Rd.,Shihlin Dist., Taipei 11174, Taiwan, Republic of China (R.O.C)

** Correspondent, Assistant Professor; TEL: 886-2-28102292-5023;*

ABSTRACT:

This paper is to explore when the rotating disk-driven cube container structure flow generated by different Reynolds numbers to observe structural reasons and swirl flow field generated in the space discretization dispersion-relation-preserving (DRP) scheme finite difference method, time item then use total variation diminishing (TVD) Runge-Kutta method format, thereby to achieve the accuracy of its value, the paper also use topological theory to analyze the characteristics of singularity, and draw a three-dimensional flow field pattern thereby to observe the structure and flow of the flow field case, with the result that the Reynolds number increased flow into the spiral point position will gradually close the bottom of the cavity, and with the impact of an increase in the Reynolds number at the bottom of the singular point significantly smaller.

Keywords: *disk-driven, Reynolds number, dispersion-relation-preserving (DRP), total variation diminishing (TVD), Runge-Kutta, topological theory*

I. INTRODUCTION

Because the relationship between today's emphases on efficiency, with essays program to deal with less fluid flow analysis, the majority are based software package for simulation analysis. However, due to physical problems, there are many possibilities and variations, this paper attempts to analyze essays program flow structure in the disk-driven under the influence of the cube.

In the past the process industries often use to drive the rotating disk-driven flow cylinder, rectangular, or cube thereby to understand the internal structure of the fluid flow. Applying a simple geometric structure of the flow field to explore rotation can help analyze and understand the principles of early and recent research literature mostly cylindrical or rectangular shape, so this article is to explore the use of a cube shape, in their daily lives the most common is the computer's CD-ROM drive, using a rotary disc pieces to bring the whole flow field, hoping to apply the same theory to understand the internal structure of the rotating disk-driven flow, the paper is a continuation of the literature Chiang et al. study [11] was made to continue. To investigate the flow structure when $\mathrm{Re} > 2000$ after arising.

Benjamin and Denny [1] with the vorticity-stream function method to simulate the two-dimensional closed pull hole course and supplemented with multi-grid method, will increase the numerical simulation of the Reynolds number to 104, expressly found that the two-dimensional geometry of a closed pulling hole course located primary vortical center and three times the corner vortical. Koseff and Street [2] employed the experimental data for a series of studies with discussion. Koseff and Street [3] were the top three drivers pulled closed experimental observation point field, when the Reynolds number is between 6000-8000, the structure of the turbulent rotating disk-driven flow for the first time the show. Fenstermacher [4] used laser-Doppler velocimetry explore concentric circles in the middle of the restricted fluid flow from the column transition situations arising from the rotation. Chenoweth and Eyret [5] found that when the Reynolds number is higher than a certain value, the main component of the two-dimensional flow field in the following structure: the geometric center of the vortical in the main (primary eddy), located at the corner of the three sub-swirl (secondary eddy).

Liao et al. [6] using numerical simulation method of rotating between the cylinder when the non-denaturing conditions axisymmetric ilk, and the use of numerical methods for solving the three-dimensional Navier-Stokes equations, the accuracy of its value on having a second-order accurate in time and space, in changing Couette-Taylor flow field, Liao et al clearly parsed revolving cylinder, transitional flow conditions and the structural characteristics of the flow patterns between. Tam et al. [7] proposed to keep the format dispersion relation scheme, the use of the best ways to improve spatial discrete wave number format analog capability. We can also use its spherical shaped segments to observe the distribution of the entire three-dimensional rotating driven cavity flow. Inamuro et al. [8] use variables to calculate the angular velocity $(R\Omega)$, drawing plane streamlines and velocity vectors to observe the driven cavity flow.

In this paper, in order to make more accurate numerical studies, spatial discrete part of the Navier-Stokes equation literature [9] ownership dispersion-relation-pressure formulation finite difference method, at the time part of discrete items literature [10] retain TVD Runge-Kutta method and for different Reynolds number of numerical results are discussed its flow structure, and to explore the reasons for its physical phenomena and secondary flow generated.

II. WORKING EQUATIONS

We consider in this paper the Navier-Stokes equations for velocity u and pressure p:

$$\frac{\partial u_i}{\partial t} + \frac{\partial}{\partial x_i}(u_m u_i) = -\frac{\partial p}{\partial x_i} + \frac{1}{\mathrm{Re}}\frac{\partial^2 u_i}{\partial x_m x_i} \tag{1}$$

The above equations of motion are under the constraint condition of fluid incompressibility,

$$\frac{\partial u_i}{\partial x_i} = 0 \tag{2}$$

The above two equations will be solved subject to the initial divergence-free velocity condition and boundary velocities to close the problem. In this primitive-variable formulation, specification of velocity boundary conditions has been rigorously proven [11]. For this study, we concentrate to steady and laminar conditions. The Reynolds number Re is defined by choosing the maximum rotation speed of the disk $(R\Omega)$ as the characteristic speed and the radius of the rotating disk (R) as the characteristic length. In this study, the pressure has been normalized by $p(R^2\Omega^2)$ where Ω denotes the angular velocity of the disk.

The rationale behind adopting the velocity -pressure formulation is that it provides closure boundary conditions [8], Referring to Figure 1, no-slip boundary conditions for velocities u_i are specified everywhere except at the upper wall, where a disk of radius 1 rotates with a constant value of Ω which is referred to as the disk angular speed. No pressure boundary condition is permitted at the boundary where velocities are specified; otherwise, the investigated elliptic system will be over determined [8].

The appearance and disappearance of non-wandering set is called bifurcation. knowledge about the changes in flow stability and bifurcation, which always coincide in nonlinear dynamics, is thus crucial to get a better understanding of the currently investigated nonlinear differential system. Another main objective in conducting this study is to explore the hydrodynamic details based on the topology theory.

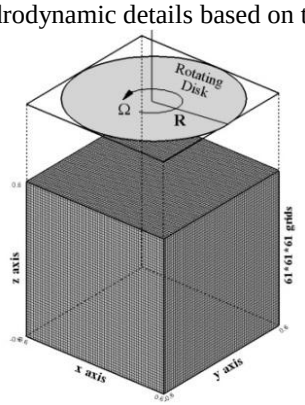

Figure 1. Description of the investigated rotating disk-driven cavity problem and the non-uniform grid distribution 61^3 on the bounding surfaces.

III. FINITE DIFFERENCE METHOD

Discrete numerical methods of solving numerical simulation of rotating disk-driven flow compression is not available to the general use of discrete intermediate pressure gradient difference method detects the unreasonable pressure field, so the literature [9-10] have proposed on the same grid size position high-precision,

high- resolution compact model and can suppress the fluctuation-induced generalized principle and the principle of stability of the momentum equation to deal with the pressure gradient term, and the other according to Tam and Webb [9] proposed dispersion-relation-preserving (DRP) scheme discrete governing equations using best of space discrete method to improve the format for the wave number of simulation capabilities. Its core idea is assumed that the function $\phi(x)$ of the Fourier transform of $\tilde{\phi}(\alpha)$, is $\partial\phi/\partial x$ the Fourier transform of $i\alpha\tilde{\phi}(\alpha)$. The corresponding difference scheme inevitably transformed with the presence of poor guide. The DRP format to maintain a certain precision, the optimized dispersion coefficient difference can lead to a minimum.

3.1. Dispersion-relation-preserving advection scheme

In this paper, the advection term in the level set equation is discretized using the DRP dual-compact scheme [12], and the advection term in the momentum equation is discretized using the multi-dimensional DRP upwinding scheme [13]. The underlying idea in the DRP method is as follows: to physically predict the first derivative term accurately, the dispersive nature embedded in it must be retained as much as possible. The reason for this is that the dispersion relation governs the relationship between the angular frequency and the wavenumber of the first-order dispersive term [9]. In other words, it is possible to predict the solution accurately provided that the dispersion relation is well preserved. To achieve this, we combine the Taylor series expansion analysis with the Fourier transform analysis to derive the discretized coefficients. For details of the derivations, the interested reader is invited to refer to [12] and [13].

3.2. Solver in non-staggered grids

Within the context of velocity-pressure formulation, one has a choice of employing a staggering [14] or a collocating [15] grid strategy for the storage of working variables. While use of both approaches can suppress node-to-node pressure oscillations, we adopt in this study the collocating grid approach for the sake of programming simplicity. When solving the incompressible Navier-Stokes equations (1-2), two well-known numerical instabilities may be encountered in cases when the convection term dominates the diffusion term. We will employ the DRP upwinding scheme detailed in [16] to resolve this numerical instability problem.

The second computational difficulty is to assure the discrete divergence-free condition for the working velocity vector. While this constraint condition can be automatically satisfied in the approach based on a mixed formulation, a much larger algebraic system needs to be solved due to the mass conservation equation. The convergent solutions for (u_i, p), which $i = 1 \sim 3$, in a domain with a large number of mesh points become much difficult to be calculated using a computationally less expensive iterative solver [17]. Derivation of a proper equation for the p replace the divergence-free equation (2) is therefore adopted in this study. This class of approaches involves using a rigorously derived integral boundary condition [18,19] and the calculation of matrix solutions becomes computationally more challenging. Due to these drawbacks, we employ in this study the fractional-step method to advance the calculation through a sequence of sub-steps.

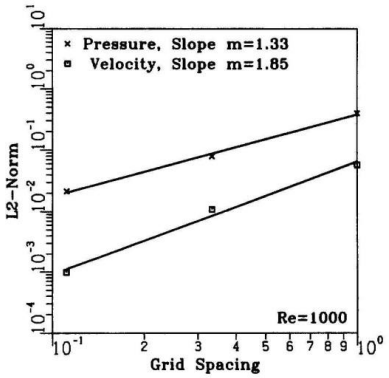

Figure 2. Rates of convergence for velocity magnitude $(u^2+v^2+w^2)^{1/2}$ well as pressure.

3.3. Velocity-pressure coupling

When solving the incompressible flow equation, special care must be taken for the velocity and pressure coupling. While a staggered grid has been demonstrated to be able to eliminate the odd-even decoupling problem, the resulting programming complexity is still a key task. For our purposes, we use a semi-staggered grid to couple the velocity and pressure [20]. The velocity vectors are stored at the edge of the cell, whereas pressure and other scalar fields are stored at the center, as shown in Figure 2. The programming complexity is much lower for this grid system, compared to the staggered grid, and the coupling may be easily achieved if one employs a pressure interpolation from cell center to edge.

We have benchmarked the computer code employed here by taking the analytic velocity vector $u(x_i, t=0)$, as given in the problem of Ethier and Steinman [21], the specified boundary velocities. In this study, solutions computed at the finest grid $(h=1/61)$ are regarded as reference va1ues for conducting the rate of convergence test. According to our previous work [8], the rates of convergence for velocities and pressure are plotted in Figure 2. The success in va1idating the analysis code provides us with strong confidence to study the driven cavity flow subjected to a rotating disk.

In this study, first chosen $\mathrm{Re}=1000$, 2000, 3000, 4000 with experimental data and references each comparison and verification can clearly be seen from Figure 2, with the increase in the number of apparent speed will increase. This article draws from the numerical results of different Reynolds numbers into the speed chart, the pressure diagram, fluid flow map, vorticity map to explore several Reynolds number is not found in the structure of the flow field in the gap is too large, and so this article will explore the entire steady since the structure of the flow field.

IV. RESULTS AND DISCUSSIONS

4.1. Problem description

The disk-container assembly is shown schematically in Figure 1. On the roof of the cavity, a disk of radius 1 is mounted coaxially with the centroid of the cubical cavity, which has a length of 2. This disk rotates constantly with an angular speed Ω , driving an initially resting liquid fluid and thereby resulting in a vortical flow. For this study, we address the effect of the rotation speed, or Reynolds number as defined in Section 2, of the disk on the established vortical flow structure. We also explore into the kinematic aspect of the primary vortical flow and the secondary flow.

On the roof of the rotating disk-cavity flow, a disk of radius 1 is mounted coaxially with the centroid of the cube, which has a length of 2. This rotating disk-cavity flow constantly with an angular speed Ω , driving an initially resting liquid fluid and thereby resulting in a vortical flow. The Reynolds number chosen for this study is defined by the lid speed, the width of the cavity, and the kinematic viscosity of the working fluid.

4.2. Disk-driven vortical flows

Figure 3 compares the rate for the z direction, from the figure that as the Reynolds number can increase the speed will be higher. Then from Figure 4 in the plane $y=0$ for four different Reynolds number flow field pattern, can be observed from the figure had one pair of swirl and eddy currents in different directions of rotation near the top center of the cavity, it is because the top a rotating disk (z direction is the angular velocity), prompting the fluid passes through the center of the chamber to flow upward, fluid particles flowing near the cavity direction downwardly into the vertical end wall, thereby forming a secondary flow structure is inverted. Different faces from Figure 5(a) z direction of the flow field, can observe all of the flow is to the middle of the stream into the boundary wall, the structure of the flow field around the rotation coupled fluid flow into the middle part caused by distortions phenomenon, in the plane $z=0.4$ can be observed that the four corners of the visible presence four secondary flow, because of the adverse pressure gradient caused by the occurrence of reflux, the formation of secondary flow in the four corners of the biggest reason is because effect of viscosity caused by shear stress.

From Figure 5(b) observed vorticity z direction, this flow field is a rotating flow it will generate vorticity, vorticity can be seen from the middle part of the vorticity maximum, because with the amount of rotation in the middle of both the shear stress so large relative vorticity is relatively large near the smaller boundary layer vorticity, and the greater the surface vorticity near the top of the disk. And from the speed can also explain why in the middle of the main vortical vorticity will be greater than four secondary flow vorticity. Topological theory can be obtained by the use of flow into the spiral point (attracting-spiral2d), at $y=\pm 0.6$, $x=\pm 0.6$, $z=-0.6$ and $z=+0.6$ has two faces, three-dimensional map plotted as Figure 6, from the figure can be found at the top of a counter-clockwise rotation of the disk can be used to drive the flow field, from each of the boundary wall flows into the direction of flow can be learned, when $\mathrm{Re}=1000$ the entire flow field flow direction are along the flow direction of rotation of disk.

When $\mathrm{Re}=3000$ when, from Figure 7 can be observed, as the Reynolds number increases speed becomes faster so the fluid flow lines are more intensive in the $z=0.4$ surface persistence of four secondary flow in $z=-0.59$ surface location can be found in the direction of rotation along four distinct swirl counterclockwise also followed a slight change in the main part of the increase in the speed of the vortical near the boundary at four whirlpool reduced, and the pressure is just the opposite this also explains why the primary vortical vorticity increased four secondary flow vorticity smaller reasons. Figure 8 can be more clearly seen in the case of the speed of each plane and the flow. In Figure 9, when $z=-0.6$, $y=\pm 0.6$, $x=\pm 0.6$, to produce a

spiral flow into the point to drive the entire flow, the entire flow way and are rotating disk-driven cavity flow counterclockwise along without any change.

V. CONCLUSIONS

This study is mainly aimed at different Reynolds number as explore its structure flow mechanism and physical behavior. Discussion In this study, the top three-dimensional rotating disk-driven cavity flow impose certain practical value of the angular velocity Ω clockwise, we will chose $500 \le Re \le 4000$, to analyze the singularity into the spiral flow characteristics calculated for each surface point using topology theory, from three-dimensional disk-driven cavity flow can understand the situation led the whole flow. At $500 \le Re \le 4000$ analysis found that the flow of the flow field is very similar, except that with the Reynolds number increases speed and pressure will change, because the speed of the flow field flow lines caused by change-intensive, but the basic structure of the flow field which no significant change in disk-driven cavity flow pattern. Topology through a singular point of theoretical calculations can be found as the Reynolds number increases to flow into the position will gradually spiral point near the bottom of the cavity, and with the impact of an increase in the Reynolds number at the bottom of the singular point significantly smaller. In the face of $z = -0.59$ four vortical continued close to the end wall, this is because as the Reynolds number increases speed along faster, so when the speed increases viscous force it will be relatively minor role to the boundary near the end wall.

ACKNOWLEDGEMENTS

The financial supports provided by the Ministry of Science and Technology under grants 102-2221-E-229-001 and 103-2221-E-229-002 are gratefully acknowledged. Computational hardware supports from the National Center of High-performance Computing and National Taiwan University are also highly appreciated.

REFERENCES

[1] X. Ruiz, M. Aguiló, J. Massons, F. Diáz. Numerical and experimental of the forced convection inside a rotating disk-cylinder configuration, Experiments in Fluids, 14, pp. 333-340, 1993.
[2] E. Lang, K. Sridhar, N. W. Wilson. Computational study of disk driven rotating flow in a cylindrical enclosure, Journal of Fluids Engineering, 116, pp. 815-820, 1994.
[3] H. P. Pao. Numerical solution of the Navier-Stokes equations for flows in the disk-cylinder system, Physics of Fluids, 15, pp. 4-11, 1972.
[4] R. Legendre. Séparation de courant l'écoulement laminaire tridimensionel. Rech. Aéro, 54, pp. 3, 1972, 1956.
[5] M. J. Lighthill. Attachment and separation in three-dimensional flow, In Laminar Boundary Layers, II, ed. L. Rosenhead. Oxford University Press, 26, pp. 72-82, 1963.
[6] Tobak Murray, D.J. Peake. Topology of three-dimensional separated flows, Annual Review of Fluid Mechanics, 14, pp. 61-85, 1982.
[7] L. A. Yates, G. T. Chapman. Streamlines, vorticity lines and vortices around three-dimensional bodies, AIAA Journal, 30(7), pp. 1819-1826, 1992.
[8] H. U. Vogel. Experimentelle Ergebnisseüber die laminare Strömung in einem zylindrischen Gehäuse mit darin rotierender Scheibe, MPI Bericht, 6. 1968.
[9] Tam K. W. Christopher, Jay C. Webb. Dispersion-relation-preserving finite difference schemes for computational acoustics, J. Comput. Phy., Vol. 107: 262-281, 1993.
[10] A. Harten, S. Osher, S. R. Chakravarthy. Uniformly high-order accurate essentially non-oscillatory schemes 3. J. Comput. Phys. Vol. 71: 231-303, 1987.
[11] T. P. Chiang, W. H. Sheu, S. F. Tsai. Topological flow structure in backward-facing step channels, Comput. Fluids, 26(4), pp. 321-337, 1997.
[12] P. H. Chiu, W. H. Sheu. On the development of a dispersion-relation-preserving dual-compact upwind scheme for convection-diffusion equation, Journal of Computational Physics, 228, pp. 3640-3655, 2009.
[13] P. H. Chiu, W. H. Sheu, R. K. Lin. Development of a dispersion-relation- preserving upwinding scheme for incompressible Navier-Stokes equations on non-staggered grids, Numerical Heat Transfer Part B: Fundamentals, 48, pp. 543-569, 2005.
[14] S. K. Lele. Compact finite difference schemes with spectral-like resolution, Journal of Computational Physics, 103, pp. 16-42, 1992.
[15] S. V. Patankar. Numerical Heat Transfer and Fluid Flow, McGraw-Hill, New York, 1980.
[16] S. Abdallah. Numerical solution for the incompressible Navier-Stokes equations in primitive variables using a non-satggered grid II, Journal of Computational Physics, 70, pp. 193-202, 1987.
[17] M. T. Wang, W. H. Sheu. An element-by-element BICGSTAB iterative method for threedimensional steady Navier-Stokes equations, Journal of Computational and Applied Mathematics, 79, pp. 147-165, 1997.
[18] L. Quartapelle, M. Napolitano. Integral conditions for the pressure in the computation of incompressible viscous flows, Journal of Computational Physics, 62, pp. 340-348, 1986.
[19] P. Lin. A sequential regularization method for time-dependent incompressible Navier-Stokes equations, SIAM J. Numer. Anal. 34(3), pp. 1051-1071, 1997.
[20] C. M. Rhie, W. L. Chow. A numerical study of the turbulent flow past on airfoil with trailing edge separation, Report AIAA-82-0988, 1982.
[21] C. R. Ethier, D. A. Steinman. Exact full 3D Navier-Stokes solutions for benchmarking, Int. J. Numer. Meth. in Fluids, 19, pp. 369-375, 1994.

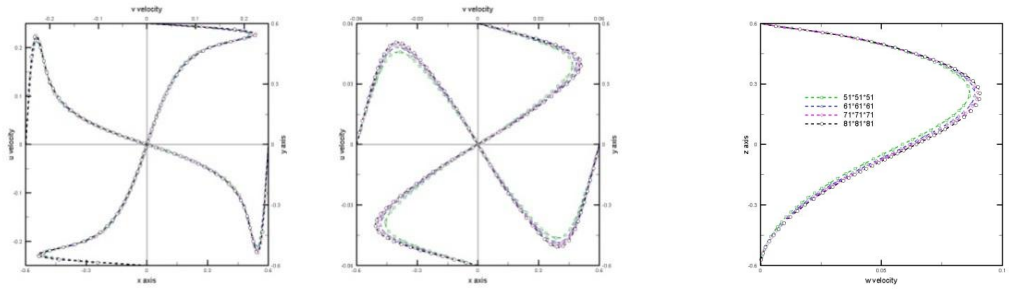

(a) (b) (c)

Figure 3. Grid independence tests for the prob1em, shown in Figure 1, with $\mathrm{Re} = 1000$: (a) $u(0, y, 0.9)$ and $v(x, 0, 0.9)$; (b) $u(0, y, 0)$ and $v(x, 0, 0)$; (c) $u(0, y, -0.9)$ and $w(0, 0, z)$.

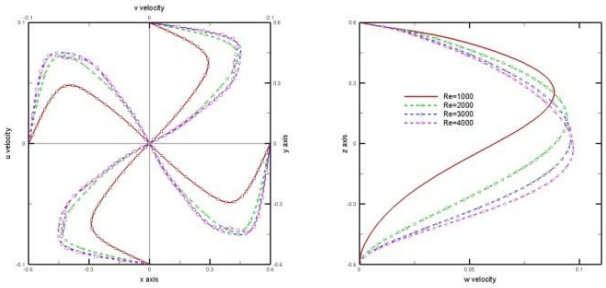

(a) (b)

Figure 4. Changes of velocity against Reynolds numbers for the case conducted on 61^3 meshes: (a) $u(0, y, 0)$ and $v(x, 0, 0)$; (b) $w(0, 0, z)$.

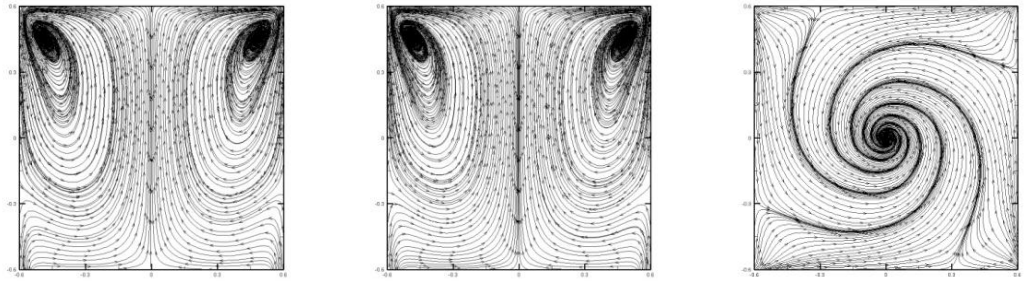

(a) (b) (c)

Figure 5. Computed secondary flow structure for the case of $\mathrm{Re} = 1000$; (a) computed pseudo-streamlines at the $x = 0$ plane; (b) computed pseudo-streamlines at the $y = 0$ plane; (c) $z = 0$ at xy plane.

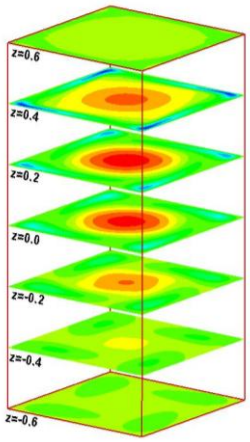

Figure 6. A three-dimensional plot for showing the positive Ω velocity component (shaded area) in the cavity which has a disk angular speed Ω in the corresponding Reynolds number of 1000.

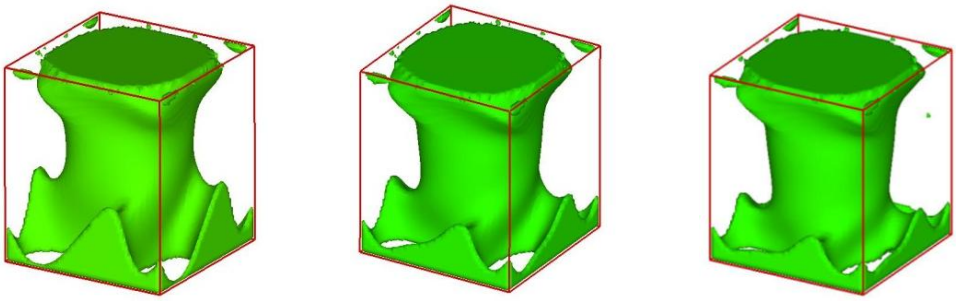

(a) (b) (c)

Figure 7. An illustration of the contour surface of $w = 0$ in the cavity for the cases of (a) $\mathrm{Re} = 2000$; (b) $\mathrm{Re} = 3000$; (c) $\mathrm{Re} = 4000$.

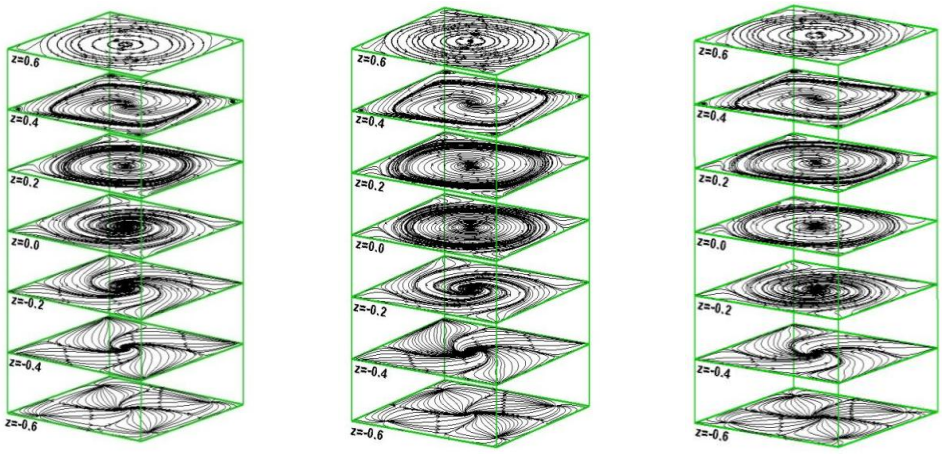

(a) (b) (c)

Figure 8. The computed pseudo-streamlines for the cases with different Reynolds numbers: (a) $\mathrm{Re} = 2000$; (b) $\mathrm{Re} = 3000$; (c) $\mathrm{Re} = 4000$.

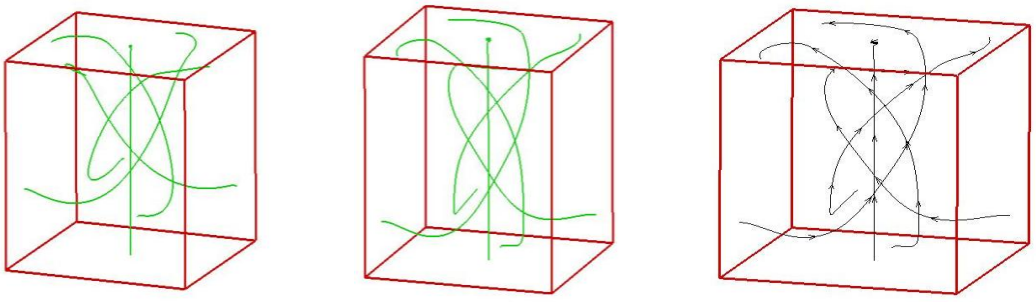

(a) (b) (c)

Figure 9. Dctai1cd flow topologies in the marked area shown in Figure 7. (a) $\mathrm{Re} = 2000$; (b) $\mathrm{Re} = 3000$; (c) $\mathrm{Re} = 4000$.

ISSN (e): 2250 – 3005 || Vol, 05 || Issue,02 || February – 2015 ||
International Journal of Computational Engineering Research (IJCER)

Optimization of Uniform Fiber Bragg Grating Reflection Spectra for Maximum Reflectivity and Narrow Bandwidth

Nagwan I. Tawfik[1], Walid S. Eldeeb[2], M. B. El_Mashade[3], A. E. Abdelnaiem[2]
[1] *Department of Electrical engineering and computer, Higher Technological Institute, 10th of Ramadan city, Egypt.*
[2] *Department of Electronics and Communications, Faculty of engineering, Zagazig University, Egypt.*
[3] *Department of Electrical Engineering, Faculty of engineering,Al Azhar University, Egypt.*

ABSTRACT

Fiber Bragg grating has made a big revolution in telecommunication systems. The existence of fiber Bragg grating is needed when an optical fiber amplifier and filter are used. They can be used as band reject filter or band pass filter for optical devices. The design parameters of the fiber Bragg grating affect the output characteristics of it. The purpose of this paper is to simulate and analyze the spectral characteristics of the uniform fiber Bragg grating (FBG) for achieving maximum reflectivity and narrow bandwidth. This can be achieved by studying the effect of the structural parameters of the uniform fiber Bragg grating such as; grating length and refractive index modulation on the reflectivity and spectral bandwidth of the FBG. The simulations are based on the numerical solution of the coupled- mode equations. The effect of changing the refractive index shape is also considered in this analysis. The simulation results show that the reflectivity of FBG will increase when the grating length and the refractive index modulation increase. Besides, the spectral bandwidth will decrease by the increase of grating length. It will also increase when the refractive index modulation increase. This study deduces that the change of the refractive index shape doesn't have any effect on the spectral response of the uniform FBG.

Keywords- *Couple mode theory, Coupling coefficient, Fiber Bragg grating, Photosensitivity, Reflectivity, Refractive index modulation, Spectral bandwidth.*

I. INTRODUCTION

Fiber Bragg grating is a periodic perturbation of the refractive index along the core of the optical fiber. It has an important role in optical communication system especially when designing optical amplifiers and filters. The modulation of the refractive index can be achieved by exposing the core of the fiber to ultra-violet radiation. This produces change in the refractive index of the core. Photosensitivity is an important characteristic in optical fiber. It was discovered at the Canadian Communication Center in 1978 by Ken Hill et al [1]. It allows the fabrication of FBG in the fiber core. Photosensitivity means the ability to change the refractive index of the core when it is irradiated by a UV light [1]. There are more factors affecting the photosensitivity of the optical fiber such as; irradiation source, fiber core composition and the past history of fiber before the irradiation. The photosensitivity of fiber can be enhanced by hydrogen loading. The first fiber grating was called (self-induced grating). It works only at the writing wavelength which is the ultraviolet wavelength. The refractive index of the core is changed permanently. Germanium doped silica fibers are used in the fabrication of FBG because it is photosensitive which means that the refractive index of the core is changed by the exposure of light. The amount of change depends on the intensity and duration of the exposure. It also depends on the photosensitivity of fiber so that for high reflectivity the level of doping with germanium must be high. There are several techniques for the fabrication of FBG such as; phase mask technique, Holographic technique and point by point technique [2]. Easy fabrication is obtained by phase mask technique. FBG has many applications in optical communication systems such as; dispersion compensation, wavelength converters, fiber grating lasers and amplifiers, laser stabilization, wavelength division multiplexing, selective mirrors and optical Code Division Multiple Access(CDMA) [3]. FBGs have many advantages such as; low losses, done into the fiber, stability, reduced maintenance, flexibility in spectral characteristics, simple structure and low insertion loss [4]. The most attractive subject in studying fiber Bragg grating is the spectral characteristics of FBG. There are several design

parameters which affect the spectral response of FBG such as: grating length, refractive index modulation and grating period [5, 6]. By choosing proper values for these parameters one can achieve maximum reflectivity and narrow bandwidth for better performance of the FBG. This paper aims to design the FBG for better performance and maximum reflectivity. Also it studies the effect of grating length and refractive index modulation on the reflectivity and spectral bandwidth of uniform FBG.

The paper is organized as follows: section I provides an introduction to the fiber Bragg grating including fabrication techniques and its applications. In section II the paper presents a study of the basic structure of fiber Bragg grating and couple mode theory which is used for the analysis of uniform FBG. The discussion and the simulation results are presented in section III with illustrated graphs for each case.

II. UNIFORM FIBER BRAGG GRATING

A. FIBER BRAGG GRATING STRUCTURE

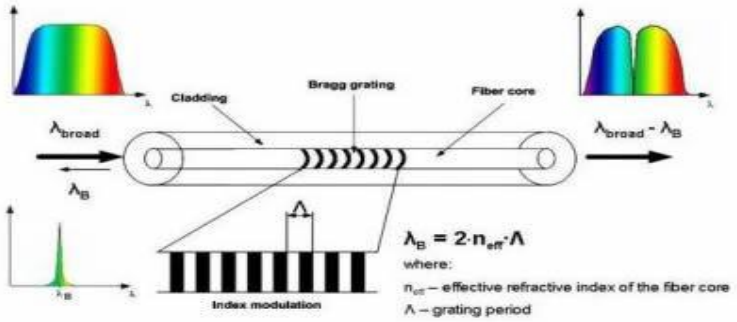

Fig 1. Basic structure of fiber Bragg grating

The basic structure of the uniform fiber Bragg grating is illustrated in Fig 1. [7]. as shown in Fig 1, the refractive index of the core is modulated by a period of Λ. When light is transmitted through the fiber which contains a segment of FBG, part of the light will be reflected. The reflected light has a wavelength equals to the Bragg wavelength so that it is reflected back to the input while others are transmitted. The term uniform means that the grating period, Λ, and the refractive index modulation, δn, are constant over the length of the grating. A grating is a device that periodically modifies the phase or the intensity of a wave reflected on, or transmitted through it [5]. The equation relating the grating spatial periodicity and the Bragg resonance wavelength is given by:$\lambda B = 2n_{eff}\,\Lambda$ where $n_{eff}$is the effective mode index and Λ is the grating period [6]. Fig. 2 shows the different types of Bragg gratings which are (a) transmission (long-period) grating (Fig. 2-A) and reflection (short-period) grating (Fig. 2-B). In reflection grating; coupling occurs between modes travelling in opposite direction, while in transmission grating; coupling occurs between modes travelling in the same direction [8].

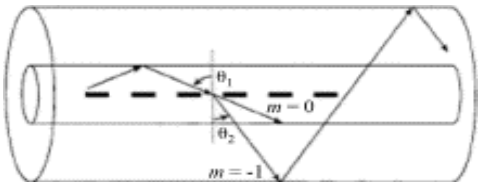

Fig 2-A. Transmission or long period grating

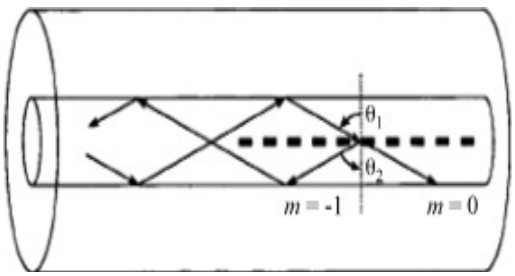

Fig 2-B. Reflection or short period grating

B. THEORY AND PRINCIPLE OF OPERATION

Studying the spectral characteristics of the uniform fiber Bragg grating is accomplished by the solution of coupled-mode equations. Coupled-mode theory is an important tool for understanding the design of fiber Bragg grating [7]. FBG can be considered as a weak waveguide structure so that the couple-mode theory can be used for the analysis of light propagation in weak waveguide structure such as FBG. The couple-mode equations that describe light propagation in FBG can be obtained using couple-mode theory. The couple mode theory was initially introduced in the early 1950's for microwave devices and later applied to optical devices in the early1970's [5]. It is the most straightforward technique as it accurately models the optical properties of the most fiber gratings [9]. Assume that the transverse component of the electric field can be written as a superposition of the ideal modes labeled j (i.e. the modes in an ideal waveguide with no grating perturbation), such that:

$$\vec{E}_t(x,y,z,t) = \sum_j [A_j(z)\exp\left(j\beta_j z\right) + C_j(z)\exp(-j\beta_j z)].\vec{e}_{jt}(x,y)\exp(-i\omega t). \quad (1.1)$$

Where $A_j(z)$ and $C_j(z)$ are slowly varying amplitude of the j[th] mode travelling in the +z and –z directions, respectively. The transverse mode fields $\vec{e}_{jt}(x,y)$ might describe the bound core or radiation LP modes, or they might describe cladding modes.

$$\beta_j = \frac{2\pi}{\lambda} n_{eff} \quad (1.2)$$

Where β_j is the mode propagation constant. While the modes are orthogonal in an ideal waveguide and hence, don't exchange energy, the presence of a dielectric perturbation cause the modes to be coupled such that the amplitudes A_j and C_j of the jth mode evolve along the z axis according to:

$$\frac{dA_j}{dz} = i\sum_k A_k(K_{kj} + K^*_{kj})\exp\left[\left(i\left(\beta_k - \beta_j\right)z\right] + i\sum_k C_k\left(K_{kj} - K^*_{kj}\right)\exp\left[-i\left(\beta_k + \beta_{j)}z\right]\right. \quad (2.1)$$

$$\frac{dC_j}{dz} = -i\sum_k A_k(K_{kj} - K^*_{kj})\exp\left[\left(i\left(\beta_k + \beta_j\right)z\right] - i\sum_k C_k\left(K_{kj} + K^*_{kj}\right)\exp\left[-i\left(\beta_k - \beta_{j)}z\right]\right. \quad (2.2)$$

Where $K_{kj}(z)$ is the transverse coupling coefficient between modes j and k and is given by:

$$K_{kj}(z) = \frac{\pi}{4}\iint_{-\infty}^{\infty} dxdy\,\Delta\varepsilon(x,y,z)\vec{e}_{kt}(x,y).\vec{e}^*_{jt}(x,y) \quad (3)$$

where $\Delta\varepsilon$ is the perturbation to the permittivity, approximately $\Delta\varepsilon \cong 2n\delta n$ when $\delta n \ll n$. The longitudinal coefficient $K^*_{kj}(z)$ is analogous to $K_{kj}(z)$ but generally $K^*_{kj}(z) \ll K_{kj}(z)$ for the fiber modes, so this coefficient is usually neglected. The two new coefficients are:

$$\sigma_{kj}(z) = \frac{\omega n_{co}}{2}\delta n_{dc}(z)\iint_{core} dxdy\,\vec{e}_{kt}(x,y).\vec{e}^*_{jt}(x,y) \quad (4)$$

$$k_{kj}(z) = \frac{\omega n_{co}}{4}\delta n_{ac}(z)\iint_{core} dxdy\,\vec{e}_{kt}(x,y).\vec{e}^*_{jt}(x,y) \quad (5)$$

Where σ is the Direct-Current (DC) (period-averaged) coupling coefficient and k is the Alternating-Current (AC) coupling coefficient. δn_{dc} is the "dc" index change over the grating length and δn_{ac} represents the distribution of the index change due to apodization.

The general coupling coefficient is given by:

$$K_{kj}(z) = \sigma_{kj}(z) + 2k_{kj}(z)\cos\left[\frac{2\pi}{\Lambda}z + \emptyset(z)\right] \quad (6)$$

Where Λ is the grating period and $\emptyset(z)$ describes grating chirp.

Equations (2) to (6) are the coupled-mode equations that describe fiber grating spectra.

For a single-mode Bragg grating the simplified coupled-mode equations can be expressed as:

$$\frac{du}{dz} = j\hat{\sigma}\,u(z) + jkv(z) \quad (7.1)$$

$$\frac{dv}{dz} = -j\hat{\sigma}\,v(z) - jku(z) \quad (7.2)$$

Where the amplitudes u and v are given by:

$$u(z) = A(z)\exp\left(i\delta z - {}^{\emptyset}/_{2}\right) \quad (7.3)$$

$$v(z) = C(z)\exp\left(-i\delta z + {}^{\emptyset}/_{2}\right) \quad (7.4)$$

The coefficient $\hat{\sigma}$ is the general "DC" coupling coefficient and is given by:

$$\hat{\sigma} = \delta + \sigma - \frac{1}{2}\frac{d\emptyset}{dz} \quad (8)$$

Where σ is the "DC" coupling coefficient. For a single mode fiber it is given by:

$$\sigma = \frac{2\pi}{\lambda}\,g[\delta n_{dc}(z) + C\delta n_{ac}(z)] \quad (9)$$

The constant C is a parameter that accounts for additional UV- induced change of the average index along the fiber. g is the overlap integral of the guided mode in the photosensitivity region.

The "AC" coupling coefficient is given by:

$$k = \frac{\pi}{\lambda}g\delta n_{ac}(z) \quad (10)$$

C. SOLVING COUPLE MODE EQUATIONS FOR UNIFORM FIBER BRAGG GRATING

For uniform fiber Bragg grating the coupled mode equations will be simplified to first-order ordinary differential equations with constant coefficients. To find the reflectivity of uniform fiber Bragg grating by applying boundary conditions:

$$u(-L/2) = 1 \text{ and } v(L/2) = 0. \quad (11)$$

So the analytical solution for the coupled mode equations for amplitude and power reflection coefficients will be:

$$\rho = \frac{-k\sinh\left(\sqrt{k^2-\hat{\sigma}^2}\,L\right)}{\hat{\sigma}\sinh\left(\sqrt{k^2-\hat{\sigma}^2}\,L\right)+i\sqrt{k^2-\hat{\sigma}^2}\cosh\left(\sqrt{k^2-\hat{\sigma}^2}\,L\right)} \quad (12)$$

$$r = \frac{\sinh^2\left(\sqrt{k^2-\hat{\sigma}^2}\,L\right)}{\cosh^2\left(\sqrt{k^2-\hat{\sigma}^2}\,L\right)-\frac{\hat{\sigma}^2}{k^2}} \quad (13)$$

For uniform fiber Bragg grating with sinusoidal refractive index variation $k = \frac{\pi\delta n\eta(V)}{\lambda}$ where $\eta(V)$ is a function of fiber V parameter and is, approximately given by:

$$\eta(V) = 1 - 1/V^2. \quad (14)$$

The detuning δ is given by:

$$\delta = 2\pi n_{eff}\left(\frac{1}{\lambda} - \frac{1}{\lambda_B}\right). \quad (15)$$

For maximum reflectivity:

$$R_{peak} = \tanh^2(kL). \quad (16)$$

Reflective bandwidth $\Delta\lambda_{FB}$ of uniform FBG is defined as wavelength bandwidth between the first zero reflective wavelength of both sides of peak reflection wavelength. It can be calculated by:

$$\Delta\lambda_{FB} \cong \frac{\lambda_B^2}{n_{eff}\pi L}\sqrt{[(kL)^2+\pi^2]}. \quad (17)$$

Where L is the grating length, n_{eff} is the effective mode index and λ_B is the Bragg wavelength.

III. RESULTS AND DISCUSSIONS

The parameters used for the simulations are; diameter of the core ($D_{core} = 1.8\mu m$), core index ($n_{co} = 1.47$), cladding index($n_{cl} = 1.457$) and Bragg wavelength($\lambda_B = 1559nm$).When choosing sinusoidal refractive index profile as shown in Fig 3., the dependence of reflectivity and spectral bandwidth on the grating length is investigated as shown in Fig 4.

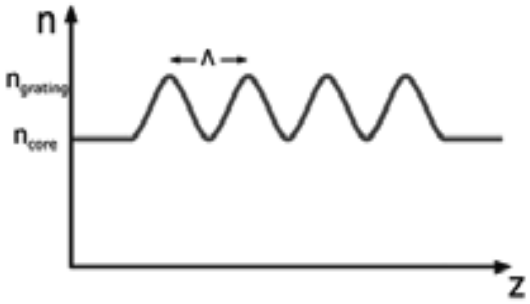

Fig 3. Sinusoidal refractive index profile

In the analysis we choose $\delta n = 4 * 10^{-4}$. It is obvious from the results of this figure that the spectral characteristics of the uniform fiber Bragg grating takes the form of sinc function. As the grating length is increased, reflectivity is increased but the spectral bandwidth is decreased. Also the side lobes are increased with the increase of the grating length. With the increase of the grating length we found that the reflectivity reaches its maximum value then it saturates. The reflectivity reaches unity at grating length equals 4mm. by the increase of the grating length the reflectivity remains unity. It was observed also that the maximum wavelength equals Bragg wavelength (λ_B) and the increase of the grating length doesn't have any effect on the maximum wavelength as it remains the same with the increase of the grating length.

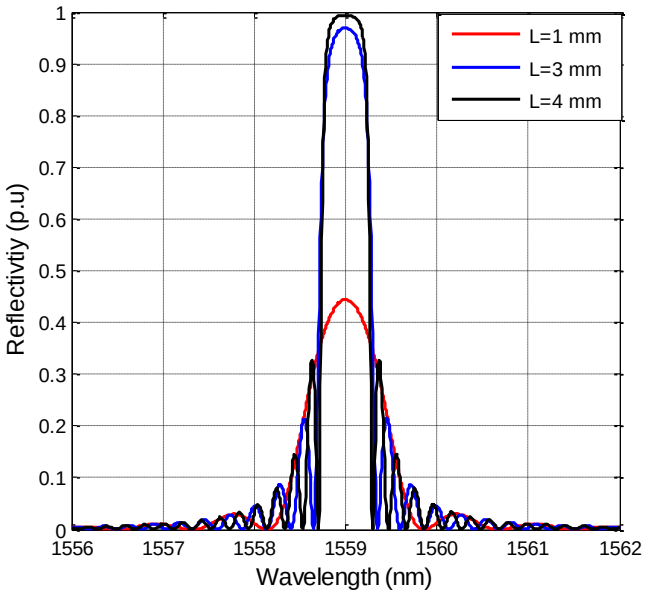

Fig 4. Reflectivity spectrum for different grating length with sinusoidal refractive index profile

Next we study the effect of refractive index modulation (δn) on the reflectivity and the spectral bandwidth as shown in Fig 5.

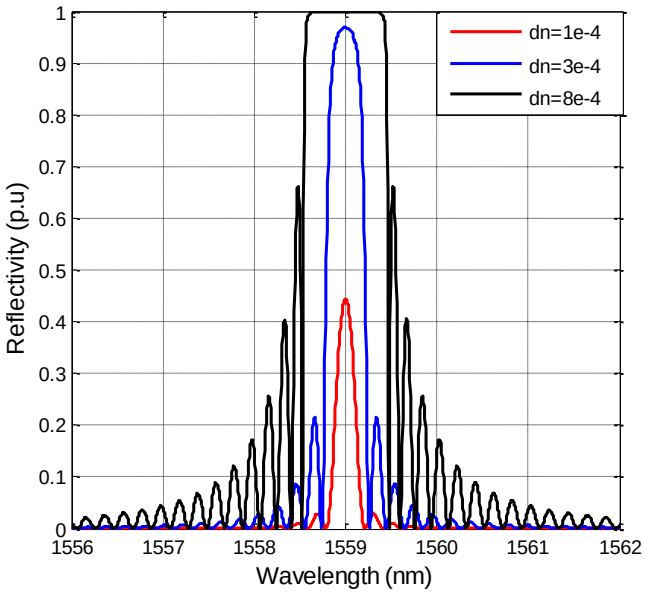

Fig 5. Reflectivity spectrum for different refractive index modulation values with sinusoidal refractive index profile

We choose L=4mm in the analysis. It can be observed that as the refractive index modulation is increased, both the reflectivity and the spectral bandwidth are increased and the side lobes are increased as well. It was obvious from the figure that the reflectivity would be increased until it reached its maximum value then it saturates at a specific value of the refractive index modulation. It reaches unity at $\delta n = 4 * 10^{-4}$ then it saturates. Also the change of refractive index modulation doesn't affect the maximum wavelength which will equal Bragg wavelength for any value of refractive index modulation.
Let us now turn our attention to the effect of square refractive index profile as shown in Fig 6.

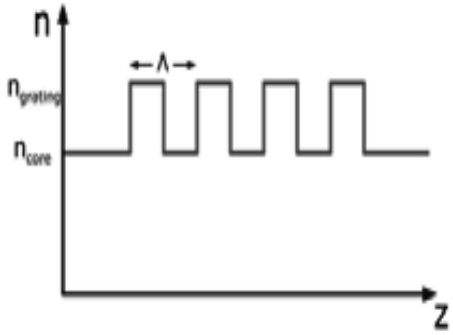

Fig 6. Square refractive index profile

When studying the effect of grating length and refractive index modulation on the reflectivity and spectral bandwidth with the new refractive index shape the following results have been obtained:

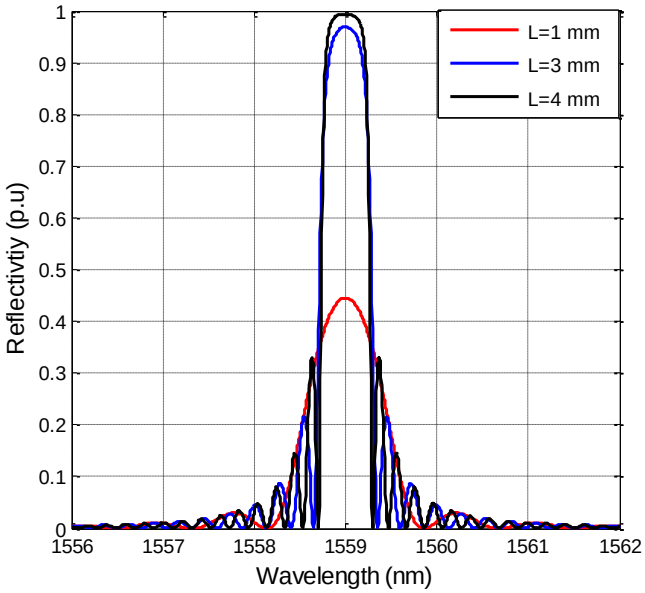

Fig 7. Reflectivity spectrum for different grating length with square refractive index profile

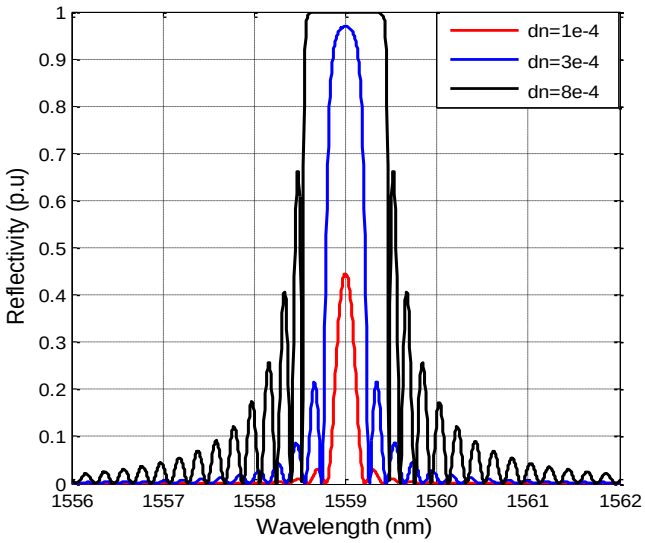

Fig 8. Reflectivity spectrum for different refractive index modulation with square refractive index profile

Figures 7 and 8 show that the shape of the refractive index profile doesn't affect the spectral characteristics of the uniform FBG. So changing the refractive index profile doesn't have any effect on the spectral characteristics of the uniform fiber Bragg grating.
In Fig 9. A relation between maximum reflectivity and grating length has been investigated.

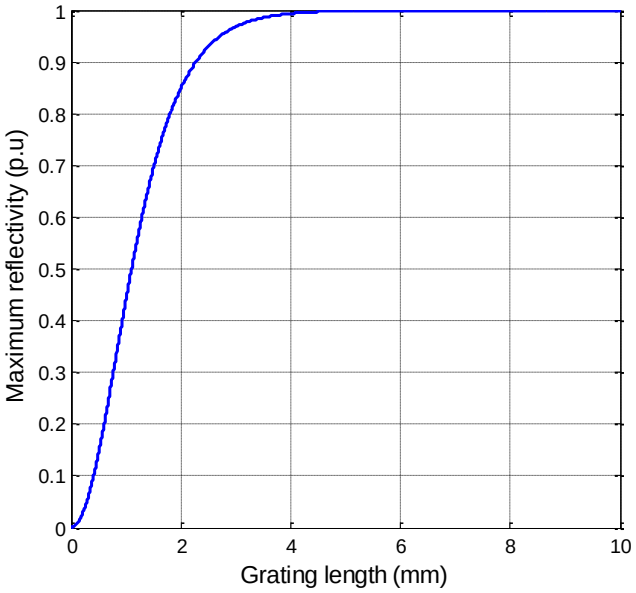

Fig 9. Relation between maximum reflectivity and grating length

It was observed that, as the grating length is increased, maximum reflectivity is obtained until it reaches its maximum value then it saturates. It will reach unity at L=4mm.
The relation between the maximum reflectivity & the refractive index modulation is shown in Fig 10.

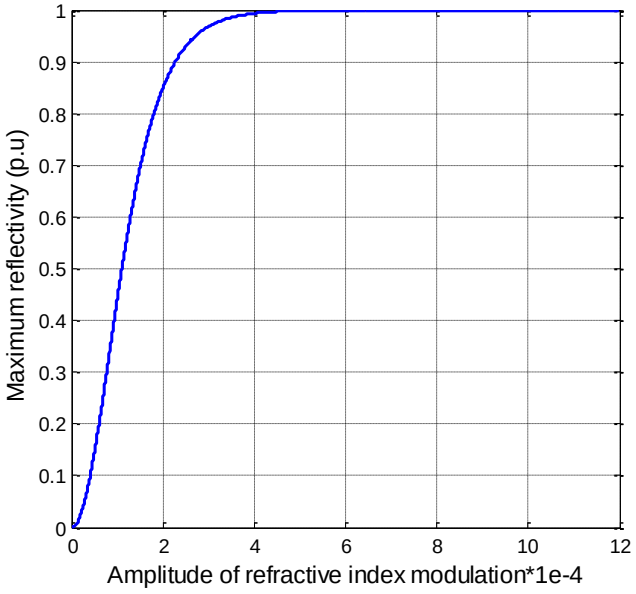

Fig 10. Relation between maximum reflectivity and refractive index modulation

It was clear that, as the refractive index modulation is increased, the maximum reflectivity is obtained and then it saturates. It will reach unity at$\delta n = 4 * 10^{-4}$. The relation between the spectral bandwidth and the grating length is shown in Fig 11.

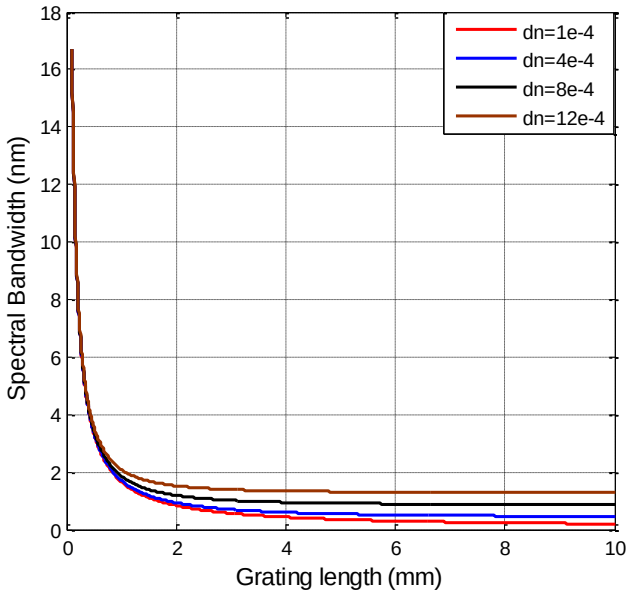

Fig 11. Relation between spectral bandwidth and grating length for different values of dn.

It was investigated that, for grating length shorter than approximately 1mm a small variation in length produces a big variation in the bandwidth. For grating length larger than approximately 5mm it was investigated that the bandwidth isn't affected by the change of grating length, while it is increased by the increase of refractive index modulation.

In Fig 12. A relation between spectral bandwidth and amplitude of refractive index modulation was investigated. It was clear that as the amplitude of refractive index modulation is increased, spectral bandwidth is increased.

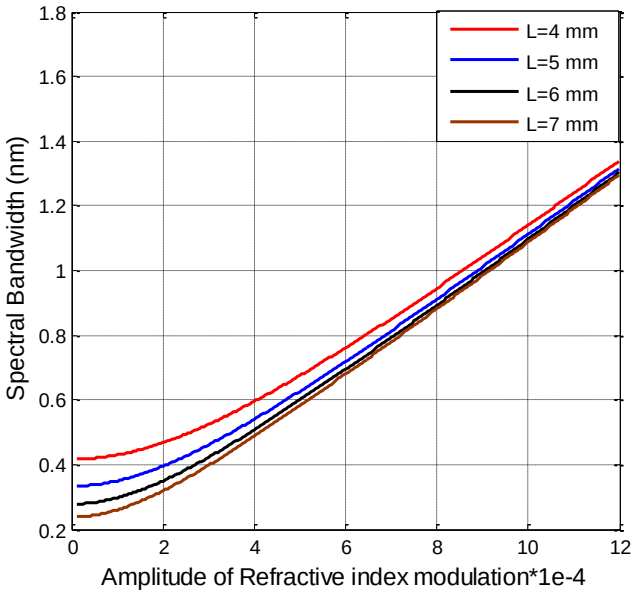

Fig 12. Relation between spectral bandwidth and refractive index modulation for different grating lengths

For better performance of the uniform FBG, proper values for L and δn must be chosen to satisfy maximum reflectivity and narrow bandwidth. If L and δn are chosen as L=5mm and $n = 4 * 10^{-4}$, the maximum reflectivity and narrow bandwidth can be obtained but the problem of side lobes can be solved by using a podization which means modulation of the amplitude δn along the grating length.

IV. CONCLUSIONS

From all the previous work it was concluded that the structural parameters of the uniform fiber Bragg grating have a significant effect on the reflectivity spectrum and the bandwidth. It was clearthat the spectral characteristics of the uniform fiber Bragg grating takes the shape of sinc function. It was investigated that as the grating length is increased, reflectivity is increased but the spectral bandwidth is decreased. With the increase of refractive index modulation both reflectivity and spectral bandwidth are increased. The shape of the refractive index profile doesn't effect on the spectral characteristics of the uniform fiber Bragg grating. For better performance of the uniform fiber Bragg grating proper values for grating length and refractive index modulation must be chosen to achieve maximum reflectivity and narrow bandwidth.

REFERENCES

[1] K. O. Hill and G. Meltz, "Fiber Bragg Grating technology: fundamentals and over-view",J Lightwave Technol, vol. 15, pages 1263–1276, 1997.
[2] Kashyap. R, "*Fiber Bragg Gratings*", San Diego: Academic Press, 1999.
[3] Abdallah Ikhlef, Rachida Hedara, Mohamed Chikh-bled. "Uniform Fiber Bragg Grating modeling and simulation used matrix transfer method". IJCSI International Journal of Computer Science Issues, Vol. 9. Pages. 368-374, 2012.
[4] Santosh Pawar, Shubhada Kumbhaj, Pratima. Sen & Pranay Kumar Sen. "Fiber Bragg Grating Filter for Optical Communication: Applications and Overview". International Journal of Advanced Electrical and Electronics Engineering, (IJAEEE), Vol.2. Pages. 51-58, 2013.
[5] Deba Kumar Mahanta. "Design of Uniform Fiber Bragg grating using Transfer matrix method". International Journal of Computational Engineering Research (IJCER). Vol. 03. Pages 8-13, 2013.
[6] Dinesh Arora, Dr.Jai Prakash, Hardeep Singh & Dr.Amit Wason. "Reflectivity and Braggs Wavelength in FBG". International Journal of Engineering (IJE), Vol. 5. Pages 341-349, 2011.
[7] Jyotsna Rani Mahapatra, Manisha Chattopadhyay. "Spectral Characteristics of uniform fiber Bragg grating using couple mode theory". International Journal of Electrical, Electronics and Data Communication, Vol.1. Pages 40-44, 2013.
[8] Turan Erdogan. T. "Fiber grating spectra". Journal of Lightwave Technology, vol.15. Pages 1277-1294, 1997.
[9] Ho Sze Phing, Jalil Ali, Rosly Abdul Rahman and Bashir Ahmed Tahir. "Fiber Bragg grating modeling, simulation and characteristics with different grating lengths". Journal of Fundamental Sciences vol.3. Pages 167-175, 2007.

ISSN (e): 2250 – 3005 || Vol, 05 || Issue,02 || February – 2015 ||
International Journal of Computational Engineering Research (IJCER)

Open CV Implementation of Object Recognition Using Artificial Neural Networks

[1]Naveen Kumar Anumula, [2]Pradeepa Katta, [3]Madhuri Basa, [4]Durga Prasad Lolla, [5]P.S.Suhasini M.S, Tech, [6]P.Venkata Ganapathi,

[1] *D.M.S.S.V.H. College of Engineering, Machilipatnam, Andhra Pradesh, India*
[2]*D.M.S.S.V.H. College of Engineering, Machilipatnam, Andhra Pradesh, India*
[3]*D.M.S.S.V.H. College of Engineering, Machilipatnam, Andhra Pradesh, India*
[4] *D.M.S.S.V.H. College of Engineering, Machilipatnam, Andhra Pradesh, India*
[5]*Associate professor in E.C.E dept., DMS SVH CE, MTM, Andhra Pradesh, India*
[6]*N.I.T (Warangal), Andhra Pradesh, India*

ABSTRACT

We present an automatic road sign detection and recognition service system for automatic driving system. Artificial neural networks are models inspired by human nervous system that is capable of learning. One of the important applications of artificial neural network is traffic symbol Recognition. The traffic symbol system has been studies for many years. It is one of the most important research area for enabling vehicle driving assistances. The automatic driving system should be simple in order to detect symbol with high responses. The challenge gets more difficult in order to make system simple while avoiding complex image processing techniques to detect symbol. It uses images taken from the Data base. The propose system consist of three main phases: image segmentation, recognition, and classification.

Keywords*—artificial neural networks; object recognition; Open CV; Visual studio; back propagation algorithm.*

I. INTRODUCTION

i. Background

Complexity of the Recognition Task a normal road in the middle of most cities in the world like the one shown for Trowbridge in Figure 1.1, presents a complex scene. It may include trees with different colors, and a number of traffic signs to control the traffic on this road. Fundamentally, if a person is asked to point out the traffic sign in the image, they can do this easily.

Figure 1.1: A Road scene near the Trowbridge.

However, from the point of view of computer vision, this image contains some difficulties which are addressed here:
• The existence of a number of similar objects (either in color or in shape) in the scene.
• The presence of obstacles in the scene which can partially or totally occlude the sign.
• The amount of information in the scene is vast and time is needed to analyze the scene and extract the desired information.

ii. Aims and Objectives of the Research

The overall aim is to develop a system that can be used for traffic sign inventory. This system can assist local or national authorities in the task of maintaining and updating their road and traffic signs by automatically detecting and classifying one or more traffic signs from a complex scene (like the one shown in Figure 1.1) by segmentation process. This process segmentation process is not our project. This process can be done by others. We are going to do our project on segmented image.

Figure 1.2: an image before segmentation

Figure 1.3: an image after segmentation

iii. ARTIFICAL NEURAL NETWORK

Artificial neural networks have been developed as generalizations of mathematical models of biological nervous systems. The basic processing elements of neural networks are called artificial neurons or simply neurons or nodes. In a simple mathematical model of neuron, the effects of the synapses are represented by connection weights that modulate the effect of associated input signals and the nonlinear characteristics exhibited by the neurons that are represented by transfer function. The neuron impulse function is calculated as the weighted sum of input signals, with the help of the transfer function. The Learning capability of artificial neurons is achieved by adjusting the weights in accordance with chosen learning algorithm. The artificial neural network can be trained into two main groups that are supervised and unsupervised learning. In supervised learning, the network learns by example with help of some training algorithm and a target value is set, whereas in unsupervised learning, no target value is set or no example is given. Unsupervised learning is very complex and difficult to implement.

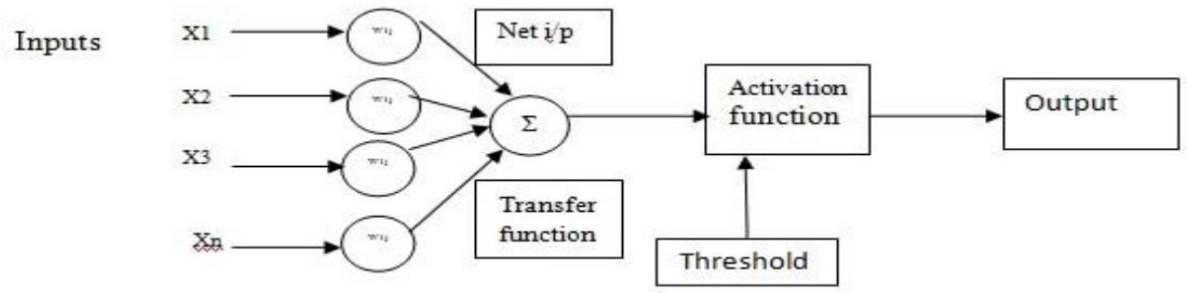

Figure 1.4: A neuron in artificial neural network

iv. Multi-Layer Artificial Neural Networks and Back Propagation

To do more complex calculations, such as analyzing the shape of a traffic sign from the input image and determining what sign it is, can be performed by adding multiple layers of neurons interconnected. This class of networks consists of multiple layers of neurons usually interconnected in a feed-forward way. Each neuron in one layer has directed connections to the neurons of the subsequent layer. In many applications the units of these networks apply a sigmoid function as an activation function. Multi-layer networks use a variety of learning techniques, the most popular being **back propagation algorithm**, In Back propagation, an abbreviation for **'Backward Propagation of Errors',** is a method used for training of artificial neural network. From the desired or actual output, the network learns from number of inputs, similar to the way a child learns to identify a car from group of toys. It is supervised learning method. It requires a dataset of desired output from set of many inputs, making up the training set. A back propagation network consists of three layers of units-input layer, hidden layer and output layer as shown in figure 2. These units are connected in feed forward manner with input units fully connected with units in hidden layer and units in hidden layer fully connected with units in output layer. When back propagation network is cycled, an input pattern is propagated forward to the output units through input to hidden and hidden to output weights. Back propagation is an iterative process that starts with last layer and moves backward through the layers until the first layer is reached. This algorithm is based upon Windrows hoff delta learning rule in which the weight adjustment is done through mean square error of output response to sample input. The rest of these sample patters are repeatedly presented to the network until the error value is minimized. Weights are adjusted according to the error present in the network.

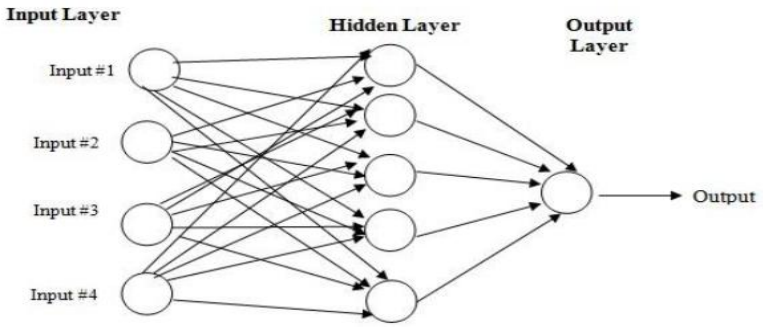

Figure 1.5: Back Propagation Network

II. TRAFFIC SIGN RECOGNITION

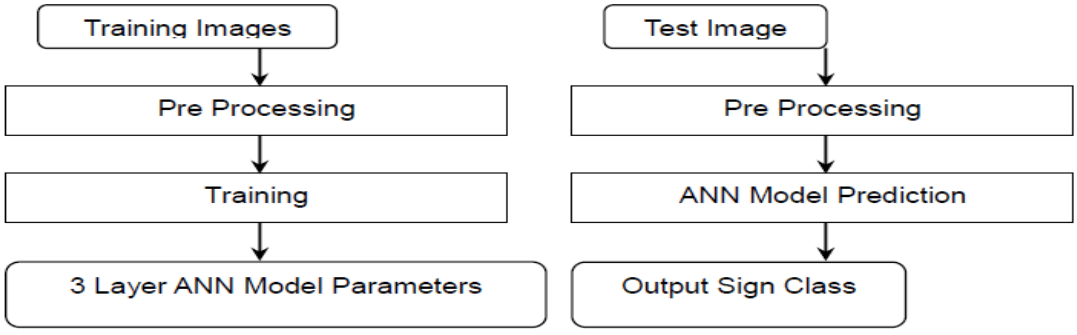

Figure 1.6: System Blocks in Training Mode and Prediction Mode

In this section, we describe the algorithm for traffic sign recognition. The image processing tool used in this paper is a free-and noncommercial Intel® Open Source Computer Vision Library (OpenCV). We used the OpenCV library function to do implement various functions of our system. Some of the function we highlighted when we felt appropriate in the paper. The traffic sign recognition system we designed consists of a Multi-Layer Feed-forward Artificial Neural Network (MLF-ANN) with 3 layers. The first layer is the input layer consisting

256 neurons, second layer is the hidden layer consisting 16 neurons and the third layer consists of 6neurons. To the 256 neurons will receives 256 binary pixels as input and the MLF-ANN produces 6 outputs for each input. Depending on the sign one of the 6 outputs of the network will be predominant which is represents the recognized traffic sign. To understand the system we shall understand the working of the designed MLF neural network. The MLF neural network operates in two modes: training and prediction mode. For the training of the MLF neural network and for the prediction using the MLF neural network we need two data sets, the training set and the set that we want to predict (test set). The training mode begins with arbitrary values of the weights -they might be random numbers -and proceeds iteratively. Each iteration of the complete training set is called an epoch. In each epoch the network adjusts the weights in the direction that reduces the error (see back-propagation algorithm). As the iterative process of incremental adjustment continues, the weights gradually converge to the locally optimal set of values. Many epochs are usually required before training is completed.

In order to train and test the neural network we need pool of traffic images. In our study, we collected our own images of traffic signs downloaded from internet. We gathered 500 images spanning around six different traffic signs. We ensured there is some level of diversity among the images we have collected. All these images need to be preprocessed before we give then to the input layer of the network. During the prepossessing, Gaussian filter is applied to each image to remove the noise, then the image is binarized and cropped to region of interest (ROI) which the area in the image where the traffic sign is placed. The image is downscaled to16x16 size. This window of 16x16 pixels are the 256 pixels required as inputs to the ANN. The preprocessing flowchart is given in the Figure.

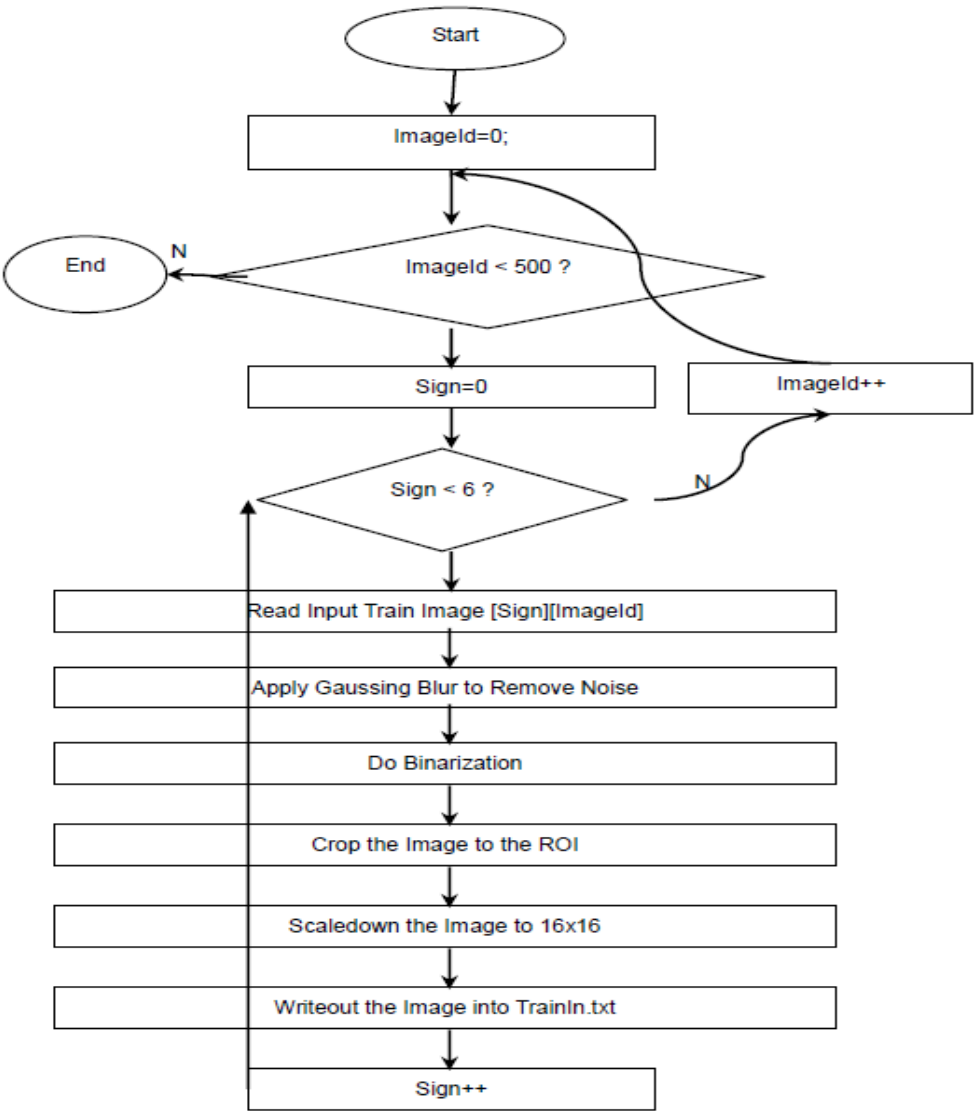

Figure 1.7: Preprocessing Flow Chart

The preprocessed binary images are later read and given as inputs to the network for training. For training we used OpenCV library functions. The OpenCV provides a C++ class called **CvANN_MLP** to model the Artificial Neural Network easily. Below are the functions of this class we used for modeling the network.

VoidCvANNMLP::create (const Mat&layerSizes, intactivateFunc, doublealpha, doublebeta)
Where
LayerSizes: Specifies the number of neurons in each layer
ActivateFunc: Specifies activation function
IntCvANN_MLP::train (const Mat& inputs, const Mat& outputs, const Mat& sampleWeights, const Mat& sampleIdx, CvANN_MLP_TrainParams params, int flags)
Inputs: Floating-point matrix of input
Outputs: Floating-point matrix of output
Sample Weights: Floating-point vector of weights for each sample
Using the above two functions we have created the ANN model of 256 input neurons, 16 hidden neurons and 6 output neurons. The train function does the training for the specified number of iterations which we set to 1000. The resulting ANN model weights are stored into an XML file. This is output of the system in training mode.

During the prediction mode, the ANN model in the recognition system shall be able to recognize any new test image given as input. To do this the ANN model is recreated with the weights obtained in the training mode using **CvANN_MLP::create** function. The test image is preprocessed in the same way we have done in the training mode. OpenCV provides **predict** function in the class **CvANN_MLP.** This function predicts the responses of the model to the new input. The preprocessed binary test image is given as input to this function which gives six responses of the network for the given input. As we discussed one of the six responses would be predominant which is considered as the label for the traffic sign recognized.

V.RESULTS

III. CONCLUSION AND FUTURE SCOPE

The application of neural network in traffic sign recognition has been a field of study recently. Neural networks are used to solve the tasks which are difficult for conventional computers or human beings to solve. This paper aims at recognition of Traffic sign image recognition using gradient descent based back propagation algorithm. The main aim of using this algorithm is to reduce the error which is difference between the computed value of neural network and desired value. By using artificial neural network methodology of Traffic sign image recognition, 99% accuracy is achieved. The method used in this paper can be further extended to recognize multilingual images.
The application of neural network in traffic sign recognition has been a field of study recently. Neural networks are used to solve the tasks which are difficult for conventional computers or human beings to solve. This paper aims at recognition of Traffic sign image recognition using gradient descent based back propagation algorithm. The main aim of using this algorithm is to reduce the error which is difference between the computed value of neural network and desired value. By using artificial neural network methodology of Traffic sign image recognition, 99% accuracy is achieved. The method used in this paper can be further extended to recognize multilingual images.

REFERENCES:

[1] R. Vicen-Bueno, R. Gil-Pita, M.P. Jarabo-Amores and F. L´opez-Ferreras, "Complexity Reduction in Neural Networks Applied to Traffic Sign Recognition", Proceedings of the 13th European Signal Processing Conference, Antalya, Turkey, September 4-8, 2005.

[2] R. Vicen-Bueno, R. Gil-Pita, M. Rosa-Zurera, M. Utrilla-Manso, and F. Lopez-Ferreras, "Multilayer Perceptron's Applied to Traffic Sign Recognition Tasks", LNCS 3512, IWANN 2005, J. Cabestany, A. Prieto, and D.F. Sandoval (Eds.), Springer-Verlag, Berlin, Heidelberg, 2005, pp. 865-872.

[3] H. X. Liu, and B. Ran, "Vision-Based Stop Sign Detection and Recognition System for Intelligent Vehicle", Transportation Research Board (TRB) Annual Meeting 2001, Washington, D.C., USA, January 7-11, 2001.

[4] H. Fleyeh, and M. Dougherty, "Road and Traffic Sign Detection and Recognition", Proceedings of the 16th Mini -EURO Conference and 10th Meeting of EWGT, pp. 644-653.

[5] C. Y. Fang, C. S. Fuh, P. S. Yen, S. Cherng, and S. W. Chen, "An Automatic Road Sign Recognition System based on a Computational Model of Human Recognition Processing", Computer Vision and Image Understanding, Vol. 96 , Issue 2 (November 2004), pp. 237 –268.

[6] Intel Corporation, "Open Source Computer Vision Library," Reference Manual, Copyright © 1999-2001, Available: www.developer.intel.com.

[7] G. Schwarzer, W. Vach, and M. Schumacher, "On the Misuses of Artificial Neural Networks for Prognostic and Diagnostic Classification in Oncology," Statistics in Medicine, 2000, Vol. 19, pp. 541-561.

[8] Henricsson, O., 1996, Analysis of image structures using color attributes and similarity relations. Unpublished PhD Thesis, Institute for Geodesy and Photogrammetry, Swish Federal Institute of Technology, Zurich, pp. 124.

[9] Marr, D., 1982, Vision: A computational investigation into the human representation and processing of visual information. W.H. Freeman and Company, New York, pp. 397.

[10] S. Kumar, "Neural Networks: A Classroom Approach", Mc Graw Hill 2005.

[11] L. Fausett, "Fundamentals of Neural Networks Architectures, Algorithms, and Applications", Prentice Hall Upper Saddle River, New Jersey, 1994.

[12]. G. Loy and N. Barnes. Fast shape-based traffic symbol detection for a driver assistance system. In Proc. IEEE Conf. Int. Robots Syst., pages 70–75, 2004.

[13]. R. Belaroussi and J. Tarel. Angle vertex and bisector geometric model for triangular traffic symbol detection. In Proc. Workshop Appl. Comput. Vis., pages 1–7, 2009.

[14]. Siti Sarah Md Sallah, Fawnizu Azmadi Hussin, and Mohd Zuki Yusoff. Road sign detection and recognition system for real time embedded applications. International Conference on Electrical, Control and Computer Engineering, Pahang, Malaysia, June 21-22 2011.

[15]. Woong-Jae Won, Sungmoon Jeong, and Minho Lee, Road traffic sign saliency map model, in Proc. Image and Vision Computing, New Zealand, pages 91–96, 2007. [

[16]. Z. T. Kardkovacs, Z. Paroczi, E. Varga, and A. S. P. Lucz, "Real-time traffic sign recognition system," IEEE-2011 International Conference on Intelligent Computation technology and Automation, 2011.

ISSN (e): 2250 – 3005 || Vol, 05 || Issue,02 ||February – 2015 ||
International Journal of Computational Engineering Research (IJCER)

Design and Analysis of a Vented Disc brake Rotor

Madu. Gowrisankar[1], Kandula deepthi[2]
[1]Mtech student, Vikas College of engineering & technology, Nunna, AP, INDIA,
[2]Guide (Asst.Professor), Vikas College of engineering & technology, Nunna, AP, INDIA.

ABSTRACT

Brakes are most important safety parts in the vehicles. Generally all of the vehicles have their own safety devices to stop their car. Brakes function to slow and stop the rotation of the wheel. To stop the wheel, braking pads are forced mechanically against the rotor disc on both surfaces. They are compulsory for all of the modern vehicles and the safe operation of vehicles. In short, brakes transform the kinetic energy of the car into heat energy, thus slowing its speed.

The increases in travelling speeds as well as the growing weights of cars have made these improvements essential. The faster a car goes and the heavier it is, the harder it is to stop. An effective braking system is needed to accomplish this task with challenging term where material need to be lighter than before and performance of the brakes must be improved. Today's cars often use a combination of disc brakes and drum brakes. For normal sedan car, normally disc brakes are located on the front two wheels and drum brakes on the back two wheels. Clearly shows that, together with the steering components and tyres represent the most important accident avoidance systems present on a motor vehicle which must reliably operate under various conditions. However, the effectiveness of braking system depends on the design itself and also the right selection of material.

The thesis consists of modeling and analysis of both solid and vented type rotor disc brakes. The main objective of the project is to conduct thermal analysis on the both rotors to study the heat and temperature distribution on disc brake rotor. The results were compared for better rotor and both results provide better understanding on the thermal characteristic of disc brake rotor and assist the automotive industry in developing optimum and effective disc brake rotor.

Key words: *Ansys, disc brake, Pro-E, Rotor, AMMS.*

I. INTRODUCTION

1.1 Disc brake rotor description

Overall idea on vehicle brake system and disc brake theories has been described as above. As similar to the type disc brake described above, the author used the disc brake rotor from normal passenger vehicle. The disc brake rotor was taken from normal passenger vehicle which having type of ventilated disc. Basically, disc brake rotor consists of rotating circular plate and cylinder disc (hat) attached and rotated to wheel hub.

The rotating circular plate which also call annular disc has two flat surfaces separated by 32 internal vanes. Figure shows the cross sectional view of ventilated disc brake rotor with outer diameter measured as 250 mm, 4.5 mm thickness of plate and having mass approximately 4 kg

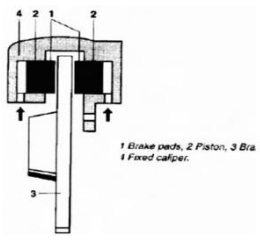

Fig.1 Disc brake rotor

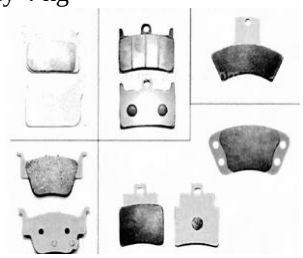

Fig.2 Sample disc pads

1.2 Brake pads

As shown in Figure.2, brake pads consist of steel carrier which the pad are bonded to the steel carrier. According to (Gerschler, 1980), organically bonded pads consist of metallic, ceramic or organic friction materials in a bonded mass such as rubber or synthetic resin. The bonded friction materials can withstand temperatures up to 750°c, with short term peaks-up to 950'~ where the friction coefficient is between 0.25 and 0.5. There is an advantage of brake pads, where most of them are poor to thermal conductivity which protects the hydraulic actuating elements from overheating. It is also ease to manufacture and low cost. However, the pads needs to inspect frequently due to rapid wear as result from higher temperatures and contact pressures associated with the operation of a brake disc.

II. MODELING BY USING PRO-E

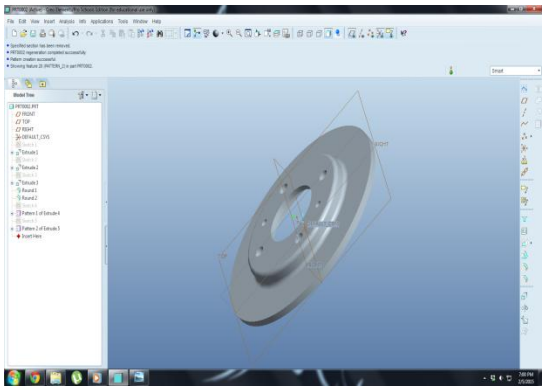

Fig.3 Solid model

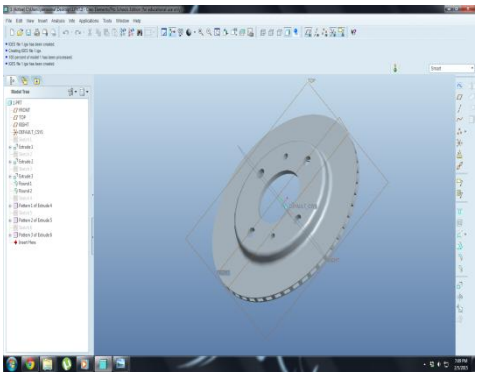

Fig.4 Vented model

2.1 Parts under analysis

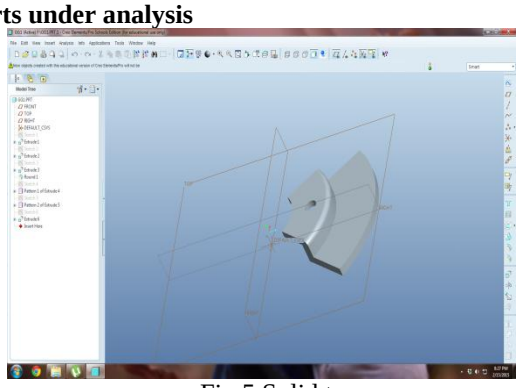

Fig.5 Solid type

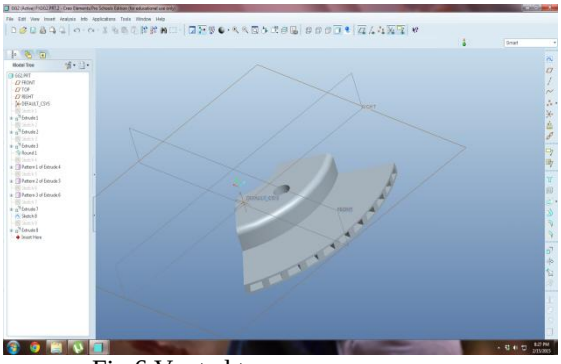

Fig.6 Vented type

III. ANALYSIS BY USING ANSYS

3.1 Imported models

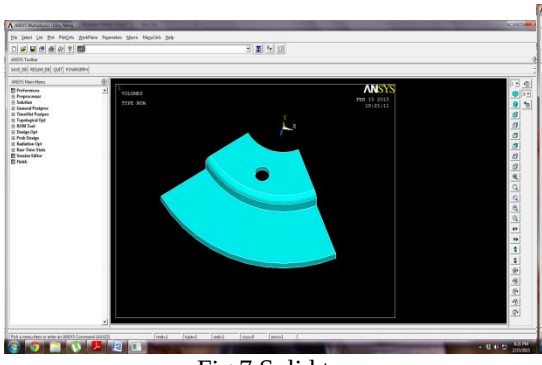

Fig.7 Solid type

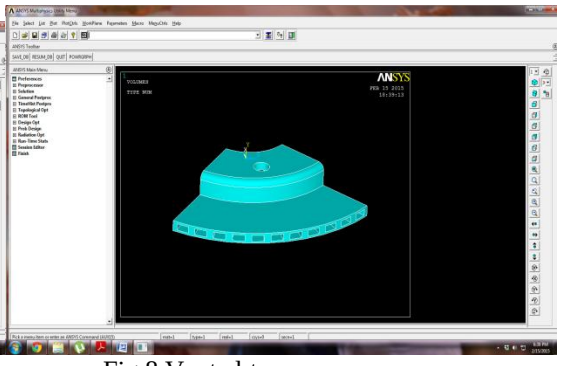

Fig.8 Vented type

3.2 meshed models

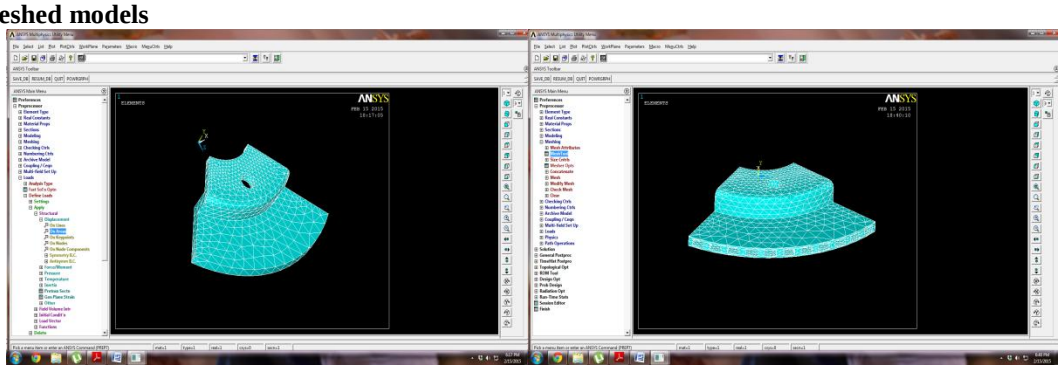

Fig.9 Solid type Fig.10 Vented type

IV. RESULTS & DISCUSSION

4.1 structural analysis results

4.1.1 Solid type

a) cast iron

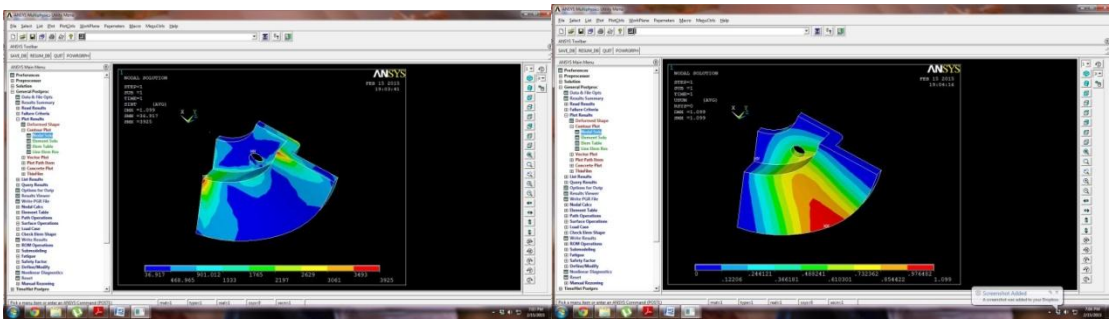

Fig.11 Stress intensity Fig.12 Deformed shape

b) Steel

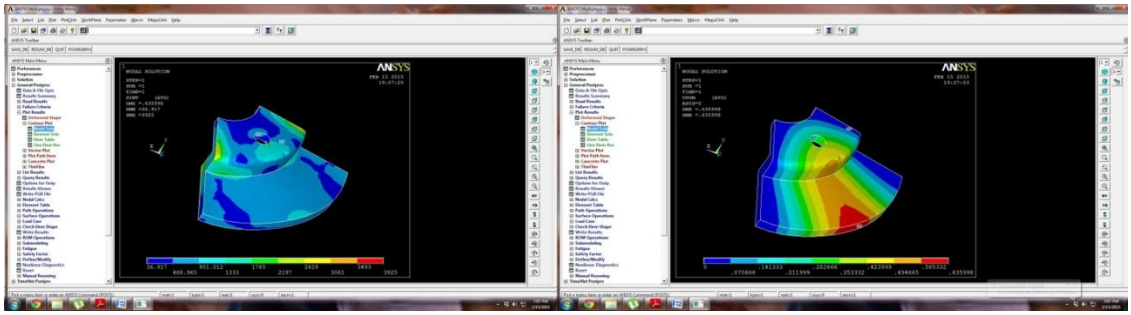

Fig.13 Stress intensity Fig.14 Deformed shape

c) AMMS

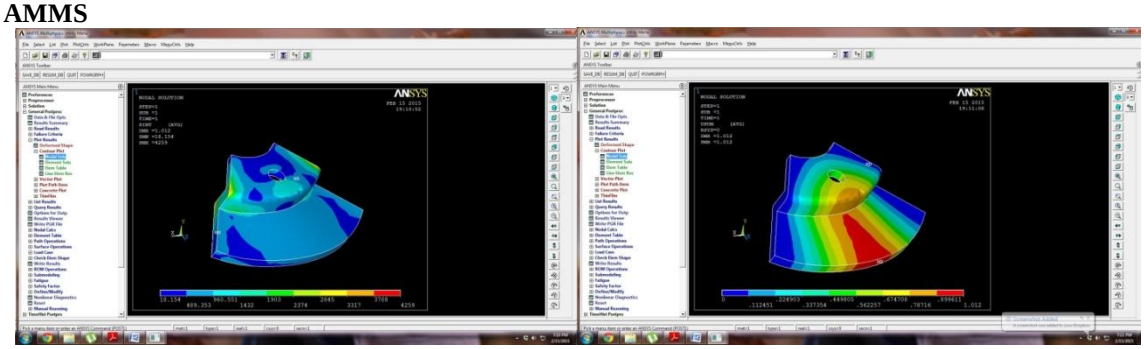

Fig.15 Stress intensity Fig.16 Deformed shape

4.1.2 Vented type

a) Cast iron

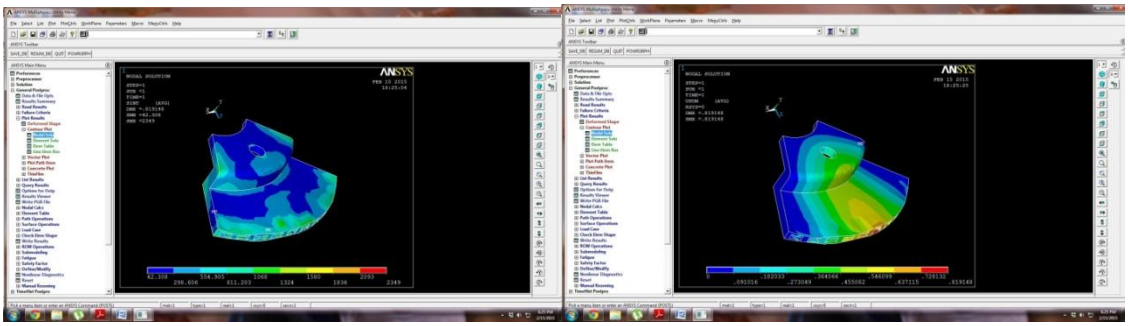

Fig.17 Stress intensity Fig.18 Deformed shape

b) Steel

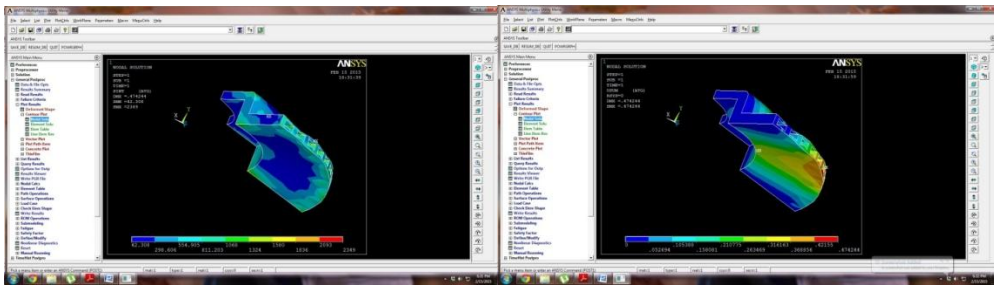

Fig.19 Stress intensity Fig.20 Deformed shape

c) AMMS

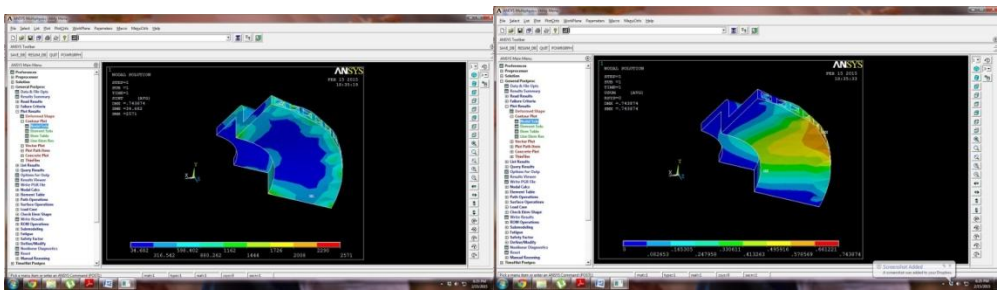

Fig.21 Stress intensity Fig.22 Deformed shape

4.2 Thermal analysis results

4.2.1 Solid type

a) Cast iron

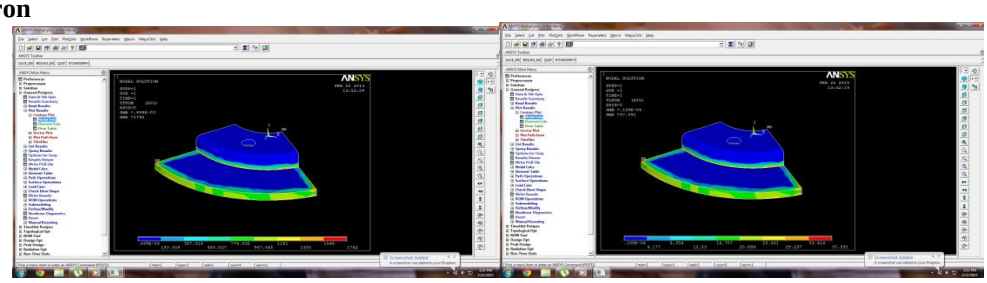

Fig.23 Thermal flux Fig.24 Thermal gradient

b) Steel

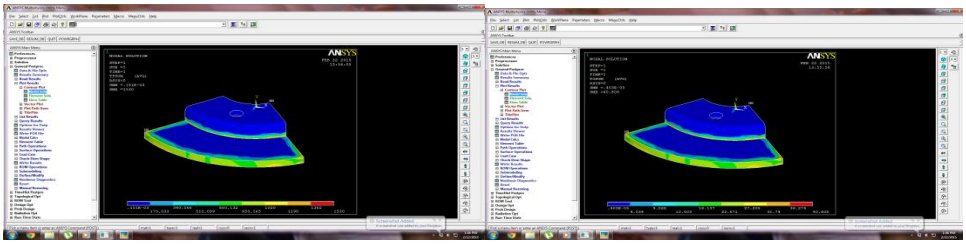

Fig.25 Thermal flux Fig.26 Thermal gradient

c) AMMS

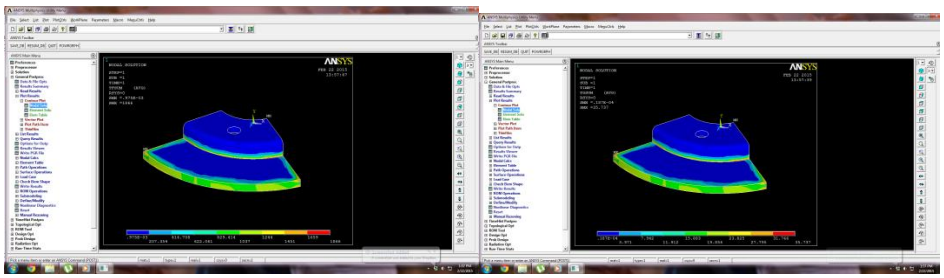

Fig.27 Thermal flux Fig.28 Thermal gradient

4.2.2 Vented type

a) Cast iron

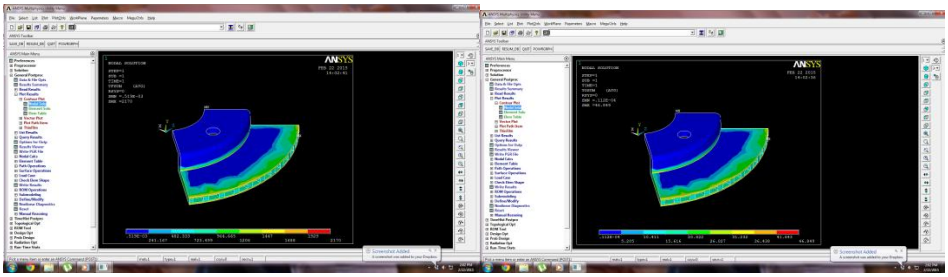

Fig.29 Thermal flux Fig.30 Thermal gradient

b) Steel

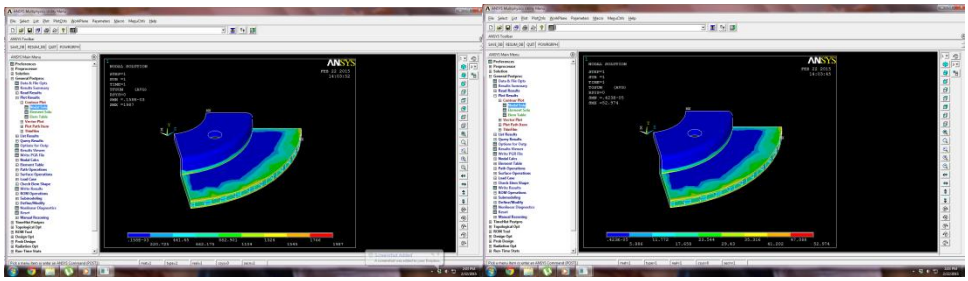

Fig.31 Thermal flux Fig.32 Thermal gradient

c) AMMS

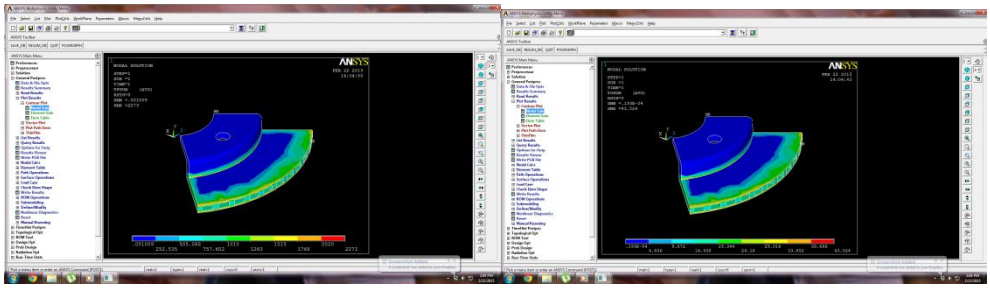

Fig.33 Thermal flux Fig.34 Thermal gradient

4.3 Results comparisons

4.3.1 Structural

Material	Stress intensity	
	Solid type	Vented type
Cast iron	3925	2349
steel	3925	2349
AMMS	4259	2571

Table.1 Stress intensity

material	Total deformation	
	Solid type	Vented type
Cast iron	1.099	0.819148
steel	0.635998	0.474244
AMMS	1.012	0.743874

Table.2 Total deformation

4.3.2 Thermal

material	Thermal gradient	
	Solid type	Vented type
Cast iron	37.591	46.849
steel	40.808	52.974
AMMS	35.737	43.524

Table.3 Thermal gradient

material	Thermal flux	
	Solid type	Vented type
Cast iron	1742	2170
steel	1530	1987
AMMS	1866	2273

Table.4 Thermal Flux

V. CONCLUSION

The modeling of the disc brake is done by using pro-e and the analysis is performed by Ansys. The project consists of two types of analysis structural and thermal. Structural analysis is done to find the strength of the model and the thermal analysis is done to check the thermal resistance of the model. Here we modeled two types of disc brakes one is solid and the other one id vented type. We did analysis on the both models by changing the materials, for this we take three different materials and done analysis on the respective model and the results were compared.

By comparing the results :

- **Structural**

The stress intensity of the vented type disc brake is lower than the solid type and the deformed values of the vented are better than the solid model. If we compare the results in the consideration of change of materials, AMMs have better results than the other two materials so by this we conclude that vented type disc brake with AMMS material is may be used in the place of solid type disc brake.

- **Thermal**

if we compare the thermal results of both solid and vented type model vented model producing better results compared to solid in the both cases of thermal gradient and thermal flux and the AMMS material is best suitable compared to the other two materials.

REFERENCES

[1.] GONSKA, H. W. AND KOLBINGER, H. J. Temperature and Deformation Calculation of Passenger Car Brake Disks, Proc. ABAQUS User.s Conference, Aachen, Germany, page 21- 232, (1993).
[2.] AKIN, J. E. Application and Implementation of Finite Element Methods, Academic Press, Orlando, FL, page 318-323, (1982).
[3.] ZAGRODZKI, P. Analysis of thermo mechanical phenomena in multi disk clutches and brakes, Wear 140, page 291-308, (1990).
[4.] COOK, R. D. Concept and Applications of Finite Element Analysis, Wiley, Canada, (1981).
[5.] 22 ZIENKIEWICZ, O. C. The Finite Element method, McGraw-Hill, New York, (1977).
[6.] 23. BEEKER, A.A. The Boundary Element Method in Engineering, McGraw-Hill, New York, (1992).
[7.] COMNINOU, M. AND DUNDURS, J. On the Barber Boundary Conditions for Thermo elastic Contact, ASME J, vol. 46, page 849-853, (1979).
[8.] BARBER, J. R. Contact Problems Involving a Cooled Punch, J. Elasticity, vol. 8, page 409- 423, (1978).
[9.] BARBER, J. R. Stability of Thermo elastic Contact, Proc. International Conference on Tribology, p Institute of Mechanical Engineers, page. 981-986,
[10.] (1987).
[11.] DOW, T. A. AND BURTON, R. A. Thermo elastic Instability of Sliding Contact in the absence of Wear, Wear, vol. 19, page 315-328, (1972).
[12.] LEE, K. AND BARBER, J.R. Frictionally-Excited Thermo elastic Instability in Automotive Disk Brakes, ASME J. Tribology, vol. 115, page 607-614, (1993).
[13.] LEE, K. AND BARBER, J. R. An Experimental Investigation of Frictionallyexcited Thermo elastic Instability in Automotive Disk Brakes under a Drag Brake Application, ASME J. Tribology, vol. 116,page 409-414, (1994).
[14.] LEE, K. AND BARBER, J. R. Effect of Intermittent Contact on the Stability of Thermo elastic Contact, ASME J. Tribology, vol. 198, page 27- 32, (1995).